Axial Response of Offshore Jacket Piles Supporting Wind Turbines

Trevon M. Joseph

St. Catherine's College

University of Oxford

A thesis submitted for the degree of

Doctor of Engineering

St Catherine's College
Michaelmas 2018

Abstract

This thesis addresses the design methods for offshore piles, and specifically the role of the end bearing of open-ended piles in contributing to capacity. In the design of offshore jacket structures, the response of open-ended tubular piles is governed by their interaction with the soil along the shaft and at the base. To estimate the total static capacity, the shaft and base capacities are estimated separately and added together. These estimates are based on empirical relationships correlated against the results of soil and pile tests. Many design methods exist for open-ended piles. However, for this research the design methods investigated are the API (2014), ICP (2005) and UWA (2005) methods. The target of these methods, is to estimate the load-carrying capacity of the designed pile, after an axial pile head displacement of $0.1D_o$. Over the last few years, much research has focused on more accurately capturing this value, and much less on the distribution of the axial load between shaft and base. It has been found that, in general, the design methods investigated, do estimate the total capacity well. However, the capacity distribution can be improved. Recent pile tests performed using double walled piles in both sands and clays have revealed more about the behaviour of the soil plug, which contributes to the base capacity in open-ended piles, and are analysed here to gain a better understanding of the overall distribution. The role of the plug, in open-ended piles, is of significant concern for designers in determining its contribution to capacity. Simplifying assumptions are often made that the pile is either fully plugged or unplugged, and these assumptions directly impact foundation stiffness and capacity. In this research project, each of the design methods investigated employ a different criterion for plugging and therefore result in different foundation solutions.

To study this problem, a one-dimensional, finite element analysis procedure has been written in MATLAB, which allows a detailed examination of the load distribution between the pile shaft and the base. This procedure can model the behaviour of open-ended piles, specifically isolating the internal and external shaft frictions, and the end bearing on the annulus. Using our existing knowledge of the components and their interactions, we can adopt the design parameters from the design methods to deduce their finite element variants and associated capacities. In addition, by examining the factors contributing to capacity in more detail, recommendations can be made to improve the finite element

procedure leading to the development of modified finite element variants of the design methods for clays, sands and layered soils. Despite these scientific variations and modifications, the variability of soil, and considering the low number of reliable open-ended pile tests in compression, which accurately distribute the applied load between shaft and base, it has been difficult to derive robust conclusions. The results have found however, that while no significant improvements were observed when the database comparisons of total capacity were analysed, the modified finite element variants of the design methods did produce pile head responses that achieved acceptable capacities based on an improved model of the soil plug.

Acknowledgements

This work was supported by grant EP/L016303/1 for Cranfield University and the University of Oxford, Centre for Doctoral Training in Renewable Energy Marine Structures - REMS (http://www.rems-cdt.ac.uk/) from the UK Engineering and Physical Sciences Research Council (EPSRC).

The Author wishes to thank Prof. Guy Houlsby for his continuous support and guidance, from the beginning and throughout the entire process, Prof. Harvey Burd for his patience and passion in conveying his detailed understanding of finite elements and Prof. Byron Byrne for his organisation of and leadership within the REMS CDT group.

From Atkins Ground Engineering, Dr. Paul Taylor who was always found time in his busy schedule to meet, chat and guide the Author throughout the process, Dr. David French, and his successor Mr. Andrew Benson, who encourage the pursuit of technical excellence within the Atkins Ground Engineering team.

The Author wishes to thank his family, friends and colleagues that were present over the duration of this research project for the help and support they provided. His family in Trinidad: Ann, Carlton, Lizanne and Ricaldo, who he knows continuously cheer him on. The Oxford team: Scott Whyte, Peter Houlston, William Beuckelaers, Stephen Suryasentana, Iona Richards and the rest of the REMS cohorts at both Oxford and Cranfield Universities. At the Institution of Civil Engineers: Neil Glover, Tim Eyles and Claire Delgal. From Atkins: Sue Rogers, Sebastien Manceau, Mark Scorer, Sarah Holmes and Alex Hall. Additionally, he would like to thank those that have guided him on his earlier geotechnical journey including Dr. Riaz Khan, Dr. Derek Gay and Dr. Richard Dean.

As for the person who has been standing at his side even before this project began, through the difficult and rewarding times, giving support and guidance daily, Ellie, I simply love you, thank you for always being there.

And now as always, the Author's strong Christian faith that has guided him throughout his life will never subside, but only grow stronger, now and always. He gives thanks.

Table of Contents

Nomenclature

A_p	=	cross sectional area of the pile ($0.25\pi\left({D_o}^2 - {D_i}^2\right)$)
A_{pl}	=	cross sectional area of the plug ($0.25\pi {D_i}^2$)
A_{rb}	=	area ratio of the pile, used in UWA method for base resistance ($1 - FFR(D_i^2/D_o^2)$)
A_{rs}	=	area ratio of the pile, used in UWA method for shaft resistance ($1 - IFR(D_i^2/D_o^2)$)
CEP	=	closed-ended pile
D, D_o	=	external pile diameter
D_{CPT}	=	diameter of the cone penetrometer used for CPT testing (0.036m)
D_i	=	internal pile diameter ($D_o - 2t$)
D_R	=	relative density
EB	=	end bearing
$F_{b,p}$	=	derived force at the base of the annulus
$F_{b,pl}$	=	derived force at the base of the plug
FFR	=	final filling ratio, MIN(1, $(D_i/1.5)^2$)
F_p	=	derived force at elevation along pile ($\sigma_p A_p$)
F_{pl}	=	derived force at elevation along plug ($\sigma_{pl} A_{pl}$)
F_t	=	force applied at the top of the pile
f/f_c	=	a factor in the UWA method for compressive or tensile loading
G	=	shear modulus
G_{vv}	=	*in-situ* shear modulus of non-cohesive material in the vertical direction
G_0	=	initial shear modulus
h	=	distance from pile base along shaft
IFR	=	incremental filling ratio
I_p	=	plasticity index
K	=	earth pressure coefficient
K_c	=	coefficient of radial effective stress for shaft after full equalisation
K_f	=	coefficient of radial effective stress for shaft at failure
L, L_P	=	length of the pile
L_a	=	active length of the plug
L_{pl}	=	length of the plug
L_{wp}	=	length of the wedged plug (L_a)
L_{up}	=	length of the un-wedged plug
M	=	constrained modulus of plug
NC	=	normally-consolidated
N_c	=	dimensionless bearing capacity factor in clays
N_q	=	dimensionless bearing capacity factor in sands

OC = over-consolidated

OCR = over-consolidation ratio

OEP = open-ended pile

P_a = atmospheric pressure (100kPa)

P_e = external perimeter of the pile

P_i = internal pile perimeter

Q = mobilised end bearing capacity

q_b = total end bearing resistance

Q_b = total end bearing capacity

$q_{b,p}$,q_{ann} end bearing resistance of annulus

$q_{b,pl}$,q_{plug} end bearing resistance on plug base

$Q_{b,p}$ = end bearing capacity of annulus

$Q_{b,pl}$ = end bearing capacity on plug base

Q_c/Q_m = capacity calculated / capacity measured

q_c = cone tip resistance (kPa)

Q_{ext} = total external shaft friction

Q_{int} = total internal shaft friction

P_e = external perimeter of the pile

P_i = internal perimeter of the pile

R = external pile radius

R_i = internal pile radius

R^* = equivalent pile radius for an OEP $\left[\left(R^2 - {R_i}^2\right)^{0.5}\right]$

R_f = failure ratio

r_m = zone of influence, “magic radius”

s_{pile} = alternative definition for pile head displacement found in literature

S_t = sensitivity of soil

s_u = undrained shear strength of the soil

t = wall thickness (WT)

UCS = unconfined compressive strength

$w_{b,p}$ = virtual displacement of the pile base

$w_{b,pl}$ = virtual displacement of the plug base

w_p = virtual displacement along the pile nodes

w_{pl} = virtual displacement along the plug nodes

w_t = (virtual) displacement of the pile head

YSR = yield stress ratio ($\sigma'_{vy}/\sigma'_{v0}$)

z = depth below the ground/seafloor level

$z_{b,p}$ = displacement of annulus base

$z_{b,pl}$ = displacement of plug base

z_c = displacement required to mobilise full base resistance

z_p = local pile displacement

z_{peak} = local pile displacement to mobilise maximum capacity

z_{pl} = local plug displacement

α = shaft friction factor in cohesive material

β = ratio of τ_i/σ'_v

δ = interface friction angle

γ = strain ($G = \tau/\gamma$)

γ' = effective unit weight

δ_{cv} = constant volume or critical state angle of interface friction

δ_f = operational peak or ultimate (residual) interface angle of friction

δ_p = plug compression

ΔI_{v0} = relative void index

ΔI_{vy} = relative void index at yield

ΔL_p = change in pile length

ΔL_{pl} = change in plug length

Δr = roughness thickness for lightly rusted steel

κ^* = coefficient of compressibility

σ_p = axial stress in the pile

σ_{pl} = axial stress in the plug

σ'_{rc} = equalised radial effective stress

σ'_{rf} = radial effective stress at point of shaft failure

σ'_{vo}, σ'_v = vertical (initial) effective overburden stress

σ'_{vi} = initial effective vertical stress

σ'_{vy} = vertical effective yield stress

τ = mobilised interface shear stress

τ_0 = shear stress at the pile shaft

$\tau_{e,i}$ = mobilised interface shear stress in the external shear zone

τ_e, τ_{ext} = design ultimate external shaft resistance

τ_f = local shear stress

τ_i, τ_{int} = design ultimate internal shaft resistance

$\tau_{i,i}$ = mobilised interface shear stress in the internal shear zone

τ_{max} = maximum interface shear stress

τ_s = shear stress of the surrounding soil

υ = Poisson's ratio

φ = interface friction value of soil

1. Introduction

This research focuses on the optimisation of open-ended piles (OEPs) which are predominantly used to support offshore jacket structures. These jacket structures are effective in converting horizontal and vertical loads from above the water surface to the seabed. These structures were originally used to support structures in the offshore oil and gas industry and are now in use in offshore wind.

Through research, the American Petroleum Institute (API) agreed upon methods to undertake the design of OEPs from as early as 1978 and has continuously updated and carefully advocated their methods to undertake these designs. The most recent of these documents is the API RP 2GEO (2014). Within this document the API sets out an OEP design method that has a proven track record of success.

Professor J.B. Burland initiated research at Imperial College (IC) London in pile-soil behaviour in 1981, which led to the research thesis by (now Professor) R. Jardine in 1985. Bond (1989) developed a specially designed, highly instrumented, closed ended, IC pile, whose work was then followed by Lehane (1992) and Chow (1996) leading to the development of the Imperial College Pile (ICP) design method published in 2005. This new method was able to improve the estimate of the capacity of OEPs and against the widely used API pile design method. The basis of the ICP method in sands is a correlation of both shaft and end bearing resistance with CPT measurements, whereas in clays, shaft resistance is related to the soil's stress history (YSR) and sensitivity (S_t). To compare both the API and ICP design methods, the API commissioned the University of Western Australia (UWA) to undertake a detailed comparison in sandy soils. The result was the development of the UWA (2005) pile design method, which lowered the variation of calculated to measured capacity in sands even further.

In each of these methods, the end bearing (EB) capacity is computed differently and each has a different means of estimating if the phenomenon of pile plugging occurs. Plugging refers to the formation of a theoretically rigid immovable plug of soil inside the base of an OEP. Piles are referred to as unplugged when no rigid plug forms but rather the pile behaves in a coring manner. To determine

whether a pile is plugged or unplugged, the API compares the internal interface capacity to the EB capacity on the plug; the ICP relates the internal diameter (D_i) to D_R and q_c in sands, and to q_c in clays; and the UWA method considers that all OEPs supporting jackets behave in a plugged manner. As found by Benson *et al*. (2013), in conducting the designs of OEPs, it is typical that the API design method gives the longest estimate of pile lengths. In some cases, however, the API design method may give shorter pile design lengths than the ICP method and this can be due to differing estimates of the whether the pile is plugged or unplugged. These differences affect the predicted stiffness of the load-displacement response. As a result of observing this discrepancy, on a major offshore wind development, this research topic was launched.

From what the industry knows on the behaviour of the soil plug in OEPs, in clays it has been found that the mobilisation of the internal soil plug under quasi-static loading is different to its mobilisation in sands. In clays, Doherty *et al*. (2010) found that there is a large proportion of pile capacity attributed to the end bearing on the annulus, but additional capacity is also gained along most of the plug length. In sands, tests performed by many researchers (Széchy, 1959; Kishida, 1967; Lehane & Gavin, 2001) found that the total load on the pile base is resisted by a solid sand core over an active plug length of up to 3 times the internal pile diameter ($3D_i$), with a large radial stress at the base. This increased radial stress was attributed to the large effective stresses at this point.

1.1. Computerised Model of an Offshore Jacket Structure

If an offshore wind turbine supported by a jacket structure is used as an example, as shown in Figure 1-1, current methods of jacket design requires both the superstructure and substructure to be modelled. This can be performed using a finite element program such as SACS (Bentley, 2018), USFOS (SINTEF, 2018) or Sesam (DNVGL, 2018). The properties of the structural members would be assigned to the model and the design load combinations applied. The resulting load effects would then be used to size the members.

The piles in these structures are modelled using the method of soil reaction curves originally established by Winkler (1867), which essentially models the progressive failure of the pile-soil interaction per layer, best replicating the pile behaviour observed when tested. Figure 1-1 shows a

typical model of an offshore wind turbine supported by a jacket structure. The piles supporting the jacket are expanded to demonstrate the arrangement of the soil reaction curves along its length. These include:

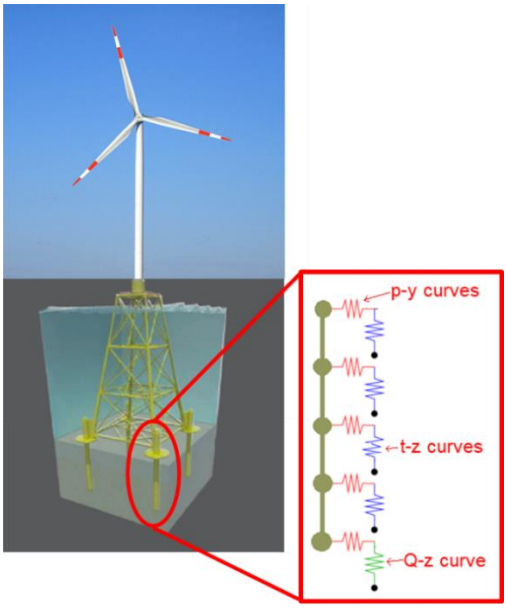

Figure 1-1 Offshore wind turbine (Atkins, 2013)

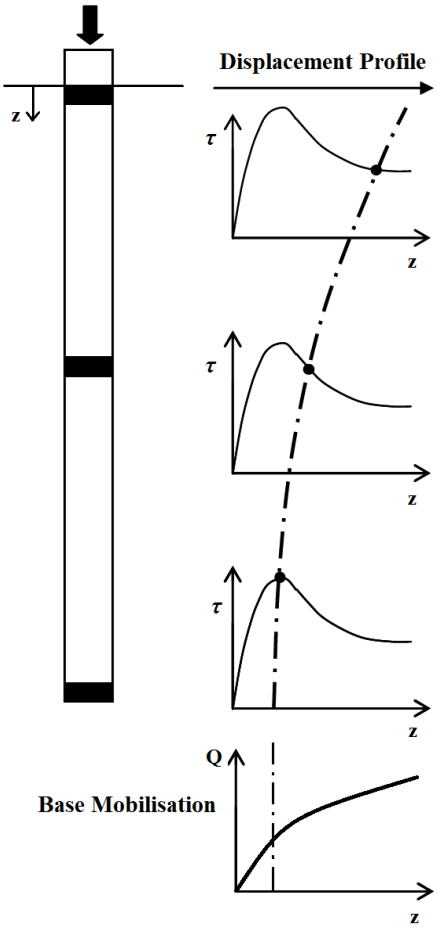

Figure 1-2 Progressive failure in clay (adapted from Doherty and Gavin (2011).

- the p-y curves which model the mobilisation of lateral soil resistance at the pile-soil interface;
- the t-z curves which model the mobilisation of axial pile-soil interface resistance along the pile length;
- and the Q-z curve which models the mobilisation of the axial base resistance of the pile.

The total capacity of any pile is usually quoted as the mobilised load after a pile head displacement (w_t) of $0.1D_o$, with the capacity separated into the shaft and the end bearing. The contribution of each component is dependent on several factors, especially the length of the pile, the pile diameter, D_o and the soil type. As an axial load is applied, the shaft resistance is mobilised along the pile length as the pile compresses and similarly, the base resistance mobilises, as the pile base displaces. As shown in Figure 1-2, after w_t=$0.1D_o$, the total shaft and EB would be at different proportions of their total capacities, dependent on the levels of strain. Considering clays, at peak capacity on the pile head load-displacement response, some elements of the shaft may be at peak resistance, with others at their ultimate values, however the EB may still be increasing in resistance. As further load is applied, the base resistance continues to increase, but the shaft may now strain to

levels that mobilise the full ultimate resistances along the entire shaft. The separation of the pile capacity into the shaft and EB contribution is therefore not straightforward. At peak pile-head load, the breakdown would not necessarily be that of a total shaft peak and maximum EB but rather a more complex result.

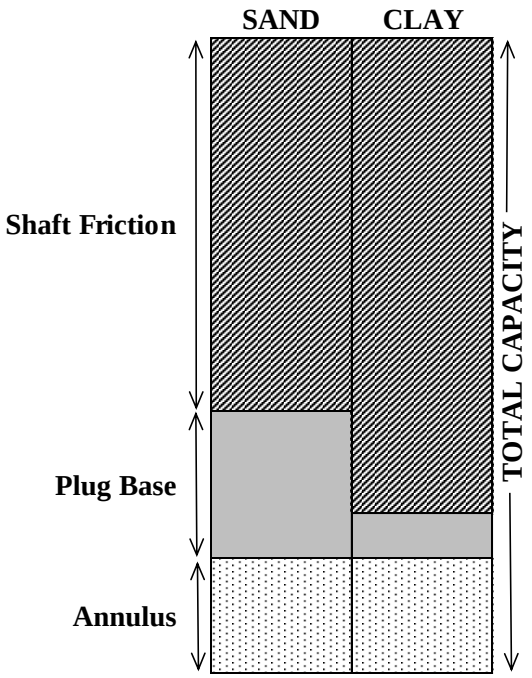

Figure 1-3 Schematic of capacity distribution in OEPs.

In addition, as the base is mobilised, the pile's annulus and plug's base attract different proportions of load. In sands and clays this load distribution is quite different, and currently not well understood or modelled. In sands, the contribution of the base can be upwards of 30% of the overall capacity and in clays it is about 20% (Chow, 1997), see Figure 1-3. With regards to the capacity distribution at the base, tests performed using double-walled piles have suggested that the annulus can attract about 30% of the base load in sands (Paik *et al*., 2003) and much more in clays.

1.2. Aim of the Research

The main aim of the research is to determine if an improved distribution of the load between the shaft and base can be found for open-ended piles. This is performed using a 1D finite element method which isolates the mobilisation of the soil plug, allowing the contribution of the shaft, annulus and plug capacities to be separated.

To facilitate this process the study is undertaken in the following stages:

- An initial investigation of the existing industry methods of computing the base capacity in open-ended piles (OEPs);
- An analysis of the three selected OEP design methods to understand their mechanics in detail;
- From the geotechnical engineering database, select OEP tests that are loaded in compression for sites in sand and clay;

- Using the database tests, estimate the static capacity of the test piles with the selected design methods;
- Write a finite element method in MATLAB which models the soil-pile-plug interaction and is capable of isolating the response of the soil plug;
- Extract design values of local shear stress (τ_f) and end bearing resistances (q_b) determined from the API, ICP and UWA design methods, and adopt these as input parameters to the finite element method. This results in the finite element variants (FEA) of the methods;
- Vary input parameters to the finite element variants of the design methods (API-FEA, ICP-FEA and UWA-FEA) to determine the sensitivity of the response to each parameter;
- Based on the accuracy of results of the sensitivity analysis, select the most representative modifications to the finite element variants of the design methods;
- Using these modifications, determine improved versions of the finite element variants of the design methods for clays, sands and layered soils.
- Compare the results of the modified methods to the original static design methods and measured values, to determine if any improvements are observed and make recommendations based on this comparison.

1.3. Limitations of Research

1.3.1. Residual Stresses

Residual stresses are not being considered in this research project. These stresses are present within the soil and pile after installation, with differing degrees of influence depending on the method of installation. The difficulty in determining these stresses can be related to that of correctly obtaining the soil's resistance to driving (SRD), which is also a difficult task with the methods that currently exist today. However, improving the accuracy of the SRD estimation would then inform the residual stresses within a pile prior to loading. If these stresses are ignored there may be a tendency to overestimate the shaft friction, by the development of positive skin friction, and underestimate the base resistance (Kraft, 1990). This factor can also be related to the databases used in this study, for if

there are many test results with high unaccounted for residual stresses, this consideration would question the accuracy of the measured results. Piles are therefore assumed to be wished-in-place.

1.3.2. Cyclic Loading

Offshore structures are subjected to numerous cycles of loading and unloading. The aim of this research, however, is to focus primarily on monotonic, quasi-static loading. During the course of the research the developed program has been updated to model cyclic loading, but these developments are not addressed here.

1.3.3. Scour

Scour occurs due to the interaction of the substructure and underwater currents. Due to this interaction, vortices are induced which erode the seabed material reducing the effective overburden stress in the soils around the pile. If unaccounted for, this phenomenon could undermine the robustness of the foundation. The effects of scour are not considered in this study.

1.3.4. Pile Type

It is anticipated that low L/D piles (such as monopiles in the offshore wind industry) are less prone to plugging and have a low contribution to axial capacity from the plug base, than the larger L/D ratios used for jacket piles. This research focuses on jacket piles with $L/D >$10.

1.4. Thesis Outline

The chapters included in this thesis are outlined as follows:

- Literature Review: This focuses on identifying the available literature on OEP design with specific emphasis on the base capacity derivation currently available in the industry.
- Finite Element Modelling of Soil Plug: Here the mechanics of the finite element model that incorporate the pile-plug-soil interaction are outlined.
- Base Capacity of Clays in the Case Studies: The database in clays is outlined and an analysis performed to determine the existing performance of the static API and ICP design methods. The results from selected sites from the database, in clays, are input into the finite element

method to determine the effects on each of the input components. Recommendations on the use of the FE variation of the methods are suggested.

- Base Capacity of Sands in the Case Studies: The database in sands is outlined and an analysis performed to determine the existing performance of the static API, ICP and UWA design methods. The results from selected sites from the database, in sands, are input into the finite element method to determine the effects on each of the input components. Recommendations on the use of the FE variation of the methods are suggested.
- New FEA Method for OEPs: The recommendations outlined in the previous sections are used to deduce new methods in sands, clays and layered soils. These results are then compared to the original static estimates from the design methods and the measured test results. The benefits of using the 1D finite element method is then discussed.
- Conclusions & Recommendations: Here, conclusions are offered based on the results of the research along with recommendations for future work.

1.5. Supplementary Material

The supplementary material contains three main items, as follows.

1.5.1. Appendix A, Paper 1: "Finite Element Analysis of Soil Plug Behaviour within Open Ended Piles"

This paper outlines the initial work undertaken during this research project. It outlines the OEP design methods that were considered and introduces the numerical process. The database used to validate the model is also outlined and comparisons are shown of the predictability of the FE variants of the design methods, with the direct consideration of the base response.

1.5.2. Appendix B, Paper 2: "One-Dimensional Finite Element Analysis of the Soil Plug Behaviour in Open-Ended Piles under Axial Load"

This paper outlines in more detail the numerical processes used in the program VIRTUPLUG. The paper details the finite element method and demonstrates the versatility of the program in estimating

the axial response of the pile, the mobilisation of the plug and annulus, and compares the finite element variants of the design methods with measured responses.

1.5.3. Appendix C: VIRTUPLUG Program Manual with Source Code

The manual outlines the numerical processes, the capability of the program and details how data is to be input. It also outlines the cyclic capabilities of the program, which are not however, directly used within this research project. The verification of the program and the source code, developed in MATLAB, are presented as part of the manual.

2. Literature Review

This work focuses on the distribution of total capacity of an open-ended pile, with specific emphasis on the contribution of the plug. In this literature review, the most applicable concepts that govern the incorporation of the soil plug into OEP design are initially investigated followed by the base capacity methods adopted by the API, ICP and UWA design methods. The estimates of shaft capacity using these methods are then briefly discussed before outlining the axial load-transfer process adopted when piles are modelled as discrete elements in the design of offshore structures. Based on the concepts outlined in this literature review, the OEP load-transfer diagram is outlined.

2.1. The Concept of Pile Plugging

When OEP's are driven or loaded it is understood that they can behave in a plugged manner whereby the core of soil within the pile is carried down with the pile; or unplugged where the core of soil remains approximately static while the pile itself moves downwards. Whilst most piles behave as unplugged during driving, principally because of dynamic effects, their subsequent behaviour during (quasi-) static loading is normally plugged (Lehane & Randolph, 2002). This thesis provides a more detailed analysis of the conditions controlling plugging post-installation under static loading. It critically assesses the published design methods that adopt different assumptions about plugging.

2.2. Types of Plugging

2.2.1. Plugging During Installation

During installation, it has been found that piles are normally driven in an unplugged manner (Paikowsky *et al*., 1990; Randolph *et al*., 1991, Schneider, 2008). This type of plugging has been investigated by a number of researchers such as White *et al*. (2005) who used cavity expansion theory to determine the flow field around the annulus of a pile. Figure 2-1 shows that as a pile is installed, the theoretical behaviour can be unplugged, partially plugged or fully plugged and the radial stress varies with the mode of installation. IFR will be explained later in Section 2.3.2.2.

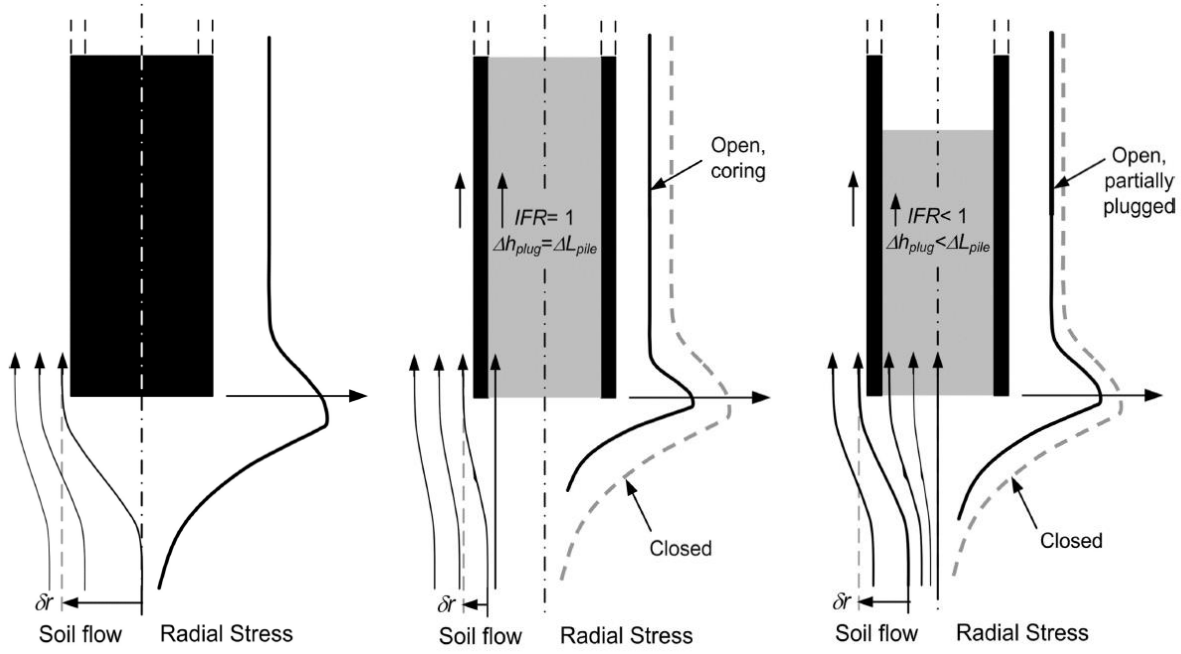

a. Plugged pile **b. Unplugged pile** **c. Partially plugged pile**

Figure 2-1 Schematic streamlines of soil flow and profiles of radial stress, δ_r (White *et al*., 2005)

2.2.2. Plugging During Static Loading

An improved understanding of the plug behaviour has been found under static loading by different researchers based on a limited number of tests that focus on the soil plug. Some of these researchers have found that piles fail in a plugged manner under static loading, such as Paikowsky *et al*. (1989) and Lehane & Randolph (2002), while others, such as Chow (1997) and Jardine *et al*. (2005), argue that this is not always the case. The bulk of this thesis will focus on the behaviour of the plug under static loading.

2.2.3. Plugging During Dynamic Loading

Only a limited number of pile tests have focused on the soil plug, with even less focus on the plug behaviour under dynamic loading. In terms of offshore wind structures, this behaviour is important for the actions of turbine and large wave loads. The behaviour of the plug under this kind of loading is not looked at in this study.

2.3. The Development of Plugging Research in Sands

The scientific understanding of how the soil plug within an OEP behaved, was under consideration for quite some time. Early publications of the API RP 2A (1984) indicated that the total end bearing (EB) should not exceed the internal shaft capacity of the plug. Prior to this, Kishida (1967) did tests

on OEP in sand and found that the plug resistance was related to the degree of compaction. Kishida & Isemoto (1977) found that the internal friction was greatest near the annulus and postulated that this was due to the creation of sand arches within the plug. In the same publication, the 9th ICSMGE (Tokyo), Klos and Tecjchman (1977) also suggested a design procedure for OEP.

The API Recommended Practice at that time, maintained the use of the α-method in total stress pile design methods, for clays, and effective stress pile design methods for sands. Here, the internal and external stresses were assumed equivalent ($\tau_i = \tau_e$). Recent developments have shown however, that this is not a correct assumption for sands.

2.3.1. Theoretical Research

2.3.1.1. Interpretation of Plugging Physics

Figure 2-2a considers a scenario where a constant static load is applied to the pile head and the arrangement is in equilibrium. A horizontal slice of the soil plug is examined as shown in Figure 2-2b. This slice of soil is cut off from the external soil. The overburden pressure, σ_v plus the shear stress along the wall of the pile, τ_i, balances the increased pressure below the slice, $\sigma_v + d\sigma_v$. The value of τ_i is directly related to the overburden pressure by the relationship $\tau_i = \beta\sigma'_v$, where the effective overburden pressure increases the internal friction.

The change from a plugged to unplugged behaviour occurs when there is slip along the entire column of the plug. This will only initiate if the cumulative internal shaft resistance is less than the ultimate base stress, q_b. As previously outlined, early researchers such as Kishida and Isemoto (1977) found that τ_i increases non-linearly towards the base of the pile.

Paikowsky, (1989) investigated plugging and explained his theory on arching within his PhD, making references to samples installed in different materials and the arches that each made under different loading types. He suggested that the silo effect occurs creating downward concave arches in piles that increase the internal shaft friction near to the base.

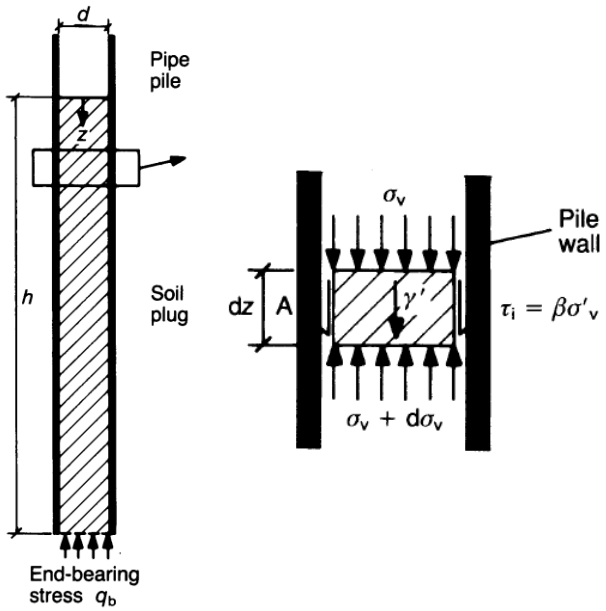

a. **b.**

Figure 2-2 Stress conditions within soil plug (Randolph *et al.*, 1991)

Randolph *et al*. (1991) suggested an explanation for this phenomenon which considered a load applied to the base of the plug, the increasing axial stress causes an increased lateral stress thereby increasing τ_i. They suggested that τ_i would increase exponentially with increasing ratio of plug length to internal pile diameter, h/D_i. In their paper, a 1D plug analysis method for drained, undrained and partially drained soil is set out. For a drained cohesionless soil, the base capacity is normally the result of the plugging of the pile brought on by the arching action within the plug. For undrained conditions, where insufficient time is available for drainage the excess pore water pressure supports the load but without an increase in τ_i, leading to an unplugged condition as a greater length of the soil plug is mobilised.

Experimentation performed by Lehane and Gavin (2001) on model piles in a testing chamber agree with the method outlined by Randolph *et al.* (1991). However, they also suggested that the sand near the annulus dilates, increasing the internal radial stress and the internal shaft friction thereby generating a plugged response.

Chow (1997) concluded that plugging in sand is a function of pile diameter, relative density and the dilative properties of the soil along the internal pile walls. Her research indicated that the greatest susceptibility to plugging occurs in small diameter piles installed in dense sand.

2.3.1.2. The 'Wedged' Plug Length

The wedged plug length is used to determine the capacity of the plug in drained soil. This is based on work undertaken by Murff *et al*. (1990), O'Neill and Raines (1991) and Randolph *et al*. (1991). This wedged length is due to the compression of the plug from the base. Without a load applied to the pile head, the base resistance of the plug, $q_{plug} = \sigma'_v = \gamma' z$ (Figure 2-3). As vertical load is applied to the top of the pile, the plug's base is mobilised and q_{plug} will increase by an amount related to the

friction along the sides of the mobilised wedge, hence $q_{plug} = \sigma'_v + \Delta q$. Where Δq will equal the integral of the internal shaft resistance along this wedged length, L_{wp}.

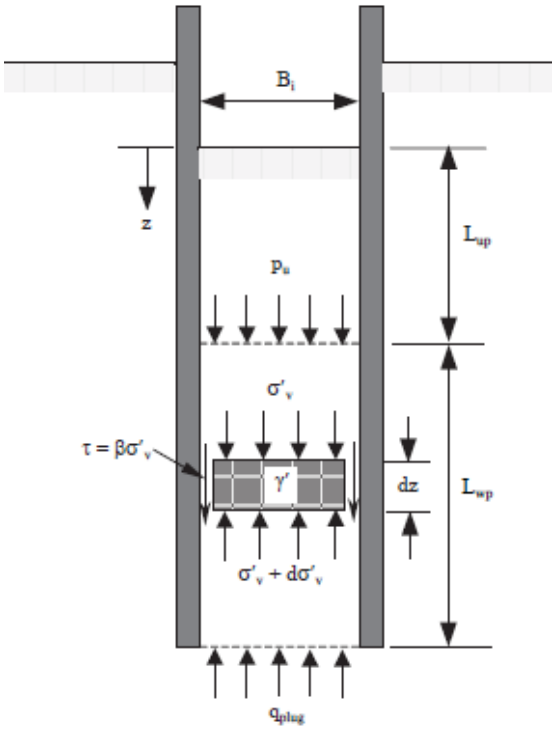

Figure 2-3 Concept of the wedged and unwedged plug length (Salgado *et al.*, 2002)

Therefore $\Delta q = \int_0^{L_{wp}} \tau_i \, . \, dz$ (where $\tau_i = \beta \sigma'_v$). As the axial load increases, the stress within the plug propagates, thereby increasing L_{wp} to balance the stress change. The value of τ_i within the plug will be a maximum at the base of the plug and decrease to zero at the top of the wedge. The soil within the un-wedged zone will only contribute to σ'_v. Using the Randolph *et al.* (1991) methodology, the vertical stress increment over the wedged plug length can be estimated from:

$$\Delta\sigma'_v = \left(e^{4\beta z/D_i} - 1\right)\left\{\gamma'\left(L_{up}\right) + \frac{D_i\,\gamma'}{4\beta}\right\} - \gamma' z \qquad (1)$$

where L_{up} is dependent on the stress change at the base balanced by the integral of τ_i. Equation (1) does not give the internal friction along the shaft of the wedged plug as this is dependent on the surface roughness and the grain size of the plug material. The wedge concept has been verified in further research by De Nicola and Randolph (1997) and later by Salgado *et al.* (2002).

2.3.1.3. Compression of the Soil at the Base of the Plug

Resistance at the pile base is provided by soil mobilised by the annulus, the plug and the soil mobilised by the plug. The overall stiffness of the base response will be as a result of the combined stiffnesses of these individual components. The resistance of the annulus has been found to be similar to that of the q_c value recorded at the depth (Chow, 1997). The resistance below the sand plug depends on the compressibility and the shear stiffness of the sand, which can be similar to the base resistance of a bored pile and can be used as a lower bound stiffness (Lehane and Randolph, 2002).

If sand is considered, the compressibility of the sand will be an important criterion in estimating the resistance. The compression of the sand will be a maximum at the base and reduces upwards through the plug. The compression of the sand can be assessed using a 1D method by Lehane and Randolph (2002) adopting the compressibility coefficient, κ*, and suggestions by Wroth and Houlsby (1991) expressing compressibility in terms of strain rather than void ratio as follows:

$$\varepsilon_v = \kappa^* ln(\sigma'_v/\sigma'_{vi}) \tag{2}$$

The compression of the sand in the plug can be determined using the stress distribution within the plug. Lehane and Randolph (2002) interpreted the stress distribution as quite substantial near to the annulus with an exponential decrease up the plug within the wedged section. The compression of the wedged section of the plug was derived as:

$$\begin{aligned} \delta_{plug} &= 0.5\kappa^*\theta\left(L_{wp}\right)^2 - \kappa^*\left[\left(A/B + L_{wp}\right)ln\left(A + BL_{wp}\right) - L_{wp} - A/B \ln A\right] \\ \theta &= 4\beta/d_i \qquad A = p\theta/\left(\gamma' + p\theta\right) \\ B &= \gamma' \theta/\left(\gamma' + p\theta\right) \qquad C = \gamma' /\left(L_{up}\right) \end{aligned} \tag{3}$$

2.3.1.4. Consideration of β and *K*

Many estimates of σ'_v within the plug have been suggested (Randolph *et al.*, 1991, Lehane and Gavin, 2001) but it is noted that its relationship with τ_i is sensitive to the values of β and K. This sensitivity leads to difficulty in applying the concept of pile plugging to general pile design (Brucy *et al.*, 1991, Leong and Randolph, 1991). Theoretical computations of β were derived by Randolph *et al.* (1991) as shown in Figure 2-4.

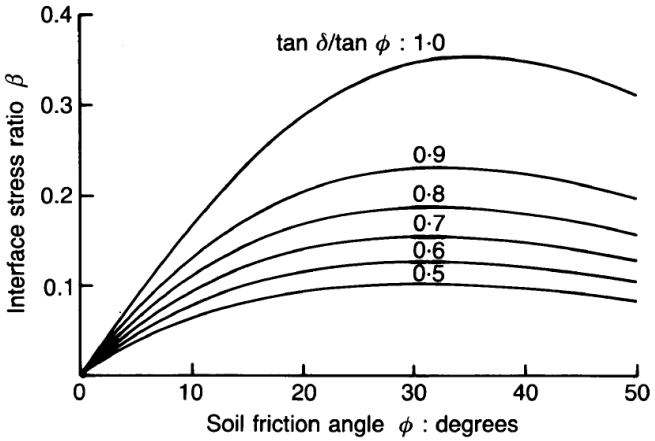

Figure 2-4 Variation of limiting stress ratio, β, with friction angles δ and ϕ (Randolph *et al.*, 1991)

De Nicola and Randolph (1997) suggested a method of determining the value of K from back analysing model tests in a centrifuge to separate the internal and external frictions and from calibrations with experimentation by Paik and Lee (1993). The process included integrating derived relationships between q_b and q_c and assuming K profiles

along the length of the soil column. This process was then iterated until the profile of K selected were consistent with the derived plug capacities. There may be merit in these derivations for driven piles, although additional work would have to be done to increase the accuracy. Figure 2-5 gives the K profile deduced.

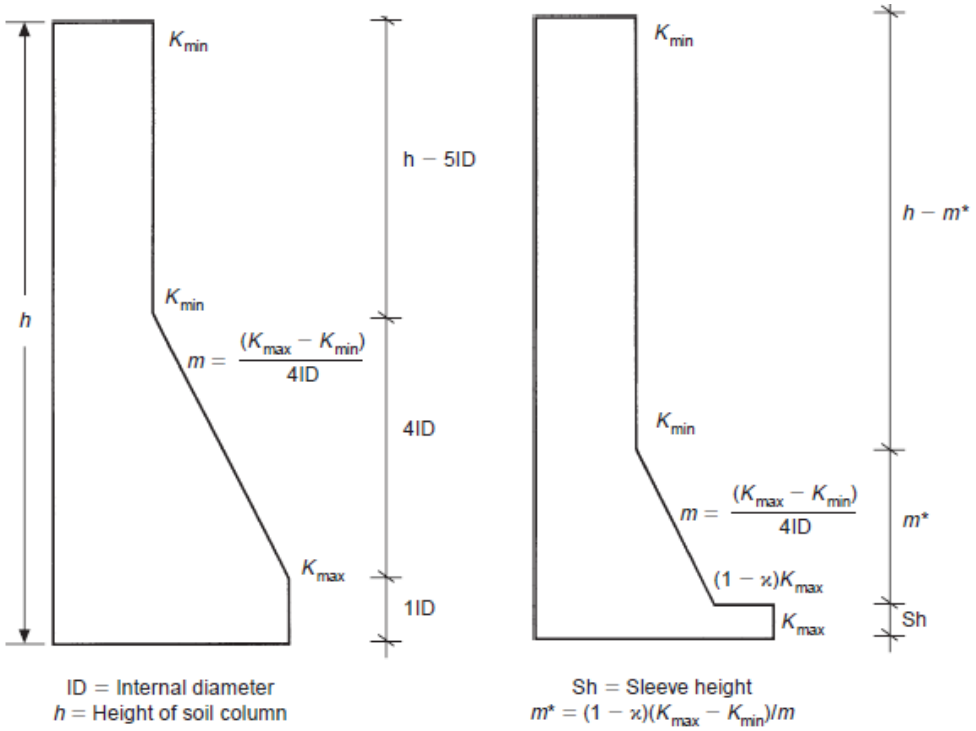

a. Without driving shoe. **b. With driving shoe.**

Figure 2-5 Lateral earth pressure coefficient (K) design profiles (De Nicola and Randolph, 1997)

Hight *et al*. (1996) indicated that the values of K would depend on the dilatational characteristics of the soil. Paik and Lee (1993) indicated that the values of K was based on the initial D_r.

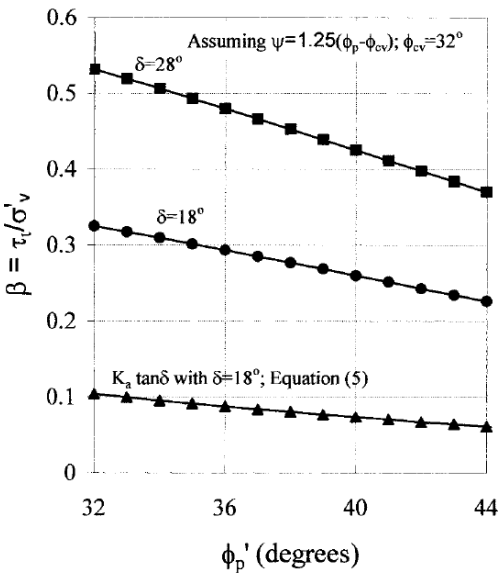

Figure 2-6 β variation with ϕ'_p (Lehane and Gavin, 2001)

Tests undertaken on jacked model piles in sands by Lehane and Gavin (2001) have shown that the value of β is relatively constant for a plug with low interface friction angles, δ. As δ increases, the β values reduce with increasing peak internal friction angles (Figure 2-6). Values of β were estimated to range from 0.08 to upper bound values of 0.45. However, the main range of β was suggested as about 0.2 to 0.3.

Paik and Lee (1993) give results of β of 0.35 to 0.25

based on their experiments. Salgado *et al*. (2002) interpreted the results of field tests and those performed in calibration chambers. Relationships were derived for estimating the EB capacity with the assumption that $K = 0.4$.

2.3.1.5. Theoretical Derivations of Plug Capacity

Randolph *et al*. (1991) produced theoretical design charts which could be used to estimate plug capacity. These charts were based on parametric studies and deduced for partially drained cases of plug capacity using the loading rate and drainage characteristics of the soil. The aim was to provide a simpler means of estimating plug response without relying on detailed numerical analyses. As a result, consolidation parameters were adapted and modified to be plotted on non-dimensional axes. Figure 2-7 and Figure 2-8 show the design charts for plug capacity and plug base displacement, respectively, in partially drained soils. In these diagrams, $h = L_{pl}$, $d = D_i$, q_{bu} is the undrained plug base resistance, σ_{crit} is the pre-consolidation stress of the soil and $E_0 = M$, when $\sigma'_v \leq \sigma_{crit}$, otherwise $E_0 = (1/m_v)(\sigma'_v/\sigma_{crit})^n$.

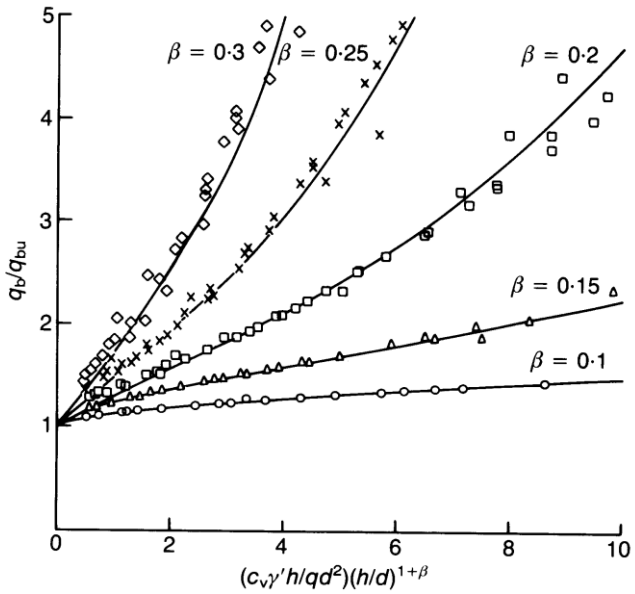

Figure 2-7 Design chart of plug capacity for partially drained conditions (Randolph *et al*., 1991)

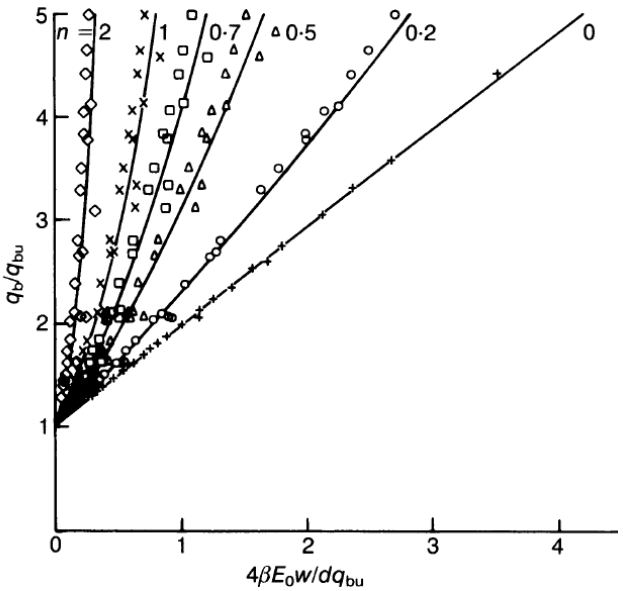

Figure 2-8 Design chart of plug base displacement at failure for partially drained conditions (Randolph *et al*, 1991)

The bearing stress below the plug was later extended by Lehane and Randolph (2002) to

$$q_{plug}/\sigma'_{v0} \approx exp\left[\left(\delta_{plug}/D_i\right)(8\beta/\kappa^*)\right]^{0.5} \text{ when } L_{wp}/L \text{ is small and}$$
$$\sigma'_{v0} \approx \gamma'(L - L_a) \qquad (4)$$

2.3.2. Empirical Research

2.3.2.1. Mobilisation of the Plug Resistance

The base displacement is computed as the summation of the compression of the plug and the compression of the soil below the plug (De Nicola and Randolph, 1999). The external shaft resistance is generally mobilised after 1% displacement (API, 2014). Randolph (1987) suggested that the displacement to mobilise the internal shaft friction was less than that of the external. He suggested that the displacement was 0.2-0.5% of the external pile diameter.

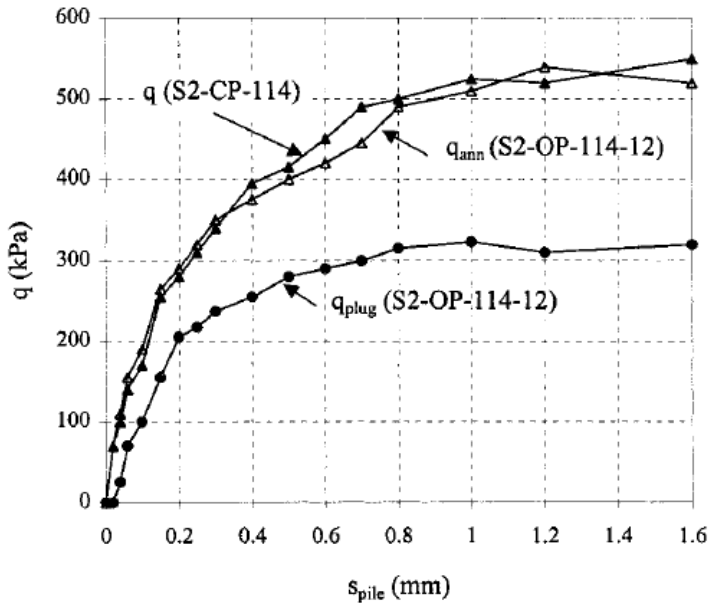

Figure 2-9 Development of EB during load test (Lehane and Gavin, 2001)

In drained cases, plugging occurs from the base. As a pile is loaded, the external shaft and EB on the annulus (q_{ann}) is mobilised initially. The EB on the plug (q_{plug}) is then slowly mobilised with an upward propagating resistance. Hence, the greater the load, the greater plug capacity mobilised. Tests performed by Lehane and Gavin (2001), in a pressure chamber in sand, show that this occurs as OEPs are loaded (Figure 2-9). The results also show that the resistance of the annulus is similar to that of a closed ended pile (CEP), represented by q (only in this diagram). The stiffness response of the annulus and a CEP of equal diameter, is also observed to be similar, however the plug's stiffness is lower than both.

Salgado and his team published two main documents on their findings from experiments on plugging in sands: a report by Salgado *et al*. (2002); and a journal paper by Paik *et al.* (2003). This experimentation was performed using an 8.24m long double walled pile, which isolates the internal and external friction. Separate layers of instruments were applied to each layer as shown in Figure 2-10. The interpretation of the base resistance mobilisation is shown in Figure 2-11. As the load increases, the resistance of the annulus is mobilised initially followed by a gradual plug mobilisation.

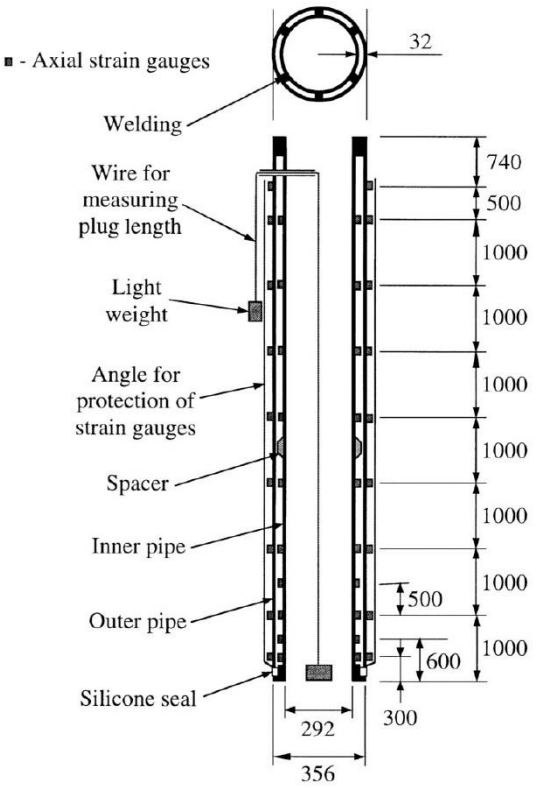

Figure 2-10 Schematic of open-ended test pile (Salgado *et al.*, 2002)

The total base resistance is then offered by the annulus and the plug. Figure 2-11 demonstrates that the annulus contributed approximately 30% of the total EB. Actual measurements indicate that the full plug capacity is mobilized over a length of 6.8 times the internal shaft diameter from the base. Figure 2-12 shows the *normalised* base resistances of the components whereby the resistances are normalised by the average value of cone tip resistance, $q_{c,b}$. The annulus resistance is highest and mobilises full capacity at a displacement of 10% of the wall thickness. The resistance of a similarly sized CEP would have a smaller base resistance than that of the annulus which can be linked to the degree of compaction at the bases of these components. This was also suggested by Lehane and Randolph (2002). The plug resistance is less than that of the base resistance of the open-ended pile as this accounts for the average resistance of the annulus and the plug over the entire base area.

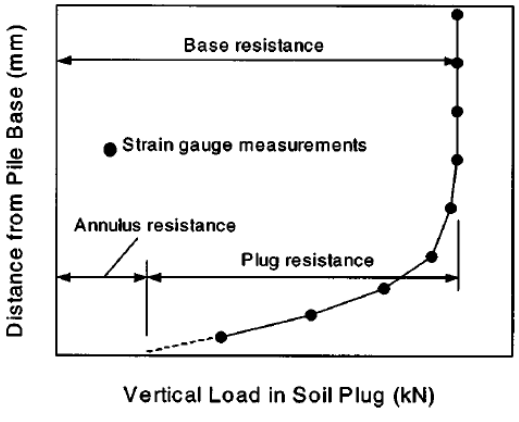

Figure 2-11 Determination of plug and annulus resistance (Paik *et al.*, 2003)

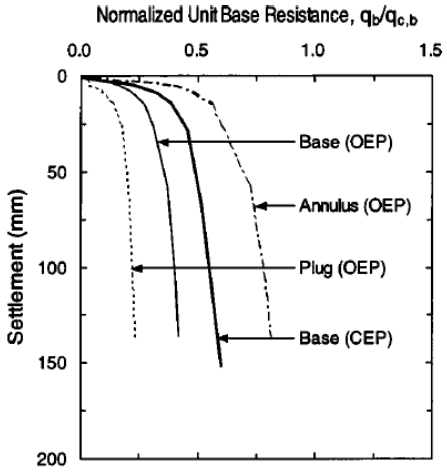

Figure 2-12 Comparison between normalised unit base resistance of open and closed-ended pile (Paik *et al.*, 2003)

Even after the full capacity of the plug is mobilised, many researchers have attributed different measures of contribution. Salgado *et al*. (2002) suggest that the annulus contributes approximately 30% of the full base capacity (Figure 2-11). Jardine *et al*. (2005) indicate that the end bearing

contribution of a plugged OEP in sand is about 50% of its closed ended counterpart. Chow (1997) indicated that considering the presence and length of the plug gave better estimates of pile capacity. The use of the plug length however was omitted from the eventual methodology of the ICP-05 due to the complexity in predicting the plug behaviour during driving.

2.3.2.2. Incremental Filling Ratio (IFR)

The IFR, although an installation parameter, is one of the key considerations of pile plugging that has been found in published literature. The IFR is a measure of the rate at which the plug length changes relative to pile penetration and computed as $\Delta L_{pl}/\Delta L_P$ (Table 2-1). The IFR has been found to depend on the internal pile diameter, soil layering, plug densification or dilation, area ratio and installation method. The final value of IFR at the depth of pile penetration is assumed critical to pile capacity.

Table 2-1 IFR Values

Mode	**IFR**
Fully Plugged Pile ($\Delta \boldsymbol{L_{pl}}$=0)	IFR = 0
Partially Plugged Pile ($\boldsymbol{0 < \Delta L_{pl} < \Delta L_p}$)	0 < IFR < 1
Coring or Unplugged Pile ($\boldsymbol{\Delta L_{pl} \geq \Delta L_p}$)	IFR $\geq$ 1

The UWA database contains 31 open-ended driven piles and of these the majority were driven with IFR values close to unity. Figure 2-13 and Figure 2-14 show the variation in IFR with pile penetration from different studies. These show the typical trends of IFR varying with D_R during installation. Loose soil tends to compact and become partially plugged, while dense soil tends to dilate and maintain unplugged behaviour.

White *et al*. (2005) suggests that the IFR is critical to estimating OEP capacity. They have indicated that the area ratio, A_{rs}, the ratio of added volume to the gross pile volume during installation, is used to estimate the degree of plugging of an OEP. This is calculated as $A_{rs} = 1 - IFR(D_i^2/D_o^2)$.

Estimates of the IFR were empirically derived by Salgado *et al*. (2002) based on tests on different sets of small-diameter piles, as shown in Figure 2-15. This relationship is presented in Figure 2-15 which adopts the plug length ratio ($PLR = L_{pl}/L_P$). Jeong *et al*. (2015) derived another version of this equation from a different database (Figure 2-16).

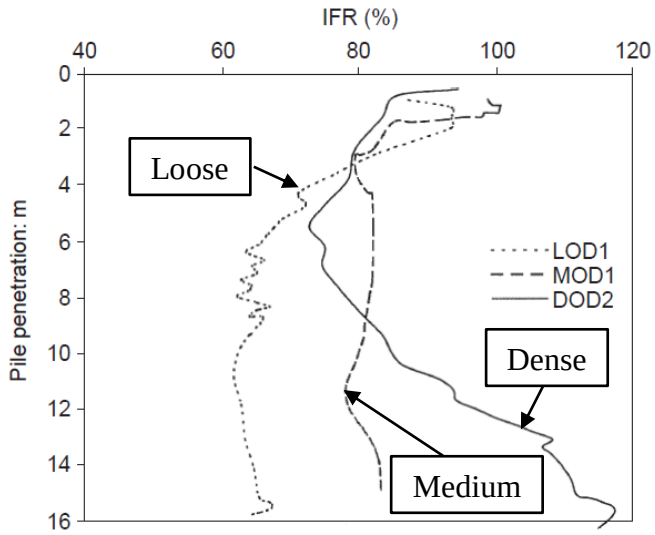

Figure 2-13 IFR vs. penetration depth for an open-ended pile (De Nicola and Randolph, 1997)

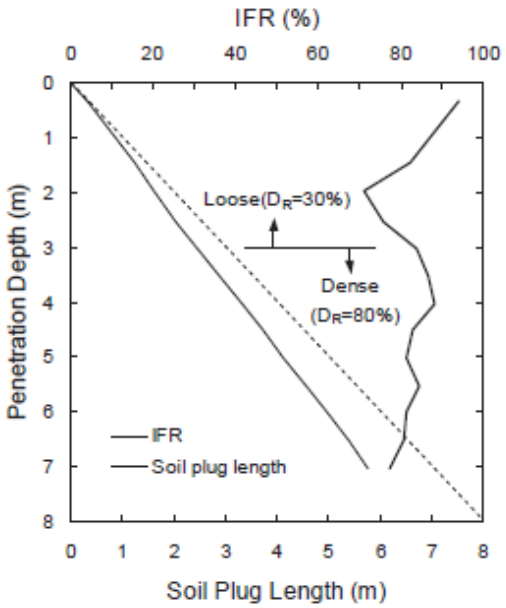

Figure 2-14 IFR and plug length vs. penetration depth for an open-ended pile (Salgado *et al.*, 2002)

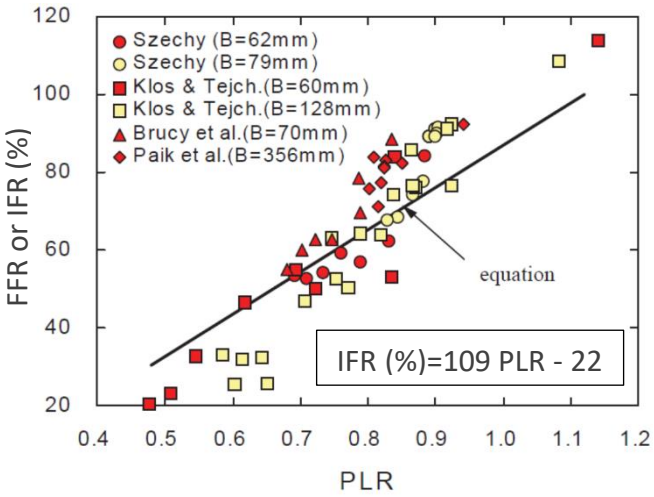

Figure 2-15 PLR vs. IFR for investigations on different pile diameters performed (adapted from Salgado *et al.*, 2002)

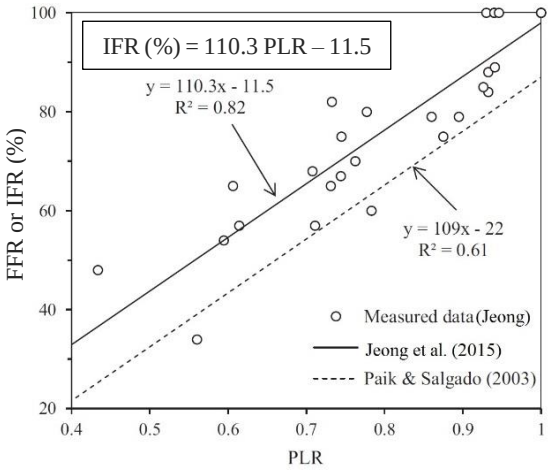

Figure 2-16 The relationship between PLR and IFR (adapted from Jeong *et al.*, 2015)

Some researchers have concluded, based on testing performed on OEP's in sand, that piles behave as fully plugged under static loading regardless of the final value of IFR (FFR) obtained (Beringen, 1979; Paikowsky *et al.*, 1989; Paik & Lee, 1993; Salgado *et al.*, 2002).

2.3.2.3. Measured Internal Shaft Frictions in Sands

Paik and Lee (1993) measured the vertical stress within the plug based on strain gauges used in double walled pile tests (L=908mm, D_o=42.7mm, D_i=35.6mm). The results are presented in Figure 2-17 and show that there is a marked increase in vertical stress within the wedged zone of the plug.

The experimentation performed by Salgado *et al.* (2002) was able to isolate τ_i. Figure 2-18 shows the load distribution along the internal pile wall under ten incremental static load tests. This shows that

the total base load is initially taken by the annular area and as the load increases, passing 0.59MN, τ_i mobilises along the internal plug. Further increases in loading show a maximum mobilised τ_i to $6.8D_i$. The values of τ_i were found to be 45% higher than τ_e.

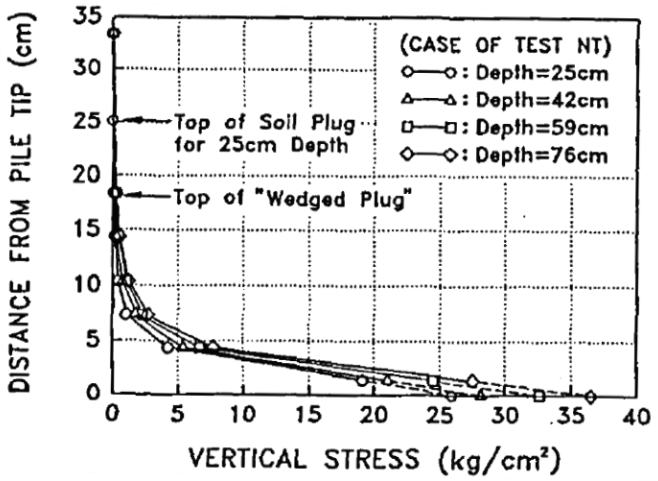

Figure 2-17 Distribution of vertical stress within soil plug (Paik & Lee, 1993)

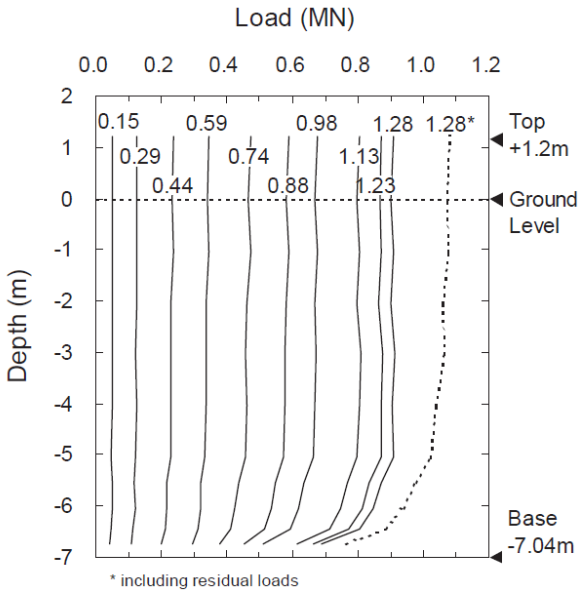

Figure 2-18 Load distribution curves for base mobilisation (Salgado *et al.*, 2002)

The internal friction allows a plug resistance to be formed and this is only possible if the friction is sufficient. Raines *et al*. (1992) suggested that as a minimum, δ=26° but Lehane and Gavin (2001) did tests on model piles and found τ_i for δ=18°.

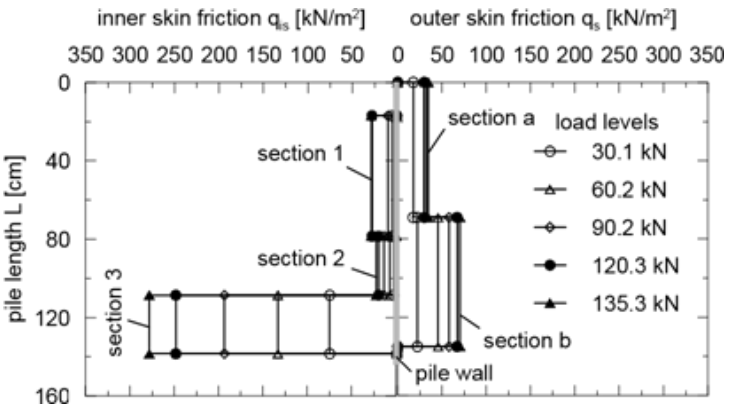

Figure 2-19 Distribution of internal shaft friction from model OEP tests (Lükeng & Kempfert, 2010)

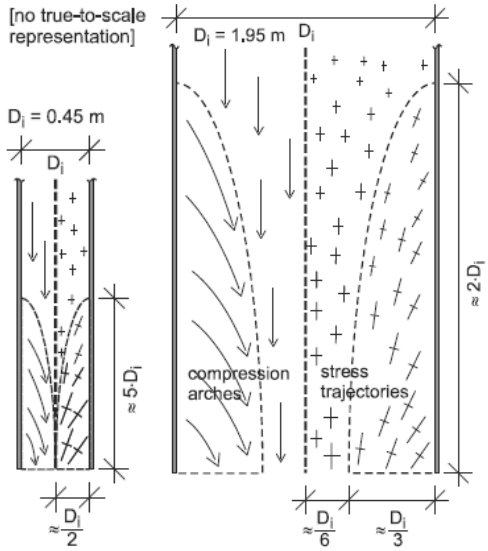

Figure 2-20 Load transfer for different pile diameters from PIV (Lükeng & Kempfert, 2013)

Lükeng & Kempfert (2010) performed tests in sand using open-ended double walled piles. These piles were instrumented and installed to 140cm with D_o=19cm, D_i=16mm. Static tests were then

performed on the pile. The internal shaft friction over the base two pile diameters also showed a marked increase in shaft friction (Figure 2-19).

In another test, particle image velocimetry (PIV) was conducted. This method allowed the displacement vectors of sand to be observed in a model pile. The study showed that the plug is created by compression arches within the sand (Figure 2-20) and these are influenced by the relative density and the internal diameter of the pile. Smaller piles showed a greater tendency to form a resistive plug.

2.3.2.4. Empirical Derivations of Plug Capacity

A number of methods have been developed to estimate the contribution of the plug to pile capacity based on OEP tests investigating the behaviour of τ_i. A few of the key methods are discussed here.

Based on the results of the centrifuge testing, De Nicola and Randolph (1997) derived a design chart relating the EB resistance of the plug to the relative density of the embedment layer (Figure 2-21).

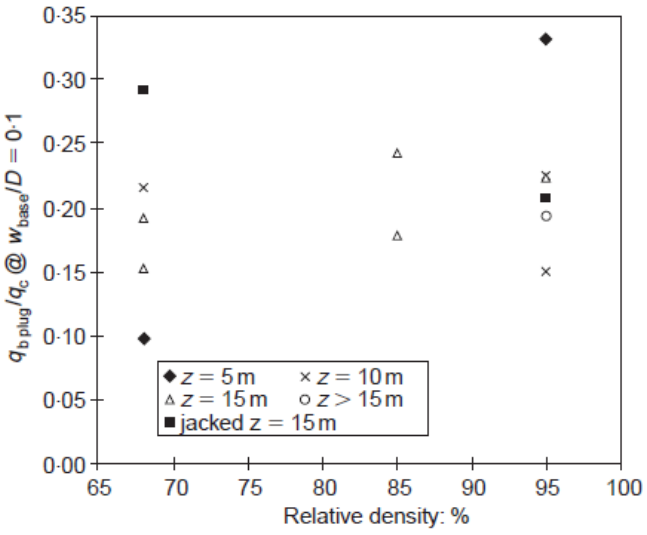

Figure 2-21 Normalised plug end-bearing resistance for open-ended piles (De Nicola and Randolph, 1997)

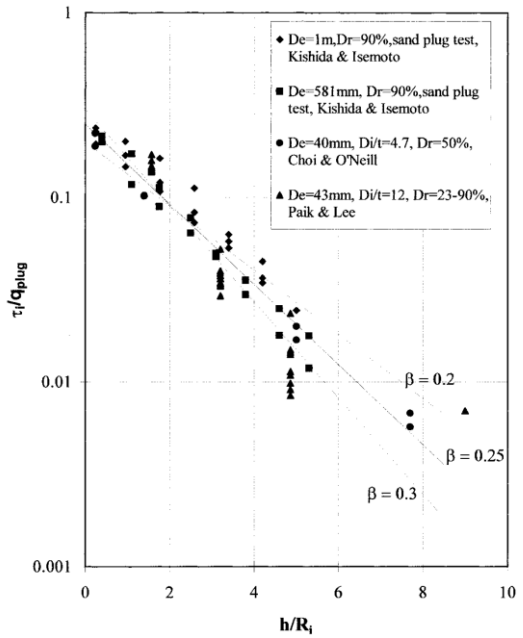

Figure 2-22 Values of τ_i/q_{plug} measured in three experimental programs (Lehane and Gavin, 2001)

Tests performed by Lehane and Gavin (2001) allowed the formation of a design chart which plots the variation in internal shaft friction with plug height when $s_{pile}/d_i \geq 0.5\%$ and $h/R_i < 4$, and if a constant ratio was assumed for $\beta = \tau_i/\sigma_v'$, then

$$\tau_i = \beta q_{plug} exp\left(\frac{-2\beta h}{R_i}\right) \quad (5)$$

Figure 2-22 shows a comparison of this relationship against the work of others.

Based on field, lab testing and available model test data, Salgado *et al*. (2002) proposed a new method to estimate the base resistance by design charts considering the plug and annulus wrt D_R, IFR and q_c (Figure 2-23).

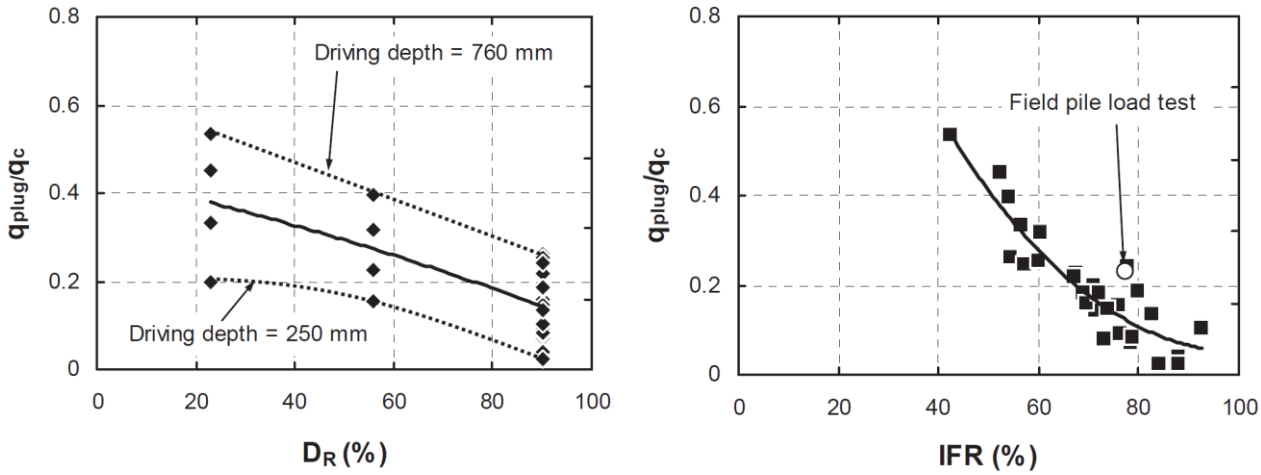

Figure 2-23 Normalized pile unit resistances for open-ended piles: q_{plug}/q_c versus D_R, and q_{plug}/q_c versus IFR (Salgado *et al.*, 2002)

Jeong *et al.* (2015) suggested a new relationship to define τ_i along the wedged length of the plug. This was based on field tests used to create an SPT based design method considering the plugging effect. This adopts the soil plug index (SPI) and an estimation of the IFR (Figure 2-24, Equation (6)).

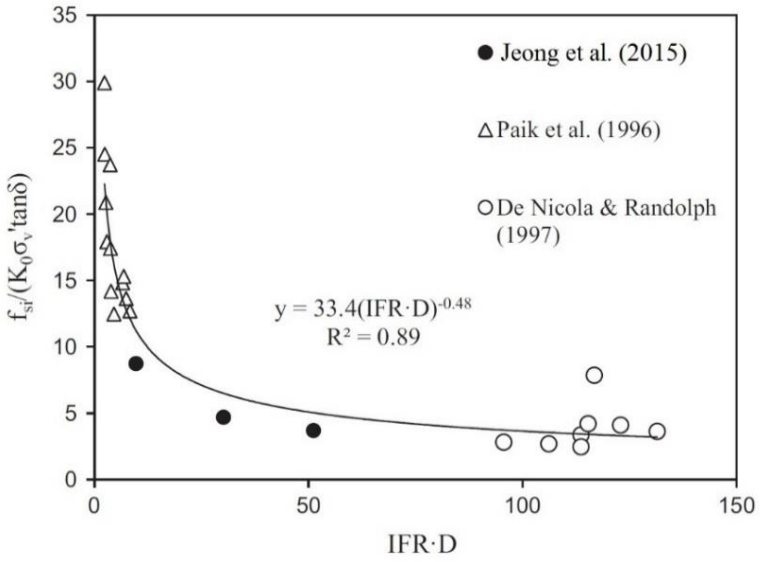

Figure 2-24 Proposed equation for internal skin friction (Jeong *et al.*, 2015)

$$SPI = -0.03D_i + 43.2 \quad \text{or} \quad SPI(\%) = L_{wp}/L_p \times 100$$
$$\frac{\tau_i}{K_0\sigma'_v \tan\delta} = 33.4\,(IFR \times D_i)^{-0.48} \tag{6}$$

2.4. The Development of Plugging Research in Clays

2.4.1. Theoretical Research

There is a limited amount of research published on the internal shaft friction capacity of piles in clay. This could be due to the lower immediate gain in strength of undrained soil plugs and the cost of these tests. If drained, the effective stresses would increase under loading, but in an undrained state, the increase in axial stress is supported by pore water pressure which does not result in increased shear strength. Randolph *et al.* (1991) outlined that under undrained conditions, the value of τ_i would be the same as that prior to loading.

2.4.2. Empirical Research

Chow (1997) indicated that only a small proportion of base capacity is obtained in clay material (~20%). In addition, she interpreted that piles with L/D>10, do not necessarily plug under static loading. A close correlation was found with cone tip resistances and base capacity in undrained conditions ($q_b = 0.8q_c$) with lower results found in fissured clays. As a comparison, drained conditions (at the Bothkennar test site) indicated that q_b can be 50% higher than in undrained clay conditions. From her database, she deduced that for OEP's in clay, piles would plug if:

$$D_i + 0.163\, q_c \leq 1.3 \qquad (7)$$

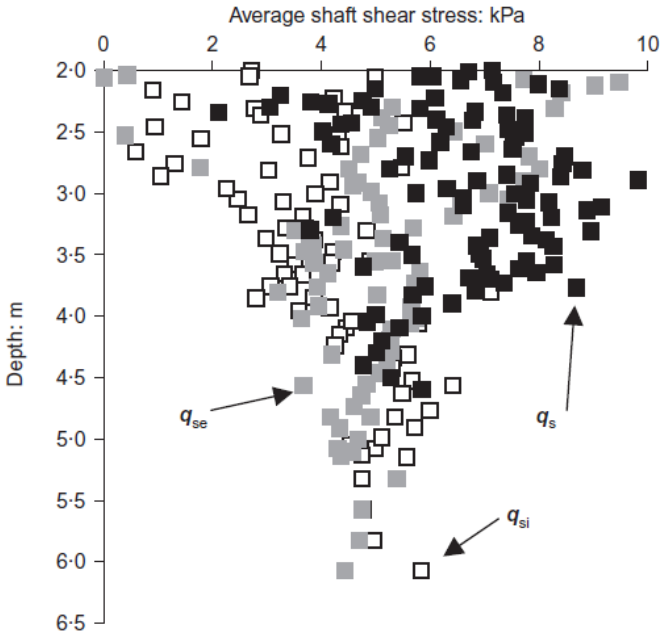

Figure 2-25 Average shaft stress results from tests (Doherty *et al.*, 2010)

More recently field work was performed at University College Dublin on OEPs in clay (Doherty *et al.*, 2010). These tests used the twin wall construction method as outlined in Section 2.3.2. Their test results, shown in Figure 2-25, found that in clays, the average internal shaft resistance (q_{si}) was smaller than the external shaft resistance (q_{se}) in an OEP, and that q_{se} was less than the external shaft friction of a CEP (therefore $q_{si} < q_{se} <$

q_s). This was applicable to depths up to 4.0m for the tested piles with equivalent L/D ratios of 23. After this depth, the OEP's behaved in a plugged manner and $q_{si} \approx q_{se}$. The results found that in clays the internal shaft friction develops immediately from installation to a maximum value and remains constant to the final penetration depth irrespective of the IFR. In terms of mobilisation, the tests found that the base was mobilised before w_t=0.1D_o. This was also found by Clarke *et al.* (1985) who installed an open-ended pile in hard clays. As for the capacity of the plug (q_{plug}), this was linked to the IFR with the following derived:

$$q_{plug} = q_c(0.8 - 0.6\,IFR) \quad (8)$$

There have only been a few tests in which the internal soil resistance has been directly tested. Referring to the tests performed in Kinnegar, Ireland (Doherty et al. 2010), the piles here were tubular steel and double walled. They were also jacked to the required depth without load tests being performed, however, these piles were highly instrumented (along a 2m section) and as a result, further insight can be gained out the behaviour of the soil plug during installation. Specifically, the increase in internal resistance from the base of the pile, upwards.

These piles were installed in clays with an initial sand layer of 1 - 2m thick. The instrumented section of pile is shown in Figure 2-26. From this diagram, the values of h/D are visible along the centreline.

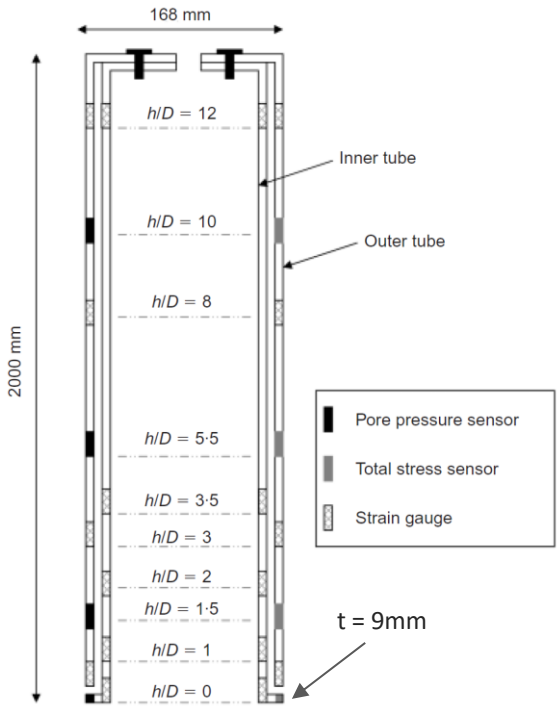

Figure 2-26 Instrumented OEP in clay (Doherty *et al.*, 2010)

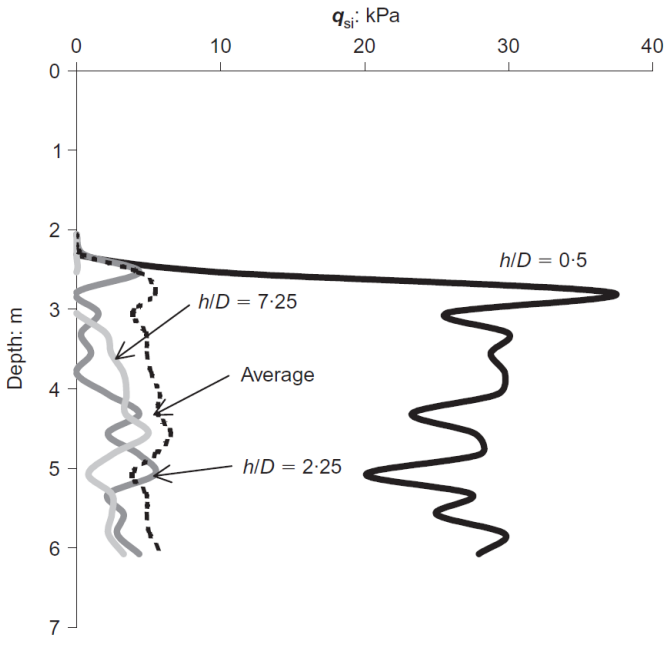

Figure 2-27 Distribution of τ_i in OEP (Doherty *et al.*, 2010)

Figure 2-27 shows that as the pile enters the cohesive soil, after approximately 2.0m, the internal friction near the base increases to a value of 30kPa and maintains this resistance throughout the installation. As the piles are jacked in, this can be viewed as a series of small load tests, most likely without sufficient time passing for pore water pressure dissipation or relaxation of circumferential arching. The higher loads experienced in these tests near to the base of the pile agree with those performed in other scenarios that show an increase in τ_i near the annulus. The results also show that further up the pile at h/D values of 2.25 and 7.25, there is still load visible in the strain gauges. This suggests that the active zone mobilised in clays is much greater than that in sands. This can be due to more of the pore water becoming activated and mobilising up the cohesive plug. In sands the behaviour is governed by the dilation of the soil increasing the stresses in the plug near the annulus. In clays, there is no dilation but the ability of the soil to influence more of the plug column (as observed in Figure 2-27) is intrinsically due to its behaviour as a material governed by the effects of excess pore water pressure. Doherty *et al*. (2010), have also found that the stress below the annulus is independent of the behaviour of the soil plug within the pile. Figure 2-28 was derived and indicates that here $q_{b,p} = q_c$.

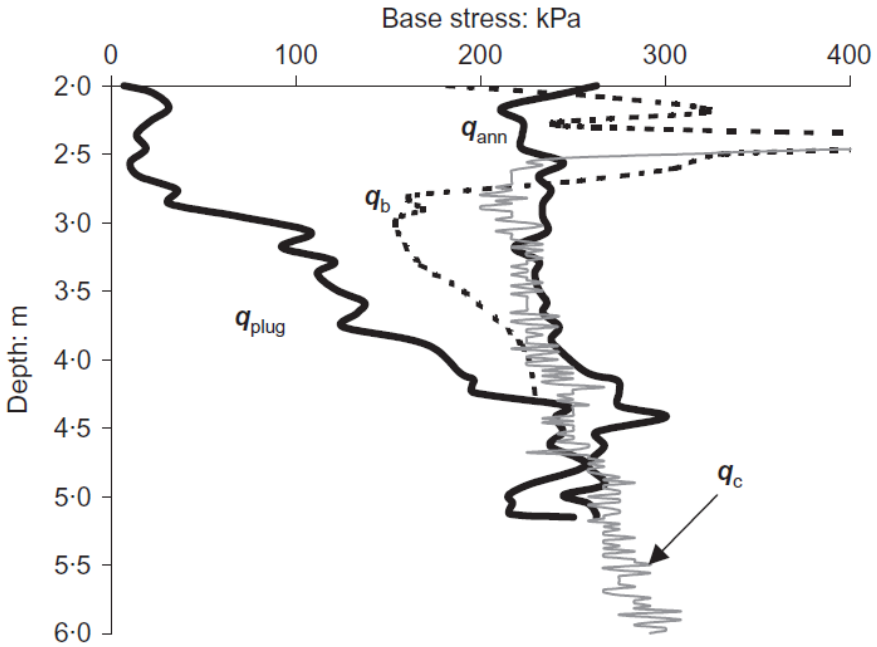

Figure 2-28 Developmemt of stress below annulus (Doherty *et al*., 2010)

2.5. End Bearing Comparison in the API, ICP and UWA Methods

In this section, the end bearing methodologies of the three selected design methods are investigated. The Author notes that there are other methods in the literature that aim to deduce the capacity of OEPs. Among the more frequently used methods is the Fugro-05 (Kolk *et al*., 2005a), however, this was removed due to misprinted equations in the guidance. Another is the NGI-05 (Clausen *et al*., 2005), which is not without merit; however limits needed to be introduced in this research. The UWA-05, Fugro-05 and NGI-05 methods are only for non-cohesive stratigraphies, and the UWA-05 method was chosen as the most promising to pursue.

2.5.1. API RP2 GEO (2011)

The API recommends that the soil plug should be considered in design and for in-place analyses. Whether a pile is plugged or unplugged is determined by a comparison of the internal shaft friction to the EB on the plug. Piles are considered unplugged when the internal shaft capacity is smaller than the plug's base capacity; or plugged in the reverse case. The capacity of the pile is computed differently for a plugged or an unplugged pile. The external shaft capacity at each unit depth is summed over the pile length for a fully plugged pile, and this is added to the EB capacity of a fully CEP.

$$Q_{PLUGGED} = Q_{e,\tau} + Q_b = \int \tau_e A_s \,.\, dz + q_b A_g \tag{9}$$

The unit shaft capacity on both the external and internal sides of the pile are added together for the unplugged condition. This is then added to the EB on the annulus.

$$Q_{UNPLUGGED} = Q_{e,\tau} + Q_{i,\tau} + Q_b = \int \tau A_{e,s} \,.\, dz + \int \tau A_{i,s} \,.\, dz + q_b A_p \tag{10}$$

The EB pressure on the base is computed differently in sands and clays. The computation for sands is $q_b = N_q \sigma'_{vo}$ (where $8 \leq N_q \leq 50$) and for clays $q_b = N_k s_u$, where N_k= 9. Other researchers (Gibbs *et al*., 1993; Chow, 1997) have found that the correlation for N_k (in clay) is not always demonstrated. The reliability of the API method has been proven through extensive use, however the variance of measured vs predicted capacities is much smaller for the newer CPT based design methods. Some of the drawbacks to the API method are listed below.

- This method is unreliable in silts and loose sands and underestimates capacity in dense sands.
- The radial effective stress, σ'_r, is proven to change with depth however K is assumed constant.
- EB is computed by the empirical relationship of $9s_u$, rather than *in-situ* q_c values.
- In sands, the internal shaft friction is assumed equal to the external side friction even though the stress regimes on both sides of the pile are very different.
- The friction during tension is assumed the same as that during compression.
- No increase in lateral stress in the soil during loading brought on by dilation or Poisson's effect.
- Interface friction angles are not influenced by relative roughness.
- The method does not consider the length or the effects of a change in length of the plug to the behaviour of the OEP under static loading. †
- No guidance is provided on the presence of a pile driving shoe at the base of the pile. †

NB. †Common to all three methods.

2.5.2. ICP-05 Method

2.5.2.1. Guidance in Sands

The Imperial College Pile Design Method is based on a series of research projects on offshore pile design from Imperial College, London. This research began in the 1980's and stemmed from Jardine (1985) to Chow (1997). This design method has a unique way of assessing the capacity of the end bearing (EB). One of the main assumptions is that total shaft friction is gained entirely from the external shaft friction and that any internal shaft friction is lumped together within the EB capacity. By doing this the separation of internal and external capacity is quite difficult. In addition, axial pile response and the effect of plug length changes are difficult to quantify. This method does not consider the capacity of the plug and neglects to interpret the plug length or any wedged or unwedged sections. This method mainly focuses on the derivation of capacity as it matches database results to its methodology. Field evidence used to justify the development of a plug in sand is presented in Figure 2-29. This diagram suggests that the maximum diameter that allows plugging is 1.4m. The method also addresses pile plugging differently in sands and clays.

In sands, plugging occurs if $D_i < 0.02 \times (D_R – 30)$ and if $D_i/D_{CPT} < 0.083 q_C/P_a$. If plugging does not occur, then the resistance is applied to the annulus of the pile only. The ratio of q_{ann}/q_c is taken as unity although estimated as 0.7 through numerical analyses performed at Imperial College. By taking the ratio as unity the extra $0.3q_c$ is adopted to consider the effect of the internal plug. This extra is considered to approximate the maximum τ_e at the annulus, applied along the internal plug up to $30t$ to $40t$ above the toe.

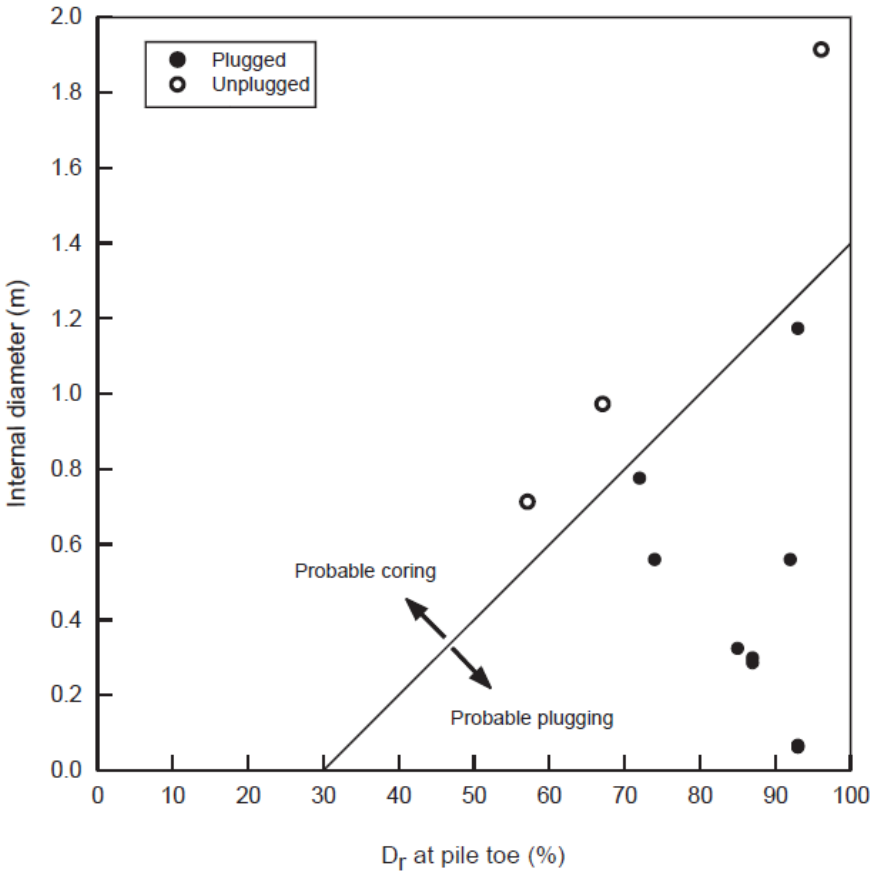

Figure 2-29 Field evidence for the adopted rigid-basal plugging criterion in sand (Jardine, 2005)

Hence, if plugging occurs:

$$Q_b = q_b \pi (D_o/2)^2 \quad \text{with} \quad q_b = q_c[0.5 - 0.25 \log(D_o/D_{CPT})] \tag{11}$$

Here the base capacity is fully mobilised after a pile head displacement of $0.1D_o$. For unplugged piles:

$$Q_b = q_{ba} \pi [(D_o/2)^2 - (D_i/2)^2] \quad \text{with} \quad q_{ba} = q_c \tag{12}$$

2.5.2.2. Guidance for Piles in Clays

Chow (1997) considered open-ended and closed-ended piles to analyse separately the capacity of the shaft and end bearing in clays. She noted that the original value of $q_b = N_c s_u$ did not estimate the end

bearing very well. The values of N_c ranged from 5 to 20, depending on D_o, as shown in Figure 2-30 and as also found by Jardine and Christoulas (1991).

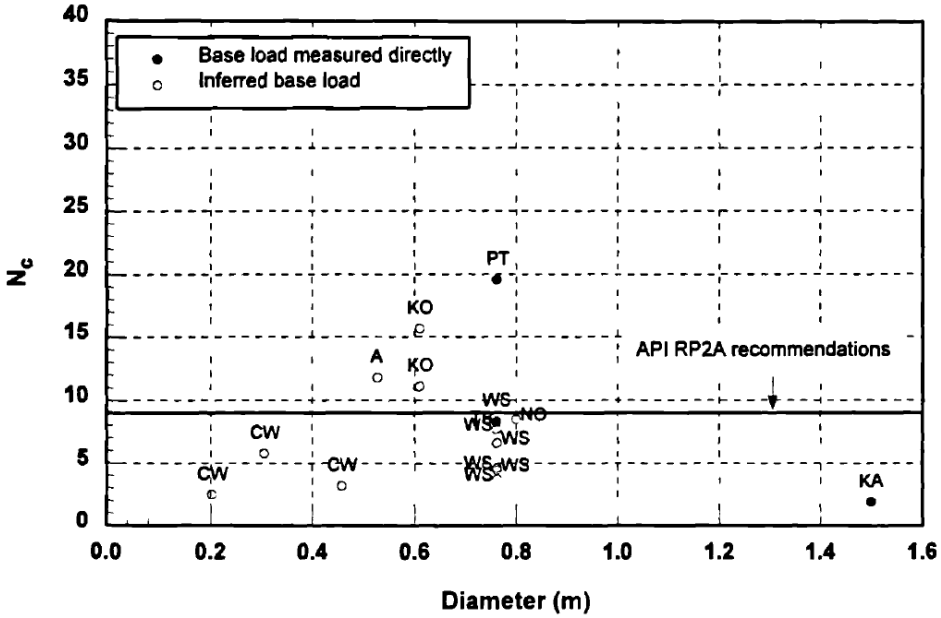

Figure 2-30 Open-ended base resistance over full pile and plug area wrt D_o (Chow, 1997).

Figure 2-31 shows the plot of the base resistance over the full base area normalised by q_c. From this diagram Chow went on to deduce the end bearing resistance in CEPs for conditions of undrained or drained clays as 0.8 and 1.3 times q_c, respectively.

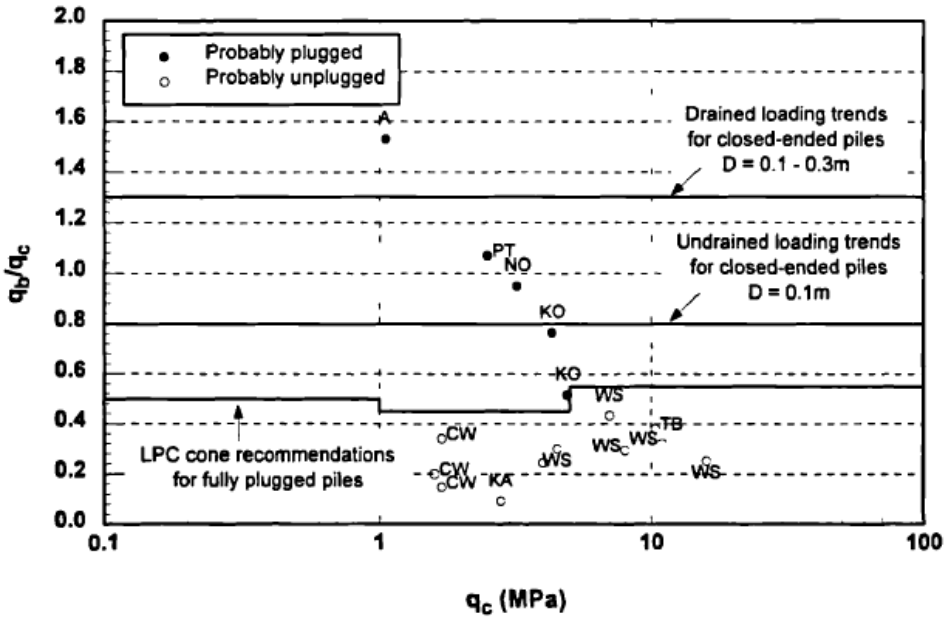

Figure 2-31 Resistance over full pile base of OEPs in clay (Chow, 1997).

While noting the limited database on which to deduce the end bearing on clays, OEPs can act in a fully plugged or unplugged manner under axial static load. From the pile testing results it was found

that in fully plugged piles the base resistance develops 50% of that in CEPs. Therefore, the end bearing resistance in fully plugged OEPs in clays was deduced:

for undrained loading $$q_b = 0.4q_c \quad (13)$$

for drained loading $$q_b = 0.65q_c \quad (14)$$

For OEPs that behave in an unplugged manner, the resistance at the base of the annulus was deduced from Figure 2-32 whereby:

for undrained loading $$q_{ba} = q_c \quad (15)$$

for drained loading $$q_{ba} = 1.6q_c \quad (16)$$

While this database used 16 OEPs, only 5 had strain gauges along the length (reduced to 3 in Jardine *et al*., 2005). The criterion for plugging was deduced from Figure 2-32 and normalised by the CPT cone diameter and P_a.

$$[(D_i/D_{CPT}) + 0.45q_c/P_a] < 36 \quad (17)$$

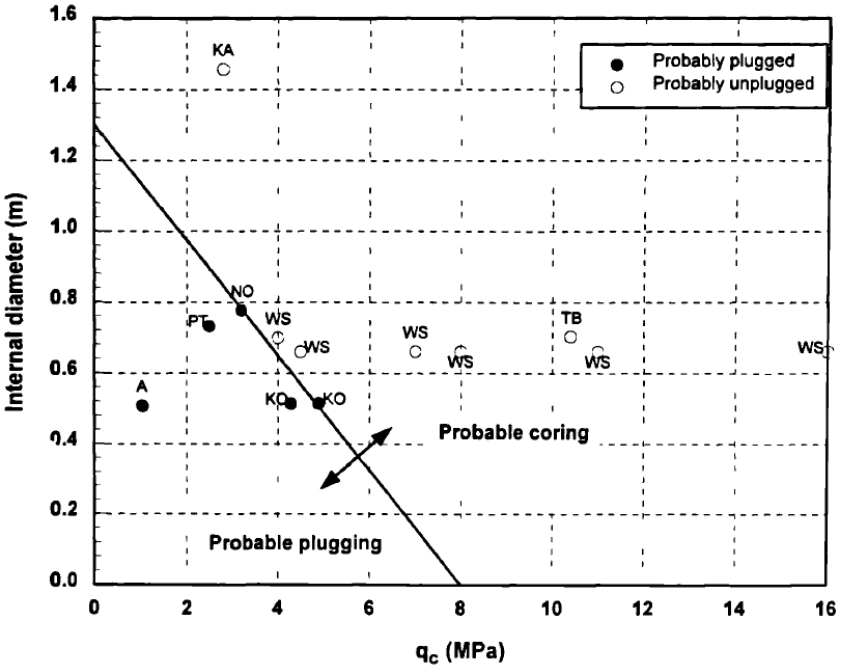

Figure 2-32 Plugging criterion for open-ended piles in clay.

The ICP method has been based on the results of geotechnical testing in the laboratory and in the field. Although relatively detailed, there are weak points within the methodology with specific reference to the plug.

- Considering unplugged piles in sand, the EB of $1.0q_c$ is adopted to the annulus area to represent the EB on the annulus of $0.7q_c$ and $0.3q_c$ to cater for the unknown contribution from the plug.

- The marginal contribution to capacity from the EB needs better interpretation for piles bearing in clay.
- None of the interpretations from published research performed on the plug (such as Salgado *et al*., 2002) and presented in Section 2.3, have been directly included in the ICP methodology.
- If the plug is sand based, internal shearing would cause an increase in the dilation of the sand thereby expanding the plug and increasing the internal shaft friction and EB on the plug.

2.5.3. UWA-05 Method

The UWA-05 method originated from research sponsored by the American Petroleum Institute (the API) to review and compare the then recently published methods of the API (2000) and three CPT based methods (Fugro-04, NGI-04 and ICP-05). The University of Western Australia's (UWA) researchers found that the predictive capability of the CPT based methods was better than the API's. The API was found to better predict the behaviour in clays, to under-predict the capacity in dense sands and to over-predict the capacity in loose sand.

After assessing the results and the use of the UWA database, the reviewers created a new design method, the UWA-05, which improved on the existing methods for OEP and CEP installed in sands. They identified that the pile base capacity can best be interpreted as a function of IFR parameter over the last few stages of installation (FFR), q_c and pile geometry. In addition to this, they identified that if the internal plug is greater than 5 internal pile diameters in length, then the pile will behave plugged under static loading regardless of pile diameter. In practice this means all piles in sand are considered plugged. The criteria for the EB of an open-ended offshore pile using the UWA-05 method is as follows:

$$Q_b = q_b \pi (D_o/2)^2 \qquad q_b = q_c[0.15 - 0.45{A_{rb}}^*]$$
$${A_{rb}}^* = 1 - FFR\left({D_i}^2/{D_o}^2\right)$$
$$FFR \approx min[1, (D_i/1.5)^{0.2}] \tag{18}$$

Not only is the behaviour of the plug interpreted differently within the UWA-05 method, but there are also shortcomings with the method itself:

- Firstly, this method is for use with sands only. Approximations are outlined in further work by Lehane *et al*. (2005) on shaft resistance in clay layers, but this is not very representative.
- No guidance is provided by this method on layered stratigraphies.
- No consideration of the length of the plug is adopted into this method.
- An EB estimate has been provided for sands but no base capacity method is outlined if the annulus bears in a clay layer.
- The UWA method adopts the FFR as the only input into the behaviour of the plug. This ratio is an empirical estimate as the minimum of 1.0 or $(D_i/1.5)^{0.2}$. This means that only the plugged pile response is considered.

Each of the main industrial design methods are inherently different due to their varying assumptions and empirically derived relationships. The resulting relationships will therefore not produce equal pile length estimates at each site.

2.6. Shaft Friction Comparison in the API, ICP and UWA Methods

The derivation of the shaft capacity is not a main focus in this research, however some salient features are outlined in the three methods being considered.

2.6.1. API

The recommendations used to estimate shaft friction have evolved over the years by the API with the most recent derived from research from Randolph and Wroth (1989). These recommendations have then been used to design many offshore installations thereby granting the method a solid track record. Figure 2-33 shows the relationship of the adhesion factor, α, to the strength ratio, s_u/σ'_v. The vertical dividing line through the chart where $s_u/\sigma'_v = 1$, reduces α for clays which are more highly consolidated where $s_u/\sigma'_v > 1$.

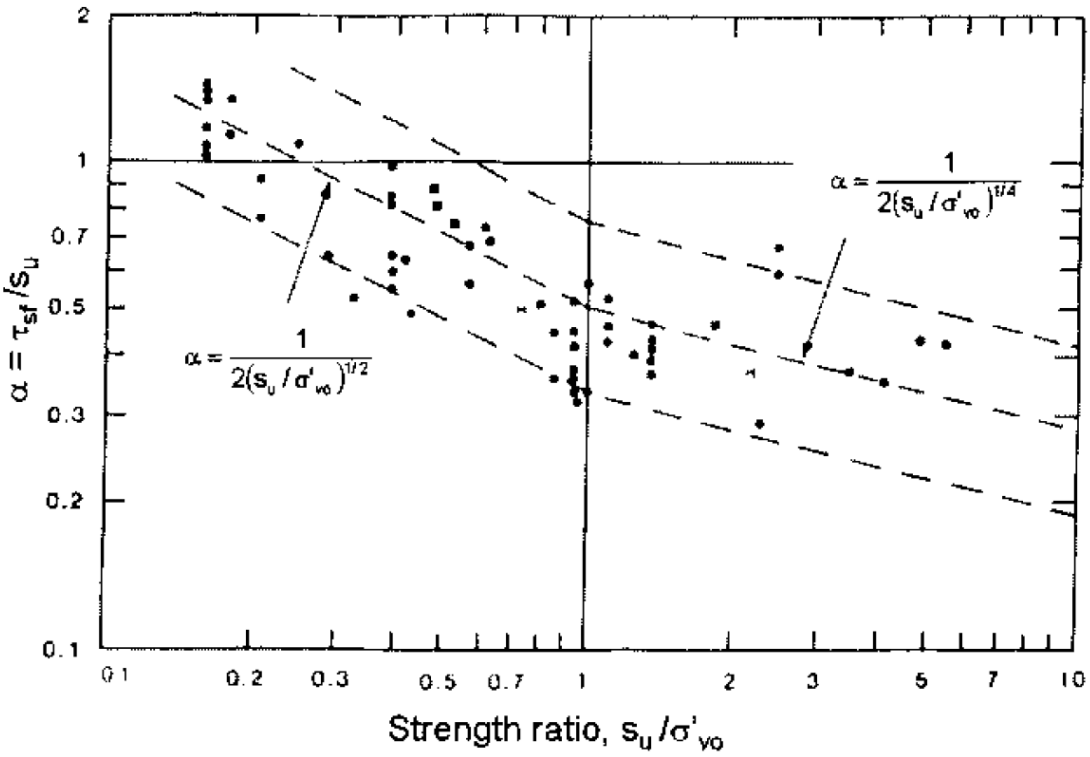

Figure 2-33 Variation of α against the strength ratio s_u/σ'_v (Randolph and Wroth, 1982).

With regards to sands, the API adopts an effective stress approach adopting the following approach:

$$\tau_f = K\sigma'_{v0}\tan\delta = (K\tan\delta)\sigma'_{v0} = \beta\sigma'_{v0} \quad (19)$$

Specific values are deduced for β, although a fixed value of 0.8 has been used for K in the past.

2.6.2. ICP

The ICP method was developed to estimate the capacity of a pile at w_t=0.1D_o. The method was derived mainly using tests performed at a number of test sites using the IC pile with the results of these tests and the procedures developed outlined in a combination of research publications including Jardine (1985), Bond (1989), Lehane (1992) and Chow (1996). These sites included: Canons Park, London, UK; Cowden, Humberside, UK; Bothkennar, UK; Pentre, UK; and Dunkirk and Labenne, France. The IC pile is a cone tipped 102mm diameter pile which has the capability of measuring the axial load, pore pressure, radial total stress and the local shear stress. Using the results from the IC pile and soil testing the following were deduced:

- The local radial effective stress, σ'_{rc} and the local shear stress, τ_f were both directly related to the measured q_c and s_u, for sands and clays respectively, on the test sites.
- In addition, it was found that the shaft resistance at a specific horizon reduces as the annulus is

advanced during installation. This was suggested to be caused by: the action of free surface effects, as the soil is pushed upwards during pile advancement; gapping during installation; and friction fatigue by the cyclic remoulding of the soil to different degrees along the pile length.

- It was also found that the normalised stress reduced quite rapidly behind the annulus.
- Pile capacity is sensitive to pile length, decay in local shear stress, the soil's OCR, pile material, installation method, sensitivity, interface friction angle and pile ageing.

Chow (1997) updated the Coulomb failure criterion for clays to:

$$\tau_f = (K_f/K_c)\sigma'_{rc}\, tan\, \delta_f = (K_f/K_c)(K_c\sigma'_{v0})\, tan\, \delta_f \quad (20)$$

$$K_c = \left[2.2 + 0.016\, YSR - 0.870\, \Delta I_{vy}\right] YSR^{0.42}(h/R)^{-0.2} \quad (21)$$

The factor K_f/K_c (= 0.8) was introduced correctly by Lehane (1992) to cater for the reduction in the overall load-displacement response due to softening after attainment of a peak load in clays. K_c was also outlined to be derived from S_t or ΔI_{v0}.

The initial ICP design methods were specifically for CEPs. Results from the strain path method were used to deduce an adjustment factor for the shaft friction mobilised externally in OEPs. The conversion to open-ended is performed by equating the unit volume of soil displaced by a CEP of radius R^*, to that of an OEP with external and internal radii, R and r, respectively, using $\pi(R^2 - r^2)$ over the pile length.

In sands, the value of τ_f was derived to be related to the measured q_c values along the pile length, the overall pile length and the dilation of the soil surrounding the pile. The shaft resistance was also found to follow a Coulomb failure criterion as follows:

$$\tau_f = \sigma'_{rf} \tan \delta_{cv} = (\sigma'_{rc} + \Delta\sigma'_{rd}) \tan \delta_{cv} \quad (22)$$

$$\sigma'_{rc} = 0.029\, q_c\, (\sigma'_{v0}/P_a)^{0.13}(h/R)^{-0.38} \quad (23)$$

$$\Delta\sigma'_{rd} = 2G\, \Delta r/R \quad (24)$$

2.6.3. UWA

The UWA method was deduced by Lehane *et al*. (2005) using a slightly modified database and by refining the factors used in the methodology of the ICP in sandy soils. Therefore, similar to the guidance outlined for the ICP method, the shaft resistance was also found to follow a Coulomb failure criterion as follows:

$$\tau_f = \sigma'_{rf} \tan \delta_{cv} = (f/f_c)\,(\sigma'_{rc} + \Delta\sigma'_{rd}) \tan \delta_{cv} \quad (25)$$

$$\sigma'_{rc} = 0.03\, q_c\, (A_{rs}{}^*)^{0.3} (h/R)^{-0.38} \quad (26)$$

$$\Delta\sigma'_{rd} = 2G\, \Delta r/R \quad (27)$$

2.7. End Bearing Mobilisation (Q-z)

The derivation of the Q-z soil reaction curve adopted by the API RP 2GEO (2014) is based on Vijayvergiya (1977). Here several pile tests were identified along with the movement required to mobilise the maximum base resistance. This database included bored piles, closed-ended steel piles, prestressed concrete square piles and open-ended steel piles. Due to the limitations of the database, no differentiation was allowed for the behaviour of piles in sands and clays and these were considered to behave in similar manners under loading. The empirical relationship that was developed based on these tests is:

$$\frac{Q}{Q_b} = \left(\frac{z_b}{z_c}\right)^{1/3} \quad (28)$$

where z_c was observed to range from 2%D_o to 9%D_o. Figure 2-34 shows this relationship which depicts the gradual mobilisation of the base resistance, Q, from zero to a maximum of Q_b.

The API modified this model and created a design method recommending a fixed z_c of 0.1D_o. This adjusted the Q-z curve to that shown in Figure 2-35 which is now the guidance provided in the API RP2 GEO (2014). The maximum values of Q_b are as outlined in Section 2.5.1.

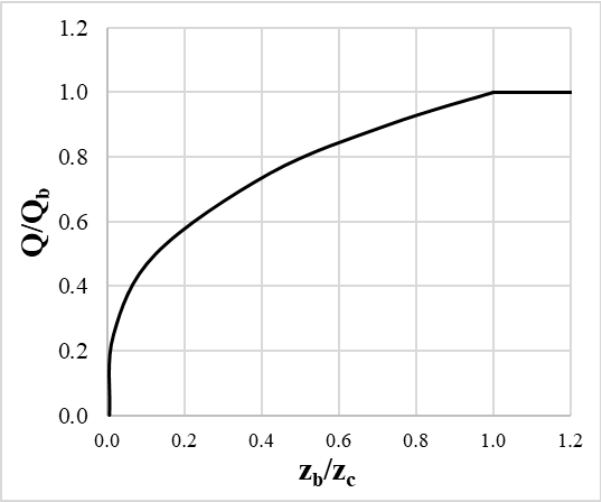

Figure 2-34 Normalised Q-z curve for sand and clay (adapted from Vijavergiya, 1977).

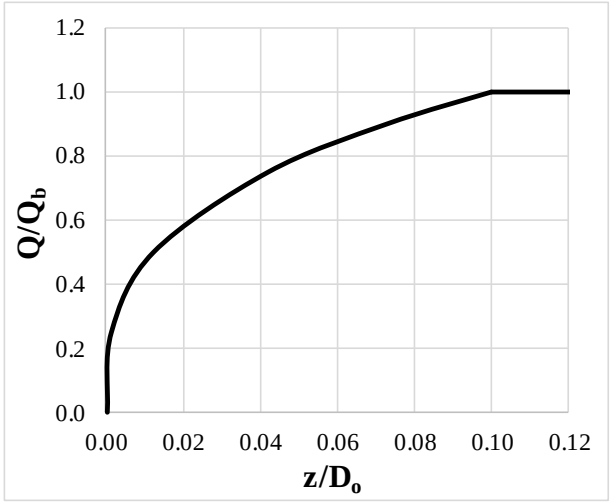

Figure 2-35 Q-z curve for sand and clay (API RP 2GEO, 2014).

2.8. Shaft Friction Mobilisation (t-z)

In a finite element model of an offshore jacket, the pile is discretised as a series of discrete continuous points connected to the surrounding soil. This interaction is modelled by a series of t-z soil reaction curves that represent the axial resistance along the length of the pile. There are different recommendations that have developed over the years for the derivation of these curves. The main form of these curves has been presented in the API and an alternative is presented in the DNV-OS-J101 (2014). Only static curves are investigated here.

2.8.1. API t-z soil reaction curves

The API t-z soil reaction curves were designed to represent the mobilisation of shaft friction for OEPs in sands and clays. These have evolved over the years being designed to fit data derived from laboratory scale and field tests performed in sands and clays. The earliest curves for clays that are similar to those used today, were derived by Coyle and Reese (1966) as shown in Figure 2-36. These curves depicted strain softening and the load transfer is normalised by the shear strength derived from the total stress approach (αs_u).

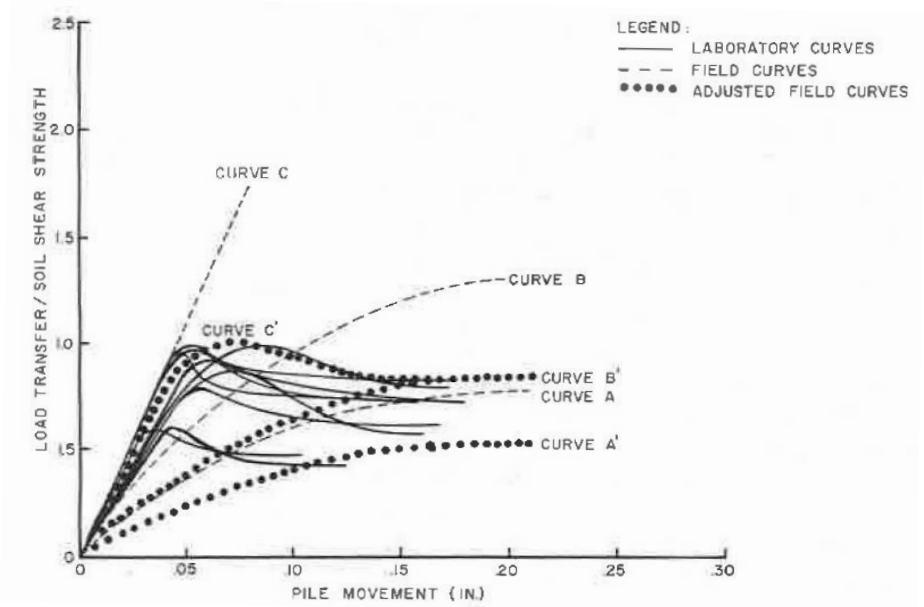

Figure 2-36 Ratio of load-transfer to soil shear strength vs pile movement for field curves in clay, laboratory curves and adjusted curves (Coyle and Reese, 1966).

Similar curves were also deduced for sands based on field and laboratory testing (Figure 2-37). The load-transfer is normalised by the shear strength derived from the effective stress ($K\ tan\ \delta$) approach.

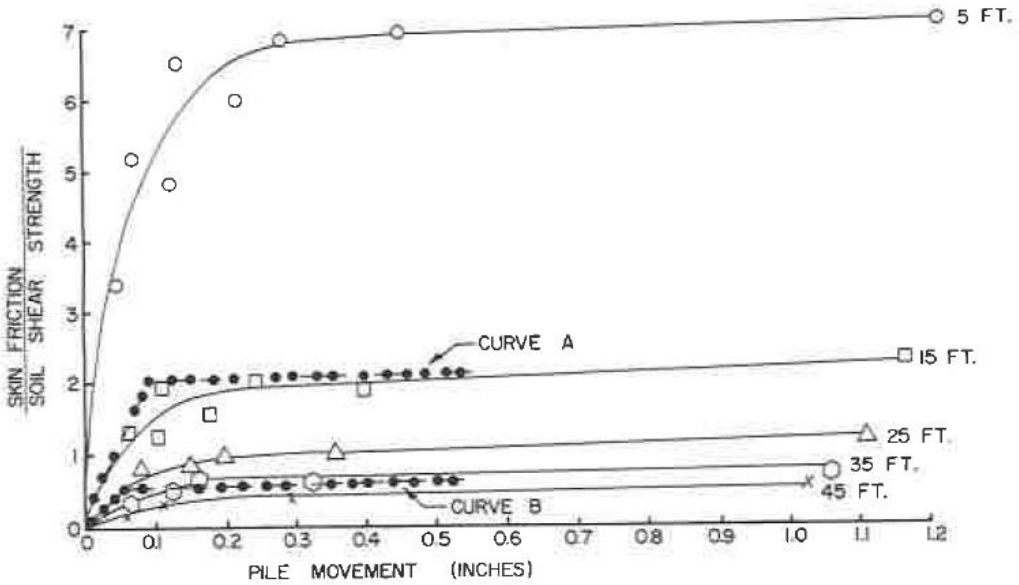

Figure 2-37 Ratio of load-transfer to soil shear strength vs pile movement for field curves in sand, laboratory curves and adjusted curves (Coyle & Sulaiman, 1967).

Further work over the next few years improved these relationships with Vijayvergiya (1977) eventually outlining the standardised form of the curve that is adopted today based on an empirical relationship. This is shown in Figure 2-38.

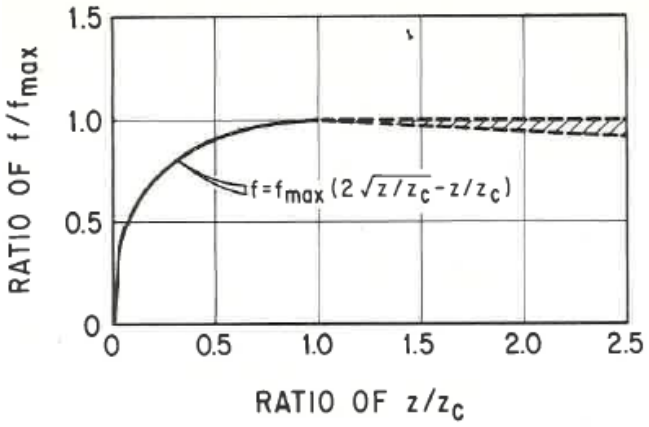

Figure 2-38 Normalised t-z curve for clay and sand (Vijayvergiya (1977).

The coordinates in Table 2-2 set out the points along the t-z reaction curves outlined in the API RP 2GEO (2014).

Table 2-2 Definition of t-z curves

z_p/z_{peak}	τ/τ_{max}	
	Clays	**Sands**
0.00	0.00	0.00
0.16	0.30	0.30
0.31	0.50	0.50
0.57	0.75	0.75
0.80	0.90	0.90
1.00	1.00	1.00
2.00	0.70 to 0.90	1.00
∞	0.70 to 0.90	1.00

2.8.2. The DNV t-z soil reaction curves

To develop the DNV curves, researchers fit load-transfer curves based on pile test results. Other teams were however developing analytical models based on the behaviour of piles.

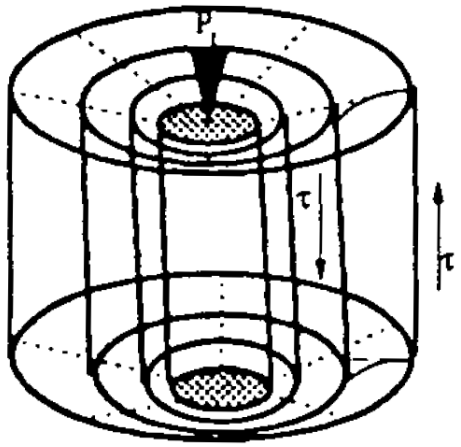

Figure 2-39 Mode of deformation of shaft (Randolph and Wroth, 1978)

Randolph and Wroth (1978) contributed to a model which adopted a cylindrical pile fully embedded in a uniform linear soil, being subjected to an axial load. This deformation was assumed to cause the load to be shed in concentric layers (Figure 2-39) surrounding the pile, out to a radius (r_m) where no further deformation occurred.

From this model an external element of soil can be extracted as shown in Figure 2-40.

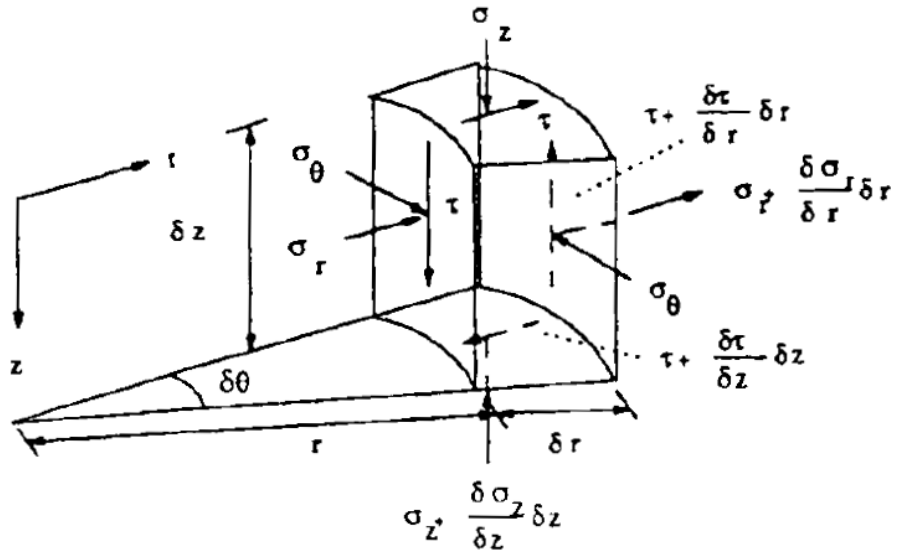

Figure 2-40 Stresses in soil element (Randolph and Wroth, 1978)

Considering the forces on the element, the vertical equilibrium of soil gave:

$$\frac{\delta}{\delta r}(r\tau) + r\frac{\delta \sigma_z}{\delta z} = 0 \tag{29}$$

Where in the context of this model, r is the radius of the pile, τ is the mobilised shear stress and σ_z is the vertical compressive stress. This is then related to the shear modulus, G, and the strains are integrated over the length of the pile to give

$$z_p = \frac{\tau_0 r_0}{G}\left[\ln\frac{r_m}{r_0}\right] \tag{30}$$

where z_p is the local pile displacement, r_m is the radius at which τ is negligible, τ_0 is the shear stress at the pile shaft, r_0 is the pile radius, and G is the shear modulus. Randolph and Wroth (1978) therefore produced a linear load-transfer relationship with a gradient of

$$K = \frac{G_0}{r_0\, ln\frac{r_m}{R}} \tag{31}$$

to model the t-z soil reaction curves. When considering non-linear soils, which achieve the same ultimate value with non-linear stiffness, several other researchers (such as Kondner, 1963; Duncan & Chang, 1970; Kraft *et al*., 1981) focused on hyperbolic relationships of the form (Pando *et al*., 2006):

$$\tau = \frac{\gamma}{\frac{1}{G_0} + \frac{\gamma}{\tau_{ult}}} \tag{32}$$

Where γ is the shear strain ($G = \tau/\gamma$). Duncan & Chang (1970) highlighted the relationship between τ_{max} and τ_{ult} was a factor R_f, where

$$\tau_{max} = R_f \tau_{ult} \tag{33}$$

Which substituted into the hyperbolic relationship, solved and integrated over the radius r_m gives

$$z_p = \frac{\tau_0 r_0}{G_0} \ln\left(\frac{\frac{r_m}{r_0} - R_f \frac{\tau_0}{\tau_{max}}}{1 - \frac{\tau_0 R_f}{\tau_{max}}}\right) \tag{34}$$

The above is recommended by DNV to deduce the t-z curves, with the slight variation that the ratio r_m/r_0 is represented by a dimensionless zone of influence, z_{IF}, as follows:

$$z_p = \frac{\tau_0 r_0}{G_0} \ln\left(\frac{z_{IF} - R_f \frac{\tau_0}{\tau_{max}}}{1 - \frac{\tau_0 R_f}{\tau_{max}}}\right) \tag{35}$$

Further guidance is then provided to estimate G_0 for clays:

based on plasticity $$\boldsymbol{G_0 = \frac{300}{I_p}\, s_u} \tag{36}$$

based on the over-consolidation ratio $$\boldsymbol{G_0 = s_u\left(600 - 170\sqrt{OCR - 1}\right)} \tag{37}$$

No guidance is given on strain softening in clays. As for sands:

$$G_0 = \frac{1000 \tan\varphi \sqrt{100 \times \sigma_v}}{2(1+\upsilon)} \tag{38}$$

2.9. OEP Load-Transfer Diagram

From the information that has been presented, Figure 2-41 demonstrates a more realistic representation of the behaviour of the soil, pile and plug when a static load is applied to the top of an OEP. The height of the active plug length will depend on many factors especially the soil properties, D_i and the installation method.

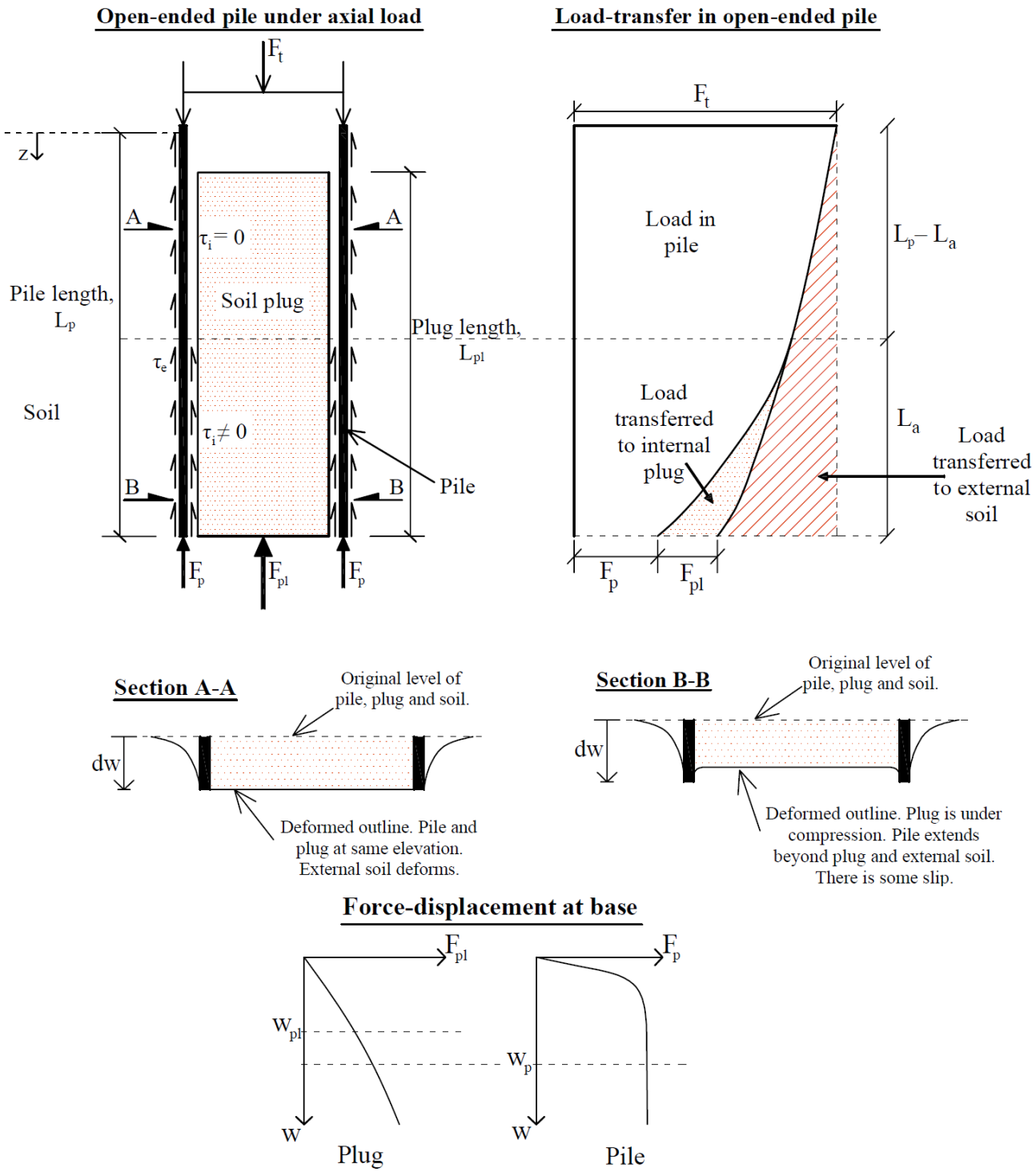

Figure 2-41 Annulus and plug behaviour under axial static load.

In the load transfer diagram, the active plug length, L_a, is the length of plug mobilised due to the interaction between the plug (column) and soil at the base of the plug.

2.10. Derivation of a new Q-z curve

It has been shown in Section 2.7 of this chapter that the existing Q-z reaction curve, which is currently used to model the non-linear response of the base of OEPs in finite element models, originated from

the paper by Vijayvergiya (1977). The methodology was derived from a variety of pile and soil types, generalised to encapsulate the database results and simplify the base response. In addition, there were (and continues to be) a very small number of OEPs available for the reliable calibration of the Q-z reaction curve. This has mainly been due to the cost of instrumentation, but also, due to the damage to the instruments during pile installation, many of the pile base capacities have been interpolated. This results in an over-conservative design method and has led to the true behaviour of the end bearing inadequately captured in the OEP design methods.

The geotechnical engineering database of pile tests contains a variety of interpretations of pile capacity. In some studies, the base capacity is with reference to the displacement of the pile toe from its original position, which is also the basis of the Q-z curve. However, in many database results, as shall be shown later in Chapter 5, at OEP test sites such as Euripides and Tokyo, the base capacity is provided relative to the displacement of the pile head. This creates an issue of consistency as after w_t=0.1D_o, differing portions of the pile may have mobilised pre-τ_{peak}, τ_{peak}, or τ_{ult} (post-τ_{peak}), as in Figure 1-2, whereas, the base may not have yet achieved its peak capacity. In the pile design methods discussed in this chapter, the base and shaft capacity are determined separately and then added to establish the capacity. This process however, gives no indication of the initial stiffness or response. As will be shown in Chapter 5, especially in sands, the capacity of the base continues to increase after w_t=0.1D_o, due to the mobilisation of the soil plug. In hindsight, the values that are indicated as the base capacity in some case studies, taken at w_t=0.1D_o, will not be the best representation of the base response.

The Q-z curve is intended to replicate the response of the base of a pile. As the base of an OEP is comprised of two main parts, this curve should therefore be designed considering input from the expected response of each component. The original derivation of the slope of this curve came about from testing and non-linear relationships outlined in Chapter 2. The main Q-z curve, used in the offshore industry for OEPs is that of the API. In the API's methodology, a plugged or unplugged pile is estimated and the maximum base capacity, Q_{max}, is derived. This is then related to the displacement of the base, which is expressed as a ratio of z/D_o. From research and test results (Salgado *et al.*, 2002;

Doherty *et al*., 2010; Ko and Jeong, 2015), full mobilisation of base capacity occurs at different displacements for both annulus and plug, and is also dependent on soil type; as some soils create larger internal arches than others, engaging more of the plug.

The method presented here illustrates a new means of deriving a load displacement (Q-z) response at the base of an OEP. This method suggests the isolation of the Q-z responses, using a finite element method as will be outlined in Chapter 3, at the base of the annulus (Figure 2-42) and plug (Figure 2-43) allowing their superposition. The full base response is then derived as an improved Q-z curve for an OEP, shown in Figure 2-44, fully mobilised at a settlement of $0.1D_i$ of the annulus. In the subsequent chapters that follow this procedure is integrated into the finite element method and not separately input.

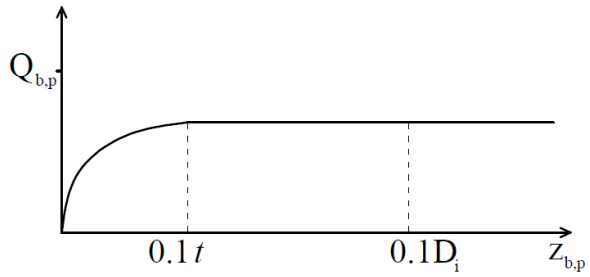

Figure 2-42 Mobilisation of EB on annulus.

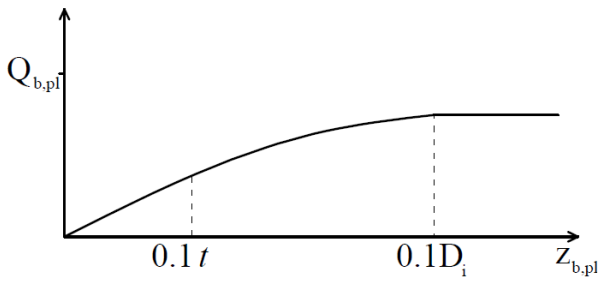

Figure 2-43 Mobilisation of EB on plug.

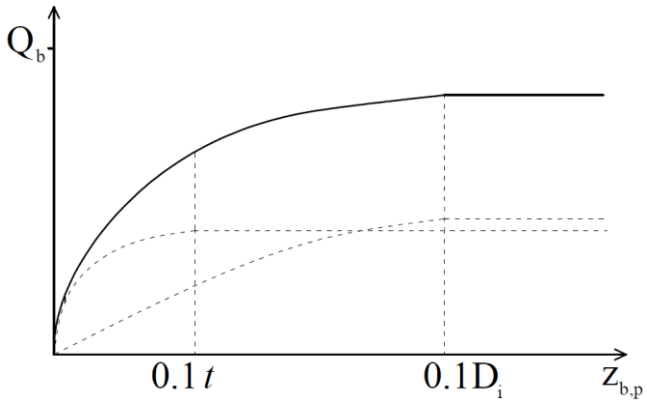

Figure 2-44 Combined base mobilisation, Q-z curve.

It is also noted that the full mobilisation of the base of an OEP requires a large degree of settlement. The design settlement at the mudline, to fulfil the serviceability requirement, is usually stated as $0.1D_o$. In very long piles, this settlement is usually achieved by the compression and displacement along the length of the pile and the displacement of the annulus. Further capacity however is gained by the mobilisation of the plug which may not achieve full capacity when the limit of the mudline settlement is reached.

3. FE Modelling Method for Soil Plug

This section develops a theoretically based method for the analysis of the soil plug. The finite element method is used to solve a 1D differential equation representing an installed pile under static vertical load. The statement of equilibrium is derived on the basis of the theory of virtual work. The soil is modelled with a linear and non-linear constitutive relationship and the Newton-Raphson method is used to converge towards the solution.

The main development of this methodology was outlined in Joseph *et al*. (2018). This paper is included as Appendix B of this document. This section expands on the development of the relationships presented the paper, but omitted due to page constraints.

3.1. Open-Ended Pile Model

Consider an OEP as in Figure 3-1 with an axially applied load F_t. In this system the elastic pile is assumed to be in equilibrium with the load applied, being balanced by the external and internal shear stress, $\tau_e(z)$ and $\tau_i(z)$, respectively, along the length of the pile plus the EB at the annulus of the pile and over the base of the internal soil plug. The vertical displacement of the pile, $w_p(z)$, and internal plug of soil, $w_{pl}(z)$, will vary with depth. The external soil, $w_s(z)$, acts as a boundary.

The shear stress or traction generated on both the internal and external sides of the pile are within an interface layer. The thickness of interface layers does vary, but for this model it is assumed to be zero. The relative displacement across the interface is dependent on the mobilisation of both the interface stiffnesses, and the soil or plug stiffnesses to that of the pile.

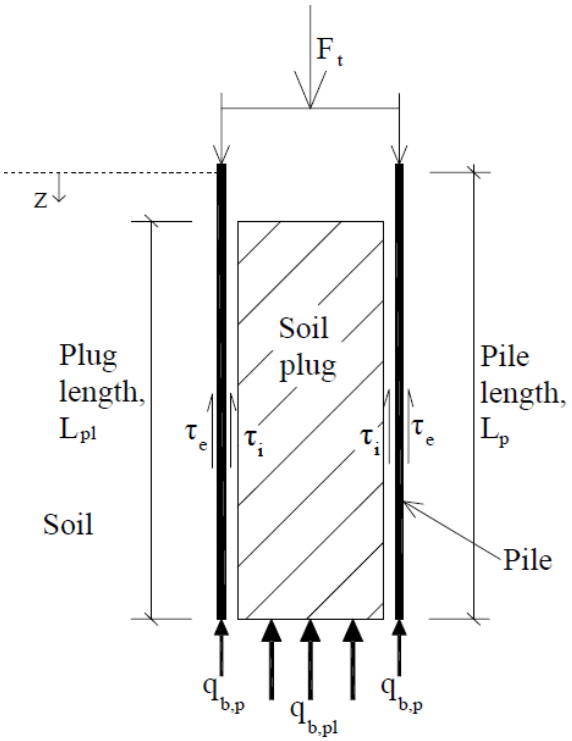

Figure 3-1. Loads and resistances surrounding pile, plug and soil.

The end-bearing of the pile and plug also have separate constitutive relationships. For the pile and plug this is based on the displacement of the annulus, $w_p(L)$ and base of the plug, $w_{pl}(L)$, respectively. The loading on the area of the annulus generates a resistance of $q_{b,p}$ and the compression of the internal plug due to τ_i generates a resistance of $q_{b,pl}$ at the base.

3.1.1. Pile

If a 1D slice were taken of the pile only, from Figure 3-1, this can be analysed as shown in Figure 3-2:

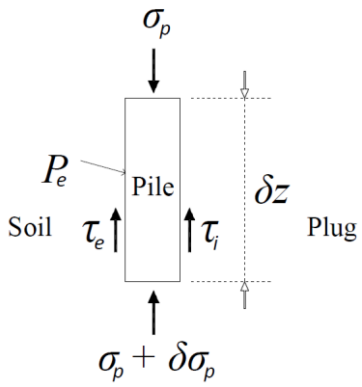

Figure 3-2. Reactions for a section of an OEP.

If compression is taken as positive:

$$\sigma_p A_p = \tau_e P_e dz + \tau_i P_i dz + \left(\sigma_p + d\sigma_p\right) A_p \tag{39}$$

$$\frac{d\sigma_p}{dz} A_p + \tau_e P_e + \tau_i P_i = 0 \tag{40}$$

3.1.2. Plug

If the plug only was considered and a 1D slice taken as shown in Figure 3-3 (again compression positive):

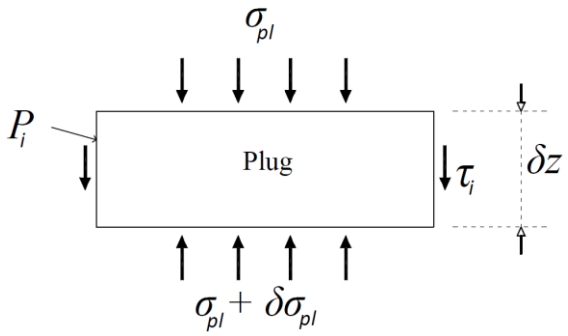

Figure 3-3. Section through plug of an OEP.

$$\sigma_{pl}A_{pl} = -\tau_i P_i dz + (\sigma_{pl} + d\sigma_{pl})A_{pl} \tag{41}$$

$$\frac{d\sigma_{pl}}{dz}A_{pl} - \tau_i P_i = 0 \tag{42}$$

3.1.3. Soil

The soil acts as a radial boundary in this model where all the load mobilised through the interface is transferred.

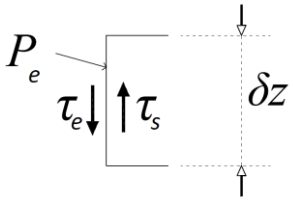

Figure 3-4. Section through plug of an OEP.

Here, as compression is positive:

$$0 = \tau_s P_e dz - \tau_e P_e dz \tag{43}$$

$$0 = (\tau_s - \tau_e)P_e \tag{44}$$

3.2. Strong and Weak Forms of the Equations of Equilibrium

Equations (40), (42) and (44) represent the strong forms of the governing equations of equilibrium necessary to represent the soil-pile-plug model.

The boundary conditions at the top of the pile (where $z = 0$) and for a pile of length L are

$$\sigma_p(0)A_p = F_t; \qquad \sigma_p(L)A_p = (F_p) \tag{45}$$

and for the pile plug are:

$$\sigma_{pl}(0)A_{pl} = 0; \qquad \sigma(L)A_{pl} = (F_{pl}) \tag{46}$$

3.2.1. Pile

Using the resistive components for the OEP, the axial stress, σ_p, in the pile satisfies the equation of equilibrium outlined in Equation (40). This equation is in the strong form and to solve this equation, it is to be converted to the weak form by multiplying by the arbitrary function, $\delta w(z)$, and integrating over the length of the pile.

$$\int_0^L \delta w_p \left(\frac{d\sigma_p}{dz} A_p + \tau_e P_e + \tau_i P_i\right) dz = 0 \tag{47}$$

3.2.2. Plug

The same is done for the plug however integrated over the plug's length.

$$\int_{L-L_{pl}}^L \delta w_{pl} \left(\frac{d\sigma_{pl}}{dz} A_{pl} - \tau_i P_i\right) dz = 0 \tag{48}$$

3.2.3. Soil

The same can be done for the soil and integrated over the pile's length.

$$\int_0^L \delta w_p \, (\tau_s - \tau_e) P_e \, dz = 0 \tag{49}$$

3.2.4. Solving

Using the boundary conditions these equations can be solved.

From Equation (47):

$$\int_0^L \delta w_p \left(\frac{d\sigma_p}{dz} A_p + \tau_e P_e + \tau_i P_i\right) dz = 0 \tag{50}$$

$$\left[\delta w_p \sigma_p A_p\right]_0^L - \int_0^L \sigma_p A_p \left(\frac{d\delta w_p}{dz}\right) dz + \int_0^L \delta w_p (\tau_e P_e) dz + \int_0^L \delta w_p (\tau_i P_i) dz = 0 \tag{51}$$

Adopting the boundary conditions

$$\left[\delta w_{b,p} F_{b,p} - \delta w_t F_t\right] - \int_0^L \sigma_p A_p \left(\frac{d\delta w_p}{dz}\right) dz + \int_0^L \delta w_p (\tau_e P_e) dz + \int_0^L \delta w_p (\tau_i P_i) dz = 0 \tag{52}$$

$$\delta w_{b,p} F_{b,p} - \delta w_t F_t - \int_0^L \sigma_p A_p \left(\frac{d\delta w_p}{dz}\right) dz + \int_0^L \delta w_p (\tau_e P_e) dz + \int_0^L \delta w_p (\tau_i P_i) dz = 0 \tag{53}$$

where b is base, and t is top.

From Equation (48), this expression is integrated over the length of the plug.

$$\int_{L-L_{pl}}^L \delta w_{pl} \left(\frac{d\sigma_{pl}}{dz} A_{pl} - \tau_i P_i\right) dz = 0 \tag{54}$$

$$\left[\delta w_{pl}\sigma_{pl}A_{pl}\right]_{L-L_{pl}}^{L} - \int_{L-L_{pl}}^{L} \sigma_{pl}A_{pl}\left(\frac{d\delta w_{pl}}{dz}\right)dz - \int_{L-L_{pl}}^{L} \delta w_{pl}(\,\tau_i P_i)\,dz = 0 \tag{55}$$

Adopting the boundary conditions,

$$\left[\delta w_{b,pl}F_{b,pl} - 0\right] - \int_{L-L_{pl}}^{L} \sigma_{pl}A_{pl}\left(\frac{d\delta w_{pl}}{dz}\right)dz - \int_{L-L_{pl}}^{L} \delta w_{pl}(\,\tau_i P_i)\,dz = 0 \tag{56}$$

$$\delta w_{b,pl}F_{b,pl} - \int_{L-L_{pl}}^{L} \sigma_{pl}A_{pl}\left(\frac{d\delta w_{pl}}{dz}\right)dz - \int_{L-L_{pl}}^{L} \delta w_{pl}(\,\tau_i P_i)\,dz = 0 \tag{57}$$

and from Equation (49), this expression is also integrated over the length of the pile.

$$\int_{0}^{L} \delta w_s(\tau_s - \,\tau_e)P_e\,dz = 0 \tag{58}$$

$$\int_{0}^{L} \delta w_s\tau_s P_e\,dz - \int_{0}^{L} \delta w_s\tau_e P_e\,dz = 0 \tag{59}$$

The summation of Equations (53), (57) and (59) is found as:

$$\begin{aligned}\delta w_t F_t = {} & w_{b,p}F_{b,p} - \int_{0}^{L} \sigma_p A_p\left(\frac{d\delta w_p}{dz}\right)dz + \delta w_{b,pl}F_{b,pl} - \int_{L-L_{pl}}^{L} \sigma_{pl}A_{pl}\left(\frac{d\delta w_{pl}}{dz}\right)dz \\ & + \int_{0}^{L} \delta w_p(\,\tau_i P_i)dz - \int_{L-L_{pl}}^{L} \delta w_{pl}(\,\tau_i P_i)\,dz + \int_{0}^{L} \delta w_p(\tau_e P_e)dz - \int_{0}^{L} \delta w_s\tau_e P_e\,dz \\ & + \int_{0}^{L} \delta w_s\tau_s P_e\,dz\end{aligned} \tag{60}$$

$$\begin{aligned}\delta w_t F_t = {} & \delta w_{b,p}F_{b,p} - \int_{0}^{L} \sigma_p A_p\left(\frac{d\delta w_p}{dz}\right)dz + \delta w_{b,pl}F_{b,pl} - \int_{L-L_{pl}}^{L} \sigma_{pl}A_{pl}\left(\frac{d\delta w_{pl}}{dz}\right)dz \\ & + \int_{L-L_{pl}}^{L} (\delta w_p - \delta w_{pl})P_i\,\tau_i dz + \int_{0}^{L} (\delta w_p - \delta w_s)P_e\tau_e dz + \int_{0}^{L} \delta w_s\tau_s P_e\,dz\end{aligned} \tag{61}$$

Equation (61) is equivalent to Equation 3 in Appendix B (Paper 2).

Joseph *et al*. (2018) goes into further detail on the derivation of expressions for the internal and external virtual work of the pile-soil-plug system and then outlines the standard Galerkin approach to solve the weak form of the equation of equilibrium. The use of 2-noded elements to model the pile, plug and soil elements are identified along with 4-noded elements to model the interfaces. Lagrangian shape functions are then used to relate the axial displacements within each element to the nodal displacements. After outlining the Galerkin form for each element, the internal force vector (F_{INT}), the stiffness matrix and the displacements vector are all assembled ($\mathbb{A}[\circ]$) and used to form the vector equation which compares F_{INT} to the externally applied load, F_{EXT}. This is then solved using the Newton-Raphson method.

The verification of this process is presented as part of the VIRTUPLUG Manual (Appendix C).

4. Base Capacity of Open Ended Piles in Clay

The mobilisation of the base capacity of OEP's in clay, and its contribution to the total capacity is investigated in this chapter. An overview of each of the test sites considered from the geotechnical engineering database is initially presented. This is then followed by the results of an analysis that evaluates the performance of the API and ICP design methods when applied directly, using the data from these sites. Using the distribution of the shaft and end bearing capacities from the design methods, an RMS-error calculation is performed to quantify the deviation from the measured values. With the input of τ_f and q_b from the API and ICP methods, into the finite element method, the FE variants of these methods are computed, resulting in the API-FEA and ICP-FEA methods. The inputs to these methods are then sequentially varied in a series of cases using the Pentre and Tilbrook test data to determine the sensitivity of each input parameter. The results of this sensitivity analysis are then compared and the summaries of the findings presented along with recommendations for improvements that best capture the behaviour.

4.1. Case Study Investigation

To perform this study, site specific data are used selecting published data from the geotechnical engineering database on piles. The case studies considered are shown in Table 4-1, which lists 21 tests performed at 8 sites, in predominantly undrained (clay) material. These sites were selected as they comprised piles with the following characteristics:

- Open-ended
- Installed by driving
- Base capacity interpreted
- Uniform cross sections
- Static compression loading
- All steel
- Circular

It is noted that no two sites or pile tests are alike, resulting in interpretations being made on available data. The variations in the selected case studies to form the pile test database for this study include sites with differing:

- Pile base configuration
- Time before testing
- Plasticity Index
- OCR states
- Initial testing direction (Compression or tension)
- Pile installation methods
- Pile diameters and wall thicknesses

It is noteworthy, that similar to Chow's (1997) database which contained 57 pile tests, only the Kansai Bridge test has a pile diameter of greater than 1m, a typical offshore pile size, with the rest of the database on smaller piles. For this research project, the primary focus is the soil plug and the variations outlined above will have an effect on the contribution of the plug to the total capacity of the pile. Following Table 4-1 is a short description of the main geological and geotechnical features at each clay site.

Table 4-1 Plug Capacity Validation in Clays

Site Number	Site	Location	Pile Test Number	Reference Authors	Length (m)	Diameter (m)	t (mm)
1	Kinnegar	Belfast Lough, N. Ireland	UCD-OE-3	Doherty *et al.* (2010)	6.1	0.168	9.0
2	Pentre - LDP	Pentre	LDP	Gibbs *et al.* (1992)	55.0	0.762	15.0
3	Tilbrook - LDP	Tilbrook	LDP	Gibbs *et al.* (1992)	30.0	0.762	30.0
4	Noetsu Bridge	Noto Peninsula, Japan	T2	Matsumoto *et al.* (1995)	8.3	0.800	12.1
5	Kansai Bridge	Osaka Bay, Japan	T1	Matsumoto *et al.* (1992)	37.1	1.500	22.0
6	Empire 1	Louisiana, USA	1	Cox and Kraft (1979)	15.2	0.356	12.0
7	Empire 2		2		15.2	0.356	12.0
8	Empire 3		3		12.2	0.356	12.0
9	Empire 4		4		12.2	0.356	12.0
10	Kontich 1	Kontich, Belgium	1 (66')	Hereema (1979)	20.1	0.610	25.4
11	Kontich 2		2 (77')		23.5	0.610	25.4
12	West Sole 1	North Sea, UK	B 6m	Clarke *et al.* (1985)	6.0	0.762	31.8
13	West Sole 2		B 9m		9.0	0.762	31.8
14	West Sole 3		B 12m		12.0	0.762	31.8
15	West Sole 4		B 15m		15.0	0.762	31.8
16	West Sole 5		B 18m		18.0	0.762	31.8
17	West Sole 6		A 6m		6.0	0.762	31.8
18	West Sole 7		A 9m		9.0	0.762	31.8
19	West Sole 8		A 12m		12.0	0.762	31.8
20	West Sole 9		A 15m		15.0	0.762	31.8
21	West Sole 10		A 18m		18.0	0.762	31.8

4.1.1. Kinnegar, Belfast Lough, Northern Ireland – Doherty *et al.* (2010)

This is a predominantly clay site with a stratigraphy that includes a 1.83m thick superficial layer of sandy gravel fill, underlain by 8.5m of Quaternary glacial drift deposits (Lehane *et al.*, 2003). There are also, to a lesser extent, traces of silts and sands. These layers were formed from rises in sea levels causing the transportation of these drift deposits via rivers, which were eventually deposited in areas such as the Belfast Lough. This material is described as a very soft clayey organic silt with high plasticity. The organic content was found to be due to the presence of course fibrous plant material. The material has a low apparent over-consolidation ratio with YSR ranging from 1 to 1.6. Despite the presence of organics and silt, permeability and consolidation tests observed behaviours similar to

clay. This material is commonly referred to as Sleech and is underlain by a harder glacial till which is predominantly sand.

4.1.2. Pentre, UK – Gibbs *et al.* (1992)

The Pentre site was selected due to the requirement to perform pile testing in soils which were similar onshore to these at typical offshore sites in the North Sea, to improve the reliability of OEP design methods in clays (Lambson *et al.*, 1992). The Holocene (surface) deposits were found to be 3-4m thick followed by Quaternary deposits of normally consolidated, low to medium plasticity, very silty clays. Gravels are also present in this layer, due to glacial lake deposition. To a depth of 15m the clays are generally uniform with low anisotropy due to continuous deposition. This is then followed by a zone of highly laminated to very finely laminated, medium to highly anisotropic layers formed by seasonal deposits. The undrained shear strength values ranged from 50-250kPa. The OCRs measured at the site were as high as 4. However, the testing at the Pentre site targeted the deeper zones which had OCR values ranging from 1 to 1.50. Due to the high anisotropy, the soil demonstrated higher permeability horizontally, a characteristic that results in faster equalisation of pore-pressures.

The OEP tested in compression at this site had 55m of penetration with a D_o of 0.762m and t of 15mm. The tests targeted the soil below 15m, therefore casing was driven to 15m then the soil plug was removed. The actual pile was then installed through the casing to 55m, making the effective pile length from 15m to 55m. At the end of driving, the soil plug was measured as 1.73m above the base of the casing. During pile driving the strain gauges below 37m were damaged.

4.1.3. Tilbrook, UK – Gibbs *et al.* (1992)

The Tilbrook site was selected due to its high OCR values. The upper clay layer is a thick 18m deposit of Lowestoft Till. The till is described as a blueish grey, silty clay with chalk and flint, and is of low to moderate plasticity. The upper bedrock of the site, underlying the till, is Oxford Clay. This is a very hard and fissile clay with concretionary nodules and bands of limestone (Lambson *et al.*, 1992). This clay is described as being uniform and having a moderate to high plasticity and is highly fissured. Its anisotropy ranges from moderate to high, increasing with depth. These layers have been subjected

to two glacial periods and two interglacial periods making the layers heavily over-consolidated. This is also observed in the liquidity indices of the clays as these are quite low and generally with negative values. The undrained shear strengths overall are high, ranging from 400 to 800kPa with apparent OCR values in the range of 20 to 50 in the top 7m and decreasing with depth to about 10 at 25m (Clarke *et al.*, 1992). The coefficient of compressibility, m_v, was between 0.01 to 0.04m²/MN, indicating that the soil was relatively incompressible, Lambson *et al.* (1992).

This OEP was driven to a penetration of 30m at this over-consolidated clay site. The pile had a D_o of 0.762m and a t of 35mm. The elevation of the soil plug at the end of driving was 13m from the pile base, a plug length ratio (L_{pl}/L_P) of 0.43. Pile tests were performed on the pile 130 days after the pile was installed.

4.1.4. Noetsu Bridge, Noto Peninsula, Japan – Matsumoto *et al.* (1995)

The superficial Holocene deposits are described as a 1.5m thick very soft clay. This is underlain by a 20m thick deposit of soft clay termed "diatomaceous mudstone" (Oka *et al.*, 2010), a highly structured and porous clay. The data available showed very low bulk densities with high water contents, which suggests that the clay is organic or that it has an extremely high plasticity. SPT and CPT resistances were generally low and consistent with soft clays. No Atterberg limit tests nor consolidation tests were performed. UCS values were also provided for the soft clays here.

4.1.5. Kansai Bridge, Osaka Bridge, Japan – Matsumoto *et al.* (1992)

The stratigraphy here includes a soft alluvial clay deposit which is approximately 10m thick. This is followed by an 8m thick layer of gravel and sand, underlain by a deposit of Pleistocene clays of at least 25m thickness. There is no further geological data available on the Kansai Bridge site. There are also no Atterberg limit tests nor consolidation tests performed although SPT data are provided.

4.1.6. Empire, Louisiana, USA – Cox and Kraft (1979)

This location is characterised as a clay site with soil parameters typical of many offshore installations (Cox and Kraft, 1979) and selected due to the normally consolidated clay stratigraphy, typical of Gulf of Mexico clays. The upper 30m soil layer comprises fine sand with layers of soft clay. This is underlain by a 24m thick firm grey clay, then an 83m thick stiff grey clay with sand seams. The

testing at this site targeted the deep clay layers. The undrained shear strength profile increases linearly with depth consistent with a normally consolidated soil. These values range from 100kPa to 125kPa at the base of the last pile test and demonstrate a high plasticity. CPT data are also available.

4.1.7. Kontich, Belgium – Hereema (1979)

Heerema (1979) gives no explicit mention of the geology of this clay site in which significant pile testing was performed. The results from limited CPT testing are available, and the undrained shear strength is shown to increase linearly with depth from 100 to 300kPa. Holeyman (2001) described separate pile tests at a site in Kontich, indicating 3m of Holocene deposits of sandy loam followed by tertiary Boom clay down to a significant depth. Belgium Boom clay is an anisotropic material of the Oligocene period. This material is a stiff, fissured, layered and over-consolidated clay. Samples obtained of the clay indicate it to be of a high plasticity.

4.1.8. West Sole, UK, North Sea – Clarke *et al.* (1985)

At this site the Holocene sediments are predominantly sand of a thickness of less than 1.0m. This sand is underlain by Pleistocene deposits comprised of Glacial Till (Boulder Clay), of a thickness of 13m overlying Lias Clay to about 24m. The Till contains sand, fragments of chalk, siltstone and granite. The undrained shear strength varies in the Till from 200kPa to about 700kPa and is an over-consolidated clay with OCR values ranging from 5-12. The Lias Clay is a hard shaly silty clay with undrained shear strength values ranging from 400kPa to 980kPa. These layers are of low to medium plasticity and also over-consolidated with OCR values ranging from 1.7 to 5.5.

4.2. Evaluation of Performance of Current Design Methods

The performance of the API and ICP methods implemented directly from their methodologies outlined in Section 2, was used to estimate the capacity of OEPs in clays using the database considered. The results of these analyses are presented in Table 4-2 where the ratio of the calculated capacity (Q_c) to the measured capacity (Q_m) is also presented for the components of the total capacity. The figures following this table show this Q_c/Q_mcomparison for the total capacity and components using the design methods.

- In Figure 4-1, the API method seems to predict total capacity well. The outlier is due to the installation of this pile by jacking.
- Figure 4-2 shows that for OEP's the ICP method seems to under-predict the total capacity.
- Figure 4-3 shows that the API method, on average, provides a good estimate of shaft capacity. However, some results are over-predicted and some are under-predicted.
- Figure 4-4 shows that the ICP method seems to under-predict the shaft friction of OEP's.
- Figure 4-5 shows that there seems to be quite a variation in the predicted base capacity of the API method.
- Figure 4-6 shows that the ICP method, in general, underestimates the base capacity of the OEPs.

Table 4-2 Comparison of estimated and measured component capacities using design methods for OEPs.

Site Number	Site	D (m)	D/t	L/D	Measured Values			API						ICP					
					Total Capacity (kN)	Total Shaft Friction (kN)	Total End Bearing (kN)	Total Capacity (kN)	Total Shaft Friction (kN)	Total End Bearing (kN)	Q_c/Q_m Total Capacity	Q_c/Q_m Total Shaft Friction	Q_c/Q_m Total End Bearing	Total Capacity (kN)	Total Shaft Friction (kN)	Total End Bearing (kN)	Q_c/Q_m Total Capacity	Q_c/Q_m Total Shaft Friction	Q_c/Q_m Total End Bearing
1	Kinnegar	0.168	18.7	36.3	16	10	6	29	24	5	1.85	2.50	0.79	22	20	2	1.40	2.05	0.35
2	Pentre - LDP	0.762	50.8	72.2	5480	4268	1212	8586	8024	562	1.57	1.88	0.46	8057	7595	462	1.47	1.78	0.38
3	Tilbrook - LDP	0.762	25.4	39.4	14900	12985	1915	14677	12709	1967	0.99	0.98	1.03	11074	10437	637	0.74	0.80	0.33
4	Noetsu Bridge[§]	0.800	66.1	10.4	4555	4055	500	5090	3066	2024	1.12	0.76	4.05	-	-	-	-	-	-
5	Kansai Bridge	1.500	68.2	24.7	11800	8900	2900	9871	8104	1767	0.84	0.91	0.61	10713	7707	3007	0.91	0.87	1.04
6	Empire 1*	0.356	29.7	42.7	900	650	250	878	827	52	0.98	1.27	0.21	373	297	77	0.41	0.46	0.31
7	Empire 2	0.356	29.7	42.7	1731	941	790	1416	1337	78	0.82	1.42	0.10	430	297	133	0.25	0.32	0.17
8	Empire 3	0.356	29.7	34.3	1839	1089	750	1451	1355	95	0.79	1.24	0.13	451	263	188	0.25	0.24	0.25
9	Empire 4	0.356	29.7	34.3	2125	995	1130	1696	1586	110	0.80	1.59	0.10	504	270	233	0.24	0.27	0.21
10	Kontich 1	0.610	24.0	33.0	2700	1740	960	3408	2782	626	1.26	1.60	0.65	1422	945	477	0.53	0.54	0.50
11	Kontich 2*	0.610	24.0	38.5	4170	3430	740	4266	3587	679	1.02	1.05	0.92	1706	1229	477	0.41	0.36	0.64
12	West Sole 1	0.762	24.0	7.9	3051	1726	1325	2859	1372	1488	0.94	0.79	1.12	1299	731	568	0.43	0.42	0.43
13	West Sole 2	0.762	24.0	11.8	5471	2642	2829	4146	2350	1796	0.76	0.89	0.63	2512	1549	963	0.46	0.59	0.34
14	West Sole 3	0.762	24.0	15.7	6681	4457	2224	5856	3598	2257	0.88	0.81	1.02	3158	2528	630	0.47	0.57	0.28
15	West Sole 4	0.762	24.0	19.7	6788	4510	2278	6751	4904	1847	0.99	1.09	0.81	3823	3331	492	0.56	0.74	0.22
16	West Sole 5*	0.762	24.0	23.6	8344	6023	2321	8055	6208	1847	0.97	1.03	0.80	4713	3981	731	0.56	0.66	0.32
17	West Sole 6	0.762	24.0	7.9	3051	2438	613	2859	1372	1488	0.94	0.56	2.43	1274	731	543	0.42	0.30	0.89
18	West Sole 7	0.762	24.0	11.8	4706	2873	1833	4146	2350	1796	0.88	0.82	0.98	3055	1549	1506	0.65	0.54	0.82
19	West Sole 8	0.762	24.0	15.7	5533	4466	1067	5856	3598	2257	1.06	0.81	2.12	3513	2528	985	0.63	0.57	0.92
20	West Sole 9	0.762	24.0	19.7	6619	5240	1379	6751	4904	1847	1.02	0.94	1.34	4101	3331	769	0.62	0.64	0.56
21	West Sole 10	0.762	24.0	23.6	8344	6734	1610	8055	6208	1847	0.97	0.92	1.15	5125	3981	1144	0.61	0.59	0.71

§ insufficient data for reliable ICP estimate.

* selected pile test which most represents site.

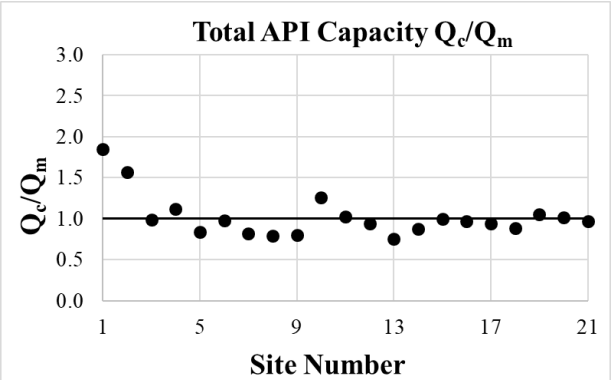

Figure 4-1 Comparison of the Q_c/Q_m of the total capacity using the API design method.

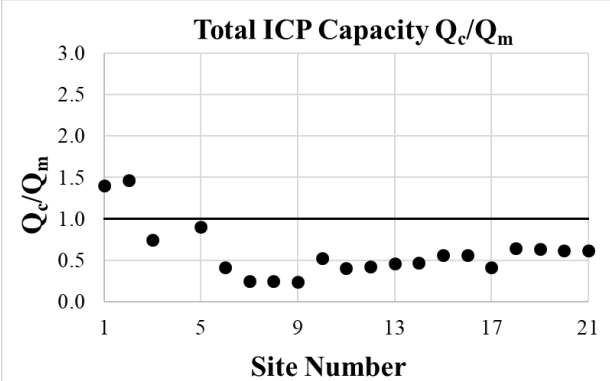

Figure 4-2 Comparison of the Q_c/Q_m of the total capacity using the ICP design method.

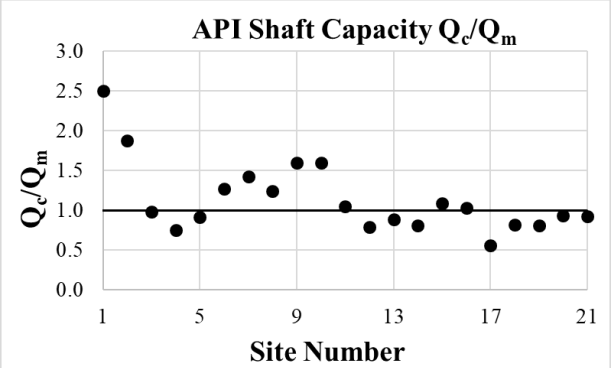

Figure 4-3 Comparison of the Q_c/Q_m of the shaft capacity using the API design method.

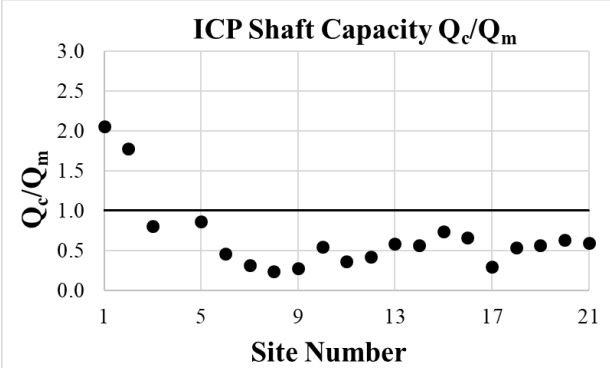

Figure 4-4 Comparison of the Q_c/Q_m of the shaft capacity using the ICP design method.

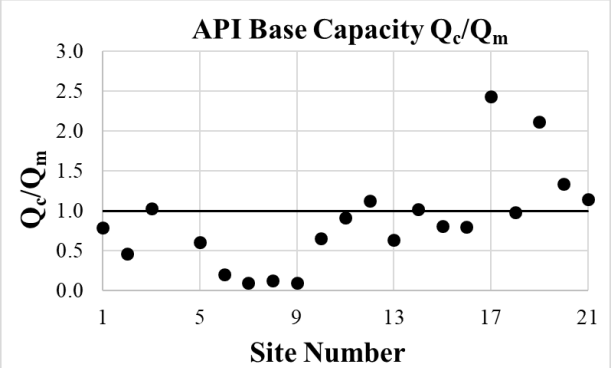

Figure 4-5 Comparison of the Q_c/Q_m of the base capacity using the API design method.

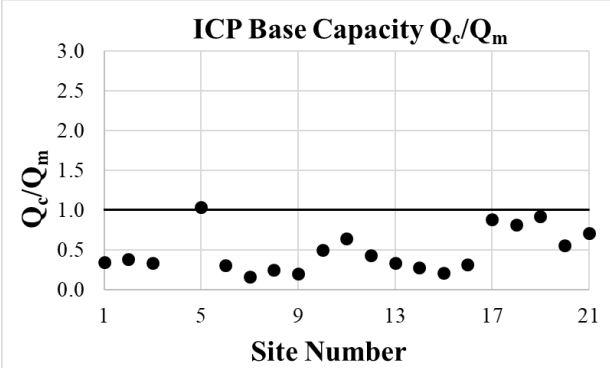

Figure 4-6 Comparison of the Q_c/Q_m of the base capacity using the ICP design method.

The mean, standard deviation and coefficient of variation for the analysis were computed and are shown in Table 4-3. This data summarises the results presented in Figure 4-1 to Figure 4-6. With the API method used directly, this method best estimates the average of the total capacity for the selected OEP's. The distribution of the capacity to the shaft and end bearing are also well averaged, although the variation is relatively quite high, especially that of the base component.

Table 4-3 Mean and standard deviation of Q_c/Q_m for the OEP validation database.

Statistic	API			ICP		
	Total Force Estimated	Shaft Friction	Total End Bearing	Total Force Estimated	Shaft Friction	Total End Bearing
μ	1.020	1.136	1.020	0.601	0.665	0.483
σ	0.261	0.453	0.910	0.331	0.464	0.265
COV	0.256	0.399	0.892	0.550	0.697	0.549

4.2.1. RMS-Error Test Specific

Based on the data available, the error in each calculation from the measured results were computed. Only one of the sites provides a value of the mobilised end bearing of the open-ended pile due to the use of the double-walled pile. This, however, is not entirely applicable as the results were extracted during the jacking process of the pile to its final depths (Site 1).

To determine the RMS-error, several stages are involved. The difference between the calculated values (Q_c) and the measured values (Q_m) is initially found. If the difference is small, this corresponds to a good estimation of the measured value. The difference is then normalised by the measured value and squared, thus proportionately enhancing the error and relating it to unity. This process was done for each site, and the square-root taken of the average sum of the squares, which gave the RMS-error for the values directly estimated by the design method. Incremental factors were then applied to the estimated end bearing and shaft friction from these design methods for each test. This procedure led to a number of values that are best displayed using a contour plot. Using this plot, the combination of factors that achieve the lowest variation to the measured value can be easily identified. If the method itself causes divergence, thereby preventing the point of lowest variation to be identified, this procedure is not applicable to the design method. Equation (62) describes the above procedure to determine the RMS-error. N is the number of sites in this expression.

$$RMS\ Error = \sqrt{\frac{\sum_1^N \left(\frac{Q_c - Q_m}{Q_m}\right)^2}{N}} \tag{62}$$

The plots in Figure 4-7 and Figure 4-8 show the contours of these RMS-errors, for the API and ICP methods respectively, plotted against the associated combination of shaft and end bearing factors.

These were derived from a specifically written MATLAB program which allows greater refinement of the factors applied.

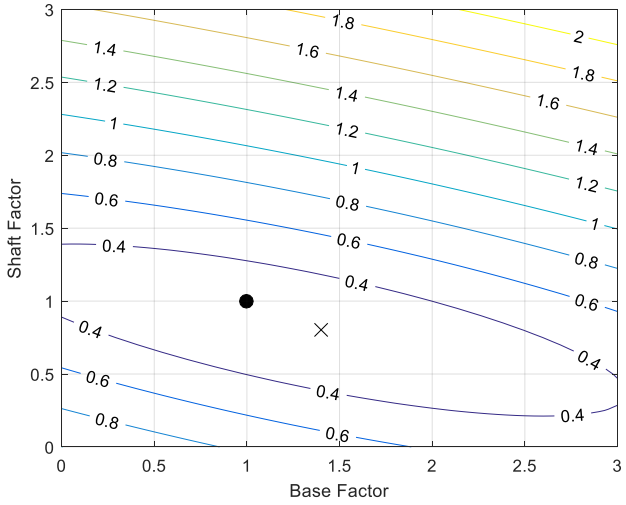

Figure 4-7 Contour Plot of the RMS-error for the API design method using OEPs.

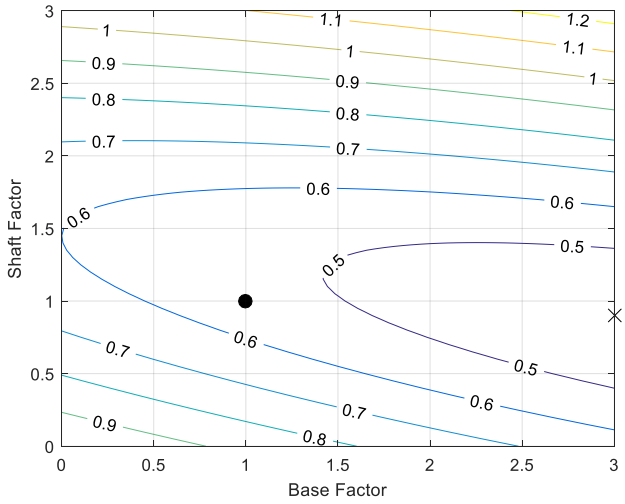

Figure 4-8 Contour Plot of the RMS-error for the ICP design method using OEPs.

In these diagrams the solid circle represents the point where a factor of unity is applied to the derived base or shaft capacity components. The position of the "×" identifies where the combination of factors on both components minimises the RMS-error.

As can be seen from Figure 4-7, the API method generally gives a better estimate of both component contributions, although it overestimates the shaft friction and underestimates the end bearing in OEPs. To reduce the RMS-error, a factor of 0.8 is required on the shaft friction and 1.4 on the base resistance. In Figure 4-8, by using the ICP method, the shaft capacity is again, in general, overestimated with a factor of 0.9 required to give the lowest variation of RMS-error. The base capacity however, is highly underestimated requiring a factor of 3.0 to reduce the error in OEPs. For the end bearing in the ICP method, this large variation is possibly due to the distribution of the shaft and base using the ICP method.

4.2.2. RMS-Error Site Specific

From Table 4-2, there are sites with more than one pile tests and with the inclusion of these, this has the effect of skewing the results. To investigate the effects of omitting these tests, the database is limited to a single pile test per site, choosing the longest pile as the most representative test for each. This new list is presented in Table 4-4.

Table 4-4 Reduced database choosing single pile test per site.

Site	Location	Pile Test Number	Reference Authors	Type of CLAY
Kinnegar	Belfast Lough, N. Ireland	UCD-OE-3	Doherty et al. (2010)	Belfast Sleech
Pentre - LDP	Pentre	LDP	Gibbs et al (1992)	Glacial Deposits
Tilbrook - LDP	Tilbrook	LDP	Gibbs et al (1992)	Lowestoft Till, Oxford Clay
Noetsu Bridge	Noto Peninsula, Japan	T2	Matsumoto et al. (1995)	Noetsu Clay
Kansai Bridge	Osaka Bay, Japan	T1	Matsumoto et al. (1992)	Osaka Bay Clay
Empire 1	Louisiana, USA	1	Cox and Kraft (1979)	Empire Clay
Kontich 2	Kontich, Belgium	2 (77')	Hereema (1979)	Belgium Boom Clay
West Sole 5	North Sea, UK	B 18m	Clarke et al (1985)	Boulder Clay, Lias Clay

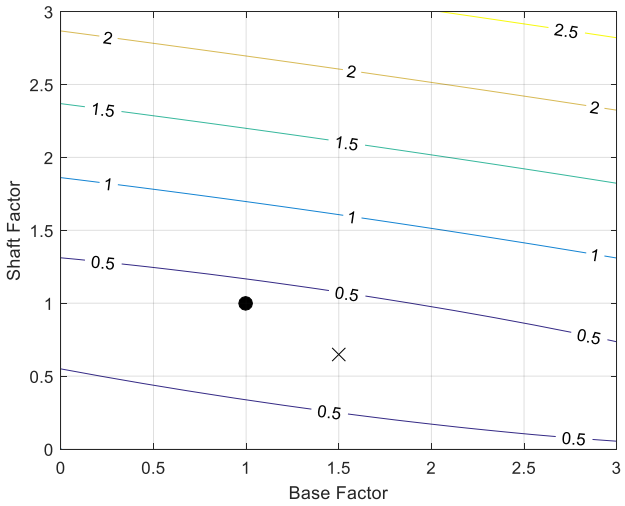

Figure 4-9 Contour Plot of the RMS-error for the API design method using OEPs.

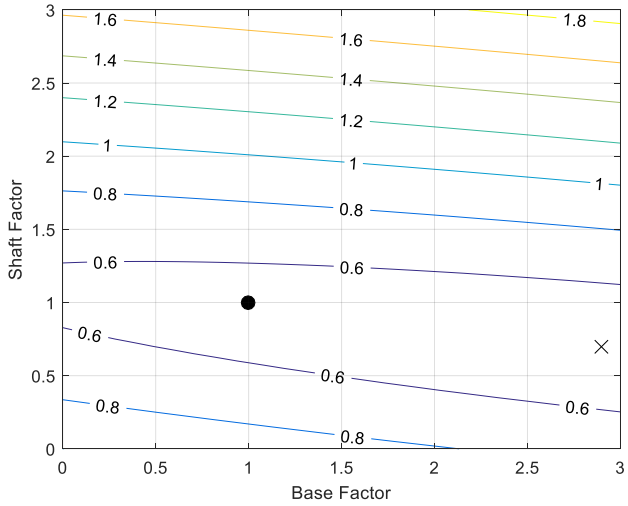

Figure 4-10 Contour Plot of the RMS-error for the ICP design method using OEPs.

From these results, the error remains large and essentially quite similar to those with the full list of test results. Here in general, the shaft capacity is again overestimated and the base capacity is underestimated in both methods in OEPs. To reduce the RMS-error using the API method, the application of a factor of 0.65 on the shaft friction and 1.5 on the base resistance is required; and by using the ICP method, a factor of 0.7 is required on the shaft friction and 2.9 on the base resistance. Due to the large error observed in the RMS-error results, these factors will not be taken forward in the analysis. This can be attributed to the variability of the soils, the method of interpreting the base capacity and the assumptions taken in the design methods.

4.3. Analysis Comparisons of Selected OEP Test Sites in Clays

The ICP design method (Jardine *et al.*, 2005) computes the ultimate capacity by applying knowledge of soil behaviour derived from sample and field testing. The results from these tests have been analysed and correlated to estimate the ultimate pile capacity using the ICP database (Chow, 1997).

This database consists of several tests on open and closed-ended piles, tested in tension and compression. The resulting method shows marked improvement in the estimation of total capacity using the full ICP database. The analysis previously shown however, demonstrates that for open-ended piles, the API is on average better at estimating the total capacity and the distribution of the shaft and end bearing capacity in both methods, can be improved.

Due to the lack of a high-quality database of instrumented OEPs, conservative estimates, that in general give acceptable results, are usually adopted with factors of safety applied to ensure that unknowns are accounted for (API RP 2GEO, 2011). Due to the obvious difficulty in the estimation of the mobilised contribution of all factors under a prescribed load, a more elegant solution is required. One of the more effective means of achieving this, is using a finite element procedure as outlined in Chapter 3. To test this procedure accurately, a large number of input parameters are required. Of all the published test sites listed in Table 4-1, only the Pentre and Tilbrook case studies have sufficient detailed information to enable this process. The shaft and end bearing parameters derived from the API and ICP methods are input into the finite element procedure to implement the API-FEA and ICP-FEA methods respectively. These results are then compared with those measured during the pile tests at both sites as outlined in Clarke *et al.* (1992).

4.3.1. Specifics on Test Cases

The results of the analyses are presented separately for each of the two sites and parameters varied individually to observe the effects and note the sensitivity of the change on the results. From these analyses, key recommendations will then be extracted and taken forward to Chapter 6 where a new modified finite element design method for OEPs in clays will be deduced. The results of these comparisons are presented in the following sections using the capability of the FE program to isolate the effects on the resistive components of the pile. An initial table is presented at the start of the API and ICP analyses which sets out the test cases being considered. The headings of this table include:

- **Case:** The test case number being considered.
- **Design Method:** The variant of the API-FEA or ICP-FEA design methods being adopted.
- **Constitutive Model, τ_{int} & τ_{ext}:** the stress-strain relationship, or stiffness, of the external soil

reaction curves. These are derived from the API RP 2GEO (2014) or DNV (2010) and τ_{ult} = $0.8\tau_{peak}$.

- $\tau_{ult} = \tau_{int}$ **&** τ_{ext}**:** the ultimate value of the local shear stress at failure in the soil layer. The ultimate value is equal on both sides of the pile but mobilised at different rates.
- z_{peak}/D_i**:** the ratio of the relative displacement to D_i where the maximum value of τ_{int} occurs.
- z_{peak}/D_o**:** the ratio of the relative displacement to D_o where the maximum value of τ_{ext} occurs.
- **Constitutive Model,** $q_{b,p}$**:** the stress-strain relationship of the base of the pile. This relationship has been derived from the slope of the Q-z curves outlined in the API RP 2GEO (2014) where the stiffness is related to the full base diameter, D_o. In this study however, this is normalised by t.
- $q_{b,p}$**:** the ultimate value of the resistance at the base of the pile.
- **Constitutive Model,** $q_{b,pl}$**:** the stress-strain relationship of the base of the plug. This relationship has also been derived from the slope of the Q-z curves outlined in the API RP 2GEO (2014) where the axial pile stiffness is related to the full base diameter, D_o. In this study however, this is normalised by D_i.
- $q_{b,pl}$**:** the ultimate value of the resistance at the base of the plug.
- M**:** the value or method of deriving the constrained modulus of the plug.
- **EB Type:** In these analyses, the end bearing is modelled using either piles with uniform thickness for its entire length or with the use of base plates positioned at the bottom of the channels to protect the instrumentation.
- **Weight:** if the weight of the pile and plug are included in the analysis.

4.3.2. Test Cases

4.3.2.1. API-FEA Analyses (Cases 1 to 10)

The API-FEA method is initially examined. In this section, the FE procedure therefore assumes the API parameters deduced from the Pentre and Tilbrook sites to derive the mobilised shaft resistance, end bearing and total capacity. Case 1 is the base case for the API-FEA method. Variations to these

cases are performed to assess the impacts on the estimated response. The analysis cases performed are outlined in Table 4-5, with the main change to the base case highlighted in blue.

Table 4-5 Details of API Analyses.

Case	Design Method	Constitutive Model: τ_{int} & τ_{ext}	τ_{ult} = τ_{int} & τ_{ext}	z_{peak}/D_i	z_{peak}/D_e	Constitutive Model: $q_{b,pile}$	$q_{b,pile}$	Constitutive Model: $q_{b,plug}$	$q_{b,plug}$	M	EB Type	Weight
1	API	API t-z curves, 20% residual	$\tau_{ext,ult}=\tau_{int,ult}$	0.0001	0.01	API Q-z to 1.0WT	N_cS_u	API Q-z, Q_{max} at $0.1D_i$	N_cS_u	G_{vv}	[1] OEP	No
2	API	API t-z curves, 20% residual	$\tau_{ext,ult}=\tau_{int,ult}$	0.100	0.01	API Q-z to 1.0WT	N_cS_u	API Q-z, Q_{max} at $0.1D_i$	N_cS_u	G_{vv}	OEP	No
	API	API t-z curves, 20% residual	$\tau_{ext,ult}=\tau_{int,ult}$	0.010	0.01	API Q-z to 1.0WT	N_cS_u	API Q-z, Q_{max} at $0.1D_i$	N_cS_u	G_{vv}	OEP	No
	API	API t-z curves, 20% residual	$\tau_{ext,ult}=\tau_{int,ult}$	0.001	0.01	API Q-z to 1.0WT	N_cS_u	API Q-z, Q_{max} at $0.1D_i$	N_cS_u	G_{vv}	OEP	No
3	API	API t-z curves, 20% residual	$\tau_{ext,ult}=\tau_{int,ult}$	0.0001	0.0025	API Q-z to 1.0WT	N_cS_u	API Q-z, Q_{max} at $0.1D_i$	N_cS_u	G_{vv}	OEP	No
	API	API t-z curves, 20% residual	$\tau_{ext,ult}=\tau_{int,ult}$	0.0001	0.0050	API Q-z to 1.0WT	N_cS_u	API Q-z, Q_{max} at $0.1D_i$	N_cS_u	G_{vv}	OEP	No
	API	API t-z curves, 20% residual	$\tau_{ext,ult}=\tau_{int,ult}$	0.0001	0.02	API Q-z to 1.0WT	N_cS_u	API Q-z, Q_{max} at $0.1D_i$	N_cS_u	G_{vv}	OEP	No
4	API	API t-z curves, 20% residual	$\tau_{ext,ult}=\tau_{int,ult}$	0.0001	0.01	API Q-z to 0.1WT	N_cS_u	API Q-z, Q_{max} at $0.1D_i$	N_cS_u	G_{vv}	OEP	No
5	API	API t-z curves, 20% residual	$\tau_{ext,ult}=\tau_{int,ult}$	0.0001	0.01	API Q-z to 1.0WT	[2] $N_c'S_u$	API Q-z, Q_{max} at $0.1D_i$	$N_c'S_u$	G_{vv}	OEP	No
	API	API t-z curves, 20% residual	$\tau_{ext,ult}=\tau_{int,ult}$	0.0001	0.01	API Q-z to 1.0WT	$0.65q_c$	API Q-z, Q_{max} at $0.1D_i$	$0.2q_c$	G_{vv}	OEP	No
	API	API t-z curves, 20% residual	$\tau_{ext,ult}=\tau_{int,ult}$	0.0001	0.01	API Q-z to 1.0WT	$1.6q_c$	API Q-z, Q_{max} at $0.1D_i$	$0.2q_c$	G_{vv}	OEP	No
6	API	API t-z curves, 20% residual	$\tau_{ext,ult}=\tau_{int,ult}$	0.0001	0.01	API Q-z to 1.0WT	N_cS_u	API Q-z, Q_{max} at $1.0D_i$	N_cS_u	G_{vv}	OEP	No
7	API	API t-z curves, 20% residual	$\tau_{ext,ult}=\tau_{int,ult}$	0.0001	0.01	API Q-z to 1.0WT	N_cS_u	API Q-z, Q_{max} at $0.1D_i$	N_cS_u	K_{water}	OEP	No
	API	API t-z curves, 20% residual	$\tau_{ext,ult}=\tau_{int,ult}$	0.0001	0.01	API Q-z to 1.0WT	N_cS_u	API Q-z, Q_{max} at $0.1D_i$	N_cS_u	[3] kS_u	OEP	No
8	API	API t-z curves, 20% residual	$\tau_{ext,ult}=\tau_{int,ult}$	0.0001	0.01	API Q-z to 1.0WT	N_cS_u	API Q-z, Q_{max} at $0.1D_i$	N_cS_u	G_{vv}	[4] Inner plates	No
9	API	API t-z curves, 20% residual	$\tau_{ext,ult}=\tau_{int,ult}$	0.0001	0.01	API Q-z to 1.0WT	N_cS_u	API Q-z, Q_{max} at $0.1D_i$	N_cS_u	G_{vv}	OEP	Yes
	API	API t-z curves, 20% residual	$\tau_{ext,ult}=\tau_{int,ult}$	0.0001	0.01	API Q-z to 1.0WT	N_cS_u	API Q-z, Q_{max} at $0.1D_i$	N_cS_u	G_{vv}	OEP	Yes + Plug Weight
10	API	API t-z curves, measured residual	$\tau_{ext,ult}=\tau_{int,ult}$	0.0001	0.01	API Q-z to 1.0WT	N_cS_u	API Q-z, Q_{max} at $0.1D_i$	N_cS_u	G_{vv}	OEP	No

[1] open-ended pile where, $\tau_{int} = \tau_{ext}$.
[2] N_c is taken as 9, but to match the measured data, N_c' is 15.8 and 8.85 for Pentre and Tilbrook respectively.
[3] k ranges from 500 to 2000 for FE convergence.
[4] open-ended pile with channel covers offset from base.

Case 1: This API-FEA sets out the base case in which subsequent API analyses are varied.

The results are displayed in the figures below where dotted lines represent values computed using the API-FEA method and solid lines represent those measured.

Pentre Site Results:

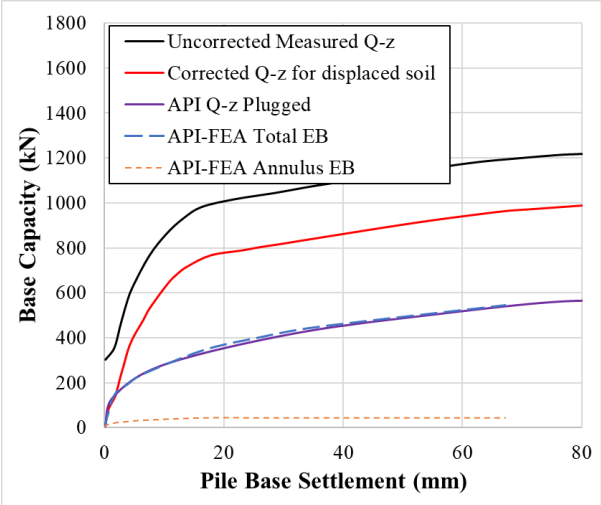

Figure 4-11 API-FEA estimation of pile base settlement vs measured load.

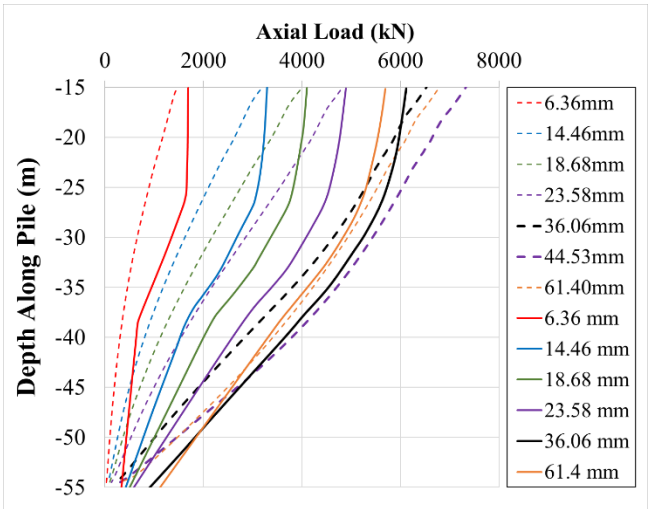

Figure 4-12 Axial load distribution in pile, API-FEA estimation vs measured.

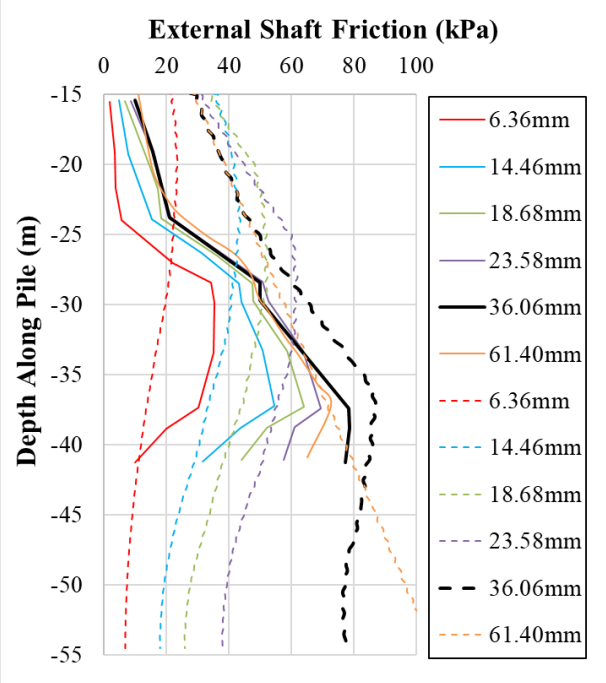

Figure 4-13 Shaft friction along pile, API-FEA estimation vs measured.

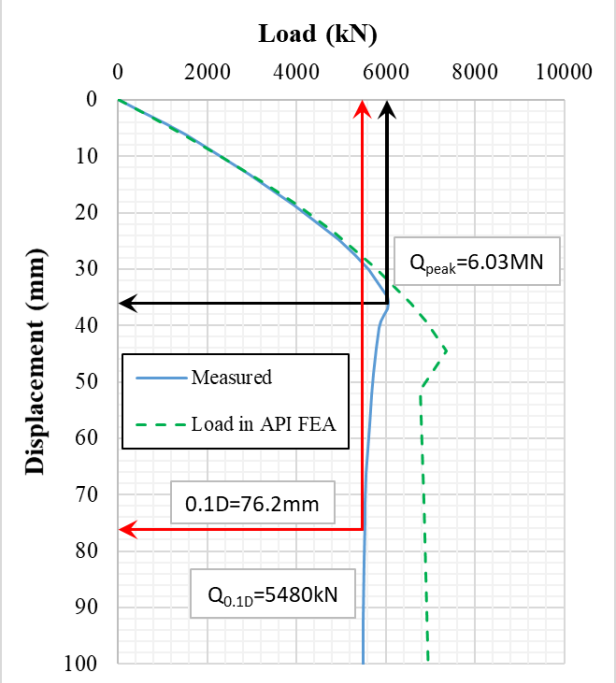

Figure 4-14 Load-displacement curve for API-FEA estimation against measured.

Figure 4-11 shows the measured end bearing results (Uncorrected Measured Q-z), interpreted corrected values (Corrected Q-z for displaced soil), Q-z curve derived from the API method which deduced a plugged pile (API Q-z Plugged), the estimated total Q-z response from the API-FEA (API-FEA Total EB) and estimated annular Q-z response from the API-FEA (API-FEA Annulus EB). The base capacity at the peak load was measured as 860kN mobilised at a pile-head displacement of 10mm (1.5%D_o). End bearing continued to increase after the peak was mobilised, but at a slower rate, possibly due the mobilisation of the plug EB capacity. At a pile-head displacement of 0.1D_o, an

annular displacement of 20mm was achieved with the measured base capacity estimated at 1,000kN. At the end of the test, the base load was measured at 1,220kN. The base response is observed to be generated by a combined response of the annulus and the plug. When using the API method directly, it was estimated that the Pentre pile behaves in a plugged manner under static loading. Adopting the base resistances associated with this assumption and separating the mobilisation of the annulus and that of the plug, the results indicate that the soil plug contributes most of the base capacity. Although N_c = 9 is recommended in the API, a larger value of $N_c \approx 16$ was estimated (by Gibbs *et al.*, 1992) to match the corrected base capacity at this site. Additionally, Gibbs *et al.* (1992) deduced that a reduction of the end bearing was necessary to cater for the soil displaced by the installation of the pile. This reduction was computed as the product of A_p and σ'_{v0} at the pile base which gave the authors' 'corrected' Q-z curve. Realistically this may have been due to a combination of factors including the residual stress in the pile after installation (about 300kN) and the increased annular area due to the covers of the instrument channels.

Figure 4-12 shows the comparison between the measured and estimated load along the pile at various pile head displacements. This shows that by using the API-FEA method, the estimated loads along the pile shaft, as a result of the pile interaction with the internal and external soil are quite well matched for these tests.

Shaft friction along the pile was deduced from the measured strains. These measurements are compared to the estimated values obtained from the API-FEA methodology and as shown in Figure 4-13, the pre- and post-peak external shaft friction is not perfectly estimated by this procedure in the top 10m of the pile but significantly improves afterwards. As load continues to be applied, strain softening occurs, and peak capacities of the deeper soil layers are mobilised. This cannot be verified however, due to the lack of measured data at these depths.

From Table 4-2, the total capacity calculated by the API method directly is 8,586kN. The peak load observed during the pile test was 6,031kN, at 36.06mm (a pile-head displacement, $0.05D_o$), as shown on Figure 4-14, with a residual load of 5,480kN at $0.1D_o$. The peak from the API-FEA was 7,358kN (Q_c/Q_m=1.2) reducing to a residual of 6,882kN (Q_c/Q_m=1.3). The computed residual continued to

increase as the capacity of the plug base increased. However, the measured capacity continued to decrease as further load was applied. Observing that the measured base continuously increased, suggests that along the shaft, more layers were mobilising ultimate resistances contributing to an overall reduction in capacity.

Tilbrook Site Results:

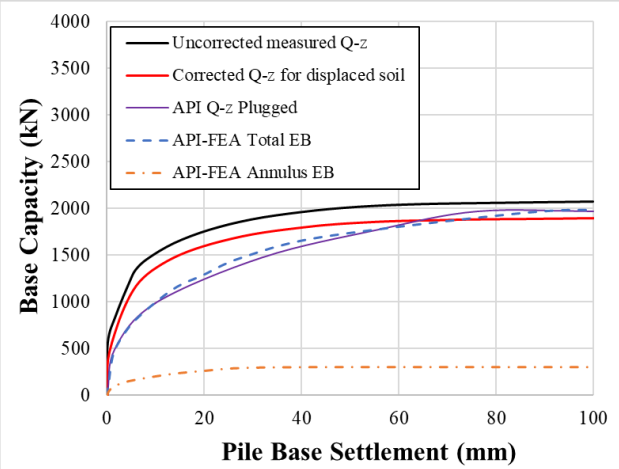

Figure 4-15 API-FEA estimation of pile base settlement vs measured load.

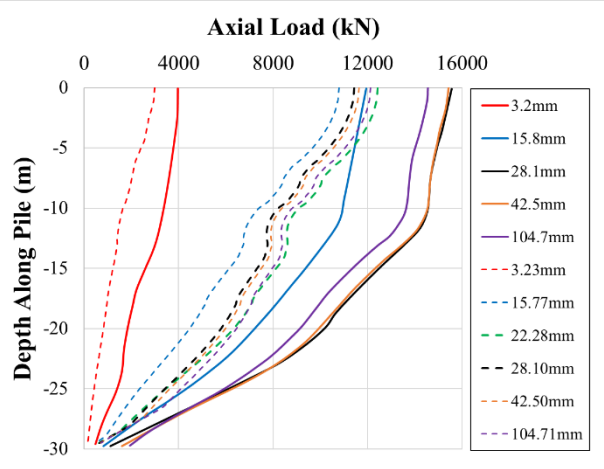

Figure 4-16 Axial load distribution in pile, API-FEA estimation vs measured.

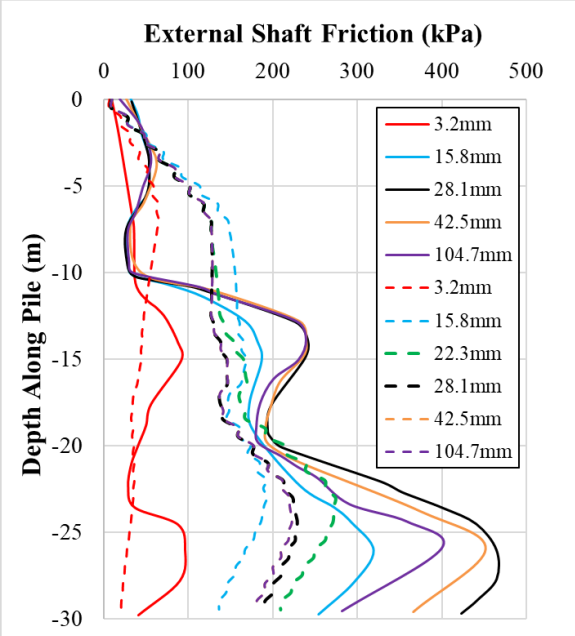

Figure 4-17 Shaft friction along pile, API-FEA τ_{ext} estimation vs measured.

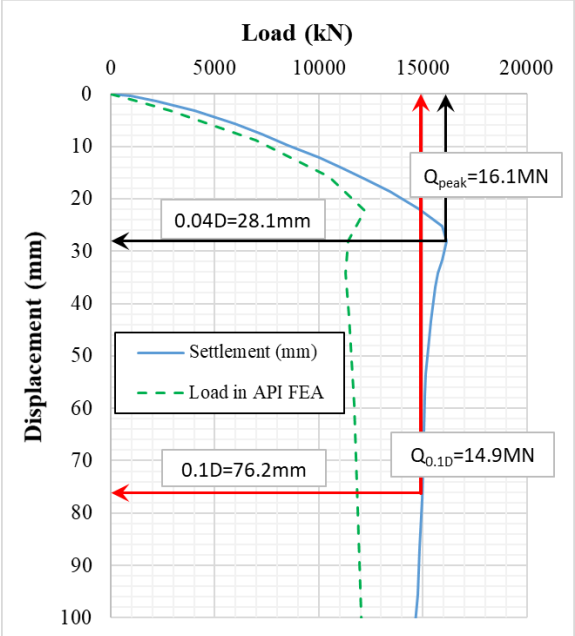

Figure 4-18 Load-displacement curve for API-FEA estimation against measured.

In Figure 4-15, the measured end bearing was 2,075kN, and this was corrected, in a similar method as the Pentre pile (see discussion for Figure 4-11), to 1,880kN at a pile base displacement of 76mm ($0.1D_o$). The direct API analysis predicts a fully plugged pile for this test case. In Figure 4-15, the plug is shown to support a much larger capacity than the annulus, with a distribution of 1,670kN and

298kN between plug and annulus, respectively. The total estimated capacity (1,968kN) mobilised, corresponds very well to the measured response. As q_b is deduced from $N_c s_u$, these results indicate that N_c = 9 is applicable. Interestingly, at peak load, the measured value of base capacity was 1,450kN, (corrected, for the soil displaced by the installation of the pile, to 1,300kN) at 8.6mm displacement ($0.01D_o$). This was also a trend observed at the Pentre tests.

The predictive capability of the API-FEA method for the axial load estimated in the pile in this Tilbrook analysis is not as good as observed in that at Pentre (Figure 4-16). Here estimated values are much less than those measured.

Figure 4-17 shows the comparison between the externally mobilised shaft friction and the measured values, showing that the shaft resistance is overestimated in the shallow layers and underestimated in the deeper layers. The resistance measured at the base of the pile (~420kPa) is almost 50% of that estimated by the API-FEA method. This difference may be addressed by the addition of τ_{int} to τ_{ext} to obtain the total mobilised shaft friction to perform the comparison with the measured results.

In terms of capacity, the peak capacity at Tilbrook was measured as 16,130kN at a pile-head displacement equal to 28.1mm ($0.04D_o$), as shown in Figure 4-18. The peak load mobilised by the API-FEA is 12,427kN (Q_c/Q_m of 0.77). The ratio of Q_c/Q_m for the ultimate axial load after a pile-head displacement of $0.1D_o$, is 0.80 (11,958kN/14,900kN).

Case 2: In this case the effects of a variation of the interface stiffness is investigated for clays.

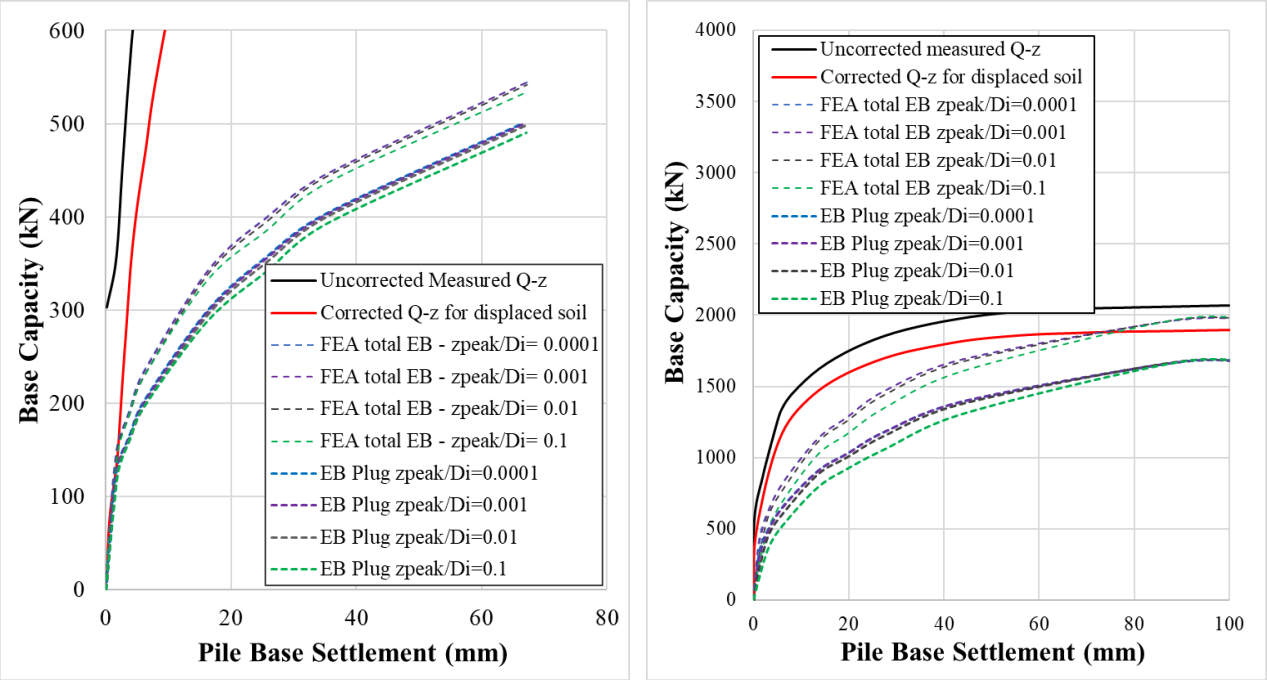

(a) Pentre results. **(b) Tilbrook results.**

Figure 4-19 Comparison of the base capacity mobilisation due to a varies interface stiffness using the API RP 2GEO (2011).

As there are no direct measurements of the internal load transfer, the effect of a variation of the interface stiffness on the estimated base response is investigated. With this variation, Figure 4-19 shows that in all cases, the higher the interface stiffness (i.e. the lower the value of z_{peak}/D_i) the better the match with the measured data. This is observed to increase the initial stiffness due to a more rapid mobilisation of the τ_{int} along the plug engaging the base resistance sooner. From these results, when z_{peak}/D_i =0.0001, the best match is found.

Case 3: In this case the displacement to peak of the t-z curves are varied. The peak resistance on tested piles has been found to range from $0.0025D_o$ to $0.02D_o$ displacement (DNV-OS-J101, 2016). For design however, this is usually taken to occur at $0.01D_o$ (API RP 2GEO, 2011). The pile response when displacements to peak mobilised load occur at $0.0025D_o$, $0.005D_o$, and $0.02D_o$, are used to investigate the effects on the pile response at both sites.

By adopting this variation at both the Pentre and Tilbrook sites, by increasing the displacement, this increases the mobilised peak and reduces the initial stiffness, as shown in Figure 4-20 (a and b),

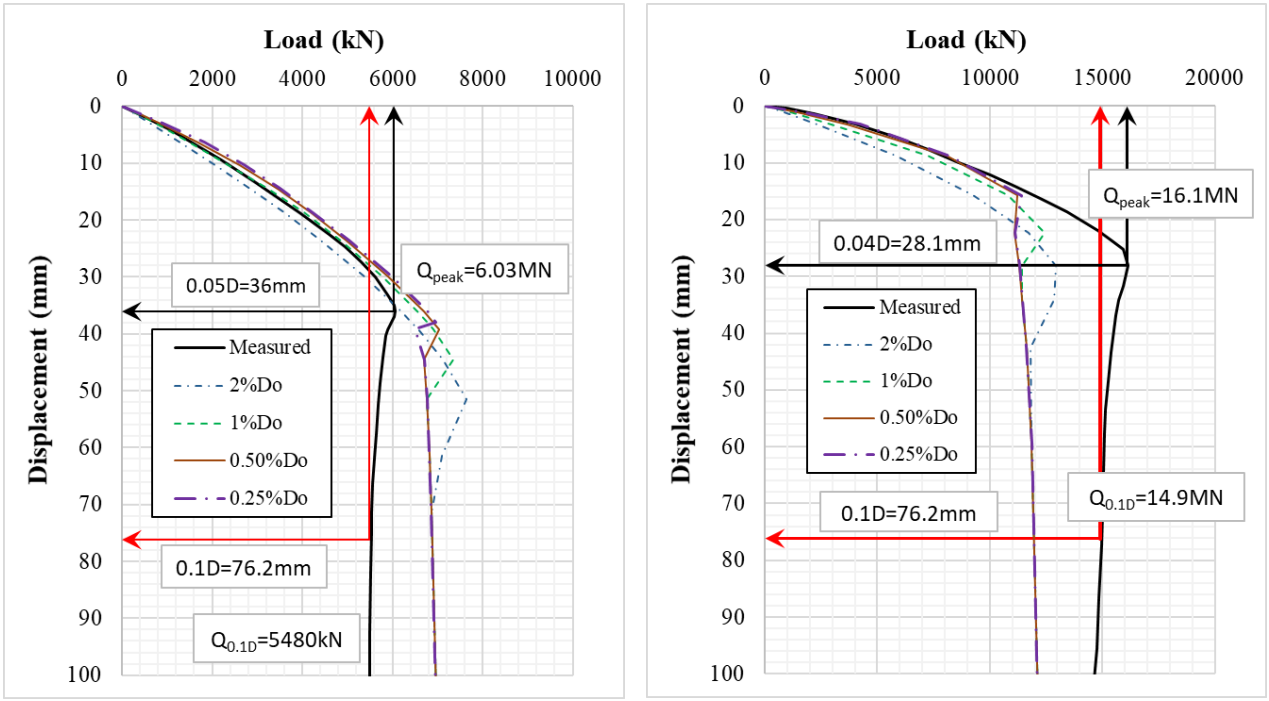

(a) Pentre results. **(b) Tilbrook results.**

Figure 4-20 Comparison of the load-displacement responses for range of t-z curves with τ_{max} from the API RP 2GEO (2011).

The results also show that the estimated responses do eventually converge to a common response after as the differing rates of shaft resistance mobilisation eventually converge to their ultimate values.

<u>Case 4</u>: Here the response of the end bearing resistance to a change in its stiffness below the annulus is investigated. Full mobilisation is set to occur at a pile base displacement of $0.1t$ as opposed to the base case which uses $1.0t$.

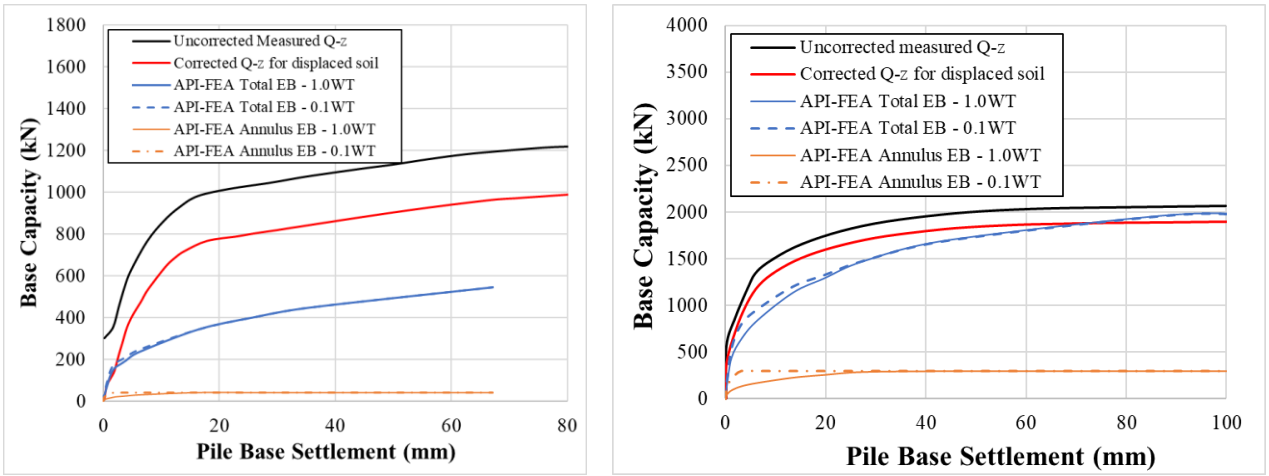

(a) Pentre results. **(b) Tilbrook results.**

Figure 4-21 API-FEA estimation of pile base settlement vs measured load adopting different displacements to achieve peak values.

As shown in Figure 4-21, as a result of choosing the stiffer initial response of the annulus, the estimated base response is much stiffer and tends to now be more representative of the measured values at both sites using the API-FEA method.

Case 5:

(a) In this case the value of N_c was changed from 9 to that estimated from the "corrected" values derived from the pile testing. This was found to be 15.8 for the Pentre site and 8.85 for the Tilbrook pile.

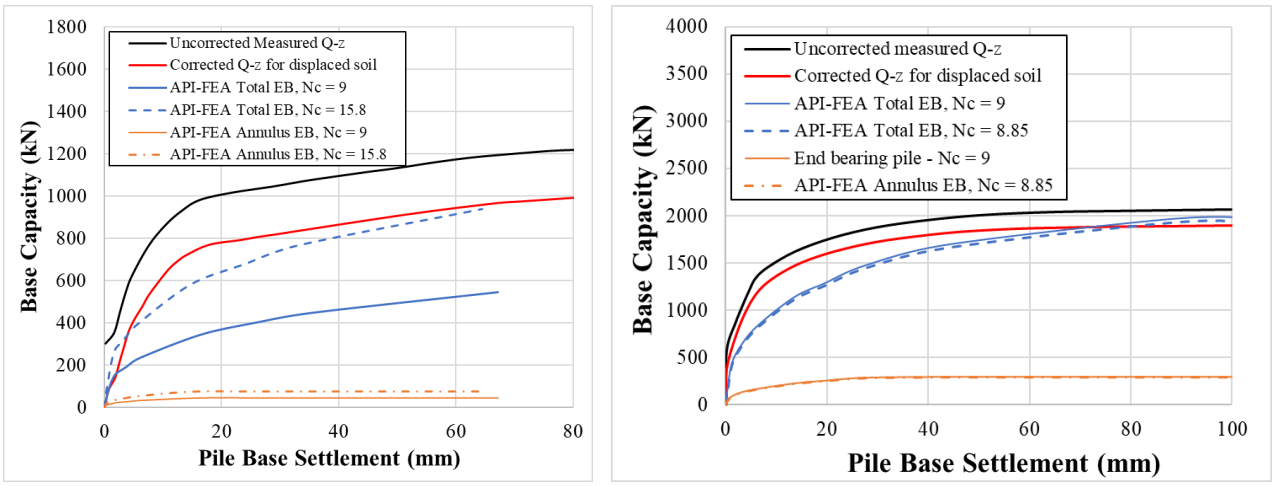

(a) Pentre results. **(b) Tilbrook results.**

Figure 4-22 API-FEA estimation of pile base settlement vs measured load adopting measured values of N_c.

As shown in Figure 4-22a for the Pentre site, using the new value of N_c, the overall base response is much more aligned to the corrected measurements after a pile head displacement of $0.1D_o$. The response is however observed to be softer. The same can be suggested for the results at the Tilbrook site (Figure 4-22b) where the modified value of N_c was used. The results here show values that are quite comparable to those estimated, noting that the adopted value was approximately 9. This may suggest that for OEPs, the value of N_c to adopt for highly over-consolidated clays is 9, this however, may be larger for NC clays.

(b) If API design parameters were applied along the shaft and a relationship factoring the measured values of q_c applied to the base, an alternative method of deriving the axial response is found. Figure 4-23 shows the variation in the base response, compared to the base case, as a result of

this process. Chow (1997) showed the variation of base resistance below the annulus and this was estimated to range considerably from about $0.65q_c$ from most of the tests, $4q_c$ at Pentre and $>8q_c$ at Noetsu. This is quite a wide range and to derive the ICP method, 0.65 was the factor on q_c adopted for undrained soils and 1.6 for drained soils. Both of these cases are considered in the figures and their effectiveness in estimating the measured response is observed. In addition, the base resistance of the plug is taken as $0.2q_c$ as per Doherty *et al*. (2014), due to the similarity of the resistance at the base of the plug and that below a bored pile.

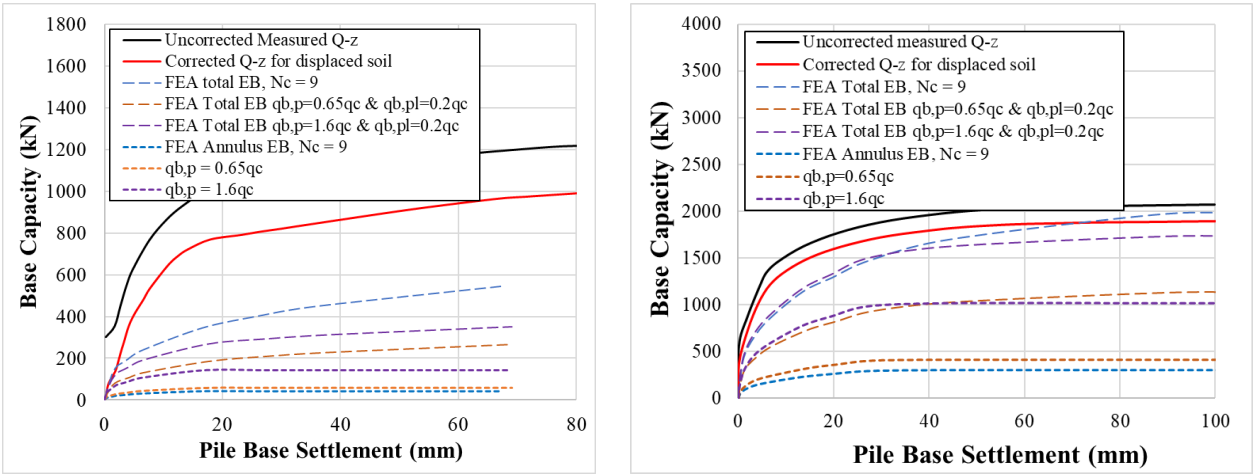

(a) Pentre results. **(b) Tilbrook results.**

Figure 4-23 Modification of API-FEA estimation adopting factored values of q_c to derive the end bearing settlement compared to measured load.

The results from Pentre show that these factors on q_c are not sufficient to estimate the measured response, however at Tilbrook, the factors seem adequate. This suggests that the soil types may need an additional factor to cater for their different consolidation states.

Case 6: Here the stiffness of the end bearing on the plug is analysed to identify if improved results are observed if its stiffness decreases. In this case, full mobilisation is set to occur at a pile base displacement of $1.0D_i$ as opposed to the base case which uses $0.1D_i$.

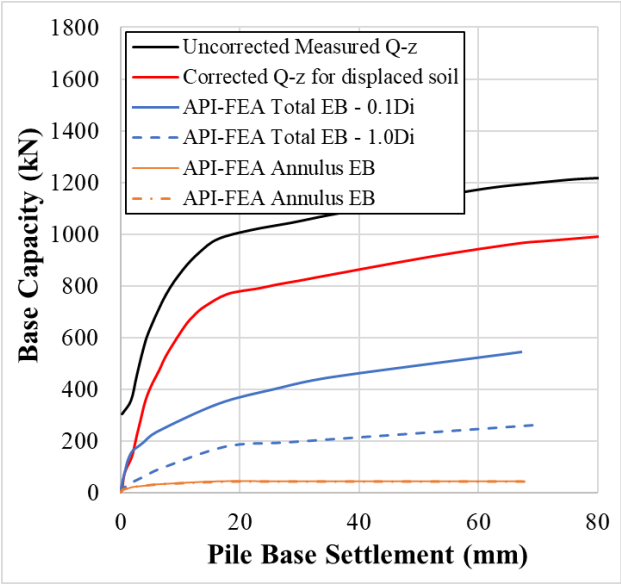

(a) Pentre results.

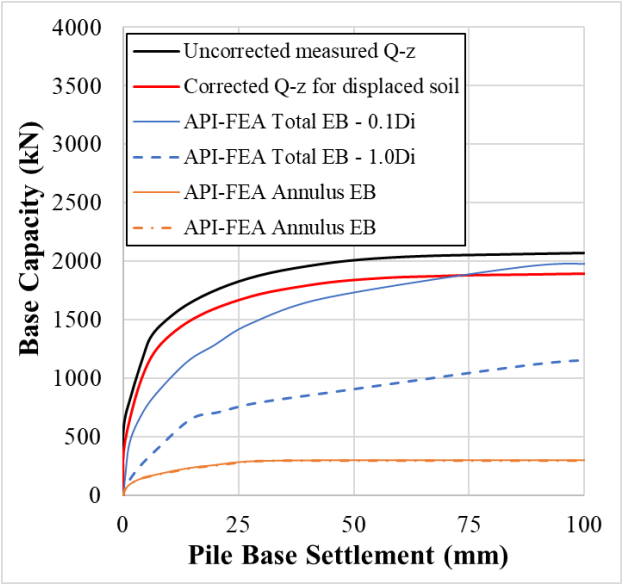

(b) Tilbrook results.

Figure 4-24 API-FEA estimation of pile base settlement vs measured load adopting different displacements to achieve peak values.

As shown in Figure 4-24 (a & b), as a result of selecting the softer initial response of the plug base, the response of the pile base is the same, but the estimated total base response is much lower and tends away from being representative of the measured values at both sites using the API-FEA method.

Case 7: In this case, the constrained modulus, M, is determined from two sources: the bulk modulus of seawater, K, taken as 2,340,000kPa; and a factored value of undrained shear strength, ks_u. $M = K$ is adopted as an upper-bound value which may occur if solely, the pore water within the full clay plug was mobilised under the action of an axial load. When $M = ks_u$, this is intended to test the range that an easily available parameter for clay can be factored to best represent the plug behaviour.

Pentre Site Results:

The results of these analyses observed that for the case of $M=ks_u$, the smallest value of k that allows convergence with the data is 2000. This suggests that with smaller values of M, there was a mis-match of component stiffness.

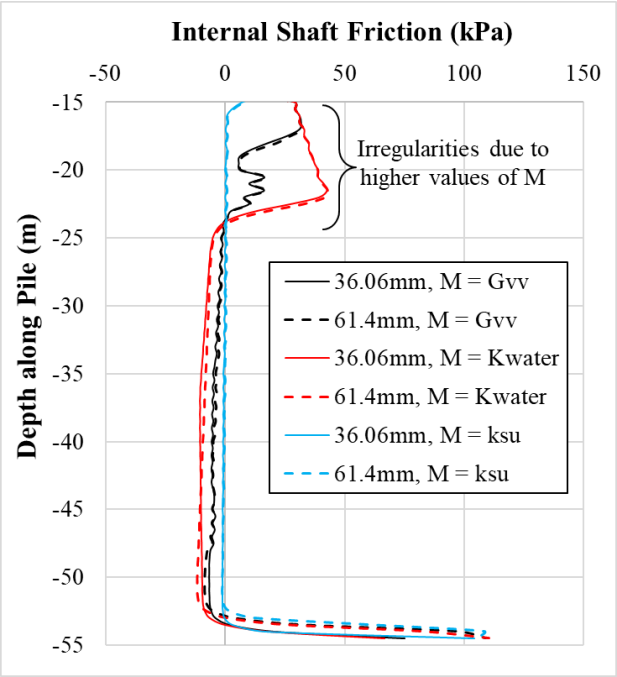

Figure 4-25 API-FEA estimated internal shaft friction along pile, with $M = G_{vv}$, K_{water} & ks_u.

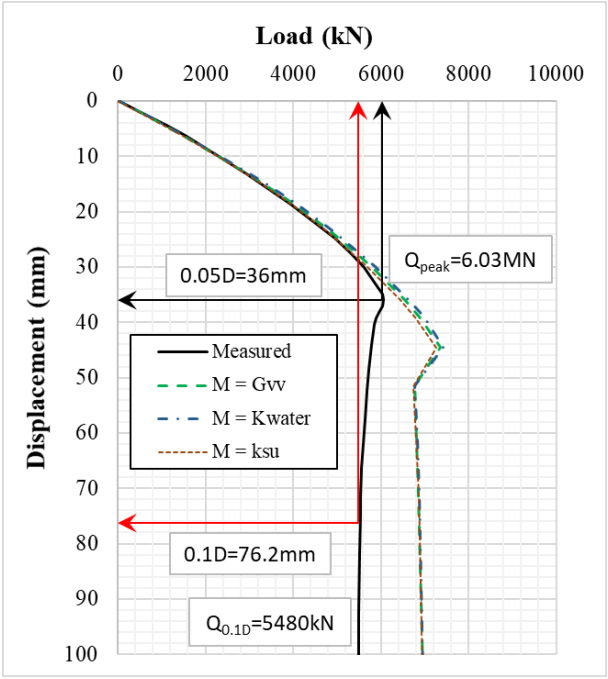

Figure 4-26 Load-displacement curve for API-FEA estimation against measured, with $M = K_{water}$ & ks_u.

Using the FE program, an estimate of the mobilised internal shaft friction along the pile, τ_{int}, can be extracted and this is shown in Figure 4-25. This shows analysis results only, as no measurements of the soil plug were extractable. Here the internal plug is shown to mobilise from the base, as the internal shaft friction mobilises and reacts against the plug's base. The maximum resistance achievable by the interface is limited to the integral of τ_{int}, along the plug surface, which reduces to a residual value after sufficient shear displacement. The value of M that is most optimum seems to occur when the plug stiffness is neither too small nor too large, and balances with the other input parameters in the analysis. This figure shows that the best results, in terms of convergence, are achieved when M=ks_u. The plug length is noted to be 13m in length from the pile base. The values above this length in the figure can therefore be ignored.

Figure 4-26 also shows that the use of any of the relationships for M does not cause a very large disparity in the estimated responses. However, there are slight variations of the peak values.

Tilbrook Site Results:

It was found here that agreement with the data occurs with a minimum value of k=500.

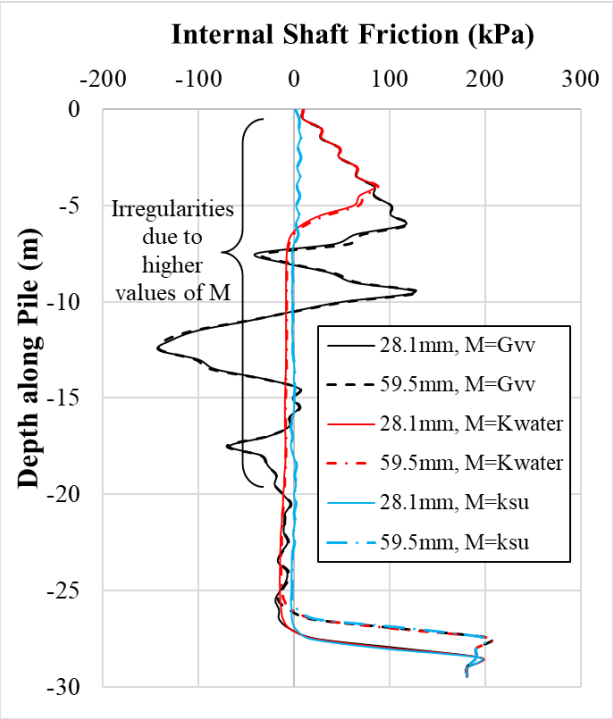

Figure 4-27 API-FEA estimated internal shaft friction along pile, with $M = G_{vv}$, K_{water} & ks_u.

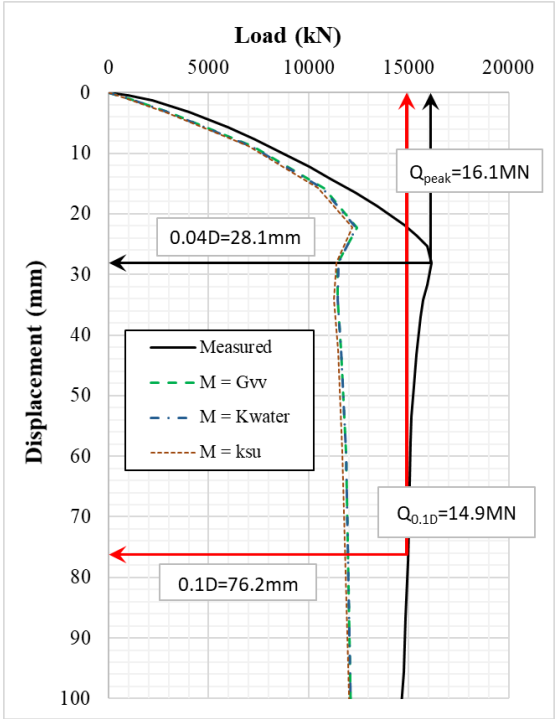

Figure 4-28 Load-displacement curve for API-FEA estimation against measured, with $M = G_{vv}$, K_{water} & ks_u.

The best representation of the expected response of τ_{int}, as shown in Figure 4-27 is again by using a factored value of undrained strength (ks_u) to determine the confined modulus, M. There is some non-convergence of the results when there is a mis-match of the stiffness, and in this case when the stiffness is too high. In all three cases however, near to the base of the pile a realistic interpretation of the behaviour is observed. Figure 4-28 gives similar results to those obtained at Pentre.

Selecting the case where $M = ks_u$, a comparison is performed between the sum of the derived τ_{ext} and τ_{int}, and the measured values. Figure 4-29 and Figure 4-30 show this comparison for both Pentre and Tilbrook tests, respectively, using the API-FEA. As shown in the figures, a better match is found when these shaft stresses are summed. For the Pentre results, there was a lack of measured results in the lower section of the pile which would have been used to validate these theories even further.

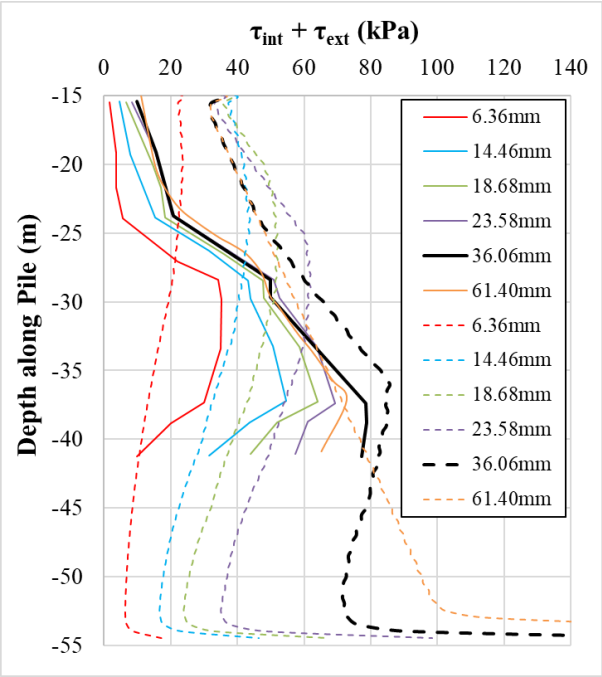

Figure 4-29 Comparison of measured τ against the summation of τ_{ext} and τ_{int} from the API-FEA for the Pentre pile test.

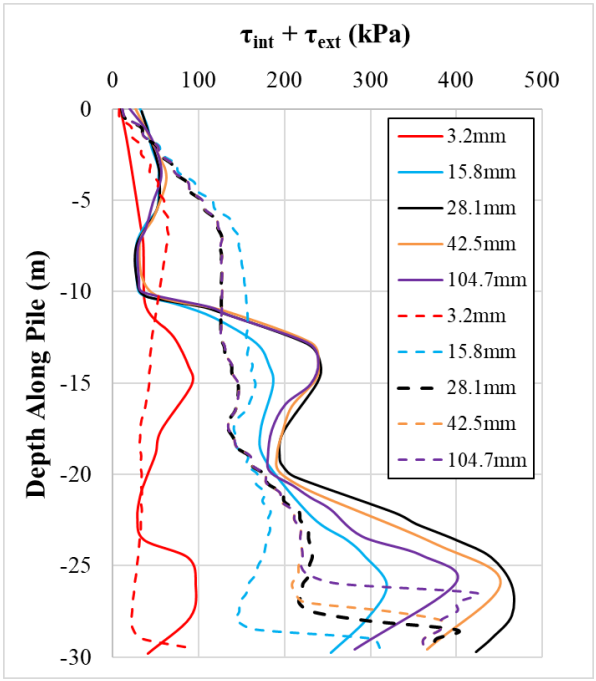

Figure 4-30 Comparison of measured τ against the summation of τ_{ext} and τ_{int} from the API-FEA for the Tilbrook pile test.

Case 8: This case focuses on a change of end bearing (EB) type, from a uniform pile, to one which includes plates within the pile. This set-up was used at both the Pentre and Tilbrook tests.

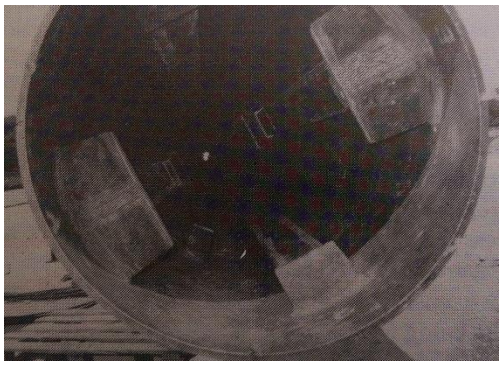

Figure 4-31 Bottom of Toe Section. Channel covers are clearly visible, Cox *et al.* (1992).

The piles were instrumented via channels along their internal walls, effectively reducing the internal cross-sectional area. In addition, a protective plate was used as a cover at the base of each channel (Figure 4-31). As outlined in Randolph (1992), these plates reduced the base plug area by 27% and the channels themselves contributed to a 16% reduction of the internal pile area. The channels would have also acted to increase the axial stiffness of the pile. The plates were positioned 0.35m above the annulus and would have increased the effective base area of the annulus, thereby attracting more load. With this arrangement, the force required to squeeze soil through the reduced area has been computed and the method incorporated in the FE analysis. The methodology effectively calculates this force and distributes it along an equivalent internal pile length. The details of this method are outlined in Section 4.4 of the VIRTUPLUG manual (Appendix C).

Pentre Site Results:

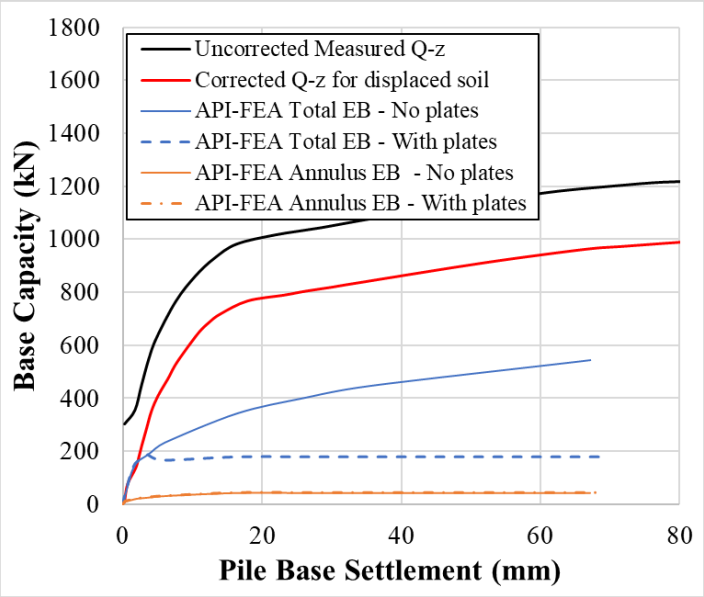

Figure 4-32 API-FEA estimation of pile base settlement vs measured load.

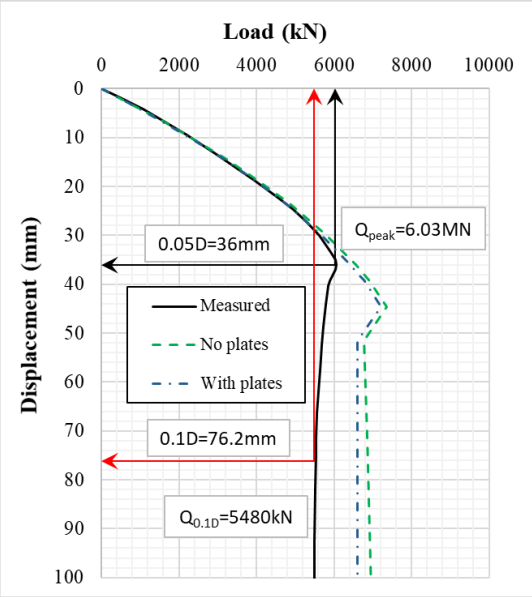

Figure 4-33 Load-displacement curve for API-FEA estimation against measured.

Within this analysis the plates are modelled to concentrate the base resistance below the plate level and remove τ_{int} above. The mobilised base capacity of the annulus is shown to remain constant (as expected) in Figure 4-32, but that of the plug has decreased. The overall contribution of the base to the total pile capacity is therefore lower as demonstrated in Figure 4-33 when compared against the base case. The peak load is not greatly affected as in this pile configuration, this is more derived from the mobilisation of the shaft and less so to that of the base. The ultimate capacity has however reduced.

Tilbrook Site Results:

The base response of the Tilbrook pile is similar to that estimated for the Pentre pile. Figure 4-34 shows this base response and some observable convergence issues brought about by the introduction of the base plates and removal of τ_{int} along a large proportion of the plug. This removal has again caused a cut-off of the full plug length and therefore its contribution to the total base capacity but has, as expected, maintained the original response of the annulus.

From Figure 4-35, the overall pile capacity that was estimated is therefore also lower than that of the base case. The peak load is again not severely affected however, quite similarly, the ultimate capacity reduces due to the capped contribution of the plug.

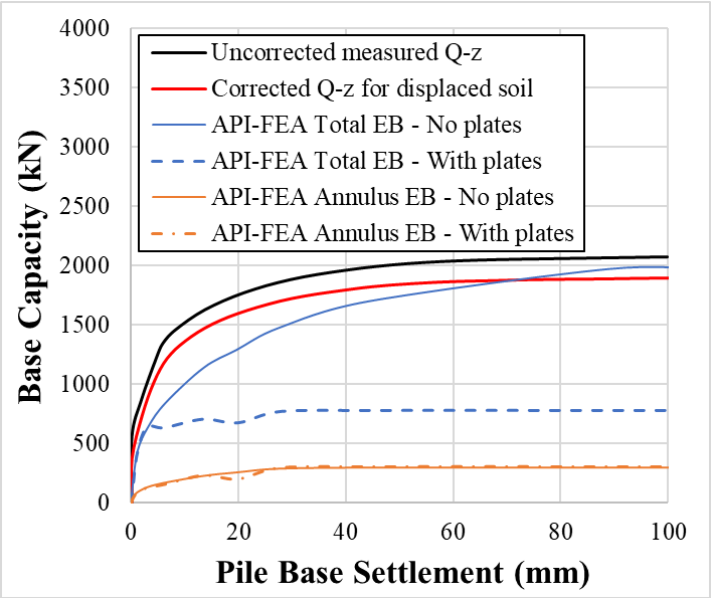

Figure 4-34 API-FEA estimation of pile base settlement vs measured load.

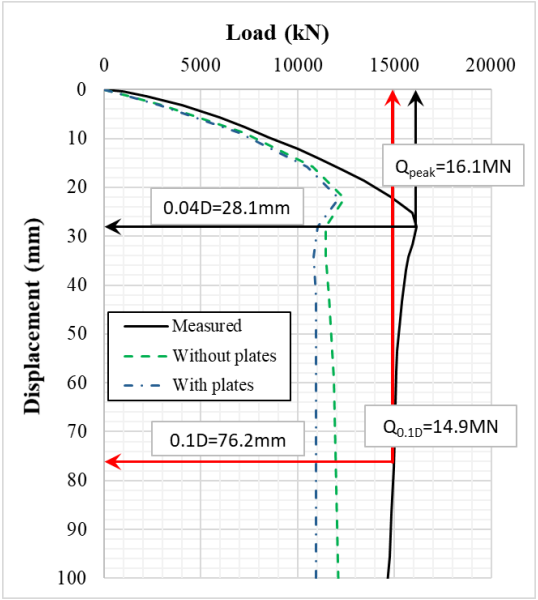

Figure 4-35 Load-displacement curve for API-FEA estimation against measured.

Case 9: This case investigated the effects of including the self-weights of the pile and plug at both the Pentre and Tilbrook piles. When the results of the analysis were compared to those when neither pile nor plug weights were included, the differences were observed to be quite small at each site. The inclusion of the self-weights of either component appears therefore to only have a limited effect on the pile response.

Case 10: In this case, measured residual values are used to compute the reduction in peak values in the t-z curves. This is assumed to occur at a displacement equal to twice the displacement to peak. The measured residuals were determined from direct and ring shear tests on undisturbed and remoulded samples extracting the ratios of residual to peak values which varied along the length of the piles. From the site data for both the Pentre and Tilbrook, the interpretation of the residual strengths are shown in Table 4-6 and Table 4-7, respectively.

With the inclusion of the measured residual strengths, Figure 4-36a shows that there is no significant change in the overall predicted load-displacement response at the Pentre site. In Figure 4-36b however where the ratios of tan δ_{ult} /tan δ_{peak} are smaller, the residual values have caused greater reduction in the estimated strengths post-peak. When compared to the measured site data, the estimations from

both the Pentre and Tilbrook analyses do not show marked improvements in the predicted responses, however, as the factor applied to the peak is meant to simulate the softening observed in clays as shear is applied, the factor will be maintained and recommended to be derived from testing.

Table 4-6 Residual δ, for Pentre.

Depth (m)	δ_{peak}°	tangent	$\delta_{residual}$°	tan ($\delta_{residual}$)°	Ratio
0.00	0.00	0.000	0.00	0.00	1.00
15.00	0.00	0.000	0.00	0.00	1.00
15.10	14.00	0.249	10.00	0.18	0.71
40.00	14.00	0.249	10.00	0.18	0.71
45.00	18.00	0.325	16.00	0.29	0.88
55.20	18.00	0.325	16.00	0.29	0.88

Table 4-7 Residual δ, for Tilbrook.

Depth (m)	δ_{peak}°	tangent	$\delta_{residual}$°	tan ($\delta_{residual}$)°	Ratio
0.00	22.00	0.404	17.00	0.31	0.76
16.99	22.00	0.404	17.00	0.31	0.76
17.00	20.50	0.374	11.50	0.20	0.54
37.00	20.50	0.374	11.50	0.20	0.54

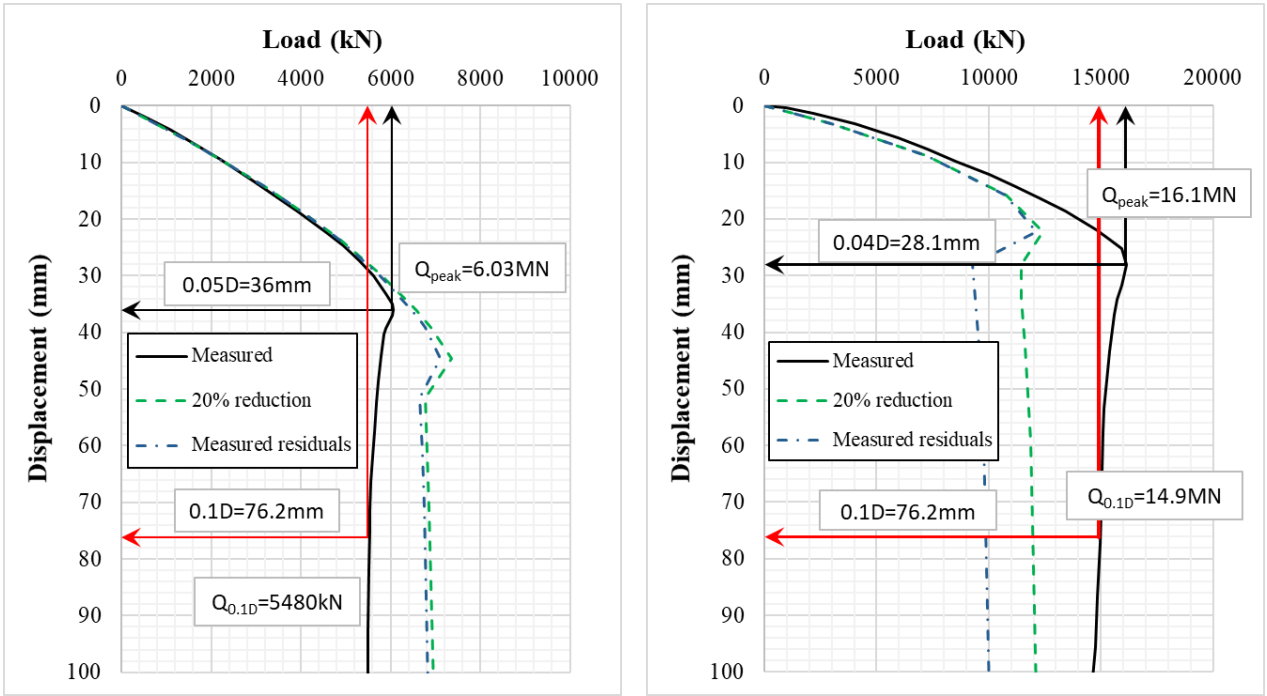

(a) Pentre results. **(b) Tilbrook results.**

Figure 4-36 API-FEA estimation of pile-head settlement vs measured load adopting measured values of strength reductions.

From the previous analyses, the most optimum conclusions are discussed and recommended in Section 4.4. The next part of this study on clays investigates the ICP-FEA, considering similar cases

as those of the API-FEA, but includes some additional analyses due to the different input parameters required in the ICP design method.

4.3.2.2. ICP-FEA Analysis (Cases 11 to 22)

Using input parameters derived from the ICP method, from both the Pentre and Tilbrook sites, the results of the ICP-FEA method can be compared to the measured results to determine if any insight can be gained on the behaviour of OEPs in clay. Case 11 is the base case for the ICP-FEA method. The analysis cases are outlined in Table 4-8. Once again, the solid lines represent measured values and the dotted lines are those estimated by the finite element method.

Table 4-8 Details of Analyses.

Case	Design Method	Constitutive Model τ_{int} & τ_{ext}	τ_{ult} = τ_{int} & τ_{ext}	τ_{int} – z_{peak}/D_i	τ_{ext} – z_{peak}/D	Constitutive Model $q_{b,pile}$	$q_{b,pile}$	Constitutive Model $q_{b,plug}$	$q_{b,plug}$	M	EB Type	Weight
11	ICP	API t-z curves	$\tau_{ext,ult}=\tau_{int,ult}$	0.0001	0.01	API Q-z to 1.0WT	$0.4q_c$	API Q-z, Q_{max} at $0.1D_i$	$0.4q_c$	G_{vv}	OEP	No
12	ICP	API t-z curves	$\tau_{ext,ult}=\tau_{int,ult}$	0.0001	0.01	API Q-z to 1.0WT	$0.65q_c$	API Q-z, Q_{max} at $0.1D_i$	$0.65q_c$	G_{vv}	OEP	No
	ICP	API t-z curves	$\tau_{ext,ult}=\tau_{int,ult}$	0.0001	0.01	API Q-z to 1.0WT	q_c	API Q-z, Q_{max} at $0.1D_i$	$0.0q_c$	G_{vv}	OEP	No
	ICP	API t-z curves	$\tau_{ext,ult}=\tau_{int,ult}$	0.0001	0.01	API Q-z to 1.0WT	$1.6q_c$	API Q-z, Q_{max} at $0.1D_i$	$0.0q_c$	G_{vv}	OEP	No
13	ICP	API t-z curves	$\tau_{ext,ult}=\tau_{int,ult}$	0.100	0.01	API Q-z to 1.0WT	$0.4q_c$	API Q-z, Q_{max} at $0.1D_i$	$0.4q_c$	G_{vv}	OEP	No
	ICP	API t-z curves	$\tau_{ext,ult}=\tau_{int,ult}$	0.010	0.01	API Q-z to 1.0WT	$0.4q_c$	API Q-z, Q_{max} at $0.1D_i$	$0.4q_c$	G_{vv}	OEP	No
	ICP	API t-z curves	$\tau_{ext,ult}=\tau_{int,ult}$	0.001	0.01	API Q-z to 1.0WT	$0.4q_c$	API Q-z, Q_{max} at $0.1D_i$	$0.4q_c$	G_{vv}	OEP	No
14	ICP	API t-z curves	$\tau_{ext,ult}=\tau_{int,ult}$	0.0001	0.0025	API Q-z to 1.0WT	$0.4q_c$	API Q-z, Q_{max} at $0.1D_i$	$0.4q_c$	G_{vv}	OEP	No
	ICP	API t-z curves	$\tau_{ext,ult}=\tau_{int,ult}$	0.0001	0.0050	API Q-z to 1.0WT	$0.4q_c$	API Q-z, Q_{max} at $0.1D_i$	$0.4q_c$	G_{vv}	OEP	No
	ICP	API t-z curves	$\tau_{ext,ult}=\tau_{int,ult}$	0.0001	0.0200	API Q-z to 1.0WT	$0.4q_c$	API Q-z, Q_{max} at $0.1D_i$	$0.4q_c$	G_{vv}	OEP	No
15	ICP	DNV t-z curves	$\tau_{ext,ult}=\tau_{int,ult}$	0.0001	DNV t-z r_f=0.98	API Q-z to 1.0WT	$0.4q_c$	API Q-z, Q_{max} at $0.1D_i$	$0.4q_c$	G_{vv}	OEP	No
	ICP	DNV t-z curves	$\tau_{ext,ult}=\tau_{int,ult}$	0.0001	DNV t-z r_f=0.50	API Q-z to 1.0WT	$0.4q_c$	API Q-z, Q_{max} at $0.1D_i$	$0.4q_c$	G_{vv}	OEP	No
16	ICP	API t-z curves	$\tau_{ext,ult}=\tau_{int,ult}$	0.0001	0.01	API Q-z to 0.1WT	$0.4q_c$	API Q-z, Q_{max} at $0.1D_i$	$0.4q_c$	G_{vv}	OEP	No
	ICP	API t-z curves	$\tau_{ext,ult}=\tau_{int,ult}$	0.0001	0.01	API Q-z to 0.1WT	$0.65q_c$	API Q-z, Q_{max} at $0.1D_i$	$0.65q_c$	G_{vv}	OEP	No
	ICP	API t-z curves	$\tau_{ext,ult}=\tau_{int,ult}$	0.0001	0.01	API Q-z to 0.1WT	q_c	API Q-z, Q_{max} at $0.1D_i$	$0.0q_c$	G_{vv}	OEP	No
	ICP	API t-z curves	$\tau_{ext,ult}=\tau_{int,ult}$	0.0001	0.01	API Q-z to 0.1WT	$1.6q_c$	API Q-z, Q_{max} at $0.1D_i$	$0.0q_c$	G_{vv}	OEP	No
17	ICP	API t-z curves	$\tau_{ext,ult}=\tau_{int,ult}$	0.0001	0.01	API Q-z to 1.0WT	q_c	API Q-z, Q_{max} at $0.1D_i$	$0.4q_c$	G_{vv}	OEP	No
18	ICP	API t-z curves	$\tau_{ext,ult}=\tau_{int,ult}$	0.0001	0.01	API Q-z to 1.0WT	$0.4q_c$	API Q-z, Q_{max} at $0.1D_i$	$0.4q_c$	K_{water}	OEP	No
	ICP	API t-z curves	$\tau_{ext,ult}=\tau_{int,ult}$	0.0001	0.01	API Q-z to 1.0WT	$0.4q_c$	API Q-z, Q_{max} at $0.1D_i$	$0.4q_c$	kS_u	OEP	No
19	ICP	API t-z curves	$\tau_{ext,ult}=\tau_{int,ult}$	0.0001	0.01	API Q-z to 1.0WT	$0.4q_c$	API Q-z, Q_{max} at $0.1D_i$	$0.4q_c$	G_{vv}	Inner plates	No
20	ICP	API t-z curves	$1.25*\tau$ ($\tau_{ext,ult}=\tau_{int,ult}$)	0.0001	0.01	API Q-z to 1.0WT	$0.4q_c$	API Q-z, Q_{max} at $0.1D_i$	$0.4q_c$	G_{vv}	OEP	No
21	ICP	API t-z curves	R instead of R* $\tau_{ext,ult}=\tau_{int,ult}$	0.0001	0.01	API Q-z to 1.0WT	$0.4q_c$	API Q-z, Q_{max} at $0.1D_i$	$0.4q_c$	G_{vv}	OEP	No
22	ICP	API t-z curves	$\tau_{ext,ult}=\tau_{int,ult}$	0.0001	0.01	API Q-z to 1.0WT	$0.4q_c$	API Q-z, Q_{max} at $0.1D_i$	$0.4q_c$	G_{vv}	OEP	Yes
	ICP	API t-z curves	$\tau_{ext,ult}=\tau_{int,ult}$	0.0001	0.01	API Q-z to 1.0WT	$0.4q_c$	API Q-z, Q_{max} at $0.1D_i$	$0.4q_c$	G_{vv}	OEP	Yes + Plug Weight

Case 11: This case sets out the base case to be used for the comparisons.

Using the direct ICP method the Pentre site predicts a plugged pile and the Tilbrook site predicts an unplugged pile. The condition however of a fully plugged undrained pile is adopted here. Figure 4-37

to Figure 4-44 compares the results of these analyses.

Pentre Site Results:

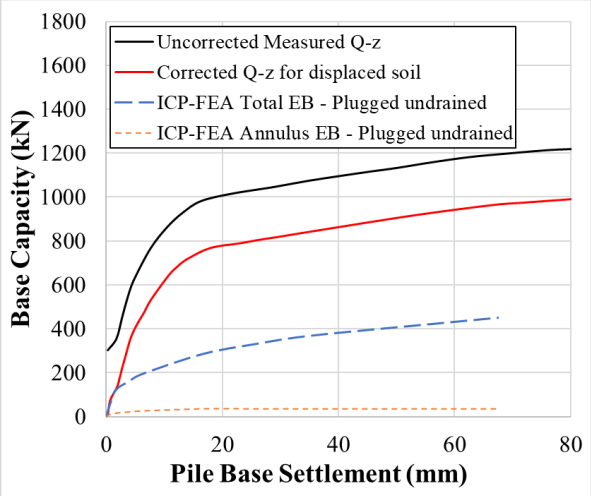

Figure 4-37 ICP-FEA estimation of pile base settlement vs measured load.

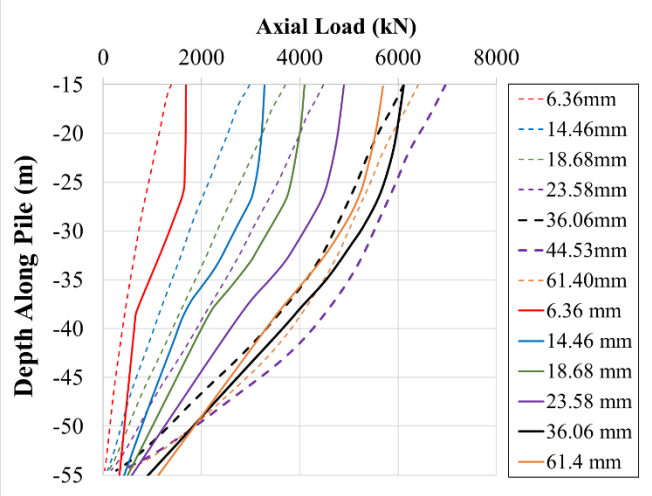

Figure 4-38 Axial load distribution in pile, ICP-FEA estimation vs measured.

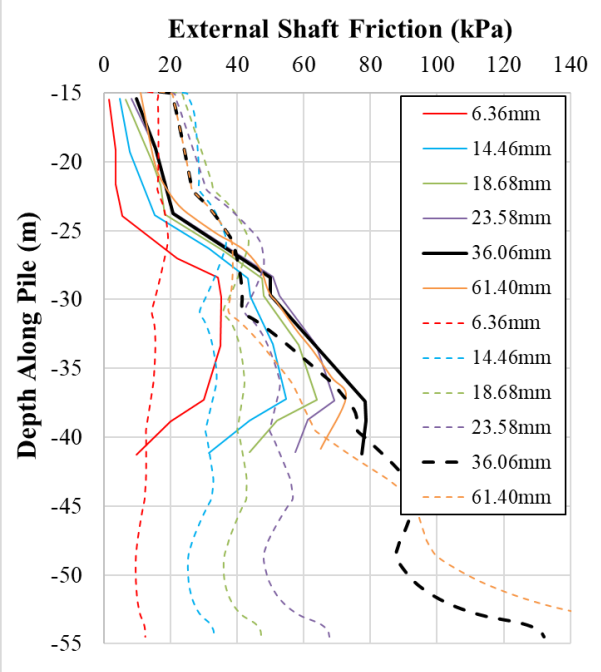

Figure 4-39 Shaft friction along pile, ICP-FEA estimation vs measured.

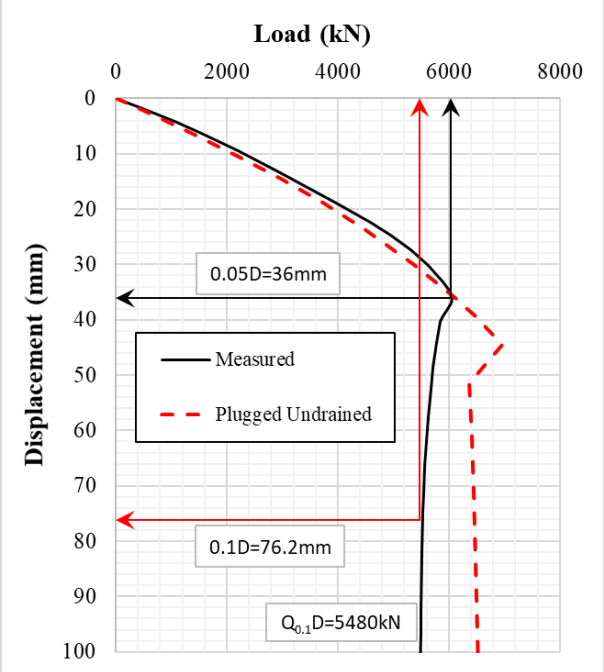

Figure 4-40 Load-displacement curve for ICP-FEA estimation against measured.

The ICP-FEA estimates that the end bearing mobilises much less than the measured data after a pile-head displacement of $0.1D_o$, which corresponds to a Q_c/Q_m value of 0.37 (Figure 4-37). The assumed ultimate limit of the pile was suggested by Gibbs *et al.* (1992) as occurring after 20mm of pile base settlement, or 2.6%D_o. The ICP prediction of a fully plugged pile adopts a uniform pressure over the full base area of the OEP and the capacity of this component is quite low (see Table 4-2). The figure plots the resistance mobilised relative to the advancement of the pile base and it is observed that the

contribution of the plug to the overall end bearing capacity is quite significant relative to that of the pile.

The distribution of the axial load in the pile at different axial pile-head displacements is well predicted as shown in Figure 4-38, however the under-estimation of the base capacity is also observed. The measured values reach the peak axial capacity after 36mm, followed by a reduced capacity. The ICP-FEA procedure captures this process with peak capacity estimated at 44.53mm displacement. Figure 4-39 also captures the efficient estimation of load transfer along the shaft, however the measured results are not available for the lower part of the pile. In terms of the overall mobilised load, Figure 4-40, the peak from the ICP-FEA was estimated at 6,962kN, a Q_c/Q_m = 1.15, and reducing to a residual of 6,688kN, a Q_c/Q_m = 1.22. A good agreement of the initial stiffness is also observed.

Tilbrook Site Results:

This interpreted behaviour shown in Figure 4-41, shows that the estimated base capacity is quite similar to those predicted using the API's Q-z approach and the measured response. In this analysis, the plugged assumption interprets a large proportion of the load supported at the base of the plug. In terms of stiffness, the initial response shows quite a good match, but some variation occurs later.

The axial load estimated at this site is not as good as that observed at Pentre, as in this case, the ICP-FEA method underestimates the shaft capacity. As shown in Figure 4-42, the axial load measured is about double that estimated with Q_c/Q_m, for the axial load at pile-head, of 0.60. Figure 4-43 demonstrates the underestimated mobilisation of τ_{ext} as incremental displacements are applied at the pile head. In terms of the overall response, Figure 4-44 shows the peak load estimated here is 10,392kN giving a Q_c/Q_m value of 0.64 and residual of 9,906kN, Q_c/Q_m of 0.66.

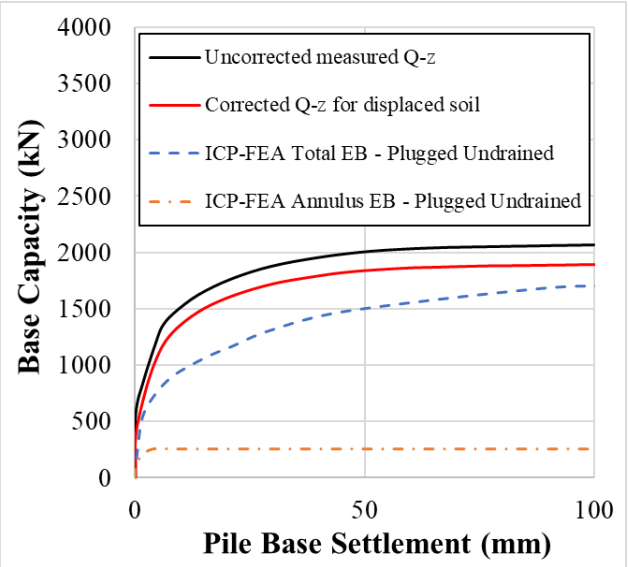

Figure 4-41 ICP-FEA estimation of pile base settlement vs measured load.

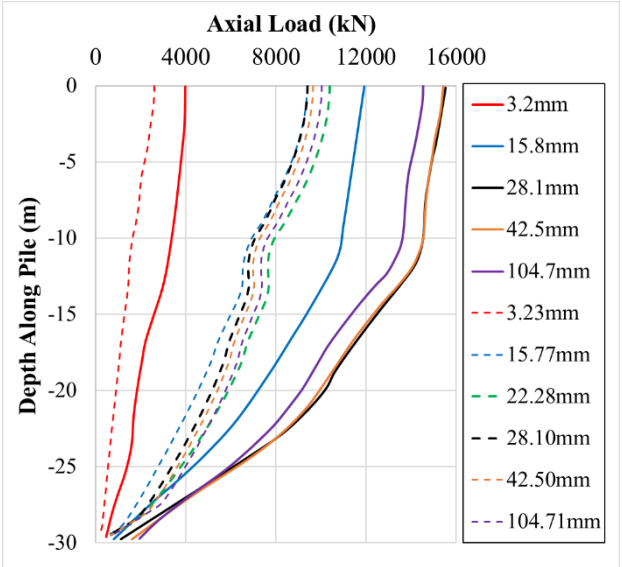

Figure 4-42 Axial load distribution in pile, ICP-FEA estimation vs measured.

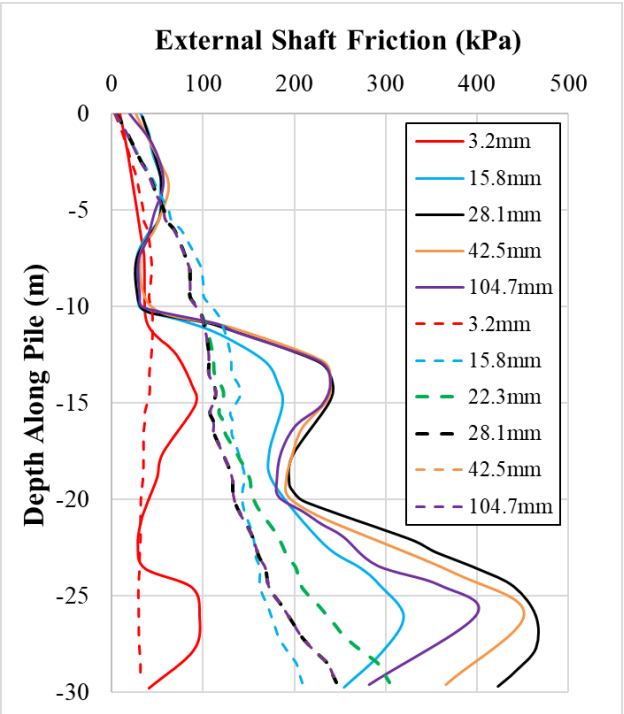

Figure 4-43 Shaft friction along pile, ICP-FEA estimation vs measured.

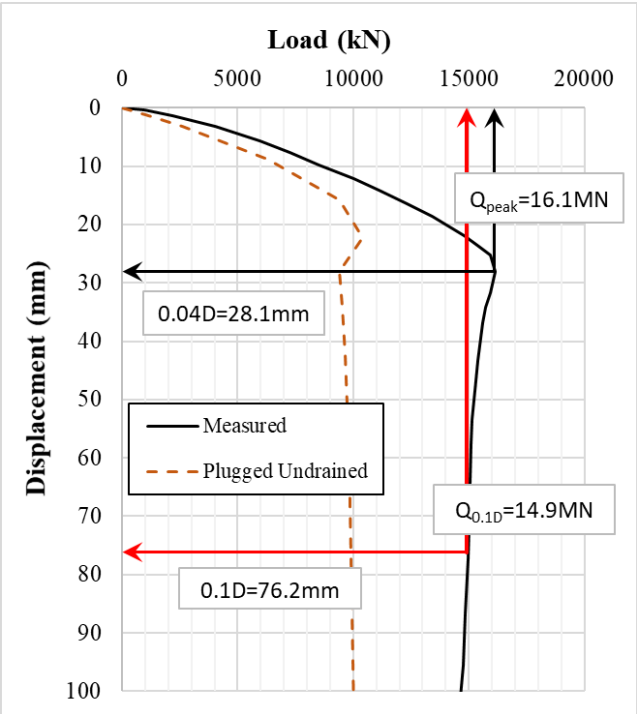

Figure 4-44 Load-displacement curve for ICP-FEA estimation against measured.

Case 12: This case compares the variation of the end bearing assumption.

These analyses can be considered direct, as the end bearing parameters are varied depending on the assumptions of the ICP method to compare the base response. Alternatively, a plugged or unplugged interpretation would be determined using the results of the FE procedure. The analyses investigated here estimate the effects of a plugged or unplugged ICP interpretation, as well as the consideration of a drained or undrained condition of the supporting soil.

Pentre Site Results:

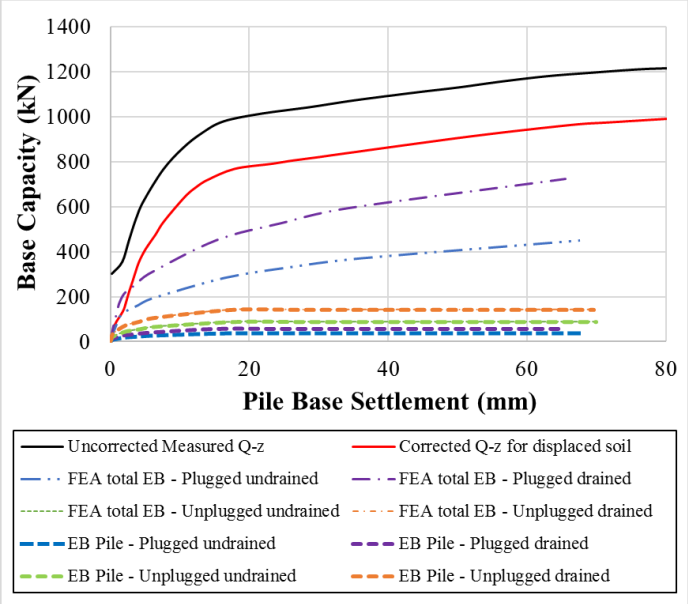

Figure 4-45 ICP-FEA estimation of pile base settlement vs measured load comparing variations in assumed base behaviour.

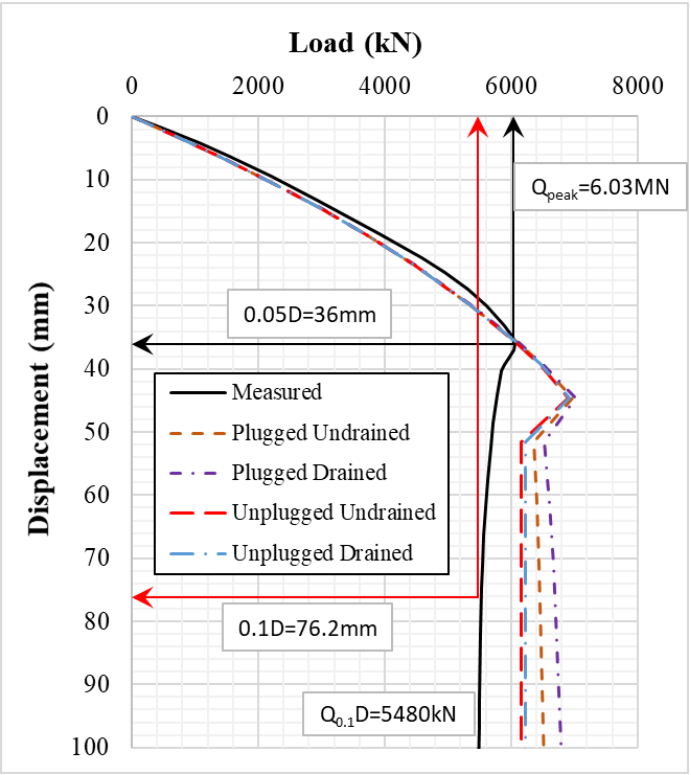

Figure 4-46 Comparison of the load-displacement responses comparing variations in assumed base behaviour.

When the plugged and drained parameters, from the ICP method are used in the FEA, the highest base and total capacities are estimated (Figure 4-45 and Figure 4-46). At the Pentre site, the measured capacities are still approximately 25% higher, suggesting that at this site, the correlation can be improved. As expected, the lowest capacity is observed when the undrained and unplugged parameters are adopted. The variation in capacity from a change in end bearing conditions mainly affects the ultimate response. Here, as the entire pile shaft is fully mobilised, any further capacity to be gained, is in the end bearing by the mobilisation of the base (Figure 4-46).

Tilbrook Site Results:

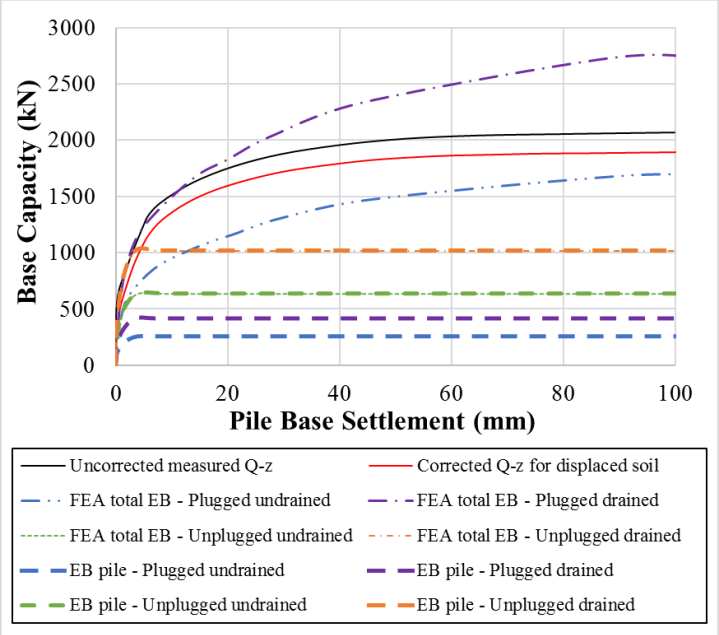

Figure 4-47 ICP-FEA estimation of pile base settlement vs measured load comparing variations in assumed base behaviour.

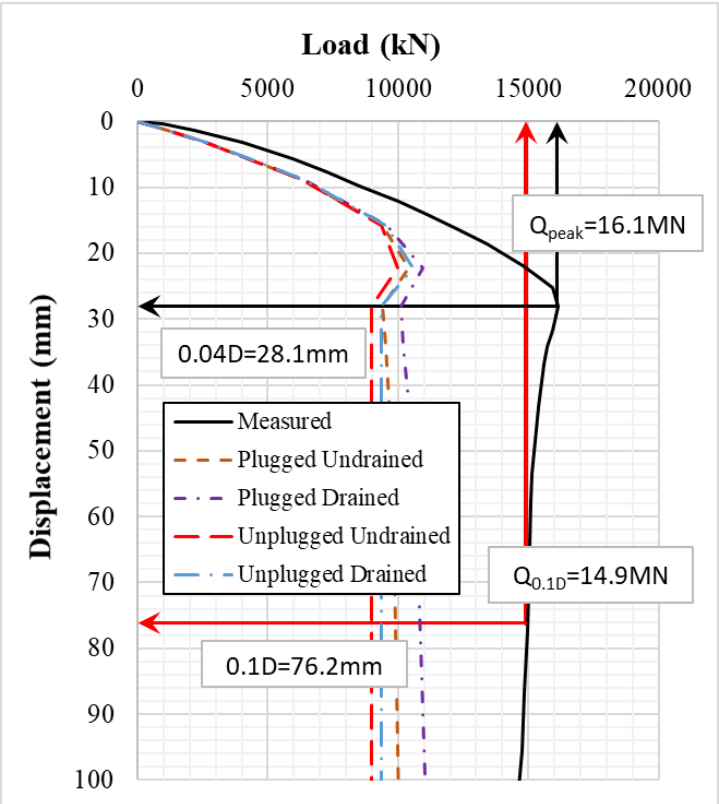

Figure 4-48 Comparison of the load-displacement responses comparing variations in assumed base behaviour.

Similar to the Pentre results, the plugged drained condition gives the highest estimated base and total capacities (Figure 4-47 and Figure 4-48). However, at this site, this combination significantly overestimates the base capacity to be greater than that measured, with Q_c/Q_m of 1.4 at $0.1D_o$ of pile base displacement. In this case the true response lies between the plugged, drained and undrained conditions.

It is demonstrated in Figure 4-48, that the initial slope of the load-displacement response is identical when the variations in end-bearing resistances are compared, but post-peak the differences between them are clearly observed.

Case 13: In this case the interface stiffness was varied. This analysis is similar to that performed in Case 2 and the results were the same as initially found: in that, the increased interface stiffness causes an increased base reaction which increases the initial slope of the total base capacity response.

Case 14: The t-z curves used in this ICP analysis are taken from API-RP 2GEO (2011). The applicability of these curves is investigated here, similar to the analysis performed in Case 3.

Pentre Site Results:

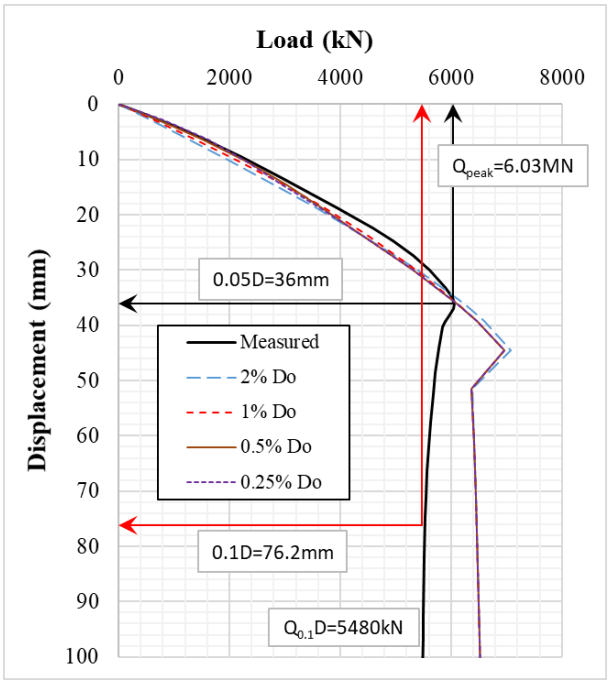

Figure 4-49 Comparison of the load-displacement responses for range of t-z curves with τ_{max} from the ICP.

As can be seen in these results from the Pentre site in Figure 4-49, there is generally very little difference in the load-displacement response using the variation in t-z stiffnesses. The peak is computed to occur at generally the same pile-head displacement when the displacement to peak ratio is varied. When the softest t-z curve is used at a displacement to peak of $0.02D_o$, there is a marginal increase in the peak capacity. As there is no variation to the end bearing conditions, the post-peak values converge to a consistent result.

Tilbrook Site Results:

This analysis uses the unplugged-undrained case.

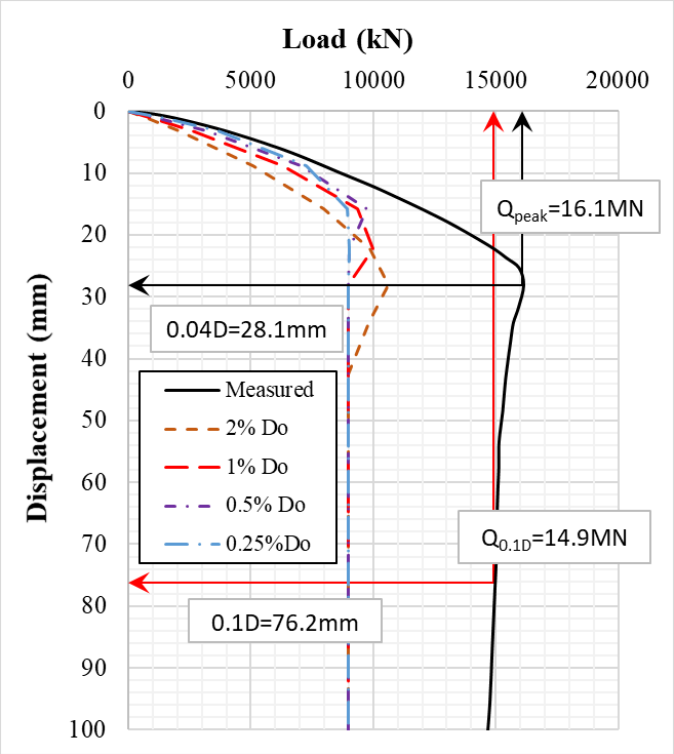

Figure 4-50 Comparison of the load-displacement responses for range of t-z curves with τ_{max} from the ICP.

As can be seen in Figure 4-50, at Tilbrook, there is a clearer trend in the load-displacement responses estimated using varied displacement to peak values. The initial slopes are quite different here when compared to the Pentre results, suggesting that the higher OCR, higher strength soil is more sensitive to t-z curve stiffness than the NC, lower strength clay, gaining strength much more rapidly.

This pile length here is 30m and the pile at Pentre is effectively 40m (55m with 15m encased). With a shorter pile, and almost three times the capacity, the stiffer transfer of shaft friction results in a higher initial load-displacement stiffness, and the displacement to peak and ultimate capacity is reduced. At a pile-head displacement of $0.1D_o$, if the t-z soil reaction curves for the Tilbrook pile is modelled with a very stiff interface, the ultimate capacity is achieved much sooner by more layers, and in the case the stiffest t-z curve ($0.25\%D_o$), no peak total capacity is observed. In the case of the softest t-z curve ($2.0\%D_o$), more of the layers would therefore be at varying levels of progressive failure, the combined effect of which is peak capacity observed at a larger displacement.

The results also suggest that with the weaker soils at Pentre, the mobilisation of stiffness along the

shaft is not very sensitive to the t-z curve stiffness. As the soil strength increases however, differing levels of strength mobilisation occurs along the pile as the t-z curve stiffness is varied.

As can be seen also, the pile here is considered unplugged and in each of the cases, the converged response is again the same.

Case 15: The t-z curves used in this analysis have been taken from DNV-OS-J101 (2016). As outlined in the literature review (Section 2.8.2), a hyperbolic t-z relationship was developed based on earlier work using an analytical model, and DNV has adopted this approach into their design guidance for offshore installations. In this analysis, a comparison is performed using these curves to determine the effect on the mobilisation of total capacity and shaft friction. These are applied as the external stress-strain relationship along the pile, selecting the limits on the ranges of the curve fitting factor, $0.5 < r_f < 0.98$, in the hyperbolic expression. Internally, τ_{int} is modelled by the stiff interface as used in the base case.

Pentre Site Results:

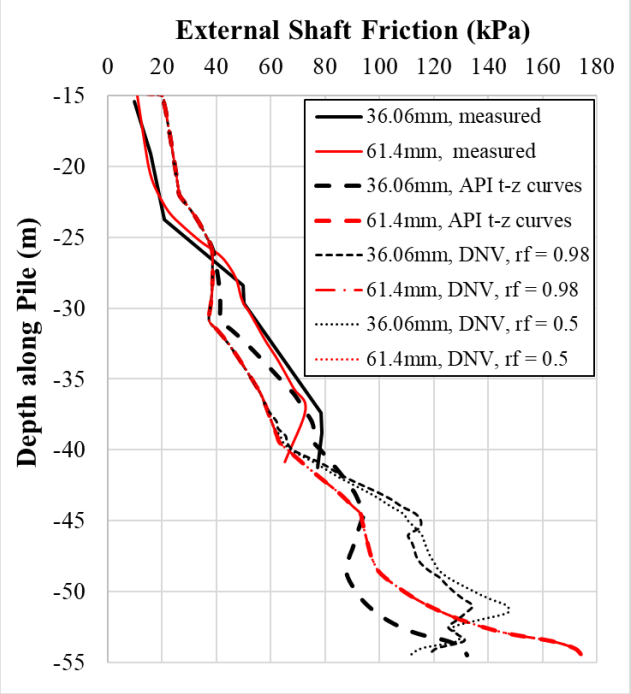

Figure 4-51 Shaft friction along pile, ICP-FEA estimation vs measured for range of t-z curves derived by the DNV-OS-J101 guidelines.

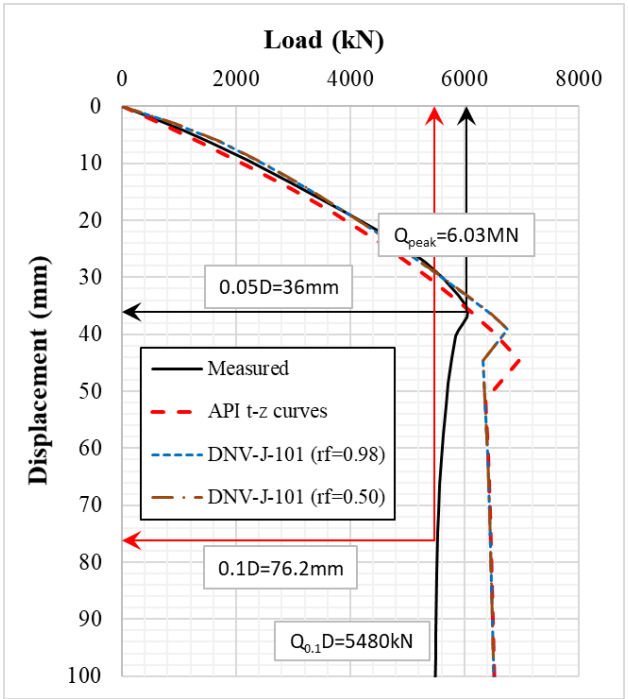

Figure 4-52 Comparison of the load-displacement responses for range of t-z curves derived by the DNV-OS-J101 guidelines.

Tilbrook Site Results:

This analysis uses the unplugged-undrained case.

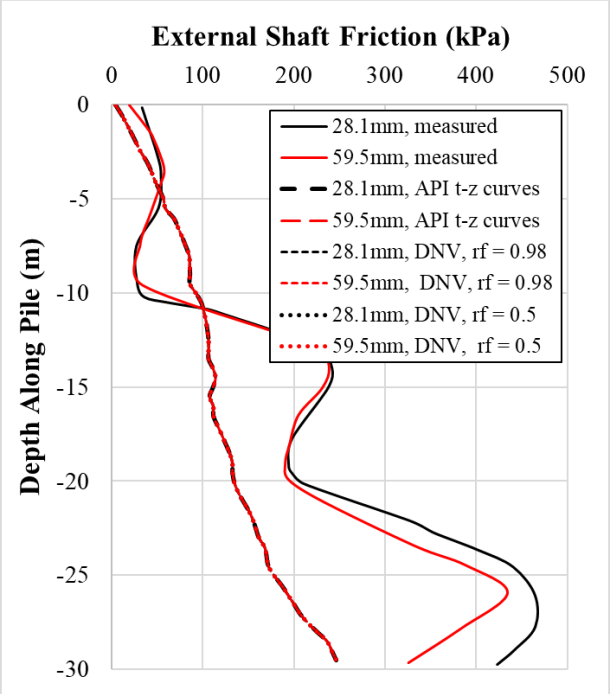

Figure 4-53 Shaft friction along pile, ICP-FEA estimation vs measured for range of t-z curves derived by the DNV-OS-J101 guidelines.

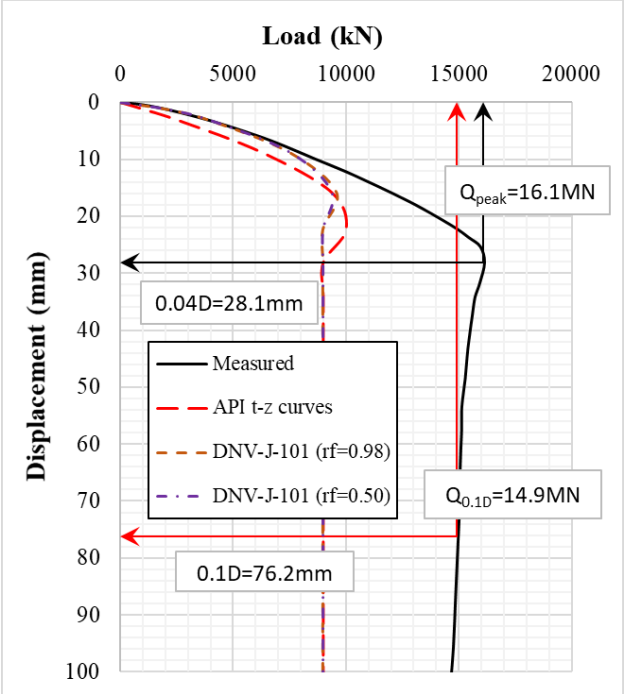

Figure 4-54 Comparison of the load-displacement responses for range of t-z curves derived by the DNV-OS-J101 guidelines.

In general, the DNV curves have a higher stiffness than those of the API, and this influences the overall mobilised response of each component. The pile at Tilbrook is shorter than that at Pentre, and this too affects the response of the components, as a shorter pile can result in a faster mobilisation of the ultimate resistances along the pile length. These effects can be observed in Figure 4-51 and Figure 4-53, at Pentre and Tilbrook respectively, with reference to τ_{ext}. The variation in resistance is observed to be much greater at Pentre than Tilbrook, with the analysis results at Pentre demonstrating varying levels of τ_{ext} mobilised, as incremental loads are applied. This is compared against a much faster achievement of the ultimate values along the pile at Tilbrook. The differences between the r_f values selected show that with higher factors used, the stiffness also increases.

At both sites, the adoption of the DNV curves produced stiffer initial responses of the total mobilised load at both Pentre (Figure 4-52) and Tilbrook (Figure 4-54) sites, when compared to the estimate using the API t-z curves. In general, these responses also matched the measured initial stiffness and the ultimate capacities. The effects of the value of r_f at both sites was also found to be negligible.

Case 16: This case looks at the full mobilisation of $q_{b,p}$ at $0.1t$ instead of $1.0t$ for the different options of base response when using the ICP design method. As the response from the other cases were very similar or very small, only the results for the plugged-undrained cases are shown (Figure 4-55).

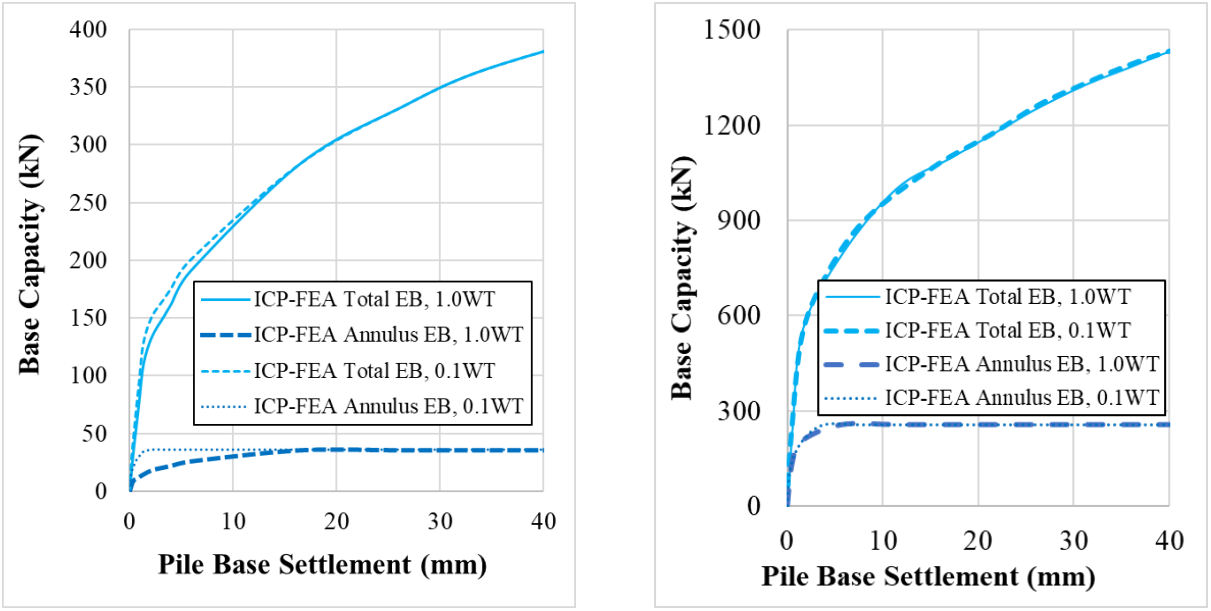

(a) Pentre results. **(b) Tilbrook results.**

Figure 4-55 ICP-FEA comparison of the measured Q-z response to the estmates choosing varying Q-z (pile) stiffnesses.

The results from the Pentre tests show that as the stiffness of the annular resistance increased, the overall base capacity is mobilised sooner. The results from Tilbrook show similar trends, although the effects are less visible as the response is already quite stiff and therefore only a slight increase is possible with the with the change in stiffness of the constitutive model employed. The high initial stiffness of the base is due to the configuration of the pile and higher shaft capacity mobilised at Tilbrook. Both sets of results show an improved match with the measured values.

Case 17: This case examines the options of equating $q_{b,p}$ to q_c and $q_{b,pl}$ to $0.4q_c$, a softer, more realistic plug base resistance.

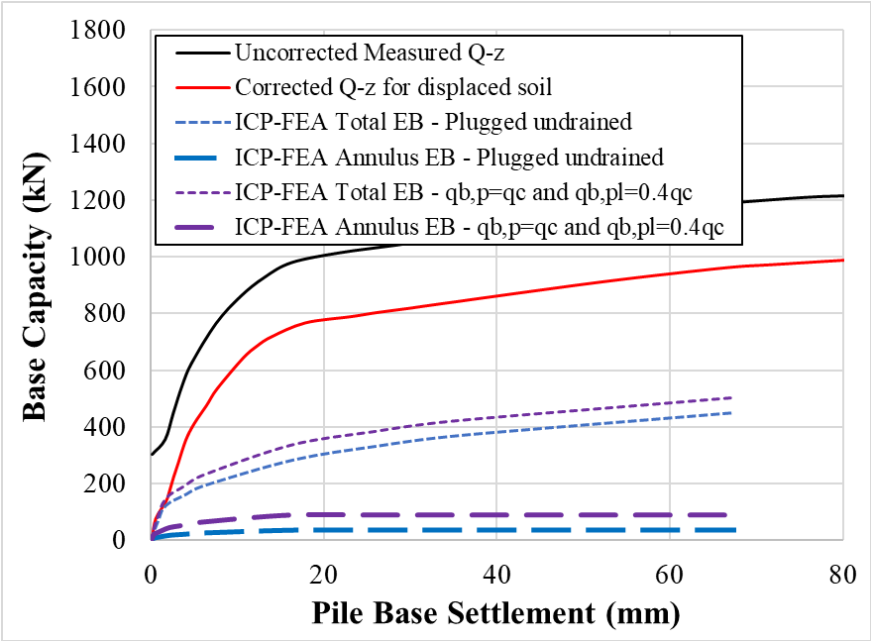

Figure 4-56 Comparison of the measured Q-z response to the ICP-FEA choosing $q_{b,p}=q_c$ and $q_{b,pl}=0.4q_c$. Pentre results.

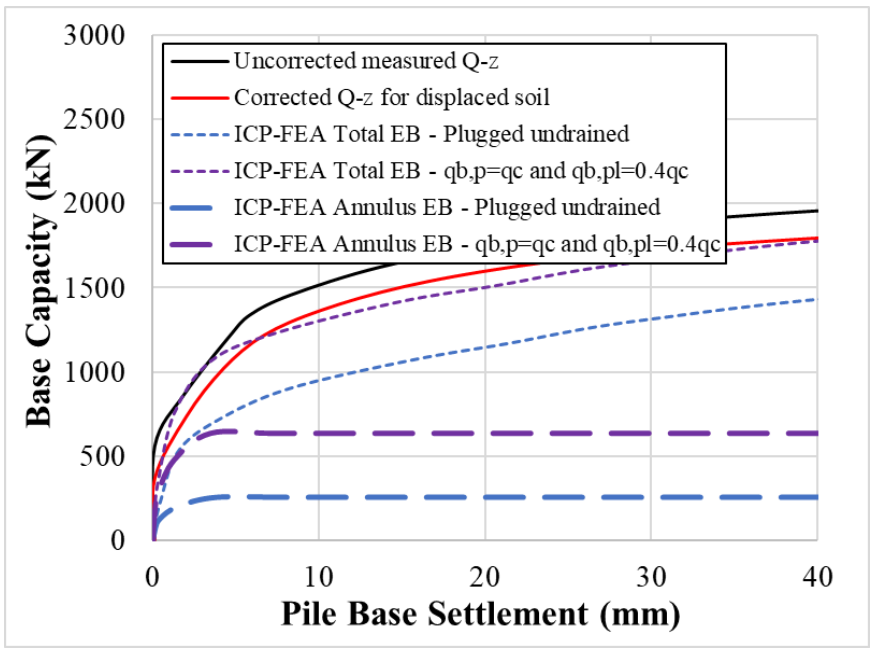

Figure 4-57 Comparison of the measured Q-z response to the ICP-FEA choosing $q_{b,p}=q_c$ and $q_{b,pl}=0.4q_c$. Tilbrook results.

In the analysis results at Pentre, the adopted ultimate resistances of the base have improved estimates compared to those obtained using the base case plugged-undrained parameters. As observed in Figure 4-56, the mobilised capacity of the base has increased the residual Q_c/Q_m from 0.66 to 0.69. Figure 4-57 shows the equivalent comparison and results sing the Tilbrook site test data. When compared to the response observed by Pentre though, the results at Tilbrook are much better, suggesting a base capacity phenomenon that is unaccounted for at Pentre but captured with the base resistance

assumptions considered here. An example of an unaccounted-for phenomenon, may be due to effects that cone tip resistance (q_c) could not obtain, such as the consolidation of the clay under sustained loading. It was found that the clays at Pentre are anisotropic and have a higher horizontal permeability. Chow (1997) also found that for Pentre, $q_{b,p}$ needed to be closer to $4q_c$ to obtain a better match and as outlined earlier, Gibbs *et al*. (1993) observed that N_c values nearer to 16 was required to be closer to the measured result. Additionally, at the Noetsu Bridge (Masumoto *et al*., 1992) found that $q_{b,p}$ was closer to $10q_c$, which was also included in Chow (1997).

Case 18: In this case different values of the constrained modulus, M, are investigated using the ICP-FEA. This is similar to Case 7 investigated earlier using the API-FEA method, where M adopts the bulk modulus of seawater, K, of 2,340,000kPa and a factored value of undrained shear strength, ks_u.

Pentre Site Results:

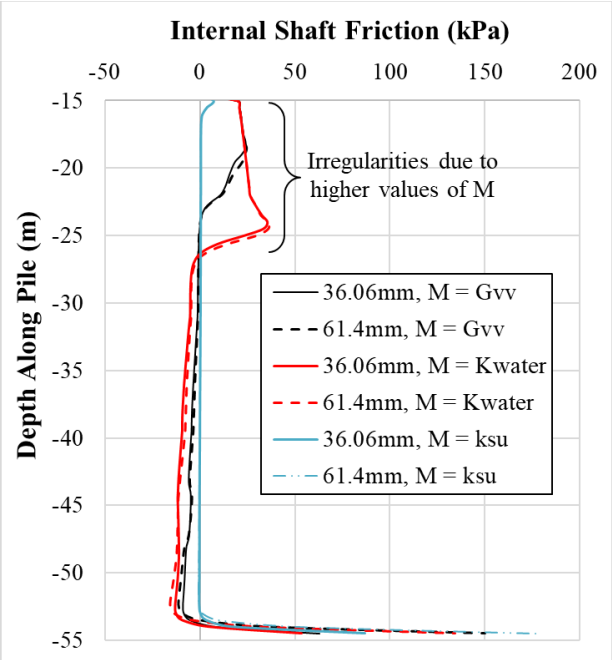

Figure 4-58 API-FEA estimated internal shaft friction along pile, estimation vs measured, with $M = K_{water}$ & ks_u.

The estimated values of τ_{int} give marginal differences when M is varied. Figure 4-58 shows that, in general, there is a zone of confinement at the base of the pile in which τ_{int} is high. This friction is generally higher in an ICP analysis, than the API, due to the Coulomb interface friction response governing τ_f. This assumption produces a much higher resistance near the base. There are also irregularities observed in the estimation of τ_{int}, similar to that found in the API-FEA, caused by a mis-match of the component stiffnesses, specifically here, to large values of M relative to the other components.

Tilbrook Site Results:

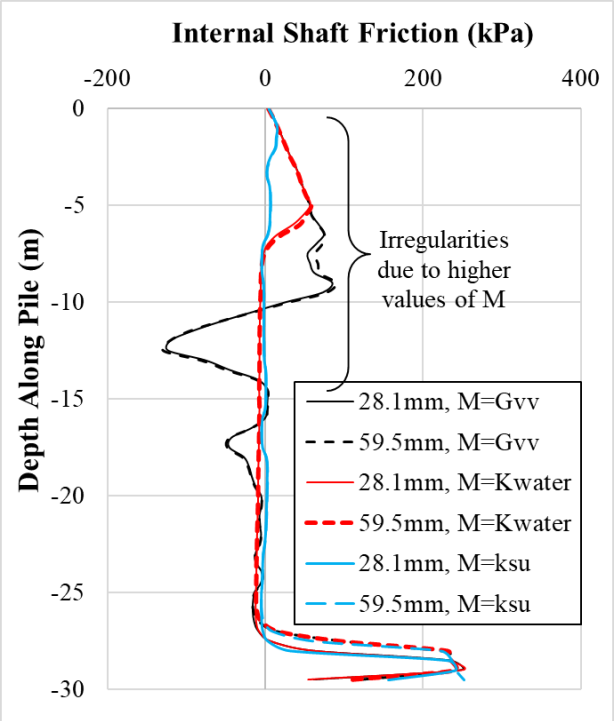

Figure 4-59 API-FEA estimated internal shaft friction along pile, estimation vs measured, with $M = K_{water}$ & ks_u.

The plugged-undrained case is analysed here. When estimating the response of τ_{int} there is a significant decrease in the observed convergence irregularities along the pile length when $M = K_{water}$ or ks_u are chosen (Figure 4-59). This was also observed when the Tilbrook analysis was performed using the API-FEA. The overall load-displacement response is not greatly affected and in general, the stiffer the soil plug, the more efficient is the load transfer to the base.

The effect is now observed of comparing the measured values and the sum of τ_{ext} and τ_{int}.

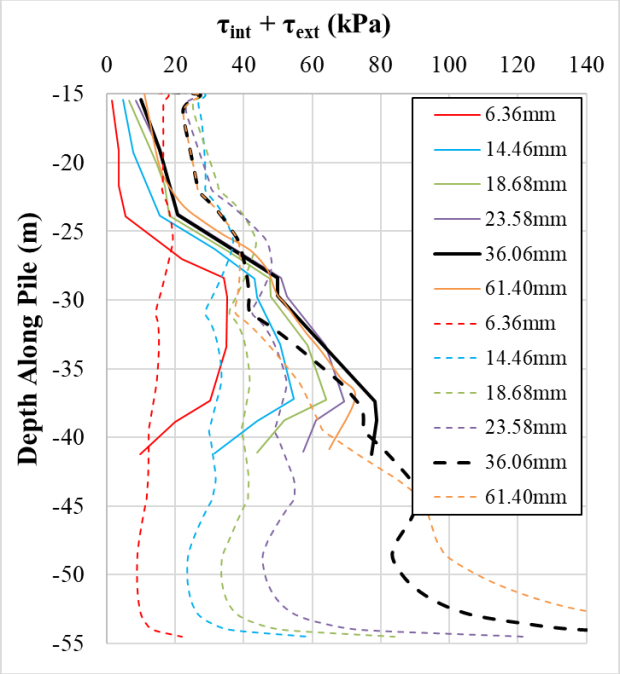

Figure 4-60 Comparison of measured τ against the summation of τ_{ext} and τ_{int} from the ICP-FEA for the Pentre pile test.

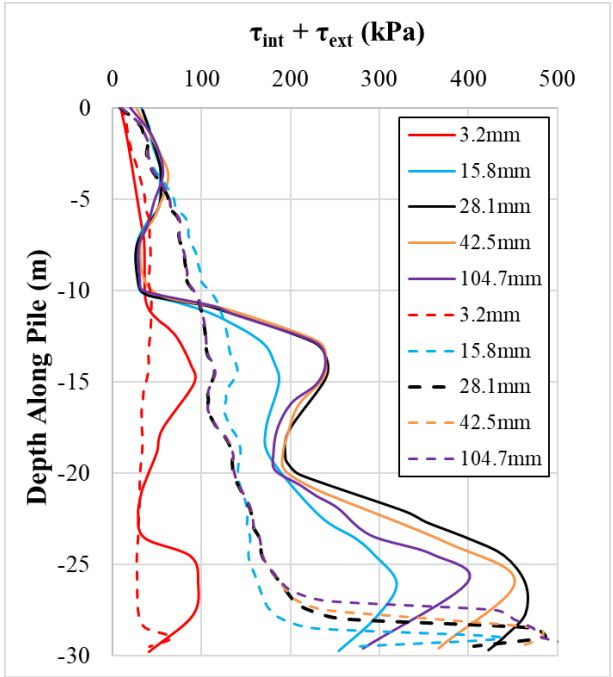

Figure 4-61 Comparison of measured τ against the summation of τ_{ext} and τ_{int} from the ICP-FEA for the Tilbrook pile test.

As can be seen from Figure 4-60 and Figure 4-61, a better match with the measured values is found when these shaft stresses are summed. In addition, the results are given for the case where $M = ks_u$ is used and gives the best match.

<u>Case 19</u>: This case focuses on a change of EB type, similar to Case 8, now using the ICP-FEA.

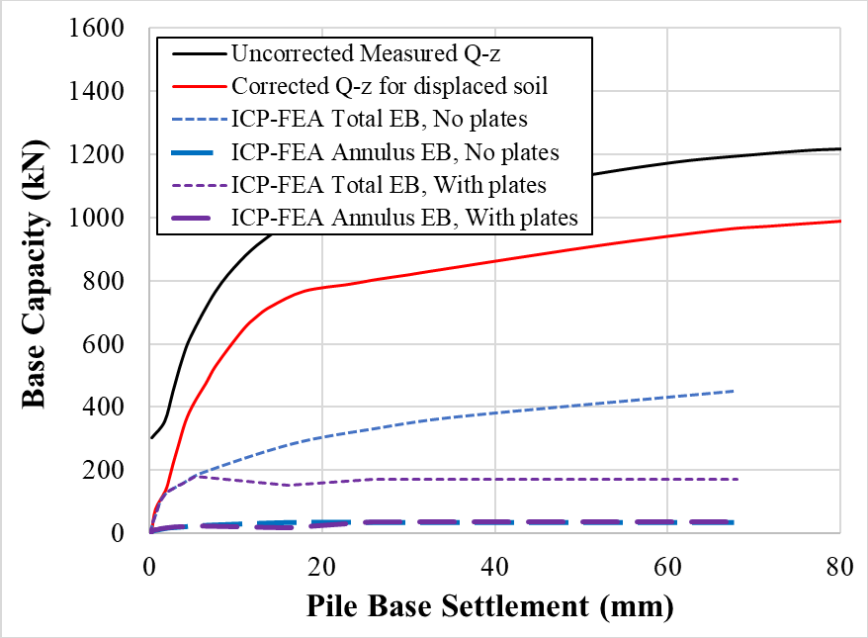

Figure 4-62 ICP-FEA comparison of the measured Q-z response to the estmates choosing varying Q-z (pile) stiffnesses. Pentre results.

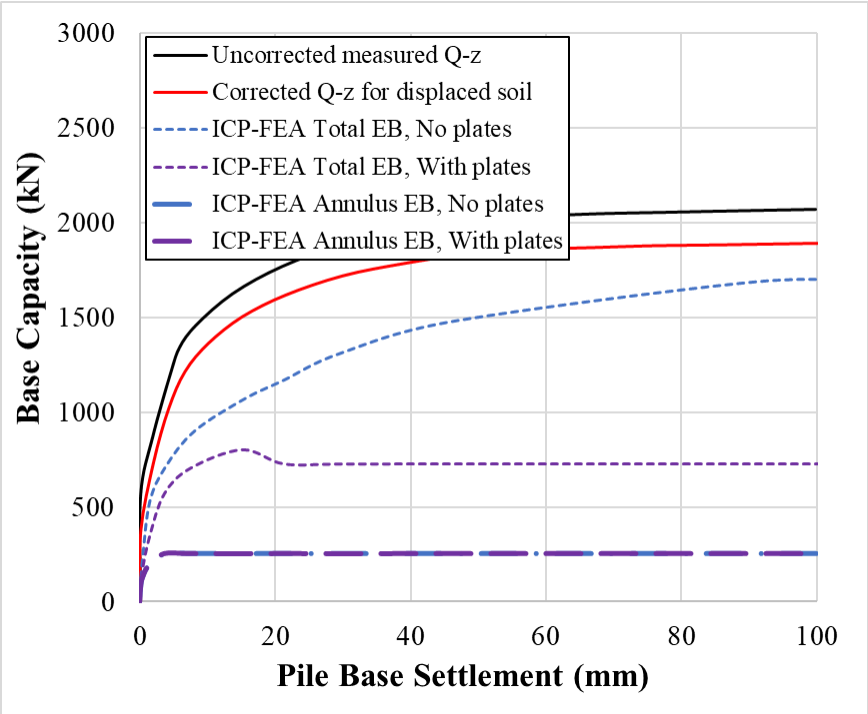

Figure 4-63 ICP-FEA comparison of the measured Q-z response to the estmates choosing varying Q-z (pile) stiffnesses. Tilbrook results.

This case has found that with the inclusion of the plates to the annular area and the removal of the τ_{int} from above the level of these plates, the mobilised capacity is again capped at a reduced level. The measured results however show, for both Pentre (Figure 4-62) and Tilbrook (Figure 4-63), that despite the presence of the plates, the pile still mobilises further τ_{int} thereby increasing the base capacity. The values of τ_{int} must therefore be considered ignoring the presence of the plates.

Case 20: Here the v is removed from the ICP methodology to compute τ_f, thereby increasing its value by a factor of 1.25. This loading factor was introduced by Lehane (1992) when it was found that the capacity of axially loaded piles in clay reduced after obtaining peak capacity with further loading applied. This reduction ranged from 1.0 to 0.8 and effectively eliminates the peak value observed in most pile tests in clay. As outlined in Chapter 1, along the pile length, the peak is not reached simultaneously in each layer. To test the effect of this factor alongside peak δ_f values and softened t-z curves, this factor is removed, and the results compared.

Pentre Site Results:

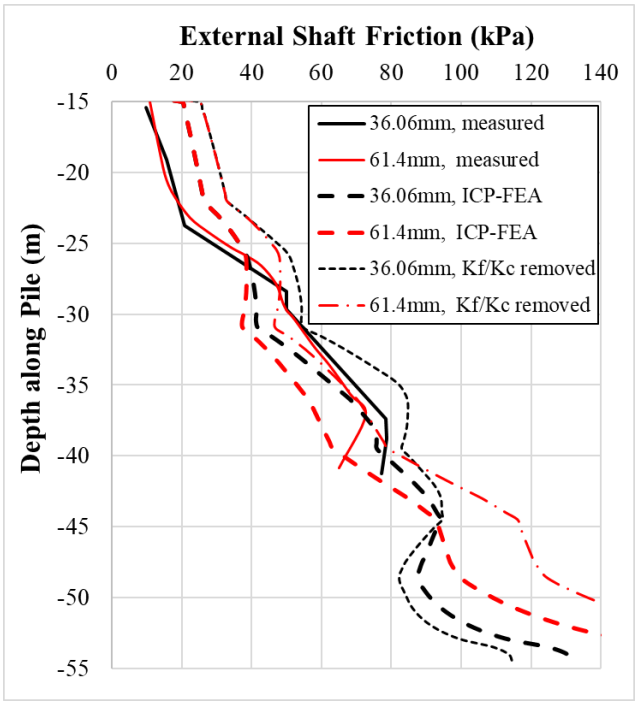

Figure 4-64 Shaft friction along pile, ICP-FEA estimation vs measured.

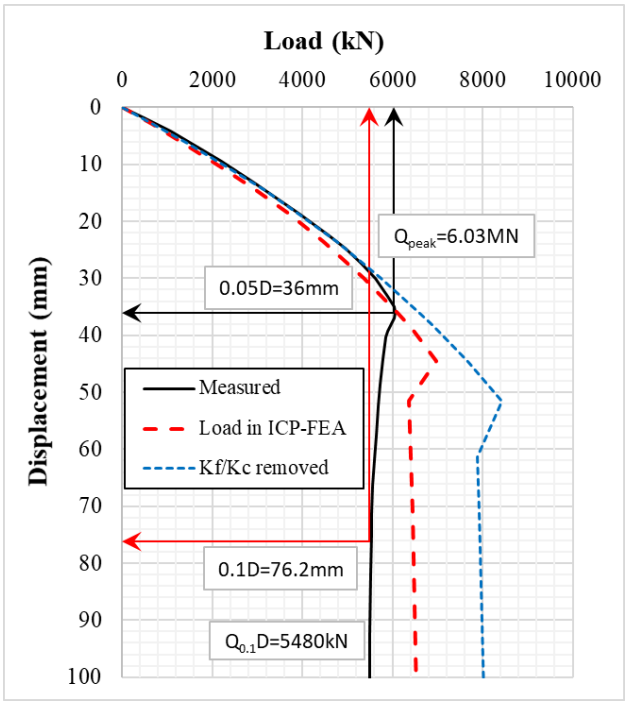

Figure 4-65 Load-displacement curve for ICP-FEA estimation against measured.

In the analysis at Pentre, the plugged-undrained condition is used as the base case. As expected, with the removal of the K_f/K_c factor, this increases the mobilised shaft resistance (Figure 4-64) and at this

site to values that are much larger than those measured. This affects the peak values that can be obtained per layer, thereby increasing the total capacity of the pile. This is demonstrated in the load-displacement response (Figure 4-65) which now shows a capacity of 7,977kN (Q_c/Q_m) of 1.45).

Tilbrook Site Results:

Here both the plugged and unplugged, undrained results are considered.

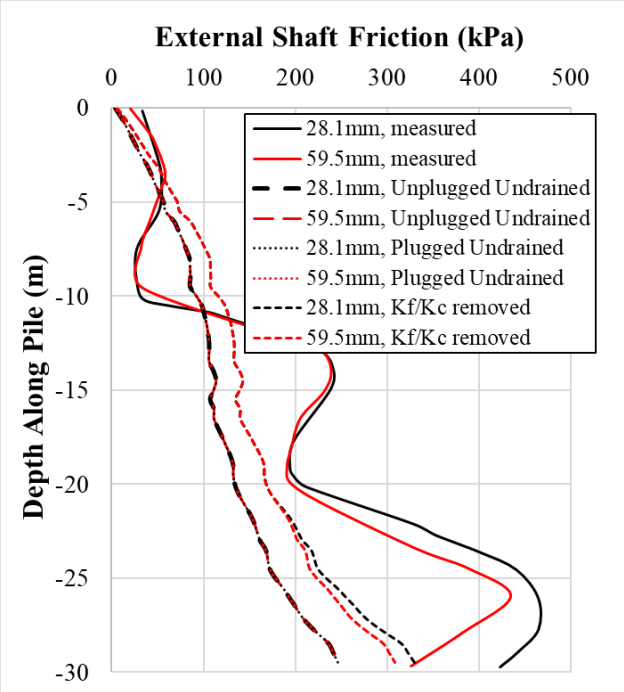

Figure 4-66 Shaft friction along pile, ICP-FEA estimation vs measured.

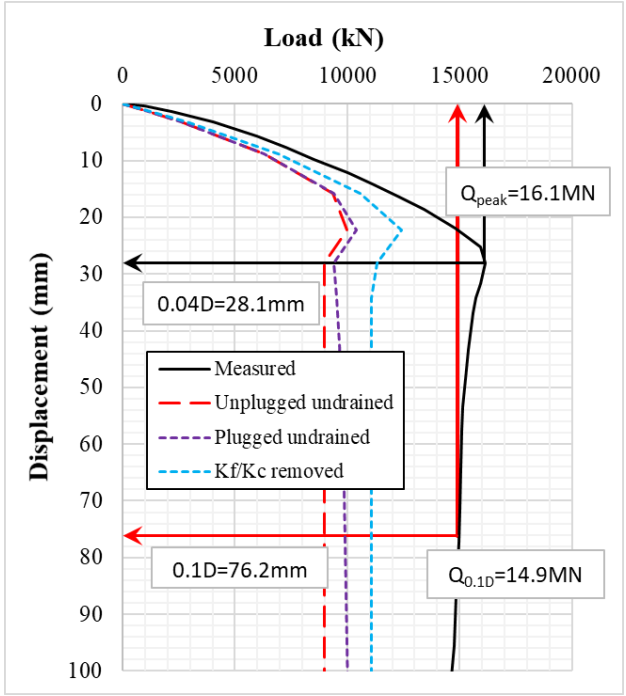

Figure 4-67 Load-displacement curve for ICP-FEA estimation against measured.

In general, this analysis shows an improvement in the estimated capacity from the removal of the K_f/K_c factor. This is observed in both the estimated shaft friction (Figure 4-66) and in the estimation of the load-displacement response (Figure 4-67). As observed, the peak and ultimate capacities remain under-predicted suggesting that changing the K_f/K_c factor is not the only requirement to improve the accuracy of predictions at this site.

Case 21: In this case the equivalent radius (R^*) that is used to convert the ICP design method for a CEP design method to that of an OEP design method is removed. This factor was introduced into the pile design method, originally outlined by Lehane (1992) for CEPs, by Chow (1997) in her thesis justifying its use in OEPs by strains obtained using the cavity expansion theory. These analyses

showed that similar displacements were obtained in soil when CEPs and OEPs of the same volume were embedded. For this analysis, R^* is replaced with R.

Pentre Site Results:

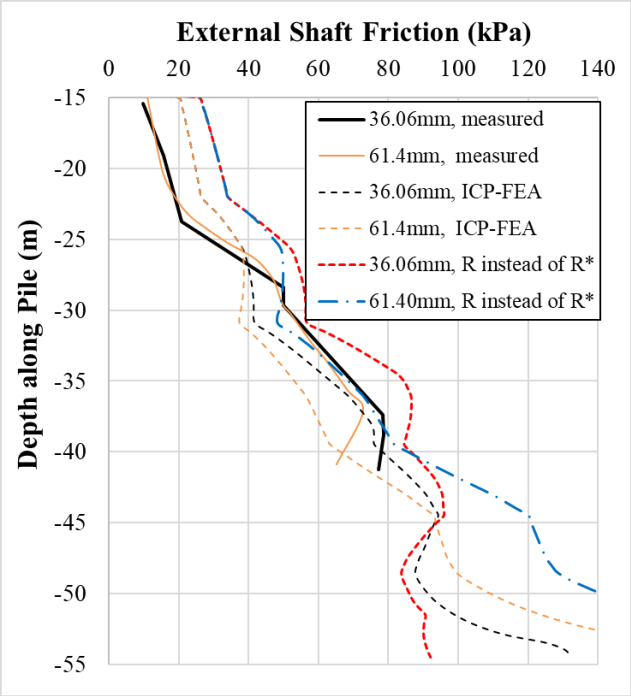

Figure 4-68 Shaft friction along pile, ICP-FEA estimation vs measured.

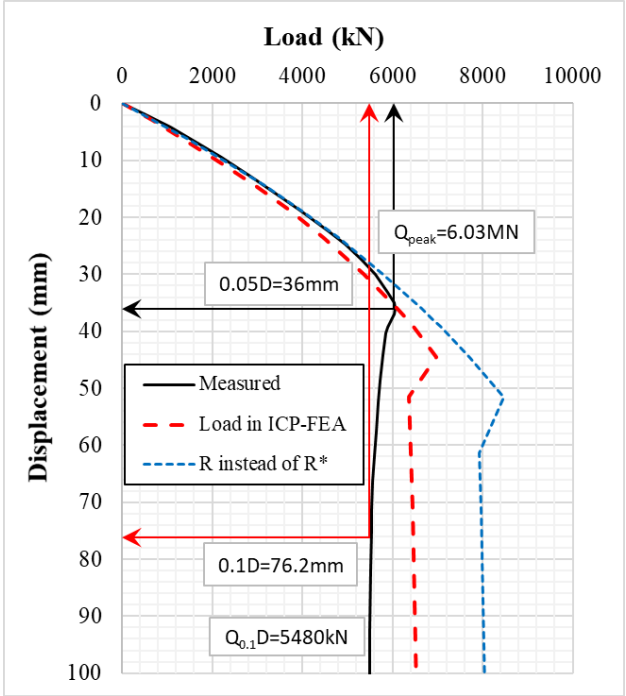

Figure 4-69 Load-displacement curve for ICP-FEA estimation against measured.

As shown in Figure 4-68 and Figure 4-69, the load estimated in the pile and the shaft friction has increased by the removal of the R^* factor. This in turn has caused the overall estimated capacity of the pile to increase.

Tilbrook Site Results:

The ICP-FEA analysis is performed using the unplugged-undrained condition as predicted from the ICP's criterion for plugging.

In Figure 4-70, where the mobilised values of τ_{ext} are equal, this is when the limiting factor of h/R (h/R^*) = 8 has been reached in both assumptions. This factor was introduced by Lehane (1992) into the ICP method to account for the reduction in σ'_{rc} as h/R increased (nearer to the top of the pile) but maintained a constant value of 8 near the pile base.

The use of the *R*-factor increases the value of K_c which increases shaft resistance τ_f. This was found to be beneficial in the Tilbrook analysis, increasing Q_c/Q_m from 0.66 to 0.70, but at Pentre this change increased Q_c/Q_m from 1.22 to 1.46.

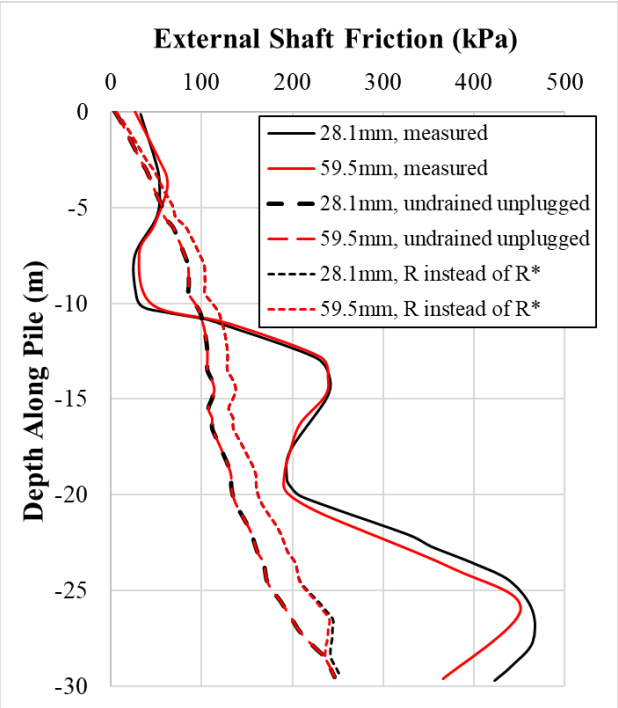

Figure 4-70 Shaft friction along pile, ICP-FEA estimation vs measured.

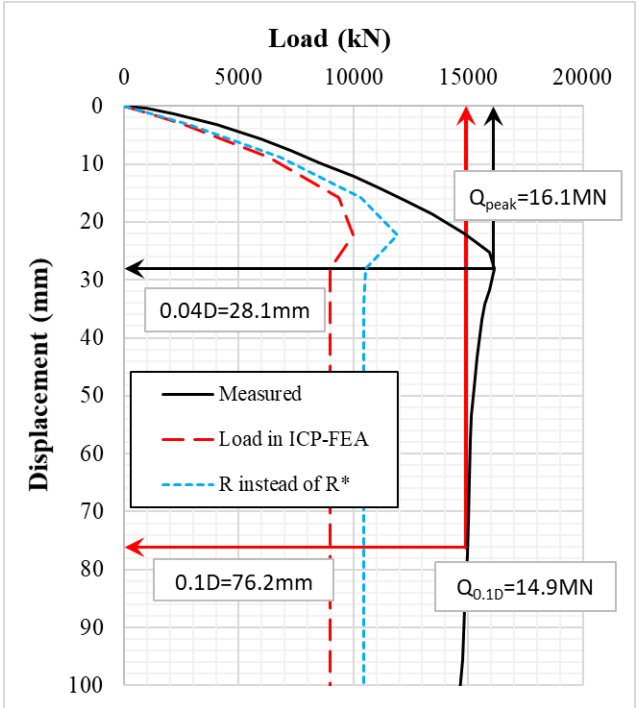

Figure 4-71 Load-displacement curve for ICP-FEA estimation against measured.

<u>Case 22</u>: In this case the additional weight from the pile only and the pile and plug are considered. The results are not shown diagrammatically; however, it was found that the difference is quite small.

4.3.2.3. Summary of Results

The results of the cases outlined above are summarised in Table 4-9, extracting the peak and residual capacities, their Q_c/Q_m ratios and the displacement to peak estimated (mm and $\%D_o$). Measured values are also included in the table for consideration.

From Table 4-9, in general it can be observed that in light of the various changes and alterations made to the API-FEA, the method continues to overestimate both the peak and residual values at the Pentre site and underestimates the peak and residual at the Tilbrook site.

Table 4-9 Summary of results.

Case	Pentre					Tilbrook				
	Peak Load (kN)	**Peak Q_c/Q_m**	**Residual Capacity (kN)**	**Residual Q_c/Q_m**	**Displacement to peak (%D_o)**	**Peak Load (kN)**	**Peak Q_c/Q_m**	**Residual Capacity (kN)**	**Residual Q_c/Q_m**	**Displacement to peak (%D_o)**
Measured	6031	-	5480	-	4.7	16130	-	14900	-	3.7
API-FEA										
1	7358.4	1.22	6881.5	1.26	5.8	12426.8	0.77	11958.46	0.80	2.9
2	7325.3	1.21	6870.5	1.25	5.8	12281.1	0.76	11904.25	0.80	2.9
	7350.4	1.22	6878.2	1.26	5.8	12376.5	0.77	11946.62	0.80	2.9
	7357.3	1.22	6881.0	1.26	5.8	12421.5	0.77	11958.08	0.80	2.9
3	6961.0	1.15	6881.5	1.26	5.0	11421.6	0.71	11958.46	0.80	2.1
	7034.8	1.17	6881.5	1.26	5.1	11240.5	0.70	11958.46	0.80	2.1
	7637.4	1.27	6881.5	1.26	6.8	12955.4	0.80	11958.46	0.80	3.7
4	7364.5	1.22	6881.5	1.26	5.8	12518.7	0.78	11958.46	0.80	2.9
5	7438.8	1.23	7213.03	1.32	5.8	12417.1	0.77	11929.38	0.80	2.9
	7294.4	1.21	6652.34	1.21	5.8	12183	0.76	11227.22	0.75	2.9
	7333.1	1.22	6736.27	1.23	5.8	12454.6	0.77	11828.72	0.79	2.9
6	7364.5	1.22	6636.36	1.21	5.8	12518.7	0.78	11136.31	0.75	2.9
7	7414.6	1.23	6884.67	1.26	5.8	12393.9	0.77	11958.21	0.80	2.9
	7262.5	1.20	6871.57	1.25	5.8	12203.4	0.76	11835.34	0.79	2.9
8	7222.5	1.20	6599.49	1.20	5.8	12140.2	0.75	10943.60	0.73	2.9
9	7368.2	1.22	6881.54	1.26	5.9	12432.2	0.77	11958.50	0.80	2.9
	7379.6	1.22	6881.59	1.26	5.9	12437	0.77	11958.55	0.80	2.9
10	7111.7	1.18	6762.07	1.23	5.8	12123.3	0.75	9863.39	0.66	2.9
ICP-FEA										
11	6962.1	1.15	6687.85	1.22	5.8	10391.6	0.64	9905.59	0.66	2.9
12	7012.3	1.16	6687.85	1.22	5.8	10939.7	0.68	10836.26	0.73	2.9
	6897.8	1.14	6165.33	1.13	5.8	10003.7	0.62	8986.64	0.60	2.9
	6919.6	1.15	6218.86	1.13	5.8	10566.2	0.66	9368.69	0.63	2.9
13	6917.2	1.15	6451.34	1.18	5.8	10416.7	0.65	9875.21	0.66	2.9
	6952.4	1.15	6455.56	1.18	5.8	10398	0.64	9897.40	0.66	2.9
	6961.2	1.15	6457.11	1.18	5.8	10391.4	0.64	9905.14	0.66	2.9
14	6962.1	1.15	6457.53	1.18	5.8	9034.62	0.56	8986.64	0.60	2.9
	6962.1	1.15	6457.53	1.18	5.8	9724.09	0.60	8986.64	0.60	2.1
	7074.2	1.17	6457.53	1.18	5.8	10595.5	0.66	8986.64	0.60	3.7
15	6751.1	1.12	6457.51	1.18	5.1	9589.65	0.59	8986.64	0.60	2.1
	6753.5	1.12	6457.51	1.18	5.1	9377.08	0.58	8986.64	0.60	2.1
16	6966.6	1.16	6457.53	1.18	5.8	10388.7	0.64	8152.30	0.55	2.9
	7019.2	1.16	6687.86	1.22	5.8	10939.7	0.68	10836.26	0.73	2.9
	6910.4	1.15	6165.33	1.13	5.8	10003.7	0.62	8986.64	0.60	2.9
	6938.6	1.15	6218.86	1.13	5.8	10566.2	0.66	9368.69	0.63	2.9

Table 4-9 (con'd) Summary of results.

Case	Pentre					Tilbrook				
	Peak Load (kN)	Peak Q_c/Q_m	Residual Capacity (kN)	Residual Q_c/Q_m	Displacement to peak (%D_o)	Peak Load (kN)	Peak Q_c/Q_m	Residual Capacity (kN)	Residual Q_c/Q_m	Displacement to peak (%D_o)
17	6979.3	1.16	6510.04	1.19	5.8	10821.1	0.67	10248.05	0.69	2.9
18	7024.0	1.16	6459.63	1.18	5.8	10442.9	0.65	9905.37	0.66	2.9
	6846.0	1.14	6451.07	1.18	5.8	10426.3	0.65	9971.09	0.67	2.9
19	6836.1	1.13	6248.41	1.14	5.8	10305.3	0.64	9075.37	0.61	2.9
20	8424.5	1.40	7948.78	1.45	6.8	12426.8	0.77	11074.10	0.74	2.9
21	8479.5	1.41	7977.35	1.46	6.8	11894.2	0.74	10462.10	0.70	2.9
22	6976.4	1.16	6457.56	1.18	5.9	10375.5	0.64	9905.68	0.66	2.9
	6994.3	1.16	6457.62	1.18	5.9	10360.0	0.64	9905.77	0.66	2.9

4.4. Recommendations from results

From an investigation of the results of the analyses performed for the Pentre and Tilbrook case studies, recommendations can be made to improve the accuracy of the prediction of the response of OEPs in clays. These recommendations focus on the improved modelling of the resistive components. If the shaft and end bearing parameters, from the API and ICP, are input into a finite element method, the API-FEA and ICP-FEA are derived, both variants of the basic method. The recommendations outlined herein will be used to form a modified (mod-) version of these finite element variants with the intention of improving the estimates of pile head response. These -mod versions will be introduced and expanded on in Chapter 6.

4.4.1. External Shaft Resistance Mobilisation, τ_{ext}

4.4.1.1. Parameters

The API pile design method is a total stress method that relates the shaft friction of a pile, τ_f, to s_u, using factors derived from σ'_{v0}. The ICP design method is determined by an effective stress method, based on a Coulomb failure approach, requiring factors including K, σ'_{v0}, δ and YSR. As shown in Table 4-3, from the database selected for this study, the API performs better overall. The Q_c/Q_m values for the total pile capacity considering the entire dataset are 1.02 and 0.60 for the API and ICP methods respectively (Table 4-3). The API therefore requires less soil parameters and performs better.

The Author recommends that for entirely clay stratigraphies, the API method of deriving τ_f is used and this recommendation will be taken forward for further analysis.

See Section 4.3.2.1, Case 1 and Section 4.3.2.2, Case 11.

4.4.1.2. Peak vs Ultimate δ_f

The interface friction angle, δ_f, accounts for the interface roughness between the pile and soil. When the API-FEA method is used, the values of τ_{ext} computed are peak values, which are reduced to their ultimate values via the t-z soil reaction curves. This procedure will be maintained for further analysis when using API derived parameters. Similarly, when using ICP parameters, the Author recommends using only δ_{peak} values to compute τ_{ext}. For an improved estimate of the reduction to the ultimate values in the t-z soil reaction curves, interface ring shear tests should be performed.

See Section 4.3.2.1, Case 1 and Section 4.3.2.2, Case 10 & Case 15.

4.4.1.3. Displacement to Peak

The displacement required to achieve the peak shaft loading is usually set at $0.01D_o$. Figure 4-72 plots the displacements required to mobilise the peak values of τ_{ext}, as a decimal of D_o, against the depth under consideration, h, normalised by D_o. These values are extracted from both Pentre and Tilbrook. The figure shows that when z_{peak} =$0.01D_o$, this is a lower-bound but as shown in Case 3, Case 14 and Case 15, this value of z_{peak} improves the prediction of the load-displacement response and is therefore recommended to be maintained in further analyses.

Another consideration can be the use of the rigidity index, I_r. This is deduced from the site measurements of G_{vv} and s_u and compared to the t-z curves measured at both Pentre and Tilbrook. According to Teh (1987), as the I_r increases, the failure zone increases (at the base of a footing). If one were to assume that

$$\frac{z_{peak}}{D_o} \propto \frac{s_u}{G_{vv}} \tag{63}$$

$$\frac{z_{peak}}{D_o} I_r = k \tag{64}$$

The *k* term is plotted against h/D_o for the OEPs at Pentre and Tilbrook as shown in Figure 4-73. From the data a constant value cannot be observed from these sites, but rather k ranges between 50 to 550.

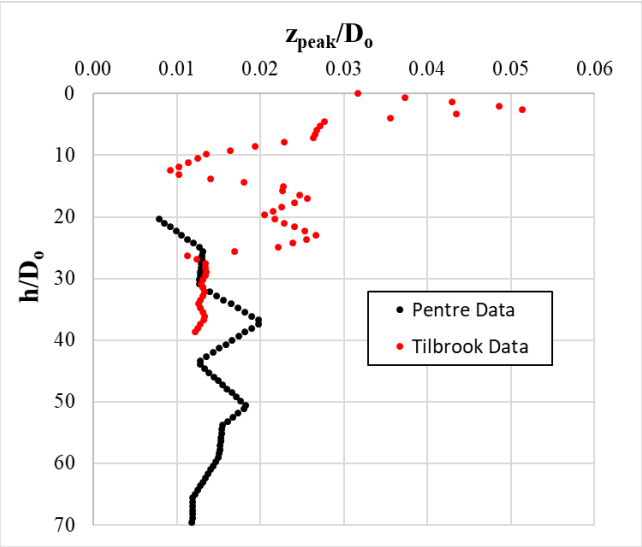

Figure 4-72 Displacement to peak ratio along pile length.

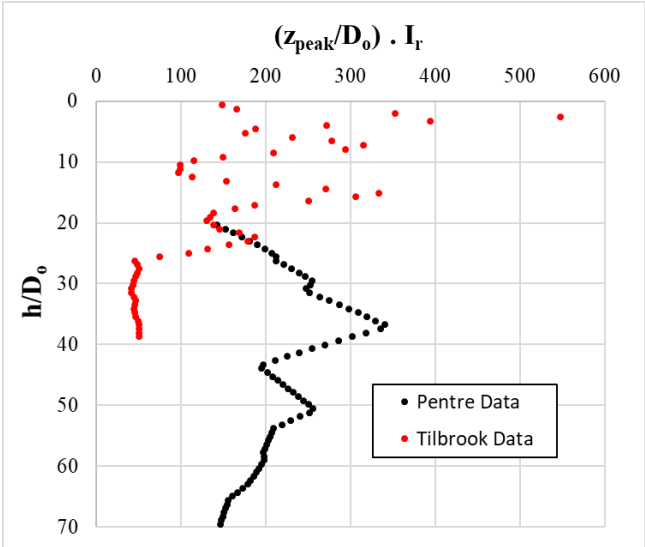

Figure 4-73 Product of displacement to peak ratio and rigidity index along pile length.

When different ratios of z_{peak}/D_o were investigated in the test cases, the load-displacement responses were found to converge to the same ultimate load-displacement result. The curves with a softer stiffness were found to achieve a slight increase in the peak response after some further displacement.

See Section 4.3.2.1, Case 3 and Section 4.3.2.2, Case 14 & Case 15.

4.4.1.4. t-z reaction curves – API vs DNV

For the case study investigated, the DNV t-z soil reaction curves were found to predict an improved stiffness response compared to the API t-z curves in the ICP-FEA method. However, the increase in accuracy was marginal and more data would be needed to advocate definitively that the DNV recommended curves are superior to the API's. In addition, there is no softening guidance provided by the DNV method. Currently the Author recommends that the API curves are used.

See Section 4.3.2.2, Case 15.

4.4.1.5. ICP - K_f/K_c

In Case 20, the ICP-FEA method was used to assess the impact of omitting the K_f/K_c term in computing τ_f. The axial load response was observed to be approximately 20% higher than the ICP base case and gave a much higher peak capacity at both the Pentre and Tilbrook sites. The values of Q_c/Q_m increased from 1.22 to 1.45 at Pentre and from 0.66 to 0.74 at Tilbrook. The ICP design method (based on Lehane, 1992) adopts a ratio of K_f/K_c of 0.8 to account for the reduction of total pile capacity to the ultimate capacity. This procedure essentially negates the development of a peak

on the load-displacement curve and targets the ultimate value. This omission is a conservative means of achieving the capacity of a pile (at $0.1D_o$) when static analyses are being performed. Static analyses use a capacity rather than a response and assumes the soil layers will mobilise their ultimate values simultaneously, no matter the length of pile. However, for non-linear analyses, where more detailed load-displacement responses are necessary, this process needs to be more precise. The Author therefore recommends that in these latter cases, the K_f/K_c term is omitted from the expression for τ_f.

See Section 4.3.2.2, Case 20.

4.4.1.6. ICP – *R** vs *R*

R is used in the ICP design method when designing CEPs and a modified R^* value used for OEPs. If R is instead used for OEP designs, this gives larger values of τ_f. Q_c/Q_m was observed to be increased by approximately 20% at both sites, specifically from 1.22 to 1.46 at Pentre and from 0.66 to 0.70 at Tilbrook. As both the omission of K_f/K_c and the change from R^* to R has the effect of increasing τ_f, when a 1D FE procedure is to be performed, the Author does not recommend altering both simultaneously and in this case R^* will continue to be used for OEPs.

See Section 4.3.2.2, Case 21.

4.4.2. Internal Shaft Resistance Mobilisation, τ_{int}

4.4.2.1. Constrained Modulus, *M*

In Case 7 and Case 18, the constrained modulus, M, was varied. This was found to be best represented when obtained by factoring the undrained shear strength, i.e. ks_u. As shown in these cases, the estimates of τ_{int} are mobilised from the bottom up as the base of the plug reacts against the soil below the plug. The results also demonstrate a good comparison when the summation of τ_{ext} and τ_{int} were compared to the measured values, suggesting a match with the other component stiffnesses. $M = ks_u$ will be brought forward for further analysis.

See Section 4.3.2.1, Case 7 and Section 4.3.2.2, Case 18.

4.4.2.2. Total shaft friction, τ

From the analysis performed using the API-FEA and the ICP-FEA, a better match is found when the shaft stresses are summed. The results showed that there is significant advantage to the combination of τ_{ext} and τ_{int}. This will therefore be performed for subsequent analyses.

See Section 4.3.2.1, Case 1 & Case 7 and Section 4.3.2.2, Case 11 & Case 18.

4.4.2.3. Internal Interface Resistance, τ_{int}

In clays, the peak value of τ_{int} is difficult to estimate as limited data is available for its validation. One of the fundamental characteristics of the soil plug is that it is completely separated from the external soil. This means that any effects that occur in clays over time, such as the reduction in pore water pressure, may not fully occur within the plug as the drainage path is quite long and offshore piles are submerged. This suggests that the soil plug will remain in an undrained or partially drained state for most of its lifetime. This is an important consideration as the design methods for OEPs estimate τ_{ext} by using either total stress (API) or effective stress (ICP) methods. Under loading, there will be no gain in strength as a result of dissipation of porewater pressure, therefore the existing effective stress of the soil will govern and the load will mainly be taken by excess porewater pressure within the plug. The ICP method derives τ_f based on soil behaviour post-equalisation, and as this will not happen, the API total stress methodology is recommended to compute, τ_{int}.

See Section 4.3.2.1, Case 7 and Section 4.3.2.2, Case 18.

4.4.2.4. z_{peak}/D_i

The ratio of the displacement-to-achieve-peak-resistance to D_i should be taken as very stiff due to the confined nature of the soil within the plug. From Case 2 and Case 13 and from studies performed by Doherty *et al*. (2010) and Matsumoto (1995), to effectively transfer the load from the pile to the plug, the assumption of a rigid interface is therefore applicable. $z_{peak}/D_i = 0.0001$, will therefore be maintained.

See Section 4.3.2.1, Case 2 and Section 4.3.2.2, Case 13.

4.4.3. Base Resistance

4.4.3.1. Resistance at pile base, $q_{b,p}$

It can be argued that at the base of the annulus, the soil will be free draining and due to installation and equalisation, can be considered drained. Also due to installation by impact driving, the soil just below the annulus will also be in a highly compacted state.

As per the API-FEA design method, $q_{b,p}$ is computed as $N_c s_u$, where N_c = 9. However, this bearing capacity factor is not necessarily the most ideal as its applicability was observed to have a limited range in the tests analysed. In the OC clays at Tilbrook, N_c = 9 was applicable, however in the NC clays at Pentre this was too small and a larger value of approximately 16 was more appropriate. Similarly, when the API-FEA method was used with a base resistance related to q_c (using a factor of 1.6) rather than s_u, an improved estimate was observed at Tilbrook but not at Pentre. The difference here may be a factor dependent on the OCR, however the data to determine this factor is limited.

In terms of the ICP-FEA design method, the base capacity of the annulus was directly analysed using a range of resistances to compare with the measured response. In general, when the base resistance was applied equally to both $q_{b,p}$ and $q_{b,pl}$ as per the ICP method, the comparisons did not match the data well, however, $q_{b,p}$ = 1.6q_c seems to be applicable. From the analyses performed, it is therefore recommended that for clays, the annular resistance and the plug resistance should not be equal. The suggested value of $q_{b,p}$ is 1.6q_c.

See Section 4.3.2.1, Case 5 and Section 4.3.2.2, Case 12, Case 16 & Case 17.

4.4.3.2. Displacement to mobilise peak resistance of pile, $z_{peak,p}/t$

The ultimate resistance at the base of the annulus should be mobilised at 10% of the wall thickness (t). This has been found to better match the results of the mobilised end bearing at both Pentre and Tilbrook sites and will be used in further analyses.

See Section 4.3.2.1, Case 4 and Section 4.3.2.2, Case 16.

4.4.3.3. Stress-strain (constitutive) model of $q_{b,p}$

The Q-z curve from the API has been used as the constitutive model of $q_{b,pl}$ and found to produce acceptable results. It is therefore recommended that this method of deriving the stress-strain relationship be maintained for $q_{b,p}$. There is however no accurate way to prove that this is the response of the pile only, as this resistance has not been effectively isolated in any of the available tests.

See Section 4.3.2.1, Case 4 and Section 4.3.2.2, Case 16.

4.4.3.4. Resistance at plug base, $q_{b,pl}$

The resistance at the base of the plug cannot be the same as that under the annulus. This is mainly due to the driving process which compresses the soil below the annulus to a greater extent than below the plug. The resistance at the base of the plug has been investigated using different values.

As per the API-FEA method, the pile was interpreted as plugged for both the Pentre and Tilbrook sites, thereby applying $q_{b,pl} = N_c s_u$ to the full base area. In addition to this, $0.2q_c$ was selected to derive $q_{b,pl}$ for different values of $q_{b,p}$. The results of these analyses showed quite varied results at both sites; at Pentre it was not possible to replicate the measured response, whereas at Tilbrook a better match was found.

As per the ICP design method, recommended values of $q_{b,pl}$ are provided for conditions where an OEP has been interpreted as fully plugged using the ICP criteria. These plug resistances, considering both drained or undrained conditions, were applied over the full base area in the ICP-FEA at the test sites. The results observed in the cases demonstrate that these resistances cannot be the same for each component as the stiffness of each is very different and found to vary. Additionally, the soil at the base of the plug can be considered as undrained, however under sustained loading, some drainage will likely occur thereby increasing the resistance. From the cases assessed, the recommended values from the ICP-FEA for $q_{b,pl}$, lie in the range $0.4q_c$ to $0.65q_c$.

It is not possible to decipher exactly how much load was supported by the plug as only the total load in the pile was measured. However, using $q_{b,pl} = 0.2q_c$, the results, especially for Tilbrook, show a better match, and this can generally be considered a conservative estimate. This recommendation will therefore be taken forward for further analyses.

See Section 4.3.2.1, Case 5 and Section 4.3.2.2, Case 12 & Case 16.

4.4.3.5. Displacement to mobilise peak resistance of plug base, $z_{peak,pl}/D_i$

The mobilisation of different pile components is necessary to mobilise the soil plug. This is done primarily through the shear-transfer along the length of the plug, causing a downward force pulling the plug to engage with the soil at its base. The relative stiffness of these components dictates the ratio of $z_{peak,pl}/D_i$. The value of D_i has a direct influence on this mobilisation. The larger this value, the less will be the confining stress needed to allow the assumption of the uniform stiffness of the layers (M) to be maintained. From the analyses performed, the full capacity of the plug was not fully reached after a pile head displacement equal to $0.1D_o$, and therefore the assumptions chosen are deemed adequate. The recommended displacement to achieve the ultimate value of $q_{b,pl}$ is therefore $0.1D_i$.

See Section 4.3.2.1, Case 6.

4.4.3.6. Stress-strain (constitutive) model of plug base

The Q-z curves from the API have been used in these analyses and produced acceptable results. It is therefore recommended that these curves be adopted as the constitutive model of $q_{b,pl}$.

See Section 4.3.2.1, Case 6.

4.4.4. Miscellaneous

4.4.4.1. Pile and plug weights

The installation of the pile will cause the soil to be displaced. Once installed, the weights of the pile and plug will act together and require support before further load is applied. The effects of these weights have been found to be marginal when compared to the design loads that OEPs offshore are required to support. It is therefore recommended that, even though these self-weights have not been found to be critical, these should remain included in the analysis.

See Section 4.3.2.1, Case 9 and Section 4.3.2.2, Case 22.

4.4.4.2. End bearing plates and channels

The plates were positioned at the base of the channels on the inside of the pile. These were not continuous and had spaces between them. The analysis performed assessed if the presence of the

plates removed the contribution of the plug length above. As greater capacity was observed than estimated, there seems to have been little effect on the base capacity by the presence of the plates, which suggests that beyond the plates, the plug length did contribute to $q_{b,pl}$.

Additionally, it is possible that the plates contributed to $q_{b,p}$, although this would have been a negligible quantity. If the base plates are to be included in the annular area, this should therefore be used in conjunction with τ_{int}, along the full plug length.

See Section 4.3.2.1, Case 8 and Section 4.3.2.2, Case 19.

5. Base Capacity of Open Ended Piles in Sand

This chapter examines the mobilisation of base capacity of OEPs in sandy soil. For this study, three OEP design methods are considered: the API, ICP and UWA methods. The study commences with an outline of each of the test sites from the geotechnical engineering database for OEPs in sand, highlighting key information. This is followed by an analysis of the performance of each design method in predicting the distribution of shaft and base capacities in each of the test sites. The results of an RMS-error calculation are shown, which is used to determine if a factor can be applied to the estimated static shaft and end bearing capacities to improve the load-distribution to these components. From the tests sites, three are selected to perform a detailed sensitivity analysis by systematically adjusting the input parameters and comparing the results from VIRTUPLUG to the measured data. The selected tests are those at the Pigeon Creek, the Kwangyang Plant and the Euripides sites. Both the Pigeon Creek and Kwangyang Plant sites adopted double walled piles, and detailed comparisons are made with the results from these. Recommendations to better estimate the behaviour of OEPs under axial load in sand are then made, using the findings of the finite element analyses.

5.1. Case Study Evaluation

In a similar way to the investigation performed on clay soil, the pile tests in Table 5-1 were selected based on the following characteristics below:

- Open-ended piles
- Uniform cross sections
- All steel
- Installed by driving
- Static compression loading
- Circular

As a comparison, this database contains 21 tests, and the Chow (1997) database contains 65.

The databases being used in this research project for sands and clays are not entirely consistent. These pile tests include an amalgamation of piles tested in compression only, tension then compression, differential degrees of residual stresses, double and single walled piles, varying pile lengths and tested at different times after initial installation. These differences, along with the inherent variation in soil, make accurate predictions of behaviour and capacity from empirical relationships difficult.

Table 5-1 Plug Capacity Validation in Sands

Site Number	Site	Location	Pile Test Number	Reference Authors	Length (m)	Diameter (m)	t (mm)
1	Pigeon creek	Pigeon River, USA	2	Salgado et al. (2002)	7.0	0.356	32.0
2	Kwangyang Plant	Korea	TP1	Ko & Jeong (2014)	8.6	0.508	50.8
3	Kwangyang Plant	Korea	TP2	Ko & Jeong (2014)	11.4	0.712	50.8
4	Kwangyang Plant	Korea	TP3	Ko & Jeong (2014)	15.5	0.914	50.8
5	Mobile Bay	AL, USA	AL-1	Mayne (2013)	15.2	0.324	25.4
6	Mobile Bay	AL, USA	AL-2	Mayne (2013)	42.7	0.324	25.4
7	Hoogzand	The Netherlands	1-C	Beringen (1979)	7.0	0.356	16.0
8	Hoogzand	The Netherlands	3-C	Beringen (1979)	5.3	0.356	20.0
9	Dunkirk	France	C1-C	Chow (1997)	10.0	0.457	13.5
10	Euripides	The Netherlands	1a	Kolk et al. (2005b)	30.5	0.763	35.6
11	Euripides	The Netherlands	1b	Kolk et al. (2005b)	38.7	0.763	35.6
12	Euripides	The Netherlands	1c	Kolk et al. (2005b)	47.0	0.763	35.6
13	Euripides	The Netherlands	II	Kolk et al. (2005b)	46.7	0.763	35.6
14	Tokyo Bay	Japan	TP	Shioi et al. (1992)	30.6	2.000	34.0
15	Drammen	Norway	16-P1-11	Tveldt & Fredriksen (2003)	11.0	0.813	12.5
16	Drammen	Norway	25-P1-15	Tveldt & Fredriksen (2003)	15.0	0.813	12.5
17	Drammen	Norway	25-P1-25	Tveldt & Fredriksen (2003)	25.0	0.813	12.5
18	Hound Point	Scotland	P(0)-C	Williams et al. (1997)	26.0	1.220	24.2
19	Shanghai	China	ST-1	Pump et al. (1998)	79.0	0.914	20.0
20	Shanghai	China	ST-2	Pump et al. (1998)	79.1	0.914	20.0
21	Ras Tanjib	Saudi Arabia	C	Helfrich et al. (1985)	18.0	0.610	28.6

The following sections outline some of the key geotechnical characteristics at each of the sites listed in Table 5-1.

5.1.1. Pigeon Creek, USA – Salgado *et al.* (2002)

The Pigeon Creek site is in Lagrange County in Indiana, USA and the soil consists predominantly of gravelly sand to 13m. The initial 2m was removed prior to pile driving to enable targeting of the required soil layer. The soil here contained no fines. The initial 3m, was found to be loose, whereas the remaining 13-14m was predominantly dense to very dense. The dry unit weights of the sand varied across the site from 18.64kN/m³ to 15.61kN/m³. The internal friction angle of the sand was 33.3°. CPT testing was performed both before and after soil testing. The CPT results measured 15-25MPa as shown in Figure 5-1, along with the sleeve friction and friction ratio.

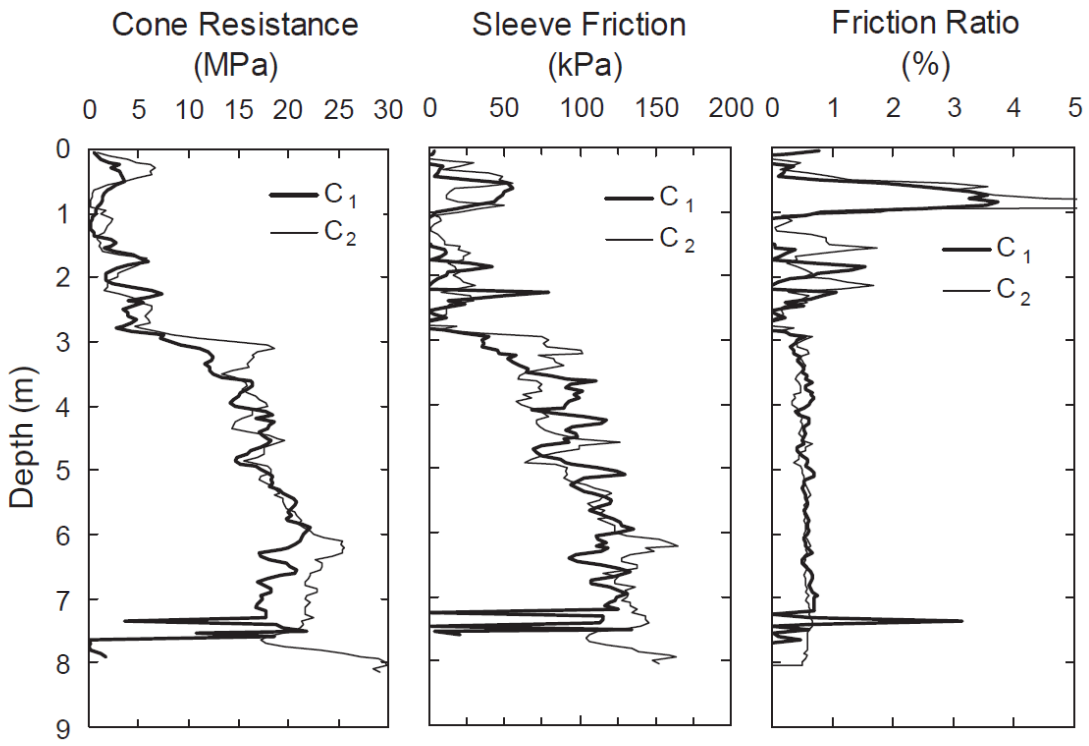

Figure 5-1 Cone resistance, sleeve friction and friction ratio (Salgado et al, 2002).

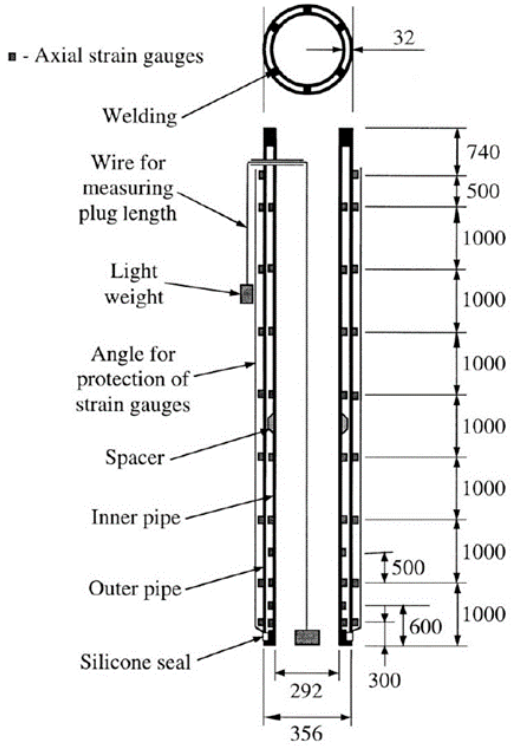

Figure 5-2 Double-walled open-ended test pile (Salgado et al., 2002).

At this site a double-walled OEP was driven to about 7m and tested. The outer and inner piles had D_o values of 356mm and 305mm respectively. Both piles in this configuration had t's of 6.4mm with strain gauges installed along the length of each pile. The arrangement is shown in Figure 5-2. There was an extra concentration of strain gauges near to the annulus to ensure that the computed load along the pile length was balanced by that interpreted near to the base. The loads were applied to the pile in small increments specifically 150, 290, 440, 590, 740, 880, 980, 1130, 1230 and 1280kN. The base of the pile was an extension of the internal pile. This was then connected to the external pile using a silicone seal which extended to a length of 30mm to ensure that no load was transferred to the external pipe.

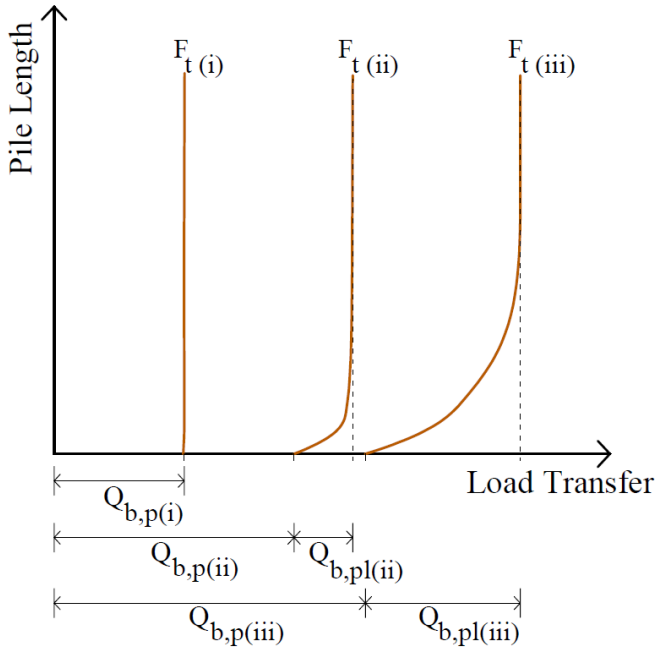

Figure 5-3 Internal interface load-transfer to base.

The results from the double wall pile tests gave strains along the internal and external piles, which allows the load-transfer to be calculated. A schematic of the load-transfer is shown in Figure 5-3. Under small incremental loads, the capacity of the annulus, $Q_{b,p}$, is usually mobilised initially at the first load increment, $F_{t(i)}$. Under additional loading, $F_{t(ii)}$, the plug capacity gradually mobilises, $Q_{b,pl}$, thereby increasing the total base capacity. During these tests however, several external strain gauges, along the lower end of the pile, failed during pile installation, so no readings were recorded at their depths.

5.1.2. Kwangyang Plant, South Korea – Ko & Jeong (2014)

This site consists of (reclaimed) sandy fill material to 14.6m, underlain by sand. No CPTs were performed, however, SPT readings are available for the site and ranged from 8 to 18. The unit weight of the fill and sand was measured as 17.6kN/m³ and 18kN/m³, respectively. The internal friction angle for the materials were 32° and 33°, respectively.

Figure 5-4 Base configuration of double walled piles (Ko & Jeong, 2015).

Three OEPs of different diameters, wall thicknesses and lengths, designated TP-1, TP-2 and TP-3, were tested at this site. The values of D_o were 508mm, 711mm and 914mm, respectively, each with a wall thickness of 50.8mm. The respective pile lengths were 8.6m, 11.4m and 15.5m. A uniform sandy fill profile was present for pile TP2 and therefore used further in this study. This pile was also double-walled, so results, similar to those outlined in Figure 5-3, are compared. In this test case, instead of a sliding mechanism, allowing both

pile walls to move independently, the bases of the two pipes were welded together using a circular steel plate, as shown in Figure 5-4, causing a small degree of load-transfer. This pile also had a 0.4m stick-up, and the initial strain gauge on the external and internal pile was located, below ground level, at 1.9m and 3.7m, respectively. Each pile (TP-1, TP-2 and TP-3) was loaded to 1000kN, 2000kN and 3000kN, respectively, after which instead of continuing to add additional load, these were maintained for about 20 minutes each and the displacement observed. The load-displacement response provided by the authors therefore suggest that these loads are the pile capacities; however, the sum of the measured loads along the inner and outer piles, and at the annulus, do not match with these loads. This leads to some difficulty in correctly estimating the true base capacity. Therefore, the sum of the loads along the internal pile and at the annulus, when the peak pile-head load was applied, was taken as the base capacity, and the sum of the loads along the external pile when the peak pile head load was applied, was taken as the shaft capacity. Due to the rate at which the loads were applied and then held, rate effects could have been the cause of these discrepancies.

5.1.3. Mobile Bay, USA – Mayne (2013)

Limited data is available for this site. Yang *et al*. (2016) present CPT results from which parameters for the design methods can be estimated. The capacities using various design methods are also presented for comparison. The measured q_c values are upwards of 30MPa at both sites.

5.1.4. Hoogzand, The Netherlands – Beringen (1979)

This site was located at Hoogzand/Oostermeer in the Netherlands. The upper 2m of the site was found to be medium dense sand, followed by a 0.5m thick sandy clay layer underlain by very dense sand to approximately 9.5m. In the dense sand layer, CPT testing produced q_c values of 24 to 64MPa and the average internal friction value was found to be 38°. The plug length ratio, or PLR (the ratio of the length of the plug to the pile length), was 0.66 and 0.77 for pile tests 1-C and 3-C, respectively.

5.1.5. Dunkirk, France – Chow (1997)

The tests were performed at the Port Authority of Dunkerque, France. This site is comprised predominantly of a 30m thick sandy alluvial deposit which is overlain by a 3m thick recent hydraulic sandy fill. The underlying sand is described as medium dense with a dry unit weight of 16.5kN/m³.

CPTs measured q_c values of more than 30MPa in the fill material; 10 to 20MPa from 8m to 10m; and 23 to 30MPa at depths greater than 10m. The water table was encountered at 4.8m below ground level.

5.1.6. Euripides, The Netherlands – Kolk *et al*. (2005b)

This site is situated in Elmshaven in the Netherlands and consisted predominantly of sand. There was 2m of made ground, which was underlain by tidal flat deposits and a layer of clayey sand near 20m. From 25m depth to about 68m below the surface there was very dense sand. The water table was found at 0.5m below ground level.

The pile tested here was a 762mm open-ended pile. This comprised a 27m long instrumented section and a 22m long add-on. The instrumented pile had a wall-thickness (t) of 35mm with that of the add-on's being 41mm, to provide sufficient bending resistance in the upper portion of the pile. The instrumentation included a combination of axial and tangential (shear) strain gauges to enhance the accuracy of the axial pile capacity results. In addition, 4 base sensors were installed on the pile to improve the measurement of the base load. The pile was driven and tested twice, and in both driving cases, the base sensors were damaged.

The tests were performed in several stages comprising three alternating series of compression and tension tests, 1a, 1b and 1c. When the pile was retrieved, re-installed and tested, at a different location at the same site, this was test 2. For this study, only test 1c will be used for a detailed analysis.

5.1.7. Tokyo Bay, Japan – Shioi *et al*. (1992)

These pile tests were used to facilitate the construction of the Trans-Tokyo Bay Highway. The water depth was 24.5m. There was a 4m thick layer of loose alluvium sandy deposit, underlain by layers of sand and clay. From 8m below the seabed, the soil was comprised of predominantly sand interspersed with thinner layers of cohesive clay. CPT testing measured q_c values that ranged from 30 to 50MPa. The q_c values in the clay layers were approximately 5MPa.

5.1.8. Drammen, Norway – Tveldt & Fredriksen (2003)

The pile tests were performed at the site of a two-lane bridge crossing the Drammen river in Norway. The stratigraphy differed at the two pile testing sites. At the middle of the bridge, Location 25-P1,

there was a 35-40m thick sand layer underlain by silty over-consolidated clay. The sand is described as medium dense with an internal friction angle of about 35°. The clay is firm, silty and slightly sensitive. At the location nearer to the bank, Location16-P1, the sand layer decreased to about 15.5m thick, again underlain by the silty clay.

5.1.9. Hound Point, Scotland – Williams *et al*. (1997)

This test was part of an extension of an existing jetty at Hound Point on the Firth of Forth, Scotland. There were three main soil units here. The initial layer was a thin unit of loose sand followed by a lightly over-consolidated glacial clay and a thick stratum of late glacial outwash of sand, gravel and cobbles. The underlying rock at the site was a mixture of limestone, sandstone and mudstone. CPT data is available for the sandy layers and shows values ranging from 10 – 40MPa. The interface friction angle was about 23°.

5.1.10. Shanghai, China – Pump *et al*. (1998)

The pile test performed here was intended for a new building in Shanghai, China. The site lay on the delta of the Yangtze River where the soil is mainly thick alluvium sediments to about 140m. The ground water on the site was about 0.5m below ground level. The stratigraphy of the sedimentary layers involved interbedded clays, silts and sands. The initial 30m was comprised mainly of clays with a large silt fraction. Underlying this were the main sand layers, of over 100m thickness, that piles in Shanghai are usually embedded. CPT testing was performed here and these sands had q_c values ranging from 11 to 22MPa.

5.1.11. Ras Tanjib, Saudi Arabia – Helfrich *et al*. (1985)

The pile tests were performed on the east coast of Saudi Arabia in Ras Tanajib. The soils in this region are quite complex due to their variability. The pile tests were performed at a site which comprised loose to medium dense Holocene deposits to about 10m, underlain by very dense Pleistocene sand. This denser sand layer is described as lightly cemented granular soil with some silt content. CPT testing found q_c values increasing from 0MPa at the surface to 45MPa at 6m depth. Below 6m, the q_c values were much greater than 45MPa.

5.2. Evaluation of Performance of Current Design Methods

Applying the API, ICP and UWA methods at these sites, Table 5-2 shows the results of using the methods directly to determine the load distribution. The total end bearing, computed as the sum of the annulus and plug capacity, is added to the shaft friction to obtain the total capacity. This table shows 21 tests from which total capacity was extracted. At 13 of these sites, the total end bearing was extracted and from these, at 4 sites, double walled piles were used.

To demonstrate the contribution of the plug, all cases assume a fully plugged end bearing condition and the resistance below the annulus and plug was equated. It is notable that the API method predicted that over 50% of the piles would behave in an unplugged manner. Figure 5-5 to Figure 5-13 demonstrate, graphically, the results shown in Table 5-2.

In terms of total capacity, the values estimated using the API method (Figure 5-5), show the widest variation to those measured. The ICP values, however, (Figure 5-6) show the best match, and the UWA values (Figure 5-7) show a relatively good match, although those values estimated using the ICP method are marginally better.

In terms of shaft friction, Figure 5-8 indicates that the shaft friction is generally underestimated when using the API method directly. With the ICP method used, a better distribution is observed (Figure 5-9) and when the UWA is used (Figure 5-10), a more uniform underestimation is observed.

Figure 5-11 to Figure 5-13 show the distribution of the estimated base capacity using the API, ICP and UWA methods respectively. In general, no method can clearly be suggested as the best, however the UWA estimations are, in general, overestimates.

Table 5-2 Direct calculation and Q_c/Q_m for the OEP validation database.

Site #	Site	D (m)	D/t	L/D	Measured			API						ICP						UWA					
					Total Capacity (kN)	Total Shaft Friction (kN)	Total End Bearing (kN)	Total Capacity (kN)	Total Shaft Friction (kN)	Total End Bearing (kN)	Q_c/Q_m Total Capacity	Q_c/Q_m Total Shaft Friction	Q_c/Q_m Total End Bearing	Total Capacity (kN)	Total Shaft Friction (kN)	Total End Bearing (kN)	Q_c/Q_m Total Capacity	Q_c/Q_m Total Shaft Friction	Q_c/Q_m Total End Bearing	Total Capacity (kN)	Total Shaft Friction (kN)	Total End Bearing (kN)	Q_c/Q_m Total Capacity	Q_c/Q_m Total Shaft Friction	Q_c/Q_m Total End Bearing
1	Pigeon creek	0.356	11	20	1029	310	719	577	189	388	0.56	0.61	0.54	1179	625	554	1.15	2.01	0.77	1271	441	831	1.24	1.42	1.16
2	Kwangyang Plant	0.508	10	17	965	651	314	807	300	507	0.84	0.46	1.62	855	515	340	0.89	0.79	1.08	1059	451	607	1.10	0.69	1.93
3	Kwangyang Plant	0.712	14	16	1777	943	834	1907	677	1231	1.07	0.72	1.48	1608	992	616	0.91	1.05	0.74	1986	843	1143	1.12	0.89	1.37
4	Kwangyang Plant	0.914	18	17	2837	1947	890	4128	1495	2633	1.46	0.77	2.96	2358	1766	592	0.83	0.91	0.67	2569	1432	1136	0.91	0.74	1.28
5	Mobile Bay	0.324	13	47	1246	-	-	946	504	443	0.76	-	-	878	696	182	0.70	-	-	796	541	254	0.64	-	-
6	Mobile Bay	0.324	13	132	3350	-	-	2675	2262	412	0.80	-	-	3210	2579	632	0.96	-	-	2193	1313	881	0.65	-	-
7	Hoogzand	0.356	22	20	2270	1310	960	702	219	483	0.31	0.17	0.50	2405	1375	1030	1.06	1.05	1.07	2254	919	1335	0.99	0.70	1.39
8	Hoogzand	0.356	18	15	1850	-	-	528	125	403	0.29	-	-	2088	883	1205	1.13	-	-	2202	592	1611	1.19	-	-
9	Dunkirk	0.457	34	22	2800	-	-	1361	521	840	0.49	-	-	2678	1445	1233	0.96	-	-	2849	1258	1591	1.02	-	-
10	Euripedes	0.763	21	40	7860	3860	4000	7907	3334	4572	1.01	0.86	1.14	9362	4876	4486	1.19	1.26	1.12	10353	2701	7652	1.32	0.70	1.91
11	Euripedes	0.763	21	51	12600	9400	3200	9833	5261	4572	0.78	0.56	1.43	16325	11674	4651	1.30	1.24	1.45	13371	5560	7811	1.06	0.59	2.44
12	Euripedes	0.763	21	62	18100	14150	3950	12178	7606	4572	0.67	0.54	1.16	22105	17171	4934	1.22	1.21	1.25	17134	7638	9496	0.95	0.54	2.40
13	Euripedes	0.763	21	61	17980	13410	4570	11674	7102	4572	0.65	0.53	1.00	19786	14635	5152	1.10	1.09	1.13	17236	7578	9658	0.96	0.57	2.11
14	Tokyo Bay	2.000	59	15	35112	25938	8958	38471	9028	29443	1.10	0.35	3.29	30683	25432	5251	0.87	0.98	0.59	27870	13053	14817	0.79	0.50	1.65
15	Drammen	0.813	65	14	1210	-	-	1441	470	971	1.19	-	-	1259	786	473	1.04	-	-	1185	521	664	0.98	-	-
16	Drammen	0.813	65	18	1890	-	-	2136	813	1324	1.13	-	-	1557	878	679	0.82	-	-	1381	419	962	0.73	-	-
17	Drammen	0.813	65	31	2700	-	-	4625	2419	2206	1.71	-	-	2464	1876	588	0.91	-	-	1675	842	833	0.62	-	-
18	Hound Point	1.220	50	21	6500	4000	2500	14706	4343	10363	2.26	1.09	4.15	5513	2547	2966	0.85	0.64	1.19	6251	1076	5175	0.96	0.27	2.07
19	Shanghai	0.914	46	86	14910	10720	4190	15100	11819	3281	1.01	1.10	0.78	16593	14489	2104	1.11	1.35	0.50	7887	4625	3261	0.53	0.43	0.78
20	Shanghai	0.914	46	87	16000	13600	2400	15123	11842	3281	0.95	0.87	1.37	13171	11066	2104	0.82	0.81	0.88	7895	4634	3261	0.49	0.34	1.36
21	Ras Tanjib	0.610	21	30	16800	-	-	3457	1317	2140	0.21	-	-	8455	5592	2863	0.50	-	-	8838	4036	4801	0.53	-	-

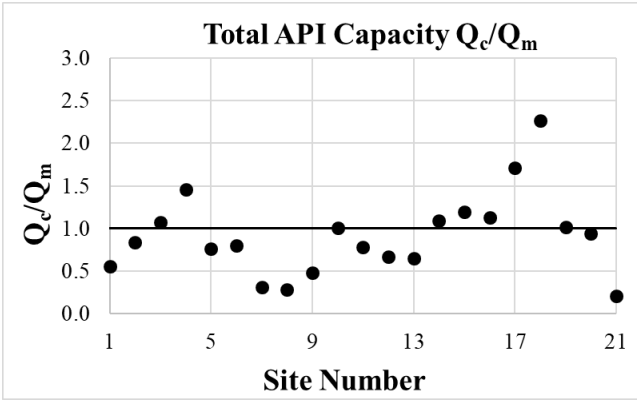

Figure 5-5 Comparison of the Q_c/Q_m of the total capacity using the API design method.

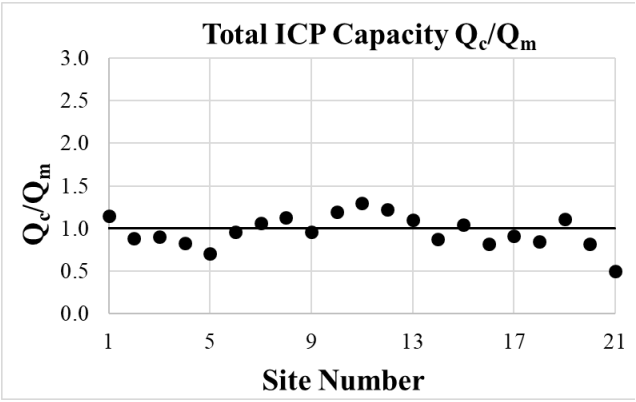

Figure 5-6 Comparison of the Q_c/Q_m of the total capacity using the ICP design method.

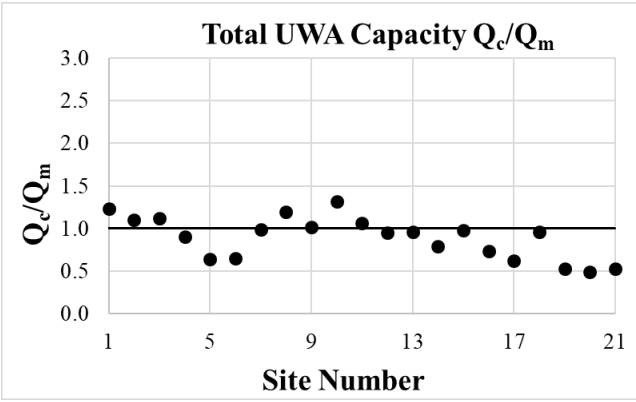

Figure 5-7 Comparison of the Q_c/Q_m of the total capacity using the UWA design method.

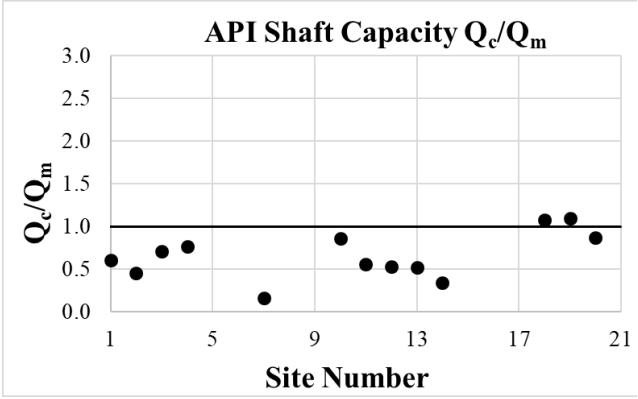

Figure 5-8 Comparison of the Q_c/Q_m of the shaft capacity using the API design method.

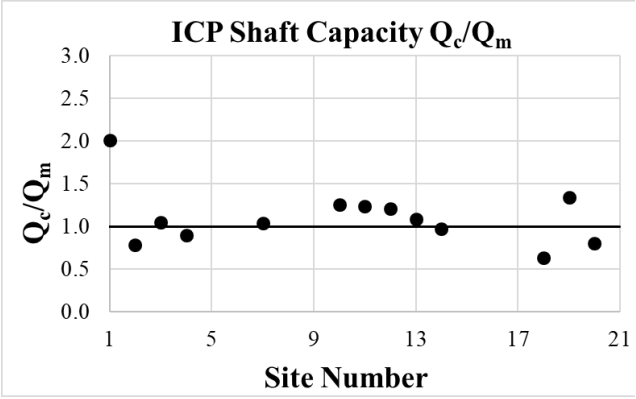

Figure 5-9 Comparison of the Q_c/Q_m of the shaft capacity using the ICP design method.

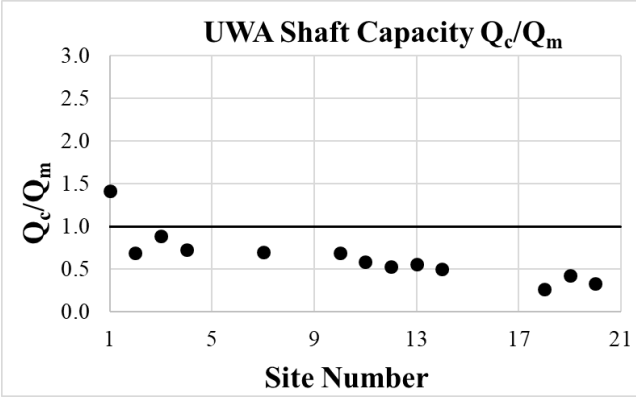

Figure 5-10 Comparison of the Q_c/Q_m of the shaft capacity using the UWA design method.

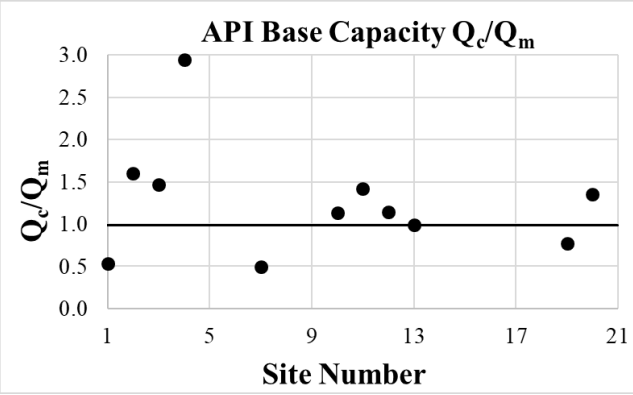

Figure 5-11 Comparison of the Q_c/Q_m of the base capacity using the API design method.

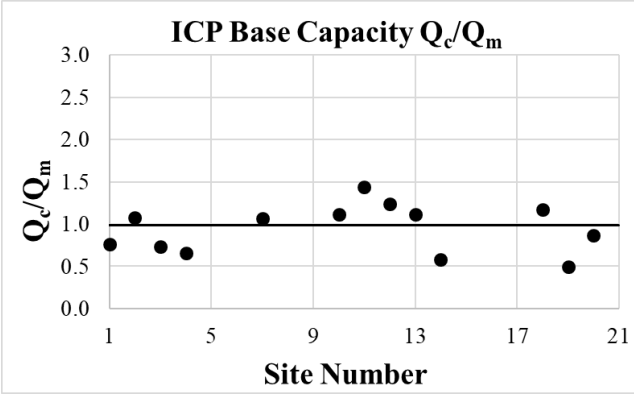

Figure 5-12 Comparison of the Q_c/Q_m of the base capacity using the ICP design method.

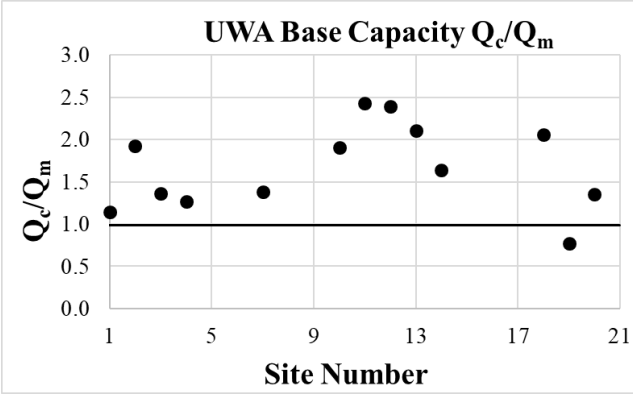

Figure 5-13 Comparison of the Q_c/Q_m of the base capacity using the UWA design method.

Table 5-3 Mean and standard deviation of Q_c/Q_m for the OEP validation database.

Statistic	API			ICP			UWA		
	Total Force Estimated	Shaft Friction	Total End Bearing	Total Force Estimated	Shaft Friction	Total End Bearing	Total Force Estimated	Shaft Friction	Total End Bearing
μ	0.916	0.663	1.646	0.968	1.108	0.956	0.894	0.823	1.682
σ	0.485	0.274	1.118	0.189	0.342	0.287	0.246	0.415	0.508
COV	0.530	0.414	0.679	0.195	0.309	0.300	0.275	0.504	0.302

Table 5-3 shows the computed mean and standard deviation, of the Q_c/Q_m values, for the database considered. This is shown separately for the end bearing, shaft friction and total capacity. The best estimation of the total capacity using the direct calculation, and considering all the sites in the database, is obtained by the ICP method. The mean Q_c/Q_m for total capacity is computed as 0.968 with a seemingly balanced split over the shaft (1.108) and end bearing (0.956). The values of standard deviation and coefficient of variation is also quite low for the estimated total capacity but increases when considering the values for the shaft and end bearing capacities separately. The UWA method gives an average Q_c/Q_m of total estimated capacity of 0.894 and the API gives 0.916. For both methods, the distribution of the load over the shaft and end bearing components is not very well balanced. In addition, the standard deviation and coefficient of variation are also quite high, suggesting that improvements can be made.

5.2.1. Contour Plots of the RMS-Error

Similar to the exercise performed in clays, by factoring the available end bearing and shaft friction results from the pile tests in sands, the root mean of the square of the normalised difference between measured and computed capacities (or RMS-error) can be found. This process is performed using Equation (62). Figure 5-11 to Figure 5-13 presents the results of the RMS-error calculation.

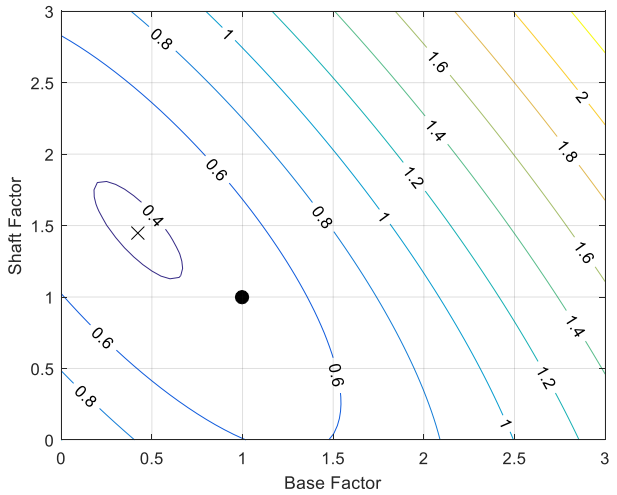

Figure 5-14 Contour Plot of the RMS-error for the API design method

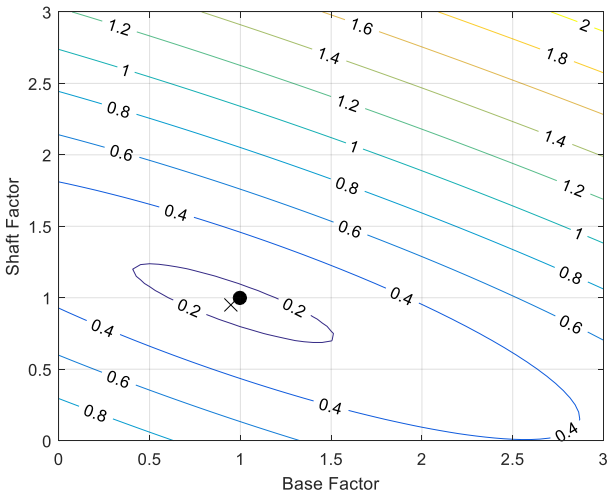

Figure 5-15 Contour Plot of the RMS-error for the ICP design method

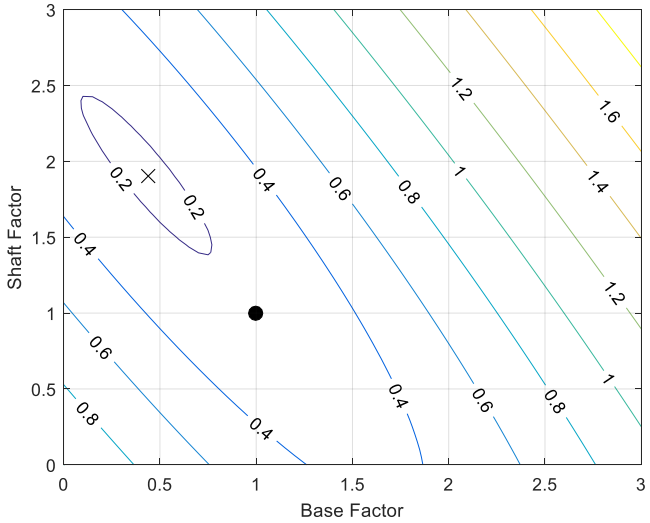

Figure 5-16 Contour Plot of the RMS-error for the UWA design method

As shown in Figure 5-14, the RMS-error deduced using the factored shaft and end bearing capacities from the API method is quite large. With no factors applied the RMS-error is about 0.50. The least error is found when the end bearing capacity is factored by 0.42 and the shaft by 1.45. The RMS-error associated with this distribution, however, is approximately 0.40.

The RMS-error is more acceptable when associated with values estimated from the ICP method. As shown in Figure 5-15, the least RMS-error is found when factors of 0.95 is applied to both the shaft and end bearing estimates of capacity. The RMS-error here is less than about 0.20, which also applies if no factors are applied.

Using the estimates of load distribution derived from the UWA method, Figure 5-16 shows that the least RMS-error would occur when a factor of 1.90 is applied to the shaft friction and a factor of 0.45 is applied to the end bearing.

5.2.2. Table of Factors Applied to the UWA method

The ICP method, when used directly, shows that when compared to the available pile tests in the database, it is clearly the best option for estimating the distribution of capacity of OEPs in sand. This suggests that the ICP methodology gives estimates of distribution that are close to the empirical error measured in the pile tests.

The UWA method is however, the most recent design method for OEPs in sand, and the results shown in Figure 5-16 suggest that the estimation of the distribution of capacity might be improved. The

results of the RMS-Error calculation suggest that factors could be applied to the shaft and base resistance in an effort to match more evenly the measured capacity distribution. An investigation was therefore launched to determine if factors can be applied to the values of σ'_{rc} and q_b, used in the UWA method, to match the measured load distribution better. The factors derived are shown in Table 5-4.

Table 5-4 Factored shaft and end bearing resistances derived to match the measured distributed loads, using the UWA method.

Site Number	Site	Location	Pile Test Number	Shaft Factor	Base Factor
1	Pigeon creek	Pigeon River, USA	2	0.67	0.86
2	Kwangyang Plant	Korea	TP1	1.50	0.52
3	Kwangyang Plant	Korea	TP2	1.13	0.73
4	Kwangyang Plant	Korea	TP3	1.39	0.78
5	Mobile Bay	AL, USA	AL-1	-	-
6	Mobile Bay	AL, USA	AL-2	-	-
7	Hoogzand	The Netherlands	1-C	1.46	0.72
8	Hoogzand	The Netherlands	3-C	-	-
9	Dunkirk	France	C1-C	-	-
10	Euripides	The Netherlands	1a	1.48	0.54
11	Euripides	The Netherlands	1b	1.75	0.41
12	Euripides	The Netherlands	1c	1.91	0.42
13	Euripides	The Netherlands	II	1.84	0.47
14	Tokyo Bay	Japan	TP	2.02	0.61
15	Drammen	Norway	16-P1-11	-	-
16	Drammen	Norway	25-P1-15	-	-
17	Drammen	Norway	25-P1-25	-	-
18	Hound Point	Scotland	P(0)-C	4.14	0.48
19	Shanghai	China	ST-1	2.53	1.28
20	Shanghai	China	ST-2	3.36	0.73
21	Ras Tanjib	Saudi Arabia	C	-	-
			Average	1.94	0.66

This produces average factors of 1.94 applied to σ'_{rc} and 0.66 applied to q_b which should give a more accurate representation of the distributed load over all the test sites. These average factors are quite similar to those derived from the RMS-error calculation results shown on Figure 5-16. Considering both sets of results, a factor of 2.0 applied to σ'_{rc} and 0.5 applied to q_b should give a better estimation of the capacity distribution. The application of these factors will be used as a test case later in this chapter, to determine the effect of this assumption on the estimated pile response.

5.3. Analysis Comparisons of Selected OEP Test Sites in Sands

This section examines in more detail, the behaviour of open-ended piles in sands. Similar to the procedure performed in clays, here, the results of the systematic variation of the input parameters to the finite element analysis are shown. This is performed to critically examine the sensitivity of the input parameters to the design methods and select the optimum input parameters to improve the estimation of the measured response.

For this study, the open-ended pile tests performed at the Pigeon Creek, Kwangyang Plant and at the Euripides site will be analysed in more detail. At these, the first two sites used a double walled pile and the third site contained highly reliable data.

5.3.1. Specifics on Test Cases

The headings set out in Table 5-5, Table 5-6 and Table 5-7 are similar to those set out for the analysis of OEPs in clay, and these descriptions, provided in Section 4.3.1, are not repeated here.

5.3.2. Test Cases

The next section outlines the test cases using the API-FEA, ICP-FEA and UWA-FEA design methods. This procedure is similar to the previous analysis done for clays, where the input parameters to these methods are varied to observe the effects and test the sensitivity of the change on the results at the test sites. Also, as with clays, using the results from these tests, key recommendations will be extracted and taken forward to Chapter 6 to deduce a modified finite element design method for OEPs in sands.

In all cases that follow, solid lines in the diagrams represent the measured values and dotted lines are those computed by the finite element procedure. Also, the symbol (*) is used to differentiate measured values.

5.3.2.1. API-FEA Analyses (Case 23 to Case 29)

The API-FEA method is initially used to analyse and compare the results between the estimated and measured values. The cases are set out in Table 5-5.

Table 5-5 API test cases analysed.

Case	Design Method	Constitutive Model τ_{int} & τ_{ext}	τ_{ult} = τ_{int} & τ_{ext}	τ_{int} – z_{peak}/D_i	τ_{ext} – z_{peak}/D_o	Constitutive Model $q_{b,pile}$	$q_{b,pile}$	Constitutive Model $q_{b,plug}$	$q_{b,plug}$	M	Weight
23	API	API t-z curves	$\tau_{ext,ult}=\tau_{int,ult}$	0.0001	0.01	API Q-z to 1.0WT	$N_q\sigma'_{v0}$	API Q-z, Q_{max} at $0.1D_i$	$N_q\sigma'_{v0}$	Lunne and Christophersen (1983)	No
24	API	API t-z curves	$\tau_{ext,ult}=\tau_{int,ult}$	0.1	0.01	API Q-z to 1.0WT	$N_q\sigma'_{v0}$	API Q-z, Q_{max} at $0.1D_i$	$N_q\sigma'_{v0}$	Lunne and Christophersen (1983)	No
	API	API t-z curves	$\tau_{ext,ult}=\tau_{int,ult}$	0.01	0.01	API Q-z to 1.0WT	$N_q\sigma'_{v0}$	API Q-z, Q_{max} at $0.1D_i$	$N_q\sigma'_{v0}$	Lunne and Christophersen (1983)	No
	API	API t-z curves	$\tau_{ext,ult}=\tau_{int,ult}$	0.001	0.01	API Q-z to 1.0WT	$N_q\sigma'_{v0}$	API Q-z, Q_{max} at $0.1D_i$	$N_q\sigma'_{v0}$	Lunne and Christophersen (1983)	No
25	API	API t-z curves	$\tau_{ext,ult}=\tau_{int,ult}$	0.0001	0.0025	API Q-z to 1.0WT	$N_q\sigma'_{v0}$	API Q-z, Q_{max} at $0.1D_i$	$N_q\sigma'_{v0}$	Lunne and Christophersen (1983)	No
	API	API t-z curves	$\tau_{ext,ult}=\tau_{int,ult}$	0.0001	0.0050	API Q-z to 1.0WT	$N_q\sigma'_{v0}$	API Q-z, Q_{max} at $0.1D_i$	$N_q\sigma'_{v0}$	Lunne and Christophersen (1983)	No
	API	API t-z curves	$\tau_{ext,ult}=\tau_{int,ult}$	0.0001	0.02	API Q-z to 1.0WT	$N_q\sigma'_{v0}$	API Q-z, Q_{max} at $0.1D_i$	$N_q\sigma'_{v0}$	Lunne and Christophersen (1983)	No
26	API	API t-z curves	$\tau_{ext,ult}=\tau_{int,ult}$	0.0001	0.01	API Q-z to 0.1WT	$N_q\sigma'_{v0}$	API Q-z, Q_{max} at $0.1D_i$	$N_q\sigma'_{v0}$	Lunne and Christophersen (1983)	No
27	API	API t-z curves	$\tau_{ext,ult}=\tau_{int,ult}$	0.0001	0.01	API Q-z to 1.0WT	$N_q\sigma'_{v0}$	API Q-z, Q_{max} at $1.0D_i$	$N_q\sigma'_{v0}$	Lunne and Christophersen (1983)	No
28	API	API t-z curves	$\tau_{ext,ult}=\tau_{int,ult}$	0.0001	0.01	API Q-z to 1.0WT	$N_q\sigma'_{v0}$	API Q-z, Q_{max} at $0.1D_i$	$N_q\sigma'_{v0}$	K_{water}	No
	API	API t-z curves	$\tau_{ext,ult}=\tau_{int,ult}$	0.0001	0.01	API Q-z to 1.0WT	$N_q\sigma'_{v0}$	API Q-z, Q_{max} at $0.1D_i$	$N_q\sigma'_{v0}$	G_{ICP}	No
	API	API t-z curves	$\tau_{ext,ult}=\tau_{int,ult}$	0.0001	0.01	API Q-z to 1.0WT	$N_q\sigma'_{v0}$	API Q-z, Q_{max} at $0.1D_i$	$N_q\sigma'_{v0}$	E_{ICP}	No
29	API	API t-z curves	$\tau_{ext,ult}=\tau_{int,ult}$	0.0001	0.01	API Q-z to 1.0WT	$N_q\sigma'_{v0}$	API Q-z, Q_{max} at $0.1D_i$	$N_q\sigma'_{v0}$	Lunne and Christophersen (1983)	Yes
	API	API t-z curves	$\tau_{ext,ult}=\tau_{int,ult}$	0.0001	0.01	API Q-z to 1.0WT	$N_q\sigma'_{v0}$	API Q-z, Q_{max} at $0.1D_i$	$N_q\sigma'_{v0}$	Lunne and Christophersen (1983)	Yes + Plug Weight

Case 23: This API-FEA analysis outlines the base case that other API-FEA analyses in this section will be compared to for each of the test sites.

Pigeon Creek Site Results:

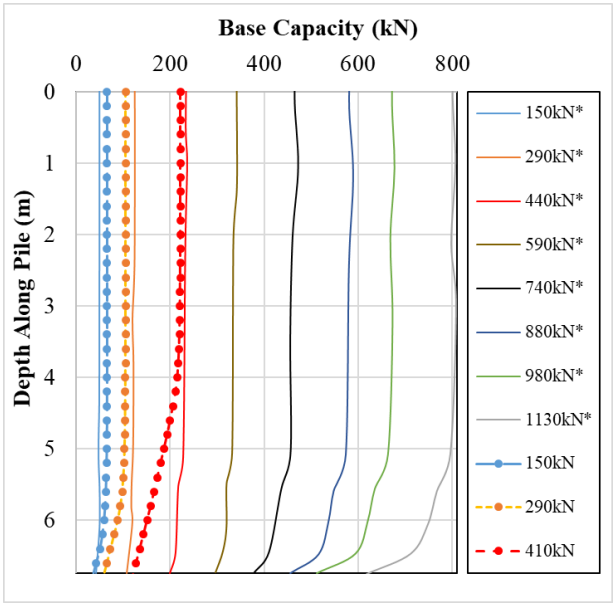

Figure 5-17 Internal shaft friction, API-FEA estimation vs measured.

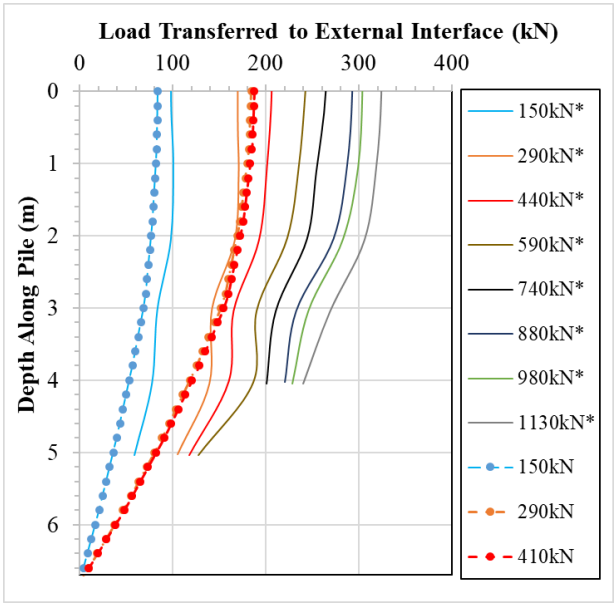

Figure 5-18 External shaft friction, API-FEA estimation vs measured.

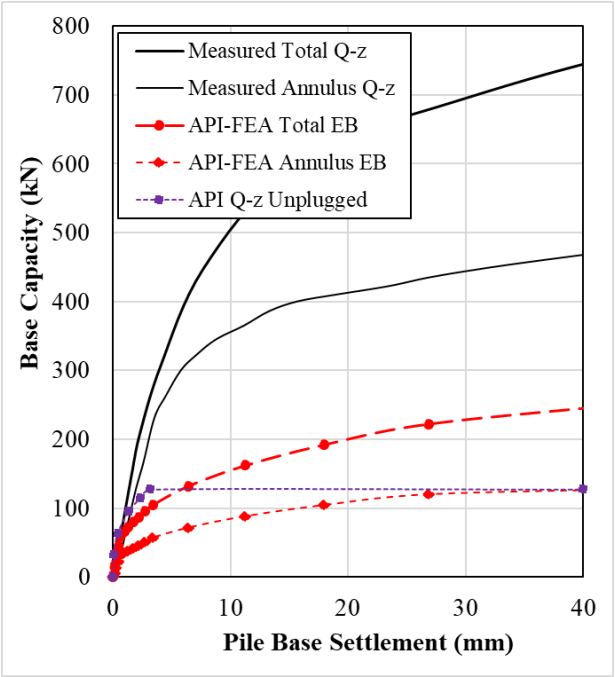

Figure 5-19 API-FEA estimation of pile base settlement vs measured load.

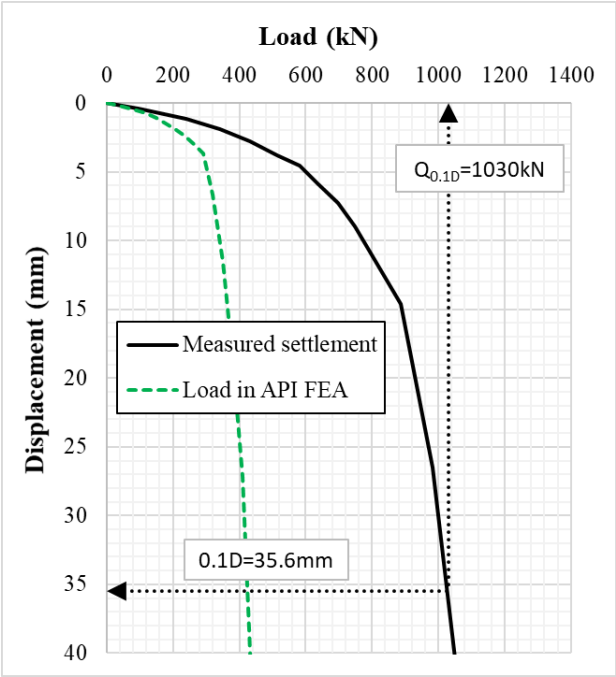

Figure 5-20 Load-displacement curve for API-FEA estimation against measured.

The mobilised base capacity, found by integrating the internal shaft friction along the plug, is shown in Figure 5-17. Here the incremental load-distribution within the pile is observed, measured along the internal pile wall, and supported by the annulus and plug base. Due to the double-walled pile configuration, the values of $Q_{b,p}$ and $Q_{b,pl}$ are easily isolated. API-FEA only mobilises a small fraction of the measured internal load with an estimated value of $Q_{b,p}$ = 150kN, whereas the measured values are approximately 450kN. This is also the case with $Q_{b,pl}$ which is estimated at approximately

100kN and measured at 275kN. The mobilised values of Q_{ext} are shown in Figure 5-18. Here, this friction is also underestimated by the API-FEA. The values tend to zero at the annulus, as the base of the pile is extended from the internal pile, therefore carrying no load. The base response, Figure 5-19, shows that the API-FEA under-predicts the capacity of the base. An unplugged pile was estimated by the direct API method, and the associated Q-z curve is observed to define a stiffer initial response that only reaches the ultimate under-predicted annular capacity. The load-displacement response, shown in Figure 5-20, demonstrates that the API-FEA underestimates the total mobilised load with a Q_c/Q_m at $0.1D_o$ of 0.41 (also in Table 5-8). It is noted that the measured load continues to increase, after a displacement of $0.10D_o$, as the plug base continues to support the additional loading.

Kwangyang Site Results:

The internal shaft friction diagram (Figure 5-21) suggests that the API-FEA gives a better distribution of base components at this site. Although, the measured values suggest that more load is taken by the annulus the trend does show an improvement from the Pigeon Creek results. The estimated values also increase linearly until 1000kN, after which the additional pile head load is now resisted mainly by the base, increasing both $Q_{b,p}$ and $Q_{b,pl}$. A good comparison is observed in the external load-transfer diagram, up to the mobilised pile head load of approximately 1400kN (Figure 5-22). The API-FEA method generates no further capacity after this load, whereas the final measured value was approximately 2000kN.

Figure 5-23 shows a lower initial total base stiffness estimated by the API-FEA method, relative to the measured response. The total base capacity is also underestimated with a Q_c/Q_m value of 0.82. The API's Q-z method, for an unplugged pile, computes a base response which is initially stiffer than that measured, and which eventually converges to the estimated annulus capacity as expected.

In terms of pile head response (Figure 5-24), the initial measured response is quite stiff until the applied pile head load of 2000kN, assumed as 1777kN due to inconsistences with the data. This measured response is atypical of OEPs in sands as usually after a very stiff initial response, where the shaft resistance is prominent, there continues to be an increase in the measured load, at a reduced stiffness, as the plug resistance mobilises. In this scenario, the ultimate value seems to have been

achieved during loading, however at the displacement in which the peak load is achieved, this is where the total pile resistance balances the load applied. Creep is then allowed to occur. The Q_c/Q_m value here is taken as 0.76.

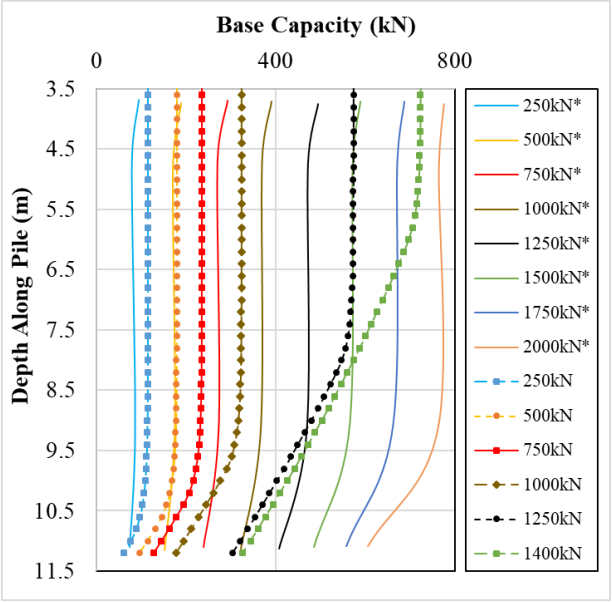

Figure 5-21 Internal shaft friction, API-FEA estimation vs measured.

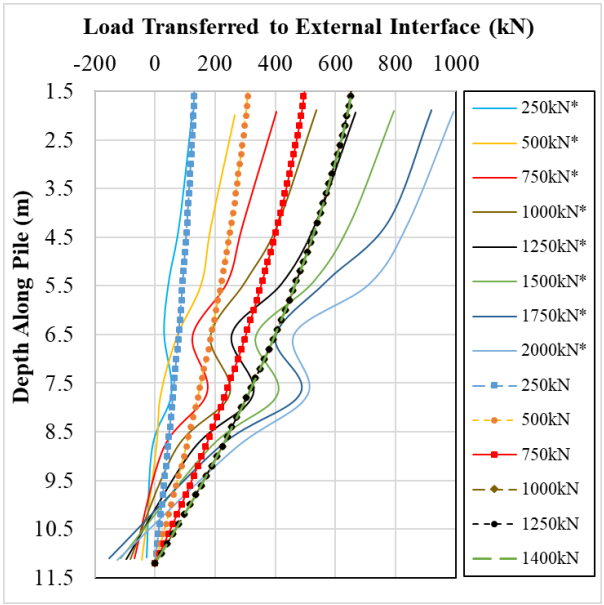

Figure 5-22 External shaft friction, API-FEA estimation vs measured.

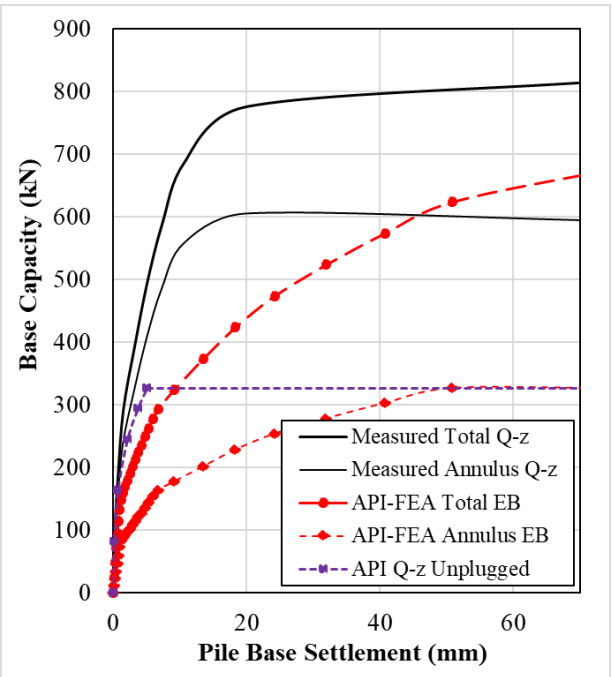

Figure 5-23 API-FEA estimation of pile base settlement vs measured load.

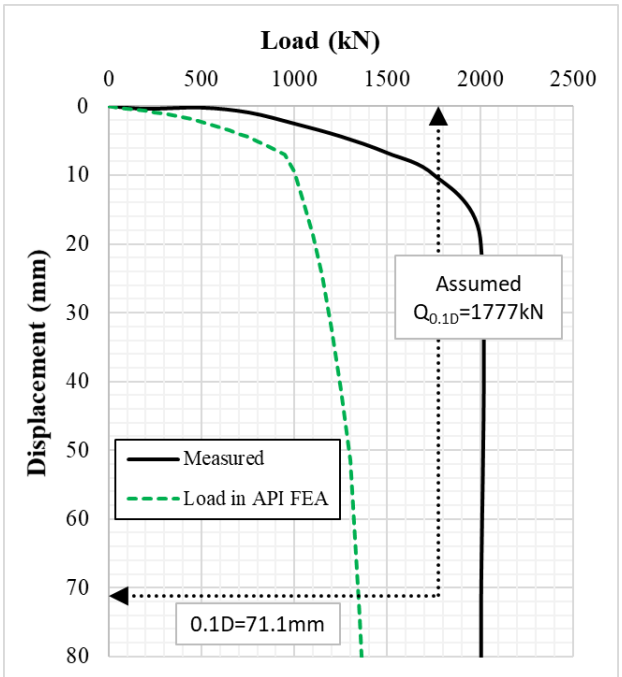

Figure 5-24 Load-displacement curve for API-FEA estimation against measured.

Euripides Site Results:

An axial load of 19,100kN (Kolk, 2005) was measured at a pile base displacement of $0.1D_o$, 76.2mm, which corresponded to a pile head settlement of 97mm. The API-FEA was therefore performed at a pile head displacement of 100mm and these results are compared to that measured. In Figure 5-25

the load estimated in the pile is much lower than that measured in the test, due to the relatively low ultimate values that the API-FEA estimates here.

The total shaft resistance measured after a pile head displacement of 100mm is compared to the sum of the estimated shaft resistances (τ_{ext} + τ_{int}) from the API-FEA at this site, in Figure 5-26. As can be observed, the estimated value is much lower than that measured. Similar results were found for the base capacity and load-displacement as presented in Figure 5-27 and Figure 5-28, respectively.

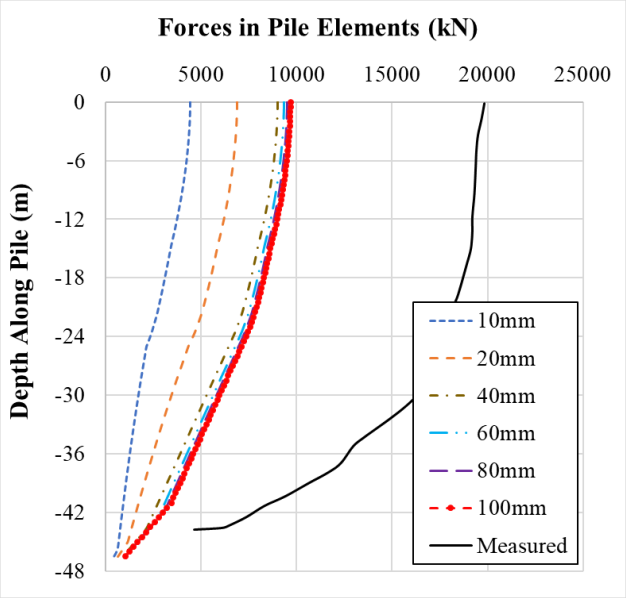

Figure 5-25 Axial load in pile, API-FEA estimation vs measured.

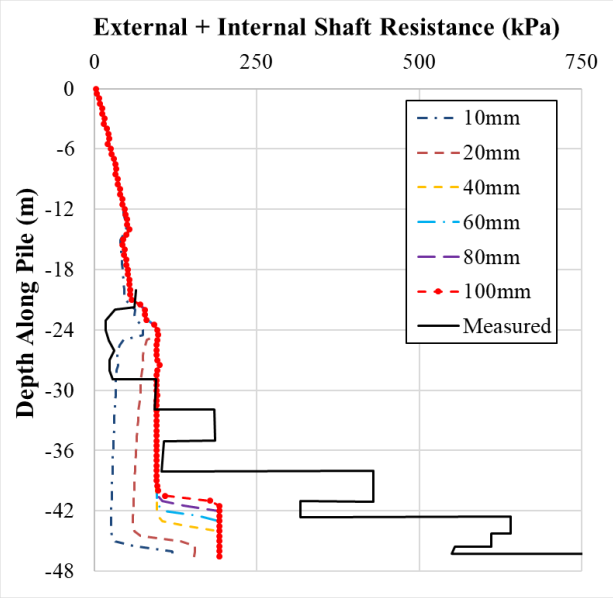

Figure 5-26 Total shaft friction, API-FEA estimation vs measured.

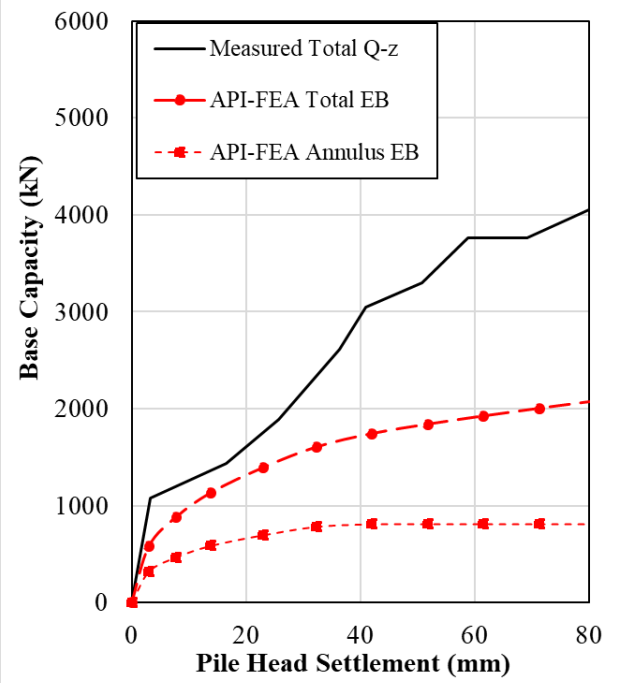

Figure 5-27 API-FEA estimation of pile head settlement vs base capacity.

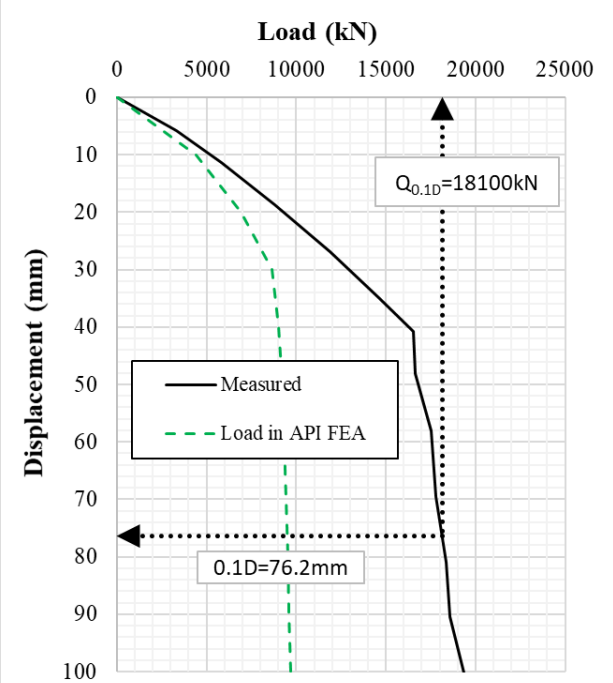

Figure 5-28 Load-displacement curve for API-FEA estimation against measured.

The API method predicts a plugged pile however the equivalent Q-z curve is not applicable here, as only the base load relative to the pile-head displacement is available whereas Q-z is relative to the annulus displacement. In terms of the load-displacement response, the API-FEA has underestimated the overall measured capacity with a Q_c/Q_m of 0.52.

Case 24: This case investigates the effect on the mobilised internal shaft resistance, τ_{int}, to a change in the stiffness of the internal soil reaction curves.

Pigeon Creek and Kwangyang Plant results:

Figure 5-29 (a & b) plot the mobilised internal friction, Q_{int} which is transferred to the base of the soil plug.

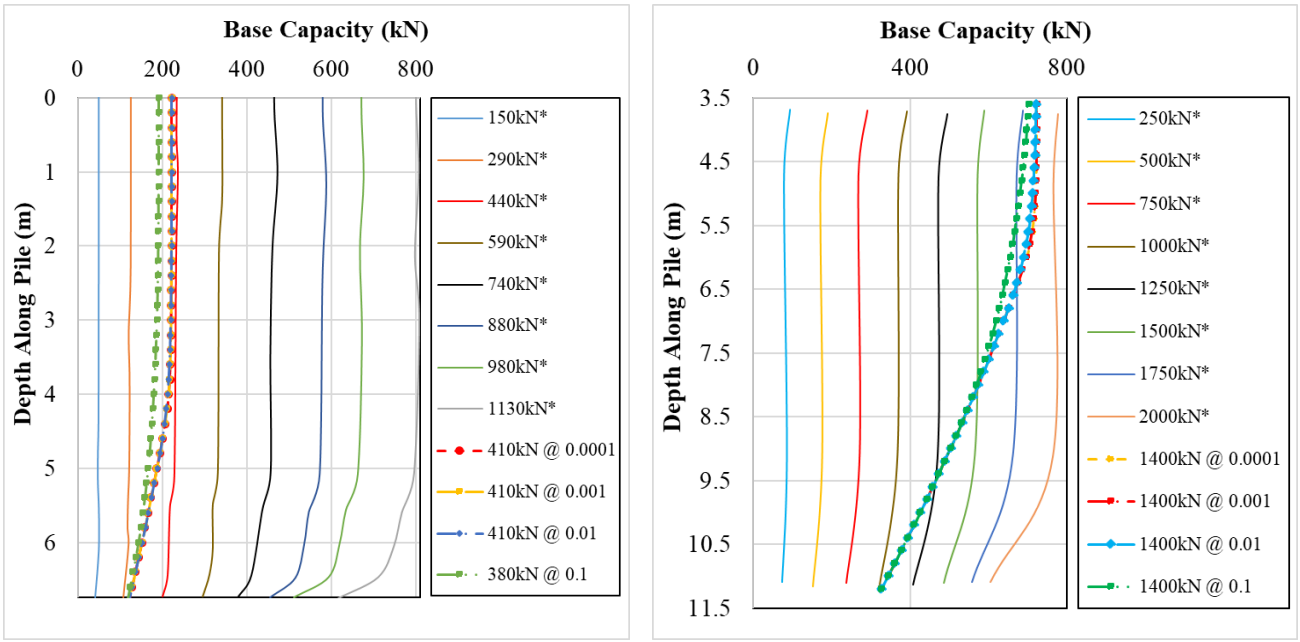

(a) Pigeon Creek results. **(b) Kwangyang Plant results.**

Figure 5-29 Comparison of the measured and estimated values of Q_{int} varying z/D_i stiffnesses. τ_{ult} derived from the API-FEA.

The initial results from Pigeon Creek demonstrate a maximum internal interface friction of approximately 200kN when a maximum pile head load of 410kN is applied (Figure 5-29a). When this load was applied using a displacement to peak ratio (z/D_i) ranging from 0.01 to 0.0001, there is very little difference in the mobilised τ_{int} and $q_{b,p}$. With a reduced stiffness, of z/D_i = 0.1, this reduces the internal interface capacity. From the analysis results of the Kwangyang Plant site (Figure 5-29b),

here the same pattern as observed at the Pigeon Creek site is observed, where as z/D_i increases, less capacity is mobilised by the internal plug.

Euripides Site Results:

At this site, since no double-walled pile configuration was used, τ_{ult}, after a pile-head settlement of 100mm, is compared with the results of the API-FEA. This is shown in Figure 5-30.

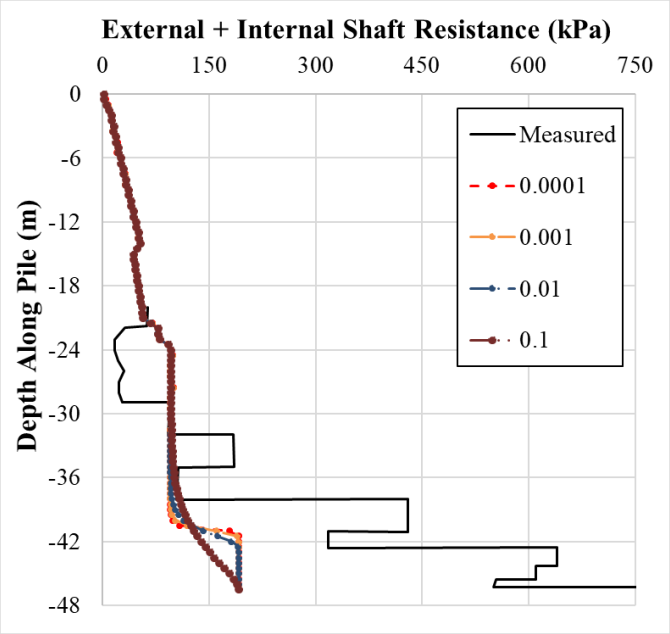

Figure 5-30 Comparison of the measured and estimated values of τ varying z/D$_i$ stiffnesses at the Euripides site. τ$_{ult}$ derived from the API-FEA.

These results show that with smaller ratios of z/D_i the internal plug can mobilise more of the ultimate values of τ_{int}, engaging greater capacity along a shorter active plug length. As observed in the previous results at Pigeon Creek and the Kwangyang Plant, most of the confining stress occurs within an even shorter active plug length than estimated. The ratio of z/D_i is therefore recommended to be small facilitating a rigid interface.

Case 25: This API analysis case compares the effects on the load-displacement curve to a change in stiffness of the t-z curves. The displacement to peak ratio, of τ_{ext}, is expressed as the ratio of z/D_o and for design, this is usually taken to occur at $0.01D_o$ (API RP 2GEO, 2011). The peak resistance on tested piles however, have been found to range from a relative displacement of $0.0025D_o$ to $0.02D_o$ (DNV-OS-J101, 2016). The load response when displacements of $0.0025D_o$, $0.005D_o$, and $0.02D_o$, are used, is investigated at the test sites.

In general, where the analysis results are quite similar, the most representative results from a specific site are presented. Here, the Kwangyang Plant results are shown.

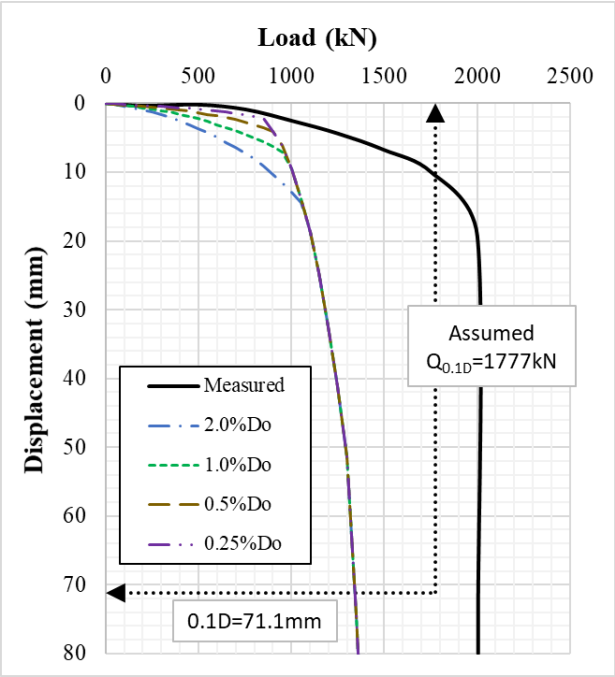

Figure 5-31 Comparison of the load-displacement responses for range of t-z curves with τ_{ult} from the API-FEA. Kwangyang Plant results.

Figure 5-31 demonstrates that the change in stiffness of τ_{ext}, only influences on the initial slope of the load-displacement response. When the displacement to peak ratio (z/D_o) is the stiffest at 0.0025, the relationship matches the measured values best. This is observed in the analysis results at each test site.

Case 26: This API-FEA analysis investigates the use of a stiffer reaction at the base of the annulus. Here the displacement to mobilise the ultimate resistance, or z, is reduced from $1.0t$ to $0.1t$. This is normally expressed as a ratio of z/t to represent the stiffness of the annulus' base resistance. The results from the Euripides analysis are shown.

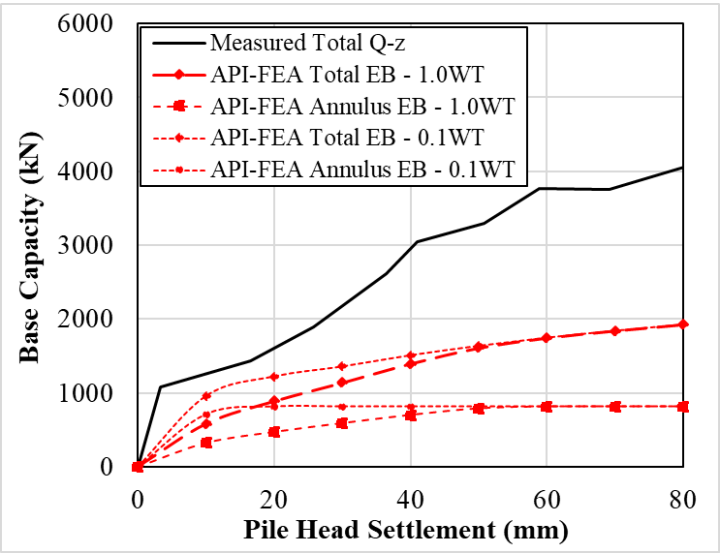

Figure 5-32 Comparison of base response with varied $q_{b,p}$ stiffness using the ICP-FEA. Euripides results.

Figure 5-32 shows that with an increased stiffness, the mobilisation of base capacity occurs much faster. In each of the cases considered, this outcome improves the prediction. This does not have an effect, however, on the ultimate capacity mobilised.

Case 27: In OEP design the base capacity is estimated to become fully mobilised after an annular displacement $0.1D_o$. As this definition does not explicitly consider the displacement of the base of the annulus or soil plug separately, this API-FEA investigates the use of a softer reaction at the base of the plug only. Here the z/D_i is increased from 0.1 to 1.0. The results from the Kwangyang Plant site are shown due to the similarity in the results for all sites.

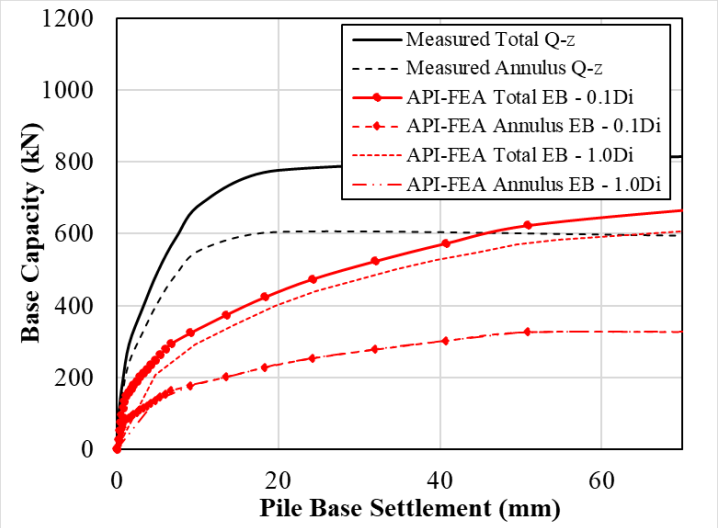

Figure 5-33 Comparison of the load-displacement responses for range of t-z curves with τ_{max} from the API-FEA. Kwangyang Plant results.

Figure 5-33 shows that using the FE method, the accuracy of the estimated overall base capacity is reduced when the base of the plug is assumed to be mobilised after a displacement equal to the diameter of the plug. As better results are obtained when the stiffer reaction curve is used, this suggests that the use of z/D_i = 0.1 is acceptable.

Case 28: In this analysis the impact of using different values of constrained modulus is investigated. This is similar to the analysis performed in Case 7 and Case 18 for clays. In the previous cases, M was derived from the specified default relationship ($M_{default}$) by Lunne and Christophersen (1983), as follows:

$$M = \begin{cases} 4q_c & ; \quad q_c < 10MPa \\ 2q_c + 20 & ; \; 10MPa \leq q_c < 50MPa \\ 120 & ; \quad q_c \geq 50MPa \end{cases} \tag{65}$$

In this case, M will consider values of K_{water}, taken as 2,340,000kPa, G_{ICP} and E_{ICP} to investigate the effects. In terms of the relative numerical value, typically $M_{default} < G_{ICP} < E_{ICP} < K_{water}$.

Pigeon Creek Site Results:

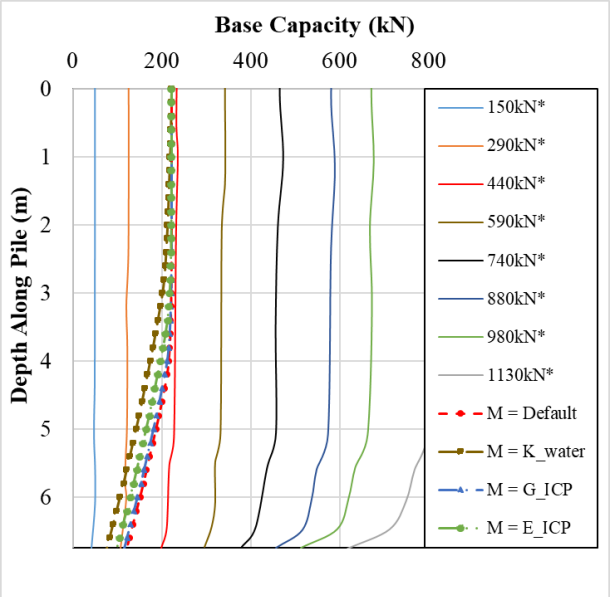

Figure 5-34 Mobilised internal shaft friction/base capacity. API-FEA estimation vs measured. Dotted lines are for F_t=410kN.

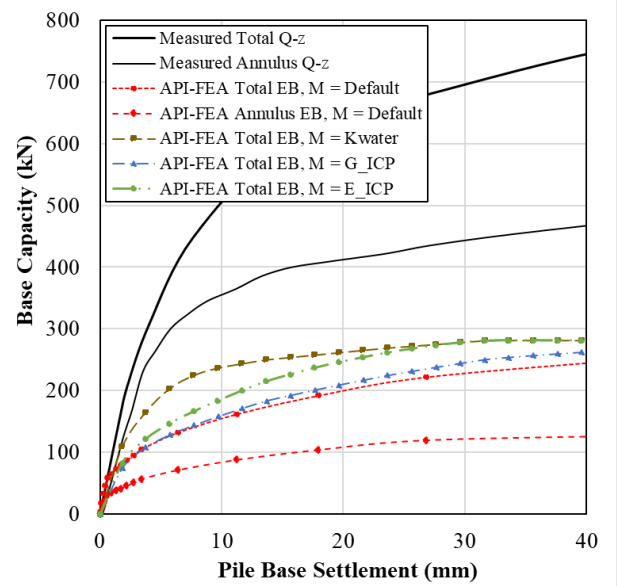

Figure 5-35 API-FEA estimation of pile base settlement vs measured load.

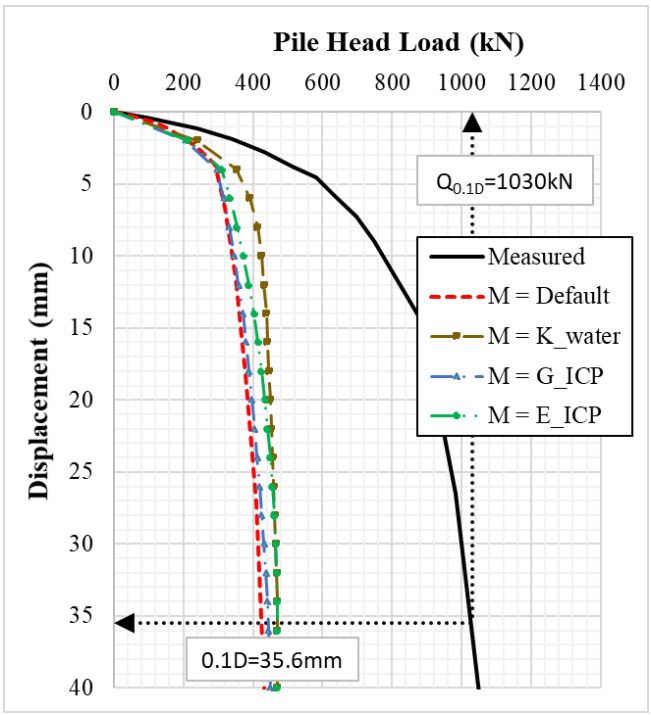

Figure 5-36 Load-displacement curve comparison of API-FEA estimates against measured.

As this site, as the plug stiffness increases, the plug capacity and the active plug length both increase. Less load is then mobilised below the annulus. This is shown in Figure 5-34 where the load-distribution under a pile-head load of 410kN is applied. In contrast, as the stiffness decreases, the plug capacity decreases, less of the plug length is mobilised (a reduced active length) and the load resisted by the annulus increases. The results of the total base capacity show that as M increases the initial stiffness of the base increases (Figure 5-35). It is also observed that the higher the value of M, the larger the base capacity, which is demonstrated when $M = K_{water}$ or E_{ICP}. The load-displacement response displays similar patterns as observed by the base response. It is shown in Figure 5-36, that with higher values of M, greater overall pile capacity is mobilised.

Kwangyang Site Results:

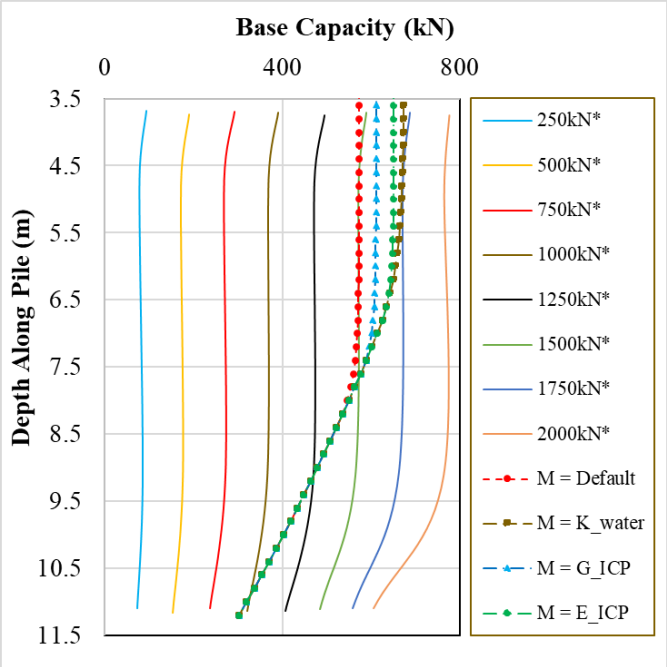

Figure 5-37 Mobilised internal shaft friction. API-FEA estimation vs measured. Dotted lines are for F_t=1250kN.

The mobilised internal shaft friction results are different here than observed at Pigeon Creek. Here the increase in plug stiffness increases the capacity of the plug without affecting the load resisted by the annulus. It does show, however, that as *M* increases the active plug length also increases (Figure 5-37).

In the other comparisons performed at the Kwangyang Plant site, the results mirror those observed at Pigeon Creek site.

Euripides Site Results:

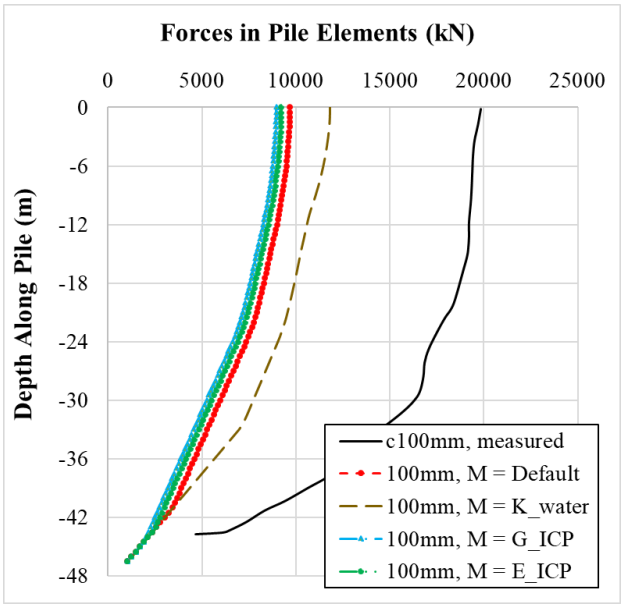

Figure 5-38 Axial load in pile, API-FEA estimation vs measured.

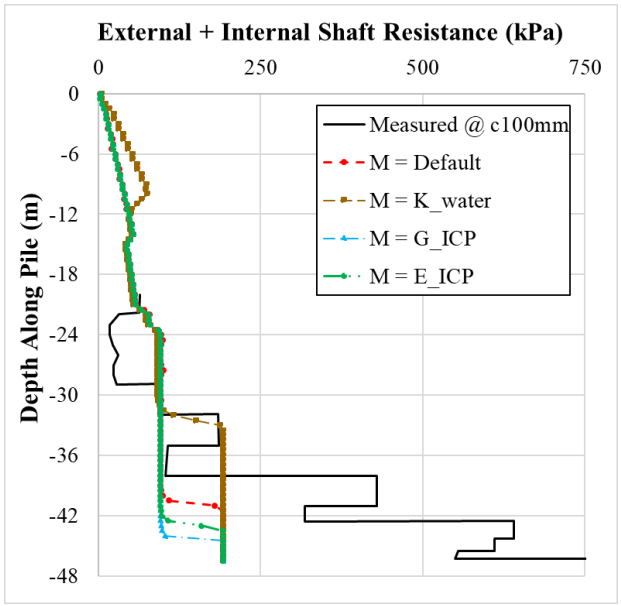

Figure 5-39 Total shaft friction, API-FEA estimation vs measured at pile head displacement of 100mm.

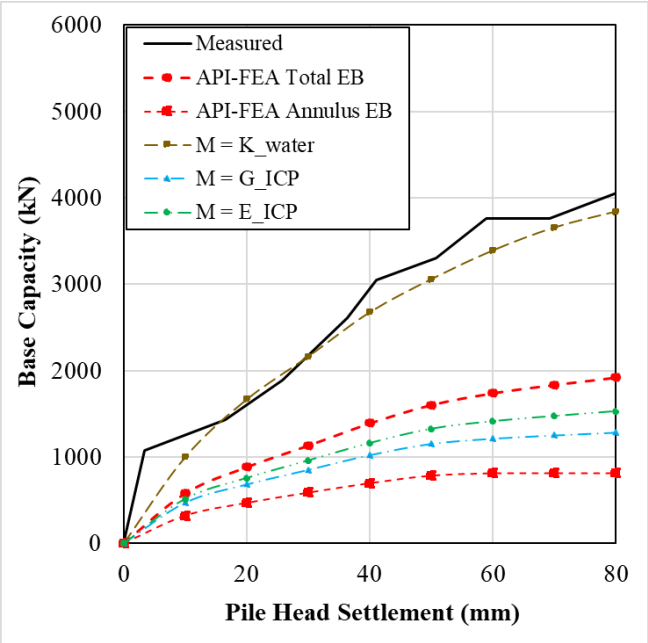

Figure 5-40 API-FEA estimation of pile head settlement vs base capacity.

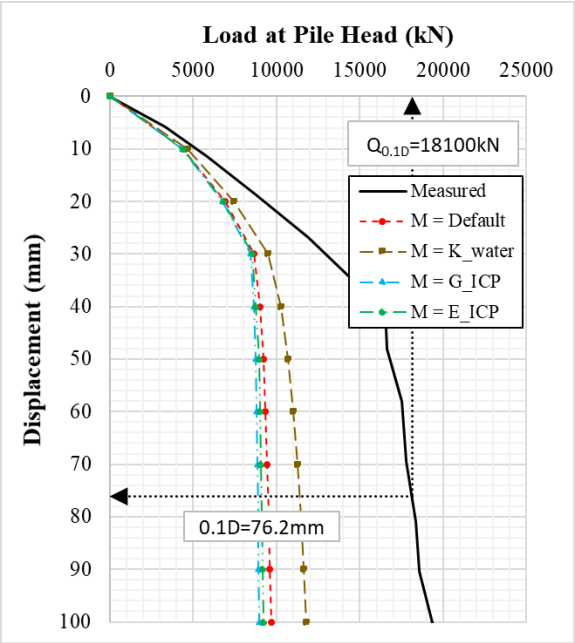

Figure 5-41 Load-displacement curve for API-FEA estimation against measured.

The results from Euripides give similar trends as the other sites. The forces in the single walled pile is unique here and suggests that the pile load also depends on M, as the larger the stiffness, the greater the load capacity of the pile (Figure 5-38). The sum of Q_{ext} and Q_{int} also shows that in a single walled pile, a higher value of M allows a greater active plug length to be mobilised (Figure 5-39). With regards to the base capacity, Figure 5-40 shows a good match observed when $M = K_{water}$, suggesting that the assumed base parameters and behaviour are closer to what exists. The overall load capacity is not well matched however, suggesting that τ_{ult} has been underestimated (Figure 5-41).

<u>Case 29</u>: This API analysis looked at the effects of including the self-weight of the pile and plug to the overall calculation. In general, it was found that with the inclusion of the weight of the pile and plug, there is little to no difference observed in general. There is only a small variation at the initial stages of loading and less so with the much longer pile at the Euripides site.

5.3.2.2. ICP-FEA Analyses (Case 30 to Case 39)

This ICP analysis uses the results from the ICP-FEA to compare the interpreted results to the measured values at the three sand sites under consideration. The cases are set out in Table 5-6.

Table 5-6 ICP-FEA test cases analysed.

Case	Design Method	Constitutive Model τ_{int} & τ_{ext}	τ_{ult} = τ_{int} & τ_{ext}	τ_{int} – z_{peak}/D_i	τ_{ext} – z_{peak}/D_o	Constitutive Model $q_{b,pile}$	$q_{b,pile}$	Constitutive Model $q_{b,plug}$	$q_{b,plug}$	M	Weight
30	ICP	API t-z curves	$\tau_{ext,ult}=\tau_{int,ult}$	0.0001	0.01	API Q-z to 1.0WT	(ICP)q_c	API Q-z, Q_{max} at $0.1D_i$	(ICP)q_c	Lunne and Christophersen (1983)	No
31	ICP	API t-z curves	$\tau_{ext,ult}=\tau_{int,ult}$	0.0001	0.01	API Q-z to 1.0WT	$1.0q_c$	API Q-z, Q_{max} at $0.1D_i$	$0.0q_c$	Lunne and Christophersen (1983)	No
	ICP	API t-z curves	$\tau_{ext,ult}=\tau_{int,ult}$	0.0001	0.01	API Q-z to 1.0WT	$0.7q_c$	API Q-z, Q_{max} at $0.1D_i$	$0.3q_c$	Lunne and Christophersen (1983)	No
32	ICP	API t-z curves	$\tau_{ext,ult}=\tau_{int,ult}$	0.1	0.01	API Q-z to 1.0WT	(ICP)q_c	API Q-z, Q_{max} at $0.1D_i$	(ICP)q_c	Lunne and Christophersen (1983)	No
	ICP	API t-z curves	$\tau_{ext,ult}=\tau_{int,ult}$	0.01	0.01	API Q-z to 1.0WT	(ICP)q_c	API Q-z, Q_{max} at $0.1D_i$	(ICP)q_c	Lunne and Christophersen (1983)	No
	ICP	API t-z curves	$\tau_{ext,ult}=\tau_{int,ult}$	0.001	0.01	API Q-z to 1.0WT	(ICP)q_c	API Q-z, Q_{max} at $0.1D_i$	(ICP)q_c	Lunne and Christophersen (1983)	No
33	ICP	API t-z curves	$\tau_{ext,ult}=\tau_{int,ult}$	0.0001	0.0025	API Q-z to 1.0WT	(ICP)q_c	API Q-z, Q_{max} at $0.1D_i$	(ICP)q_c	Lunne and Christophersen (1983)	No
	ICP	API t-z curves	$\tau_{ext,ult}=\tau_{int,ult}$	0.0001	0.0050	API Q-z to 1.0WT	(ICP)q_c	API Q-z, Q_{max} at $0.1D_i$	(ICP)q_c	Lunne and Christophersen (1983)	No
	ICP	API t-z curves	$\tau_{ext,ult}=\tau_{int,ult}$	0.0001	0.0200	API Q-z to 1.0WT	(ICP)q_c	API Q-z, Q_{max} at $0.1D_i$	(ICP)q_c	Lunne and Christophersen (1983)	No
34	ICP	DNV t-z curves	$\tau_{ext,ult}=\tau_{int,ult}$	0.0001	DNV t-z r_f=0.98	API Q-z to 1.0WT	(ICP)q_c	API Q-z, Q_{max} at $0.1D_i$	(ICP)q_c	Lunne and Christophersen (1983)	No
	ICP	DNV t-z curves	$\tau_{ext,ult}=\tau_{int,ult}$	0.0001	DNV t-z r_f=0.50	API Q-z to 1.0WT	(ICP)q_c	API Q-z, Q_{max} at $0.1D_i$	(ICP)q_c	Lunne and Christophersen (1983)	No
35	ICP	API t-z curves	$\tau_{ext,ult}=\tau_{int,ult}$	0.0001	0.01	API Q-z to 0.1WT	(ICP)q_c	API Q-z, Q_{max} at $0.1D_i$	(ICP)q_c	Lunne and Christophersen (1983)	No
36	ICP	API t-z curves	$\tau_{ext,ult}=\tau_{int,ult}$	0.0001	0.01	API Q-z to 1.0WT	(ICP)q_c	API Q-z, Q_{max} at $1.0D_i$	(ICP)q_c	Lunne and Christophersen (1983)	No
37	ICP	API t-z curves	$\tau_{ext,ult}=\tau_{int,ult}$	0.0001	0.01	API Q-z to 1.0WT	(ICP)q_c	API Q-z, Q_{max} at $0.1D_i$	(ICP)q_c	K_{water}	No
	ICP	API t-z curves	$\tau_{ext,ult}=\tau_{int,ult}$	0.0001	0.01	API Q-z to 1.0WT	(ICP)q_c	API Q-z, Q_{max} at $0.1D_i$	(ICP)q_c	G_{ICP}	No
	ICP	API t-z curves	$\tau_{ext,ult}=\tau_{int,ult}$	0.0001	0.01	API Q-z to 1.0WT	(ICP)q_c	API Q-z, Q_{max} at $0.1D_i$	(ICP)q_c	E_{ICP}	No
38	ICP	API t-z curves	$\tau_{ext,ult}=\tau_{int,ult}$	0.0001	0.01	API Q-z to 1.0WT	(ICP)q_c	API Q-z, Q_{max} at $0.1D_i$	(ICP)q_c	Lunne and Christophersen (1983)	Yes
	ICP	API t-z curves	$\tau_{ext,ult}=\tau_{int,ult}$	0.0001	0.01	API Q-z to 1.0WT	(ICP)q_c	API Q-z, Q_{max} at $0.1D_i$	(ICP)q_c	Lunne and Christophersen (1983)	Yes + Plug Weight
39	ICP	API t-z curves	R instead of R* $\tau_{ext,ult}=\tau_{int,ult}$	0.0001	0.01	API Q-z to 1.0WT	(ICP)q_c	API Q-z, Q_{max} at $0.1D_i$	(ICP)q_c	Lunne and Christophersen (1983)	No

Case 30: This is the base case using the ICP-FEA results.

Pigeon Creek Site Results:

The ICP method predicts that the pile will behave in a plugged manner, under static load, and this

scenario is investigated here.

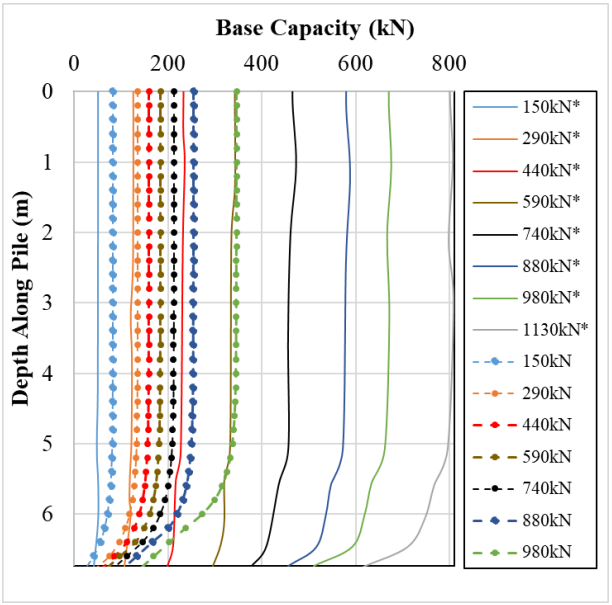

Figure 5-42 Internal shaft friction, ICP-FEA estimation vs measured.

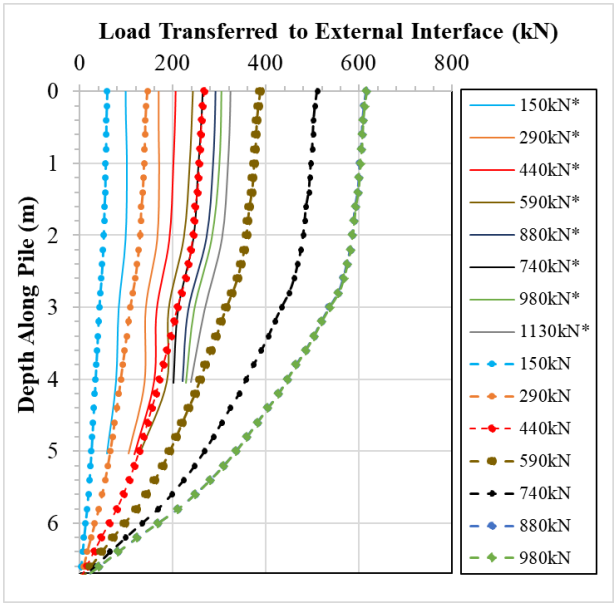

Figure 5-43 External shaft friction, ICP-FEA estimation vs measured.

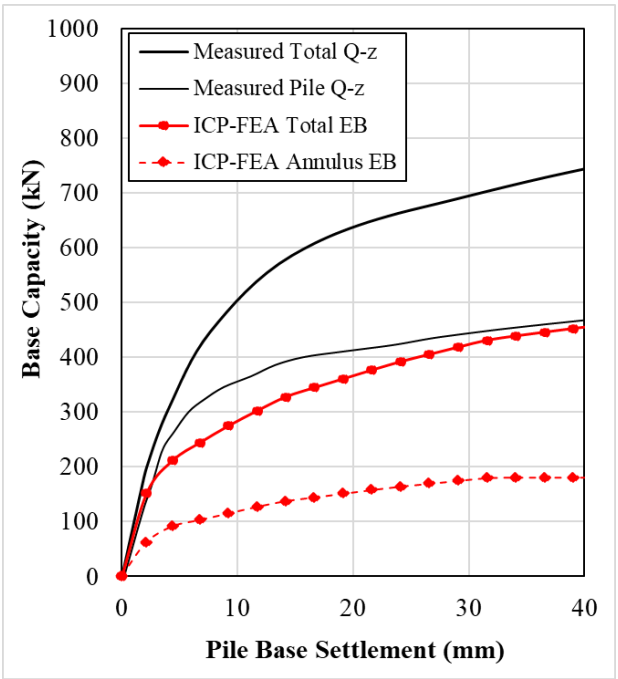

Figure 5-44 ICP-FEA estimation of pile base settlement vs measured load.

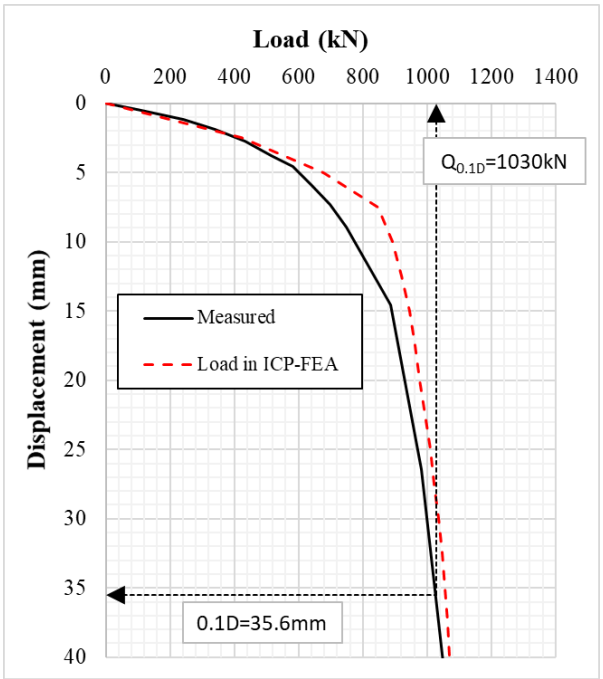

Figure 5-45 Load-displacement curve for ICP-FEA estimation against measured.

When compared to the API-FEA for Pigeon Creek, the ICP-FEA estimates a much larger capacity; however, the load that the internal shaft friction attracts remains quite low (Figure 5-42). The measured values show results of internal shaft friction when a pile head load of 1130kN is applied, which is not achieved by the ICP-FEA. As demonstrated in Figure 5-43, the ICP-FEA considerably overestimates the external shaft friction (Q_{ext}). As can be seen in the figure, Q_{ext} is approximately 2.0 times that measured under a pile head load of 980kN. This overestimation improves the match of

the load-displacement response. The end bearing capacity, at this site, is found to be underestimated by the ICP-FEA (Figure 5-44). In terms of estimated total base capacity, the Q_c/Q_m = 0.62. And with regards to the load-displacement response, Figure 5-45 shows that the ICP-FEA marginally overestimates this response; however, the capacity is generally achieved at a pile head displacement of $0.1D_o$. Here Q_c/Q_m = 1.03 even though the ratios of the base and shaft capacities are essentially 0.5 and 2.0, respectively, times that measured.

Kwangyang Site Results:

The ICP method predicts an unplugged pile at this site, however this condition is covered in the next case and a plugged pile is considered here.

The comparison of the mobilisation of the internal shaft friction (Q_{int}) is shown in Figure 5-46. At this site, with an applied pile head load of 2000kN, the ICP-FEA estimates the mobilisation of Q_{int} to a maximum achievable pile head load of 1500kN. The mobilisation of Q_{ext} is shown in Figure 5-47 and a good match to those measured is observed. The estimated initial stiffness of the annulus and total base, shown in Figure 5-48, is underestimated, and for the base capacity, Q_c/Q_m = 0.64 here. Figure 5-49 shows that the overall load-displacement response is underestimated by the ICP-FEA method when using the plugged pile input parameters with Q_c/Q_m = 0.85 in this case. The initial overall stiffness is also underestimated.

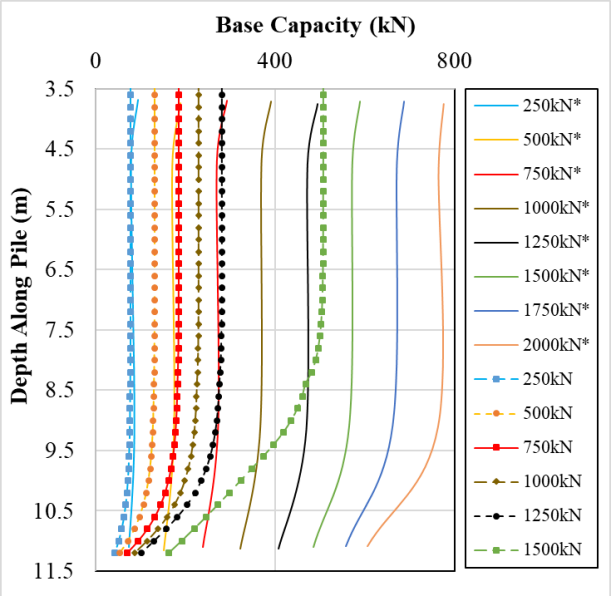

Figure 5-46 Internal shaft friction, ICP-FEA estimation vs measured.

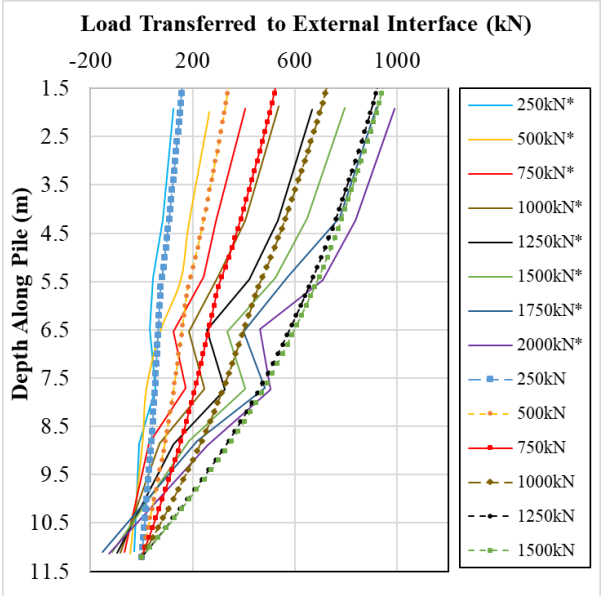

Figure 5-47 External shaft friction, ICP-FEA estimation vs measured.

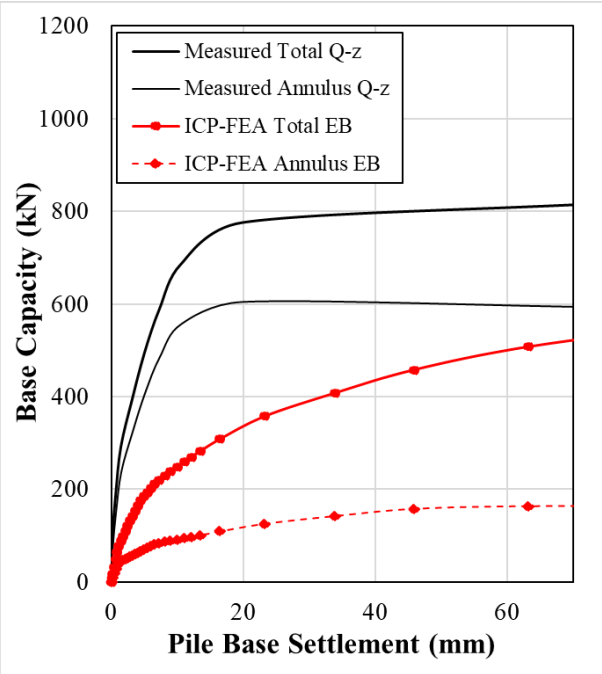

Figure 5-48 ICP-FEA estimation of pile base settlement vs measured load.

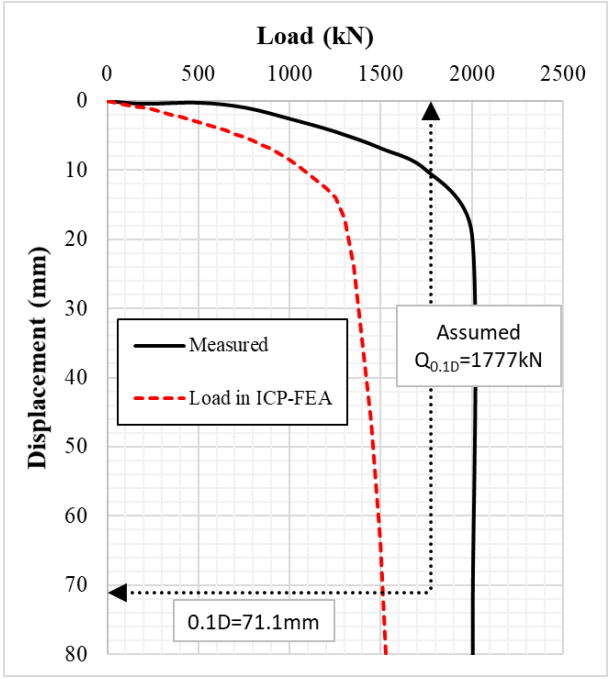

Figure 5-49 Load-displacement curve for ICP-FEA estimation against measured.

Euripides Site Results:

In the ICP design manual there is an example of the use of this method applied to the 47m pile from the Euripides pile test. The q_c profile that is outlined in this ICP example adopts a smoother lower bound version to that measured, effectively reducing the estimated capacity. In this analysis, no reductions to the q_c values are applied.

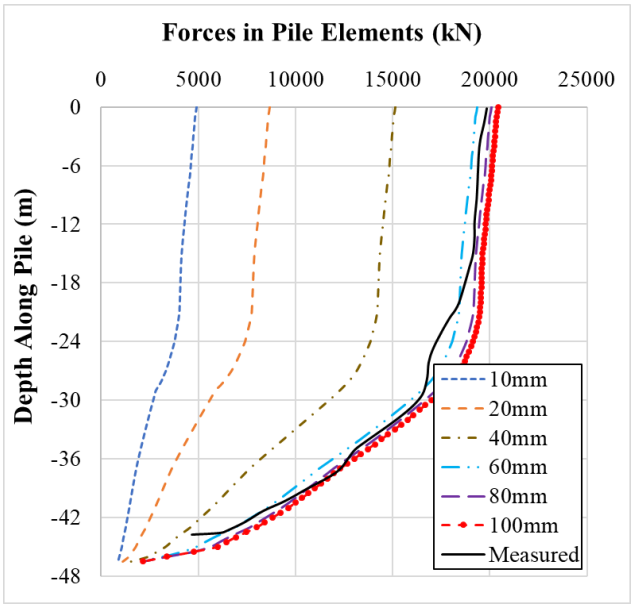

Figure 5-50 Axial load in pile, ICP-FEA estimation vs measured.

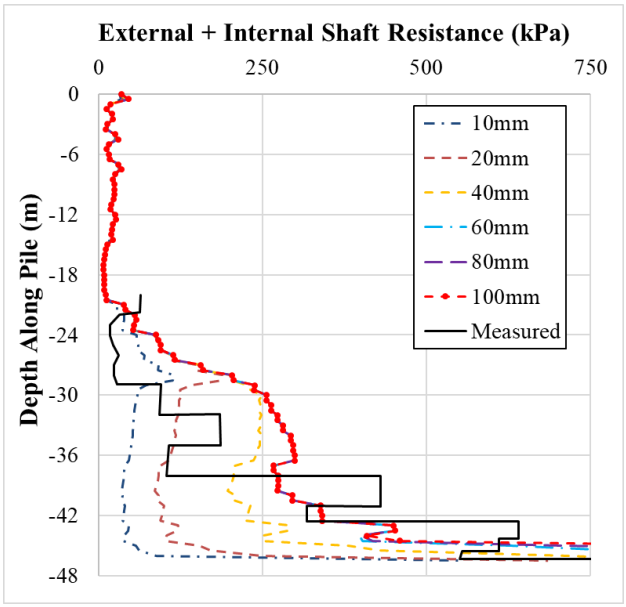

Figure 5-51 Total shaft friction, ICP-FEA estimation vs measured.

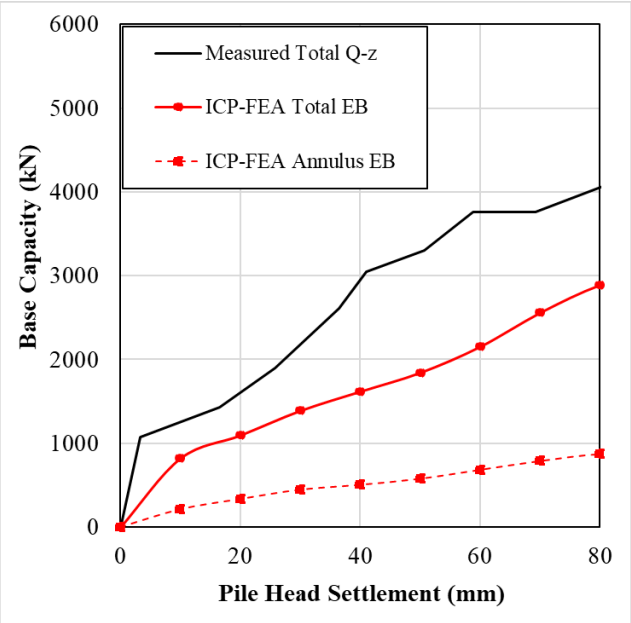

Figure 5-52 ICP-FEA estimation of pile head settlement vs base capacity.

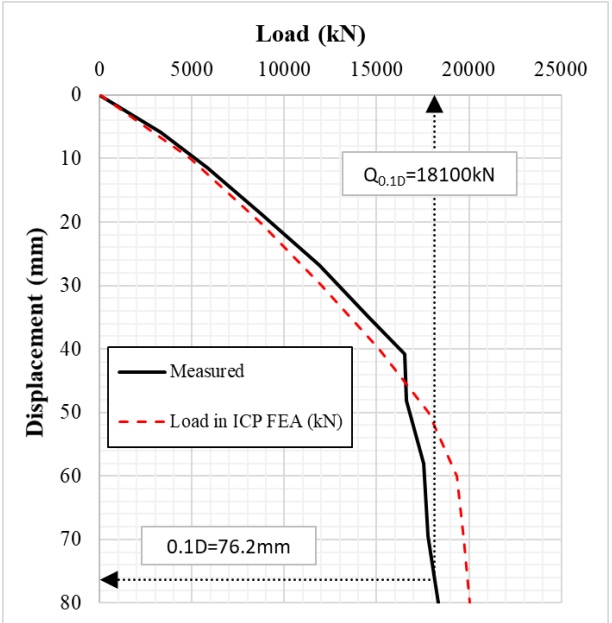

Figure 5-53 Load-displacement curve for ICP -FEA estimation against measured.

The ICP-FEA well estimates the axial load in the pile at a pile-head displacement of approximately 100mm (Figure 5-50). The comparison of the stresses is shown in Figure 5-51. The measured stresses are due to the coupled action of the soil on both sides of the pile causing axial strain. The measured results are therefore compared with the summation of τ_{int} and τ_{ext}. The results show that there is a good match between the estimated values and those predicted by the ICP-FEA method. The pile base response is shown in Figure 5-52 and the overall load response is well matched (Figure 5-53) with a Q_c/Q_m of 1.10.

<u>Case 31</u>: This ICP-FEA analysis investigates the use of varying base resistances along the annulus and soil plug. Here the results using an unplugged pile with q_c applied to the base of the annulus and using a direct distribution of $0.7q_c$ and $0.3q_c$ applied to the pile and plug, respectively, is compared to the base case.

Pigeon Creek Site Results:

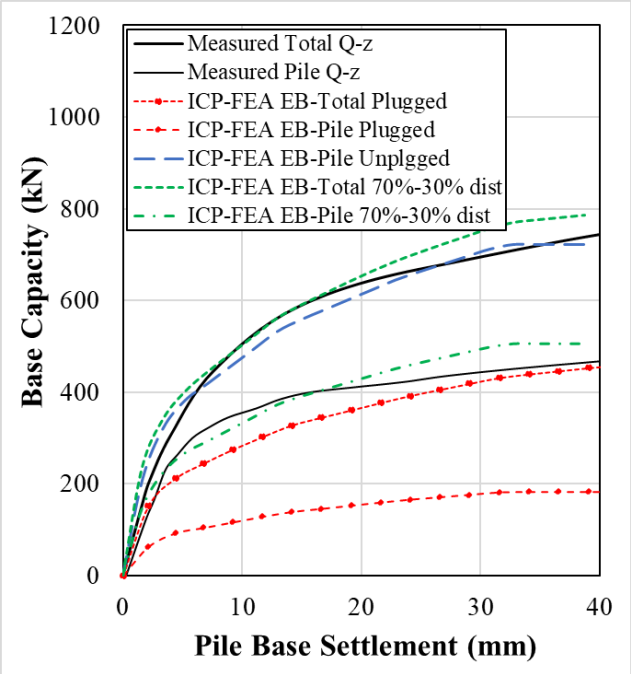

Figure 5-54 ICP-FEA estimation of pile base settlement vs measured load.

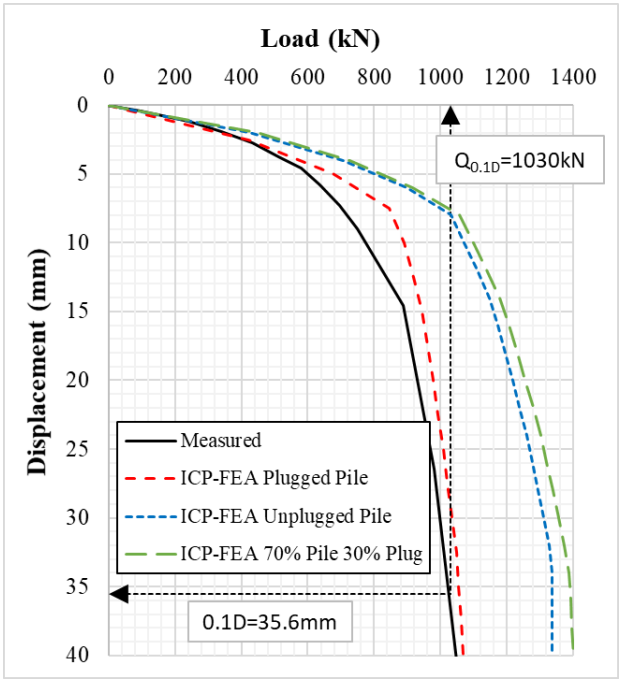

Figure 5-55 Load-displacement curve for ICP-FEA estimation against measured.

There is quite a wide variation in the estimated base response (Figure 5-54). However, the best representation is the distributed q_c case ($0.7q_c$ on the annulus and $0.3q_c$ on the plug base) where the load is well matched to that measured. In addition, the base capacity is well captured when the pile is assumed unplugged and $1.0q_c$ is applied as $q_{b,p}$. As a result of this variation of the base resistance however, the overall initial stiffness is overestimated and this increases the ultimate capacity to Q_c/Q_m = 1.35, as shown in Figure 5-55. The unplugged condition gives Q_c/Q_m = 1.30.

Kwangyang Site Results:

The results from using both the unplugged condition and that of the distributed load, both overestimate the ultimate base capacity measured at this site (Figure 5-56). The initial stiffness of the unplugged pile slightly underestimates the measured stiffness and using the distributed load, the annulus' stiffness does not match that measured. The predicted pile base capacity is best matched however, when $q_{b,p}$ = $0.7q_c$. Both the unplugged and distributed load cases underestimate the initial stiffness of the total capacity; however, the ultimate capacity is seemingly well matched (Figure 5-57).

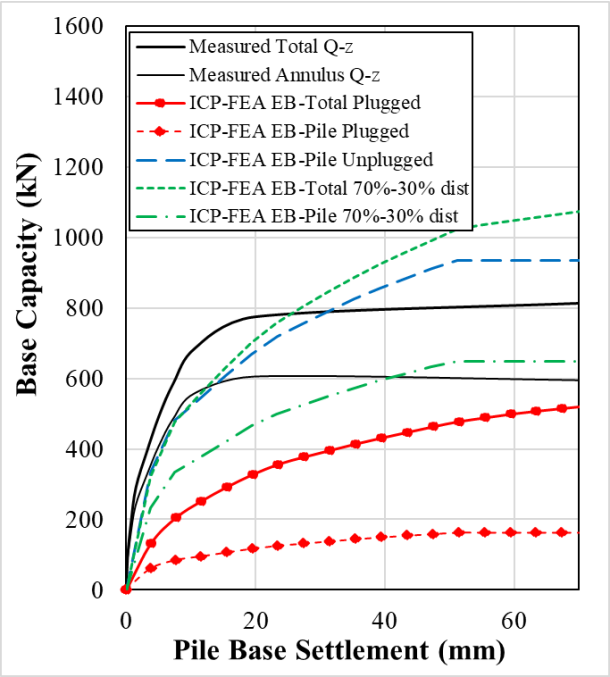

Figure 5-56 ICP-FEA estimation of pile base settlement vs measured load.

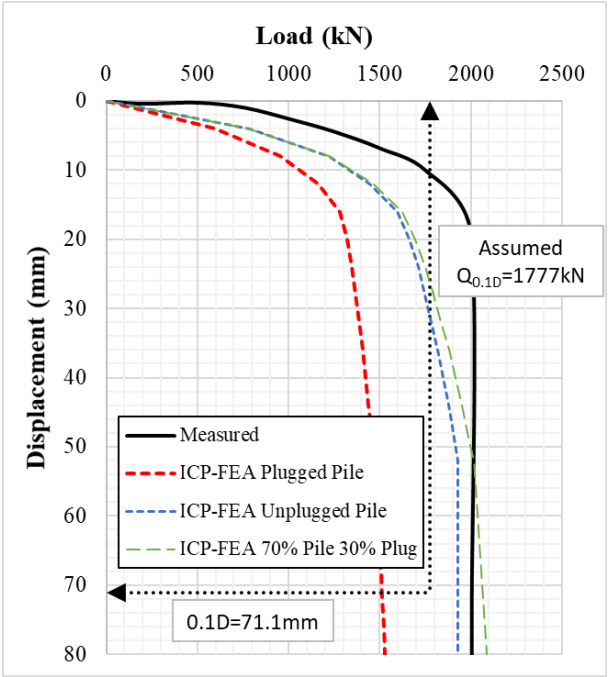

Figure 5-57 Load-displacement curve for ICP-FEA estimation against measured.

Euripides Site Results:

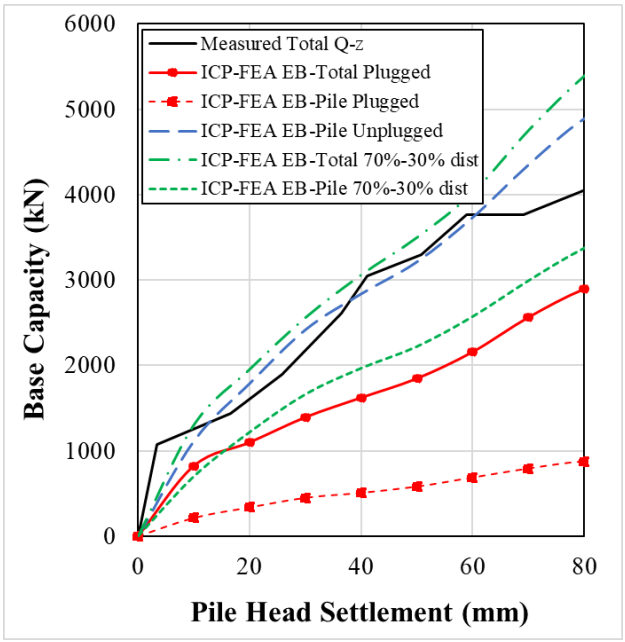

Figure 5-58 ICP-FEA estimation of pile head settlement vs base capacity.

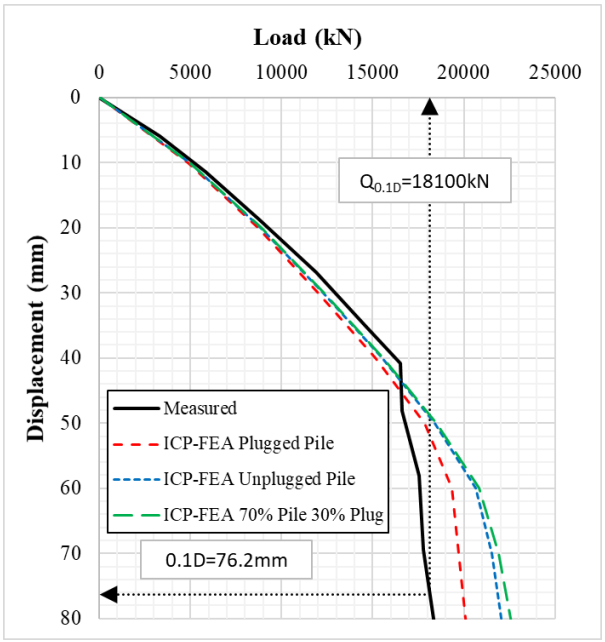

Figure 5-59 Load-displacement curve for ICP-FEA estimation against measured.

The results here are quite similar to those of the other sites. Figure 5-58 shows that the ultimate base capacity is marginally overestimated for both cases of unplugged and distributed loads. The initial stiffness matches, suggesting that the mobilised proportion of the load at the base of the plug, using $q_{b,pl} = 0.3q_c$, or the ICP's interpretation of the $q_{b,pl}$ for an unplugged pile, is applicable. The overall load-displacement stiffness is, in general, not affected by the end-condition until after the shaft

reaches its ultimate capacity (Figure 5-59). After this, the results are quite similar to those of the base response.

Case 32: This ICP-FEA investigated the effect of varying the stiffness of τ_{int}, along the pile. This was performed by applying a range of relative displacement to internal diameter (z/D_i) ratios from 0.1 to 0.0001. Due to similarity, results are only presented from the Pigeon Creek analysis.

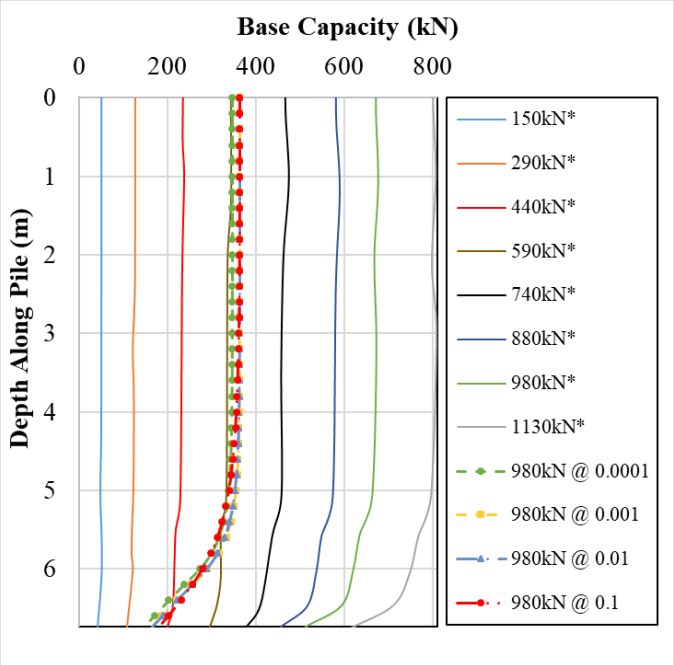

Figure 5-60 Comparison of the measured and estimated values of Q_i varying z/D_i stiffnesses. τ_{ult} derived from the ICP-FEA. Pigeon Creek results.

In general, there seems to be no overall effect on the mobilised pile or plug capacity. However, Figure 5-60 shows that with a decreasing z/D_i ratio the mobilised capacity of the pile slightly reduces. These results are for a pile head load of 980kN.

Case 33: Similar to the analysis performed for clays, and previously in Case 25, the stiffness of τ_{ext} is investigated here for displacement to peak ratios of $0.0025D_o$, $0.005D_o$, and $0.02D_o$. The constitutive model of the t-z curves used in this ICP analysis have been taken from API-RP 2GEO (2011).

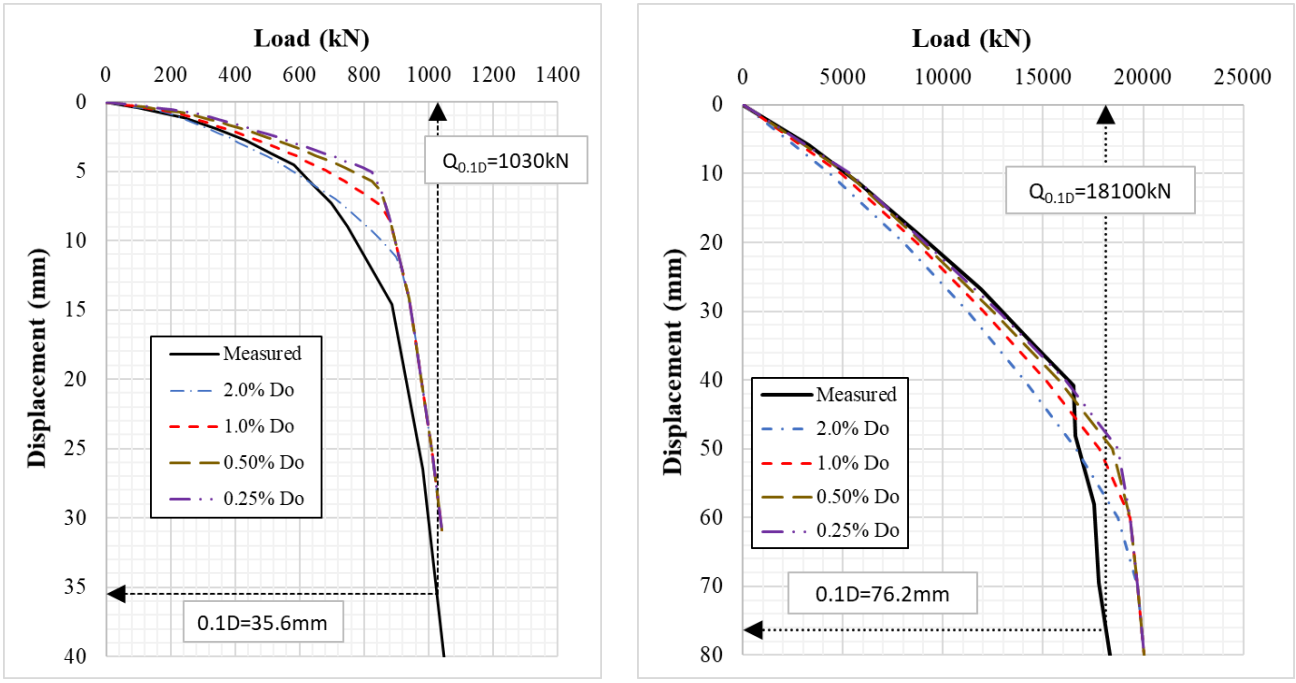

(a) Pigeon Creek results. **(b) Euripides results.**

Figure 5-61 Comparison of the load-displacement responses for range of t-z curves with τ_{max} from the ICP-FEA.

The results from the Pigeon creek site are shown in Figure 5-61a. Here, this shows that as the displacement to mobilise the peak resistance reduces, the t-z reaction curves become stiffer and the initial stiffness of the load-displacement curve is significantly increased. At this site, the lowest stiffness, at z/D_o of 2.0%, best matches the measured result. At both the Kwangyang Plant (not shown) and Euripides (Figure 5-61b) sites, the highest stiffness at z/D_o = 0.0025, gave the best match.

<u>Case 34</u>: In this ICP-FEA analysis the t-z curves have been derived from DNV-OS-J101 (2016). A similar analysis was performed for the pile tests in clays in the previous section. As outlined in the literature review (Chapter 2), a hyperbolic t-z relationship was used, based on earlier work on an analytical model by various researchers. DNV has adopted these curves into their design guidance for offshore installations. These curves are applied as the external stress-strain relationship of the pile adopting the limits on the ranges of the curve fitting factor, $0.5 < r_f < 0.98$, in the hyperbolic expression. In this case τ_{int} assumes the stiff interface which has been used in the previous cases. In addition, as this loading is in sand the curves do not soften to a residual value.

In some results, the use of the API curves give a stiffer response than those of the DNV, such as at Pigeon Creek (not shown) and at Euripides (Figure 5-63), and here these results better match the data.

At the Kwangyang Plant site (Figure 5-62), the reverse was the case and the DNV curves better matched the data. In general, with regards to the DNV curves, their stiffness increases as r_f reduces and here, the stiffer curves occur at r_f = 0.5. There was marginal observable difference on the separate pile components and these are not shown here. In addition, the curves mainly influence the initial slopes of the load-displacement response due to the shaft of the pile resisting the load as it is applied. The responses merge as τ_{ult} is achieved along the entire length and base resistance further adds to the total capacity.

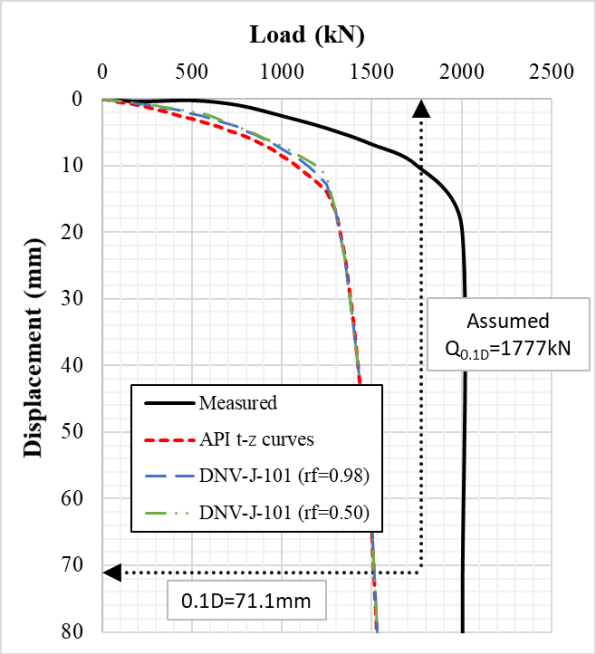

Figure 5-62 Load-displacement curve for ICP-FEA estimation against measured. Kwangyang Plant site.

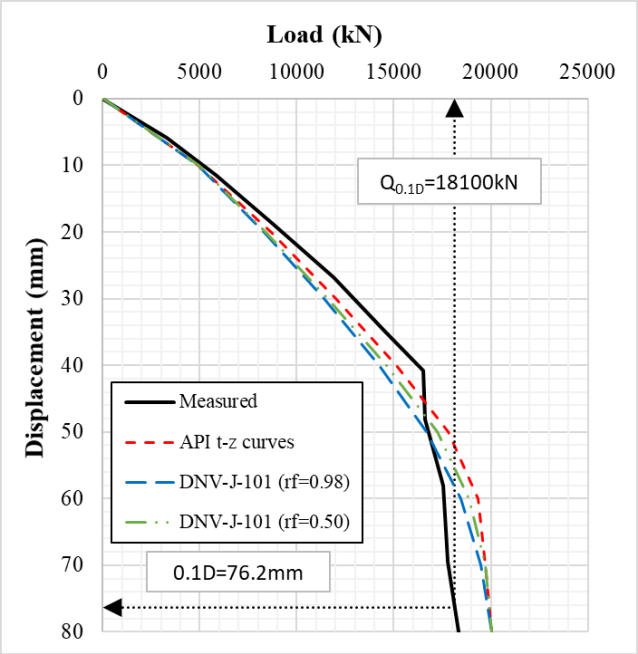

Figure 5-63 Load-displacement curve for ICP-FEA estimation against measured. Euripides site.

Case 35: Similar to Case 26, this ICP-FEA analysis investigates the use of a stiffer reaction at the base of the annulus. Here z/t is reduced from 1.0 to 0.1. Results are only shown for Pigeon Creek as the results were similar for each site.

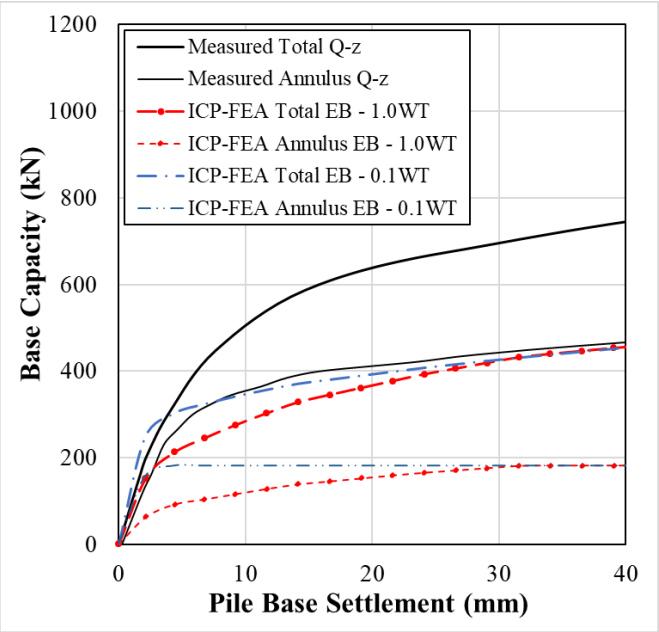

Figure 5-64 Comparison of base response with varied $q_{b,p}$ stiffness using the ICP-FEA. Pigeon Creek results.

Figure 5-64 shows that, for all the sites, when the stiffness of the reaction at the base of the pile is increased, this causes the annulus to achieve its ultimate capacity much earlier. This then has the effect of increasing the total base stiffness. The different ratios of z/t only affect the initial base response as these responses eventually merge as the displacement increases.

Case 36: This ICP-FEA investigates the use of a softer reaction at the base of the plug. Here the z/D_i ratio is increased from 0.1 to 1.0.

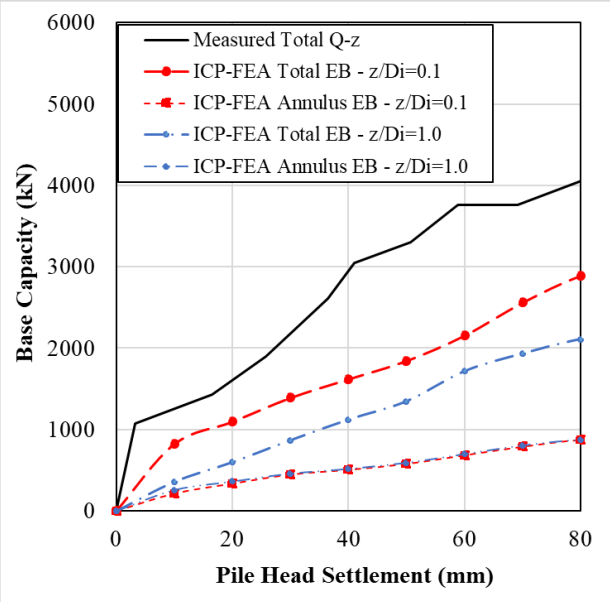

Figure 5-65 Comparison of base response with varied $q_{b,pl}$ stiffness using the ICP-FEA. Euripides results.

Figure 5-65 shows the comparison of the measured and estimated base responses at the Euripides site. In each of the analyses performed, using a softened plug base reaction for $q_{b,pl}$, causes much less total capacity to be gained from each pile base.

Case 37: This case considers the variation of the constrained modulus, M, here investigating the impact of this parameter on the results of the ICP-FEA (similar to Case 28). For this analysis, M will

be varied using, as before, K_{water}, G_{ICP} and E_{ICP}. These are compared to the results adopted for the default value of M, derived from the Lunne and Christophersen (1993), where, in general, $M_{default} < G_{ICP} < E_{ICP} < K_{water}$.

The analysis of the Pigeon Creek, Kwangyang Plant and Euripides sites, again all showed similar trends from varying M. Here the results from the Euripides analysis are shown.

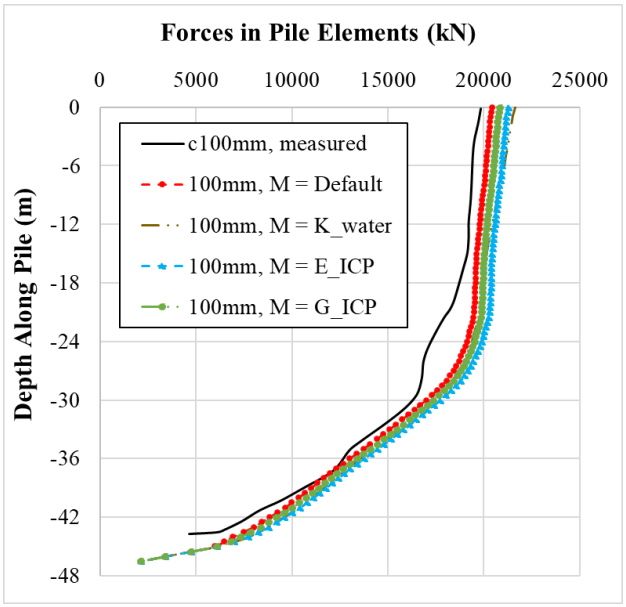

Figure 5-66 Axial load in pile, ICP-FEA estimation vs measured.

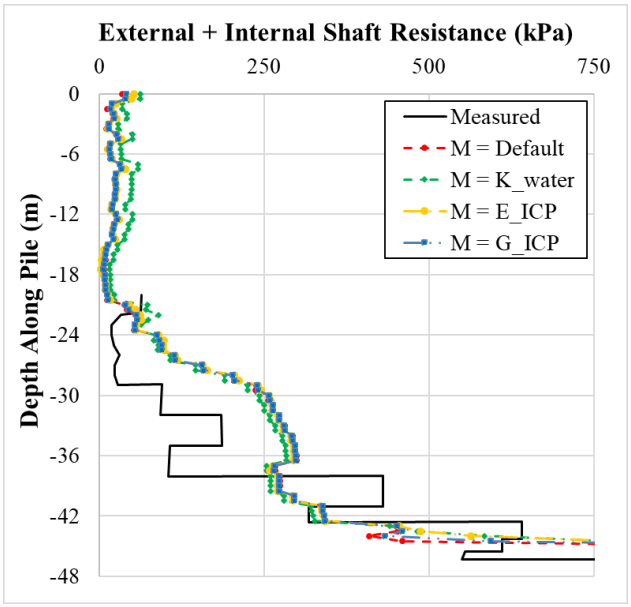

Figure 5-67 Total shaft friction, ICP-FEA estimation vs measured at pile head displacement of 100mm.

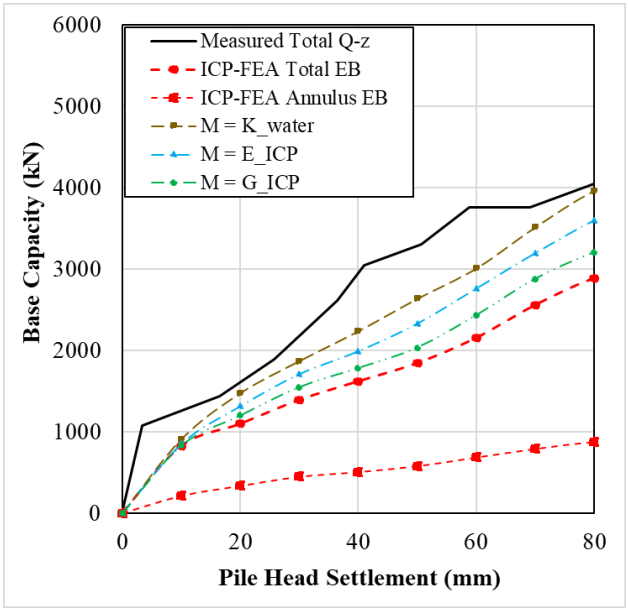

Figure 5-68 ICP-FEA estimation of pile head settlement vs base capacity.

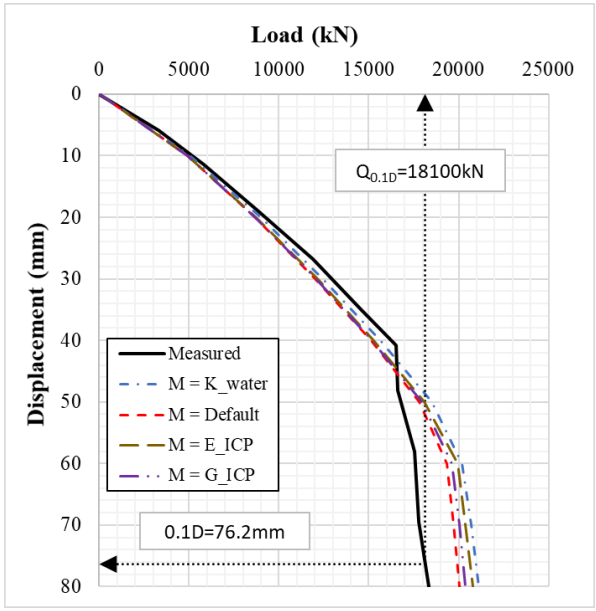

Figure 5-69 Load-displacement curve for ICP-FEA estimation against measured.

In general, the value of M affects all components simultaneously. When the value of M is at its highest, the load in the pile is estimated to be highest. The default value of M however, seems to give

the most acceptable prediction of the forces in the pile, as observed in Figure 5-66, after a pile head displacement of 100mm. In terms of estimated stresses, Figure 5-67 demonstrates that these are, in general, quite similar and using the ICP-FEA follows the measured data quite well. This is also the case for the total base load (Figure 5-68) when the highest value of M is used. Figure 5-69 shows the load-displacement results from the analysis. Here the largest estimation of load is predicted when $M = K_{water}$ (highest) but this also overestimates the ultimate value with Q_c/Q_m of 1.16, reducing to 1.12 when $M = G_{ICP}$, the lowest modulus is considered. In this case however, when $M = K_{water}$, this predicts the best estimation of initial stiffness.

Case 38: This ICP-FEA case investigated the inclusion of the weight of pile and plug into the analysis. Here the results showed a small variation in the estimated load-displacement response when these weights were included in the analysis.

Case 39: This ICP-FEA analysis investigates the calculation of the "equivalent radius" for an OEP. Currently, this factor is included in the ICP method to convert from the solution of CEPs to OEPs by adopting an equivalent radius $R^*=\sqrt{{R_o}^2 + {R_i}^2}$, where $R_o = R$. Here we investigate the alternative assumption of $R^* = R$. This is similar to the analysis in Case 21 for clay.

For this example, the effects are illustrated using the results at the Kwangyang Plant and Euripides sites. The results at Pigeon Creek were very similar but showed a slightly smaller effect.

In general, the change in R, does not affect the annulus capacity but reduces the capacity of the plug and increases the external shaft friction. The reduction in plug capacity is observed in Figure 5-70, under the 1500kN pile head load, using R instead of R^*. Figure 5-71 shows that by adopting R, slightly more load is resisted by the external shaft friction. This was the general trend for all sites. In terms of the load-displacement, the use of R, can improve the estimation of the pile head response, as shown for the Kwangyang Plant site (Figure 5-72) but can also overestimate this response as observed at Euripides (Figure 5-73).

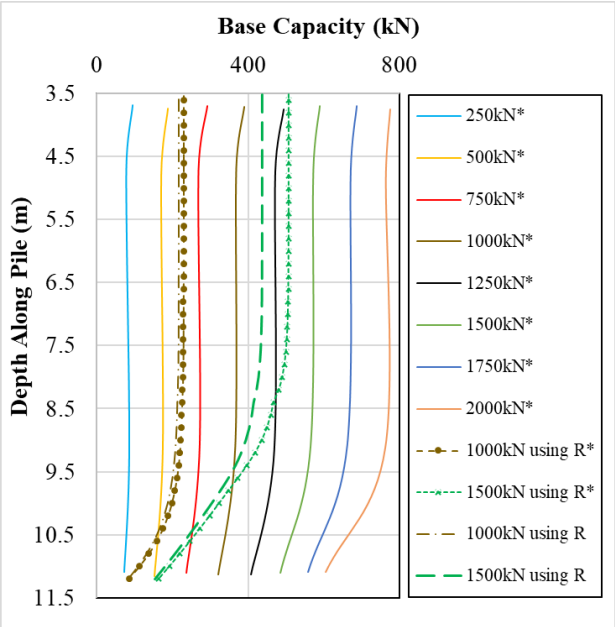

Figure 5-70 Internal shaft friction, ICP-FEA estimation vs measured. Kwangyang Plant site.

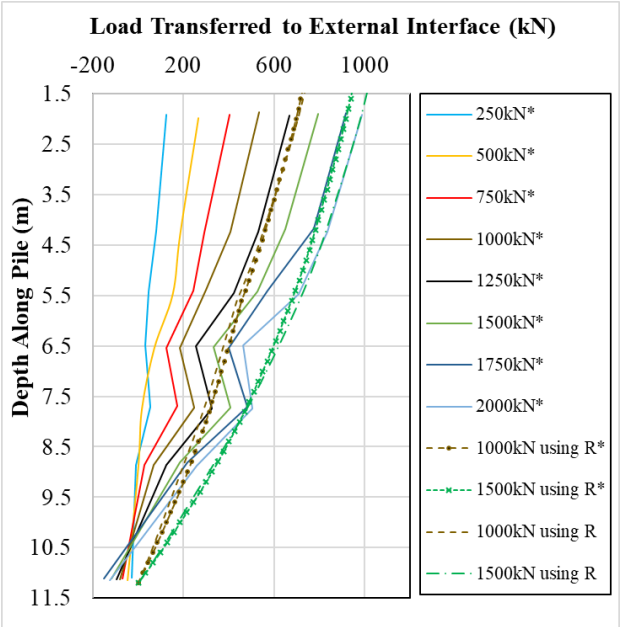

Figure 5-71 External shaft friction, ICP-FEA estimation vs measured. Kwangyang Plant site.

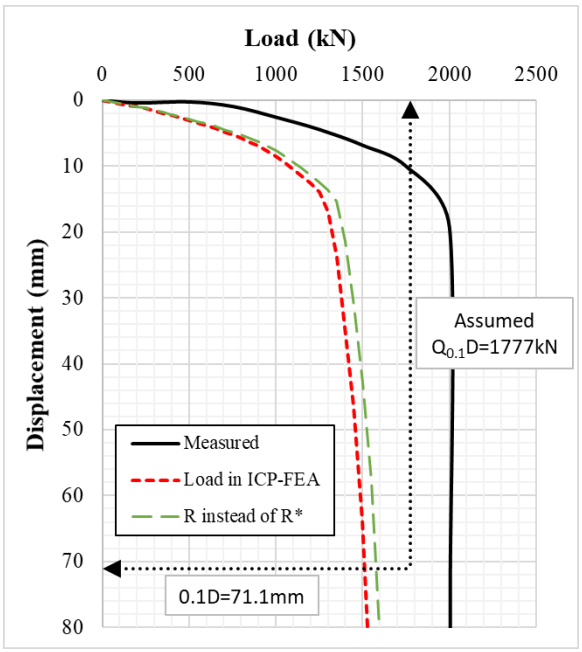

Figure 5-72 Load-displacement curve for ICP-FEA estimation against measured. Kwangyang Plant site.

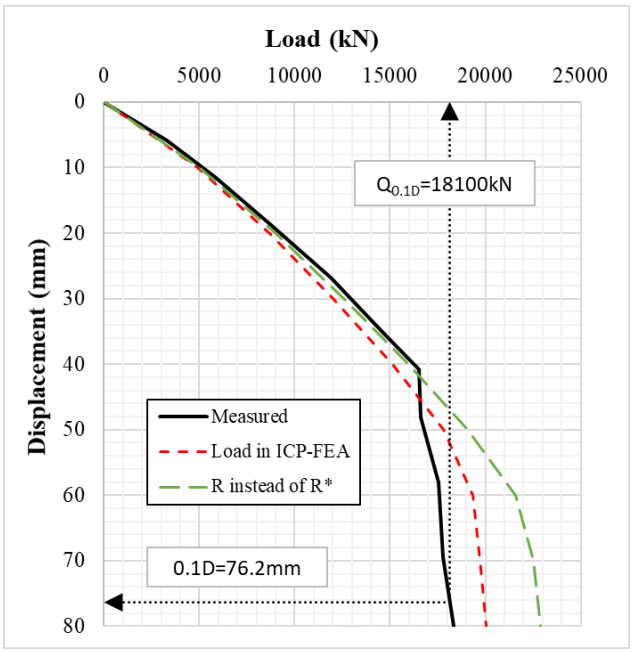

Figure 5-73 Load-displacement curve for ICP-FEA estimation against measured. Euripides site.

5.3.2.3. UWA-FEA Analyses (Case 40 to Case 48)

The UWA-FEA method is used here to compare against the results of the previous cases. This method is examined for sands as there is no UWA method for clays. In this method all OEPs are considered fully plugged under axial static loading. The cases are set out in Table 5-7.

Table 5-7 UWA test cases analysed.

Case	Design Method	Constitutive Model τ_{int} & τ_{ext}	τ_{ult} = τ_{int} & τ_{ext}	τ_{int} – z_{peak}/D_i	τ_{ext} – z_{peak}/D_o	Constitutive Model $q_{b,pile}$	$q_{b,pile}$	Constitutive Model $q_{b,plug}$	$q_{b,plug}$	M	Weight
40	UWA	API t-z curves	$\tau_{ext,ult}=\tau_{int,ult}$	0.0001	0.01	API Q-z to 1.0WT	(UWA)q_c	API Q-z, Q_{max} at 0.1D_i	(UWA)q_c	Lunne and Christophersen (1983)	No
41	UWA	API t-z curves	$\tau_{ext,ult}=\tau_{int,ult}$	0.0001	0.01	API Q-z to 1.0WT	0.6q_c	API Q-z, Q_{max} at 0.1D_i	0.1q_c	Lunne and Christophersen (1983)	No
	UWA	API t-z curves	$\tau_{ext,ult}=\tau_{int,ult}$	0.0001	0.01	API Q-z to 1.0WT	0.5 x UWA's q_b	API Q-z, Q_{max} at 0.1D_i	0.5 x UWA's q_b	Lunne and Christophersen (1983)	No
	UWA	API t-z curves	$\tau_{ext,ult}=\tau_{int,ult}$	0.0001	0.01	API Q-z to 1.0WT	0.6q_c	API Q-z, Q_{max} at 0.1D_i	0.3q_c	Lunne and Christophersen (1983)	No
42	UWA	API t-z curves	$\tau_{ext,ult}=\tau_{int,ult}$	0.1	0.01	API Q-z to 1.0WT	UWA's q_b	API Q-z, Q_{max} at 0.1D_i	UWA's q_b	Lunne and Christophersen (1983)	No
	UWA	API t-z curves	$\tau_{ext,ult}=\tau_{int,ult}$	0.01	0.01	API Q-z to 1.0WT	UWA's q_b	API Q-z, Q_{max} at 0.1D_i	UWA's q_b	Lunne and Christophersen (1983)	No
	UWA	API t-z curves	$\tau_{ext,ult}=\tau_{int,ult}$	0.001	0.01	API Q-z to 1.0WT	UWA's q_b	API Q-z, Q_{max} at 0.1D_i	UWA's q_b	Lunne and Christophersen (1983)	No
43	UWA	API t-z curves	$\tau_{ext,ult}=\tau_{int,ult}$	0.0001	0.0025	API Q-z to 1.0WT	UWA's q_b	API Q-z, Q_{max} at 0.1D_i	UWA's q_b	Lunne and Christophersen (1983)	No
	UWA	API t-z curves	$\tau_{ext,ult}=\tau_{int,ult}$	0.0001	0.0050	API Q-z to 1.0WT	UWA's q_b	API Q-z, Q_{max} at 0.1D_i	UWA's q_b	Lunne and Christophersen (1983)	No
	UWA	API t-z curves	$\tau_{ext,ult}=\tau_{int,ult}$	0.0001	0.0200	API Q-z to 1.0WT	UWA's q_b	API Q-z, Q_{max} at 0.1D_i	UWA's q_b	Lunne and Christophersen (1983)	No
44	UWA	DNV t-z curves	$\tau_{ext,ult}=\tau_{int,ult}$	0.0001	DNV t-z r_f=0.98	API Q-z to 1.0WT	UWA's q_b	API Q-z, Q_{max} at 0.1D_i	UWA's q_b	Lunne and Christophersen (1983)	No
	UWA	DNV t-z curves	$\tau_{ext,ult}=\tau_{int,ult}$	0.0001	DNV t-z r_f=0.50	API Q-z to 1.0WT	UWA's q_b	API Q-z, Q_{max} at 0.1D_i	UWA's q_b	Lunne and Christophersen (1983)	No
45	UWA	API t-z curves	$\tau_{ext,ult}=\tau_{int,ult}$	0.0001	0.01	API Q-z to 1.0WT	UWA's q_b	API Q-z, Q_{max} at 1.0D_i	UWA's q_b	Lunne and Christophersen (1983)	No
46	UWA	API t-z curves	$\tau_{ext,ult}=\tau_{int,ult}$	0.0001	0.01	API Q-z to 1.0WT	UWA's q_b	API Q-z, Q_{max} at 0.1D_i	UWA's q_b	K_{water}	No
	UWA	API t-z curves	$\tau_{ext,ult}=\tau_{int,ult}$	0.0001	0.01	API Q-z to 1.0WT	UWA's q_b	API Q-z, Q_{max} at 0.1D_i	UWA's q_b	G_{UWA}	No
	UWA	API t-z curves	$\tau_{ext,ult}=\tau_{int,ult}$	0.0001	0.01	API Q-z to 1.0WT	UWA's q_b	API Q-z, Q_{max} at 0.1D_i	UWA's q_b	E_{UWA}	No
47	UWA	API t-z curves	$\tau_{ext,ult}=\tau_{int,ult}$	0.0001	0.01	API Q-z to 1.0WT	UWA's q_b	API Q-z, Q_{max} at 0.1D_i	UWA's q_b	Lunne and Christophersen (1983)	Yes
	UWA	API t-z curves	$\tau_{ext,ult}=\tau_{int,ult}$	0.0001	0.01	API Q-z to 1.0WT	UWA's q_b	API Q-z, Q_{max} at 0.1D_i	UWA's q_b	Lunne and Christophersen (1983)	Yes + Plug Weight
48	UWA	API t-z curves	2.0 x UWA's τ ($\tau_{ext,ult}=\tau_{int,ult}$)	0.0001	0.01	API Q-z to 1.0WT	UWA's q_b	API Q-z, Q_{max} at 0.1D_i	UWA's q_b	Lunne and Christophersen (1983)	No

<u>Case 40</u>: The UWA-FEA analysis in this case is used as the base case for this section.

Pigeon Creek Site Results:

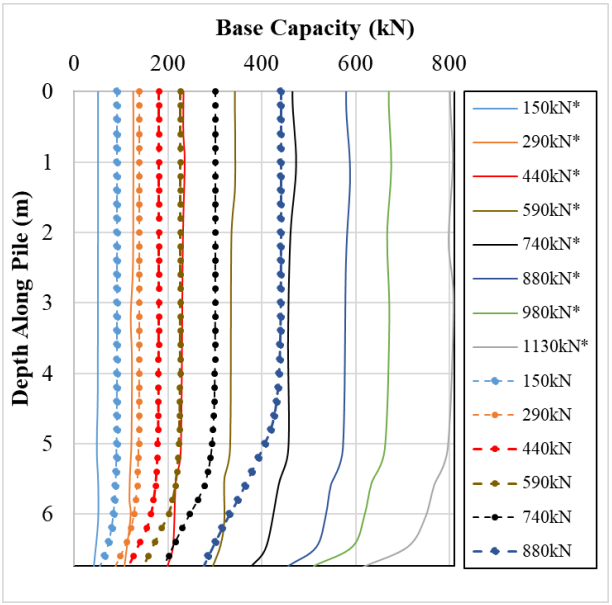

Figure 5-74 Internal shaft friction, UWA-FEA estimation vs measured.

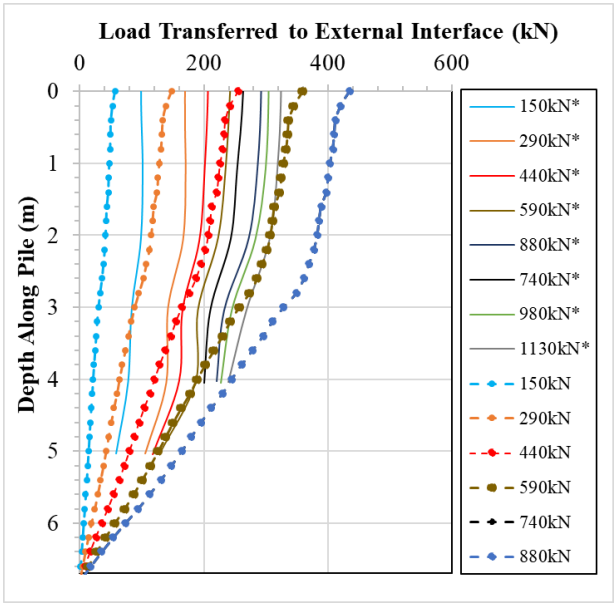

Figure 5-75 External shaft friction, UWA-FEA estimation vs measured.

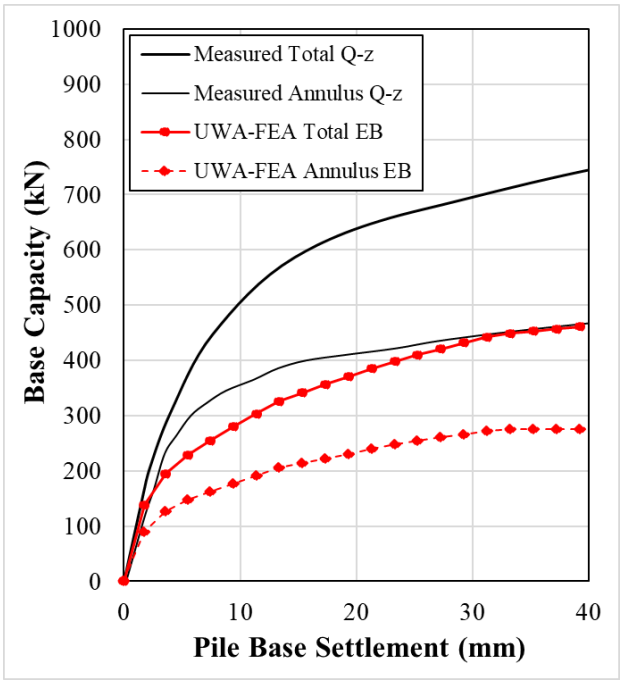

Figure 5-76 UWA-FEA estimation of pile base settlement vs measured load.

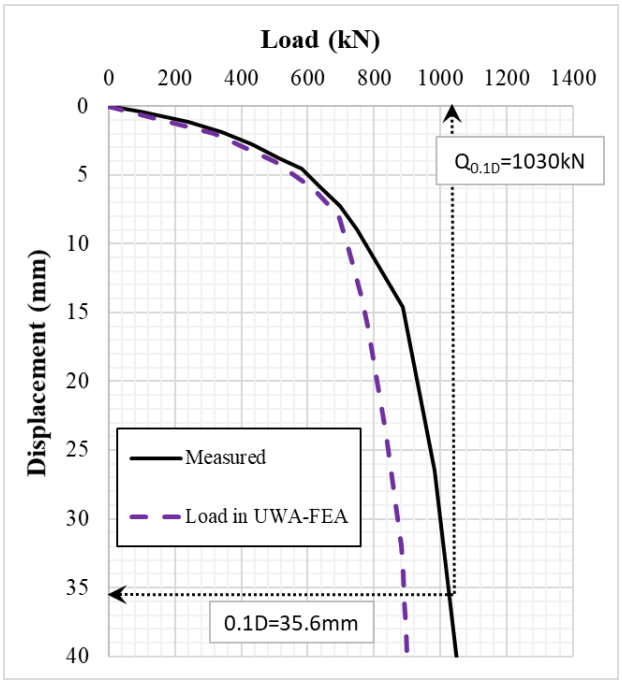

Figure 5-77 Load-displacement curve for UWA-FEA estimation against measured.

The response of the mobilised internal shaft friction is shown in Figure 5-74. Here the load estimated by the UWA-FEA method does not fully match the measured values of Q_{int}. The maximum load supported by the internal shaft under a pile head load of 880kN is approximately 440kN as compared to a measured 590kN. However, compared to the API-FEA and the ICP-FEA, this is the best match. The load transferred to the base is also observed to be underestimated. With regards to the load transferred to the external interface, Figure 5-75 shows that under a pile head load of 880kN, the

measured external load in the pile is approximately 300kN whilst that estimated is 440kN. The base response is shown in Figure 5-76. It is observed here that the UWA underestimates the base capacity with a Q_c/Q_m of 0.64 (454/712). The initial stiffness of the load-displacement, Figure 5-77, is observed to match the measured stiffness however during the latter stages of loading, the total capacity reduces below that measured, to a Q_c/Q_m of 0.87.

Kwangyang Site Results:

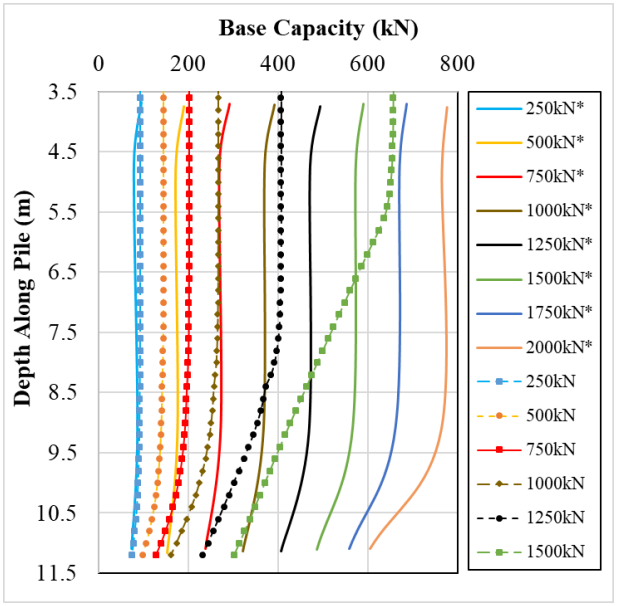

Figure 5-78 Internal shaft friction, UWA-FEA estimation vs measured.

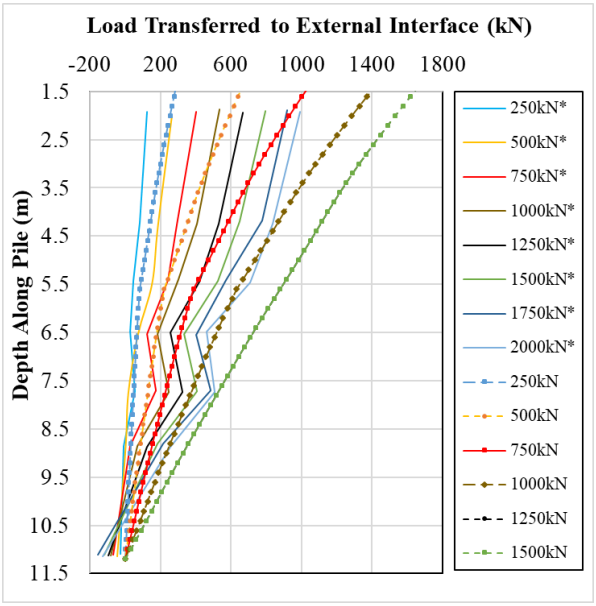

Figure 5-79 External shaft friction, UWA-FEA estimation vs measured.

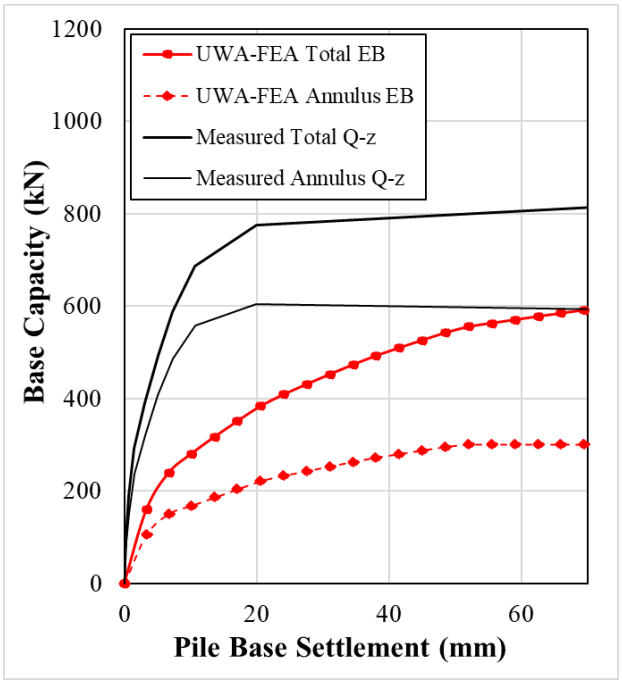

Figure 5-80 UWA-FEA estimation of pile base settlement vs measured load.

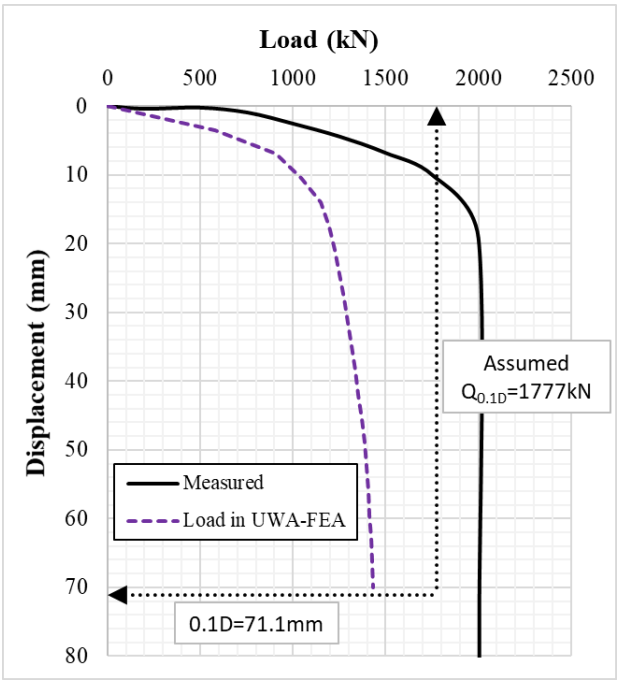

Figure 5-81 Load-displacement curve for UWA-FEA estimation against measured.

The comparison of the measured and estimated internal shaft capacity is shown in Figure 5-78. Here, the UWA-FEA underestimates the load on the pile and overestimates the load on the plug, at a pile head load of 1500kN. The total base load is comparable to the measured values; however, no further internal capacity is calculated with the UWA-FEA. Figure 5-79 shows that the UWA-FEA over-predicts the load transferred to the external shaft friction. In this case, it is observed that the estimated values are more than double those measured. The base capacity is under-predicted by the UWA-FEA in the comparison shown in Figure 5-80. The Q_c/Q_m here is 0.73 (594/815). The load-displacement response is also under-predicted, with a Q_c/Q_m value of 0.81 (Figure 5-81).

Euripides Site Results:

The q_c profile that is adopted here is directly extracted from the values measured at the Euripides site. No averaged or lower bound values are used.

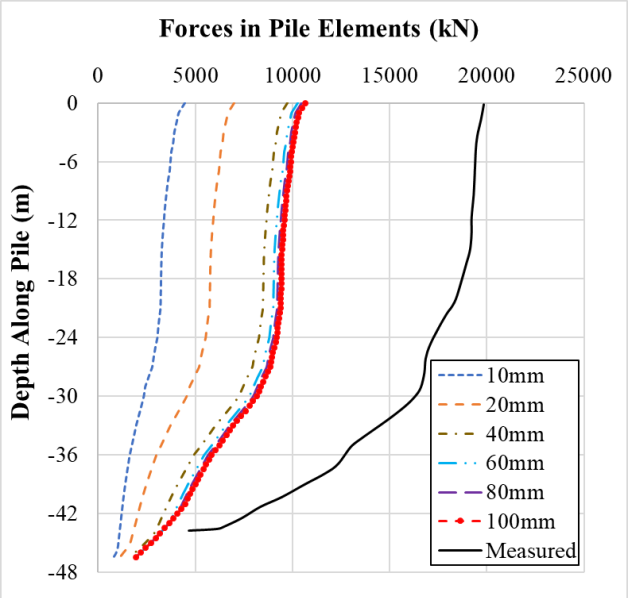

Figure 5-82 Axial load in pile, UWA-FEA estimation vs measured.

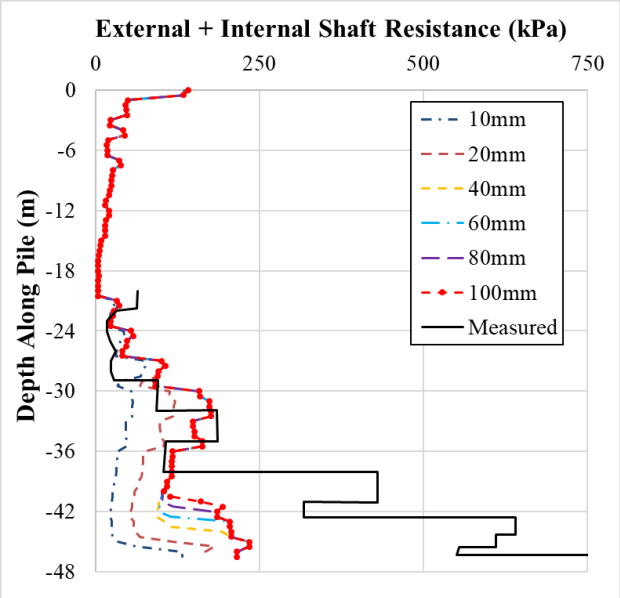

Figure 5-83 Total shaft friction, UWA-FEA estimation vs measured.

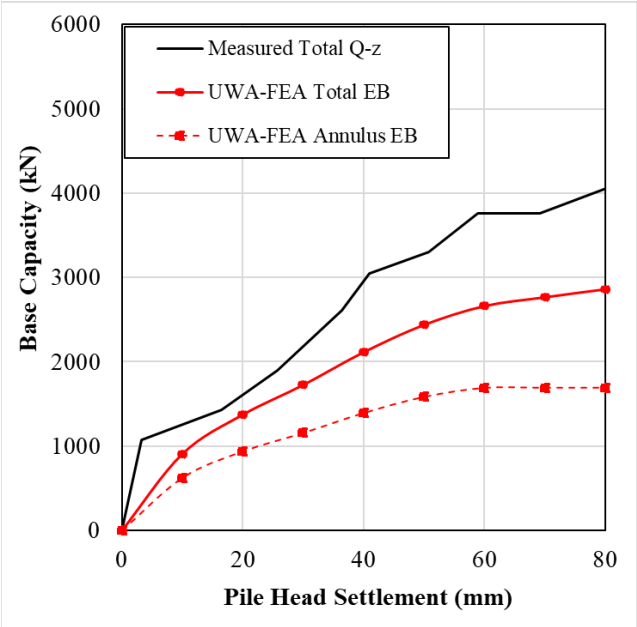

Figure 5-84 UWA-FEA estimation of pile head settlement vs measured load.

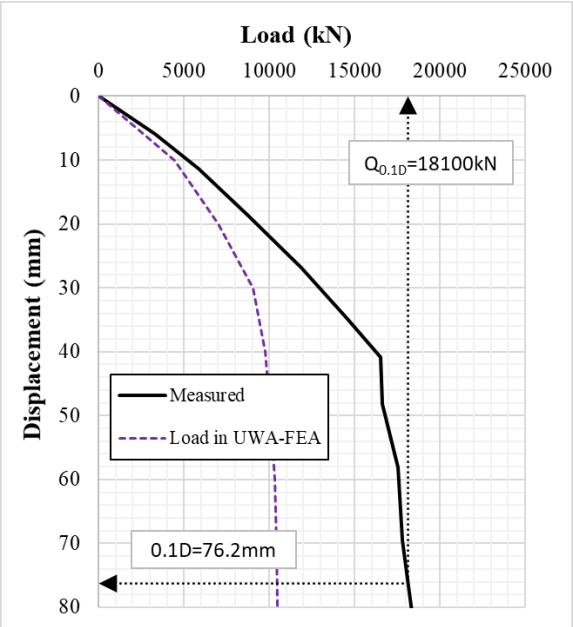

Figure 5-85 Load-displacement curve for UWA-FEA estimation against measured.

At this site the UWA-FEA method underestimates all the load components. Figure 5-82 shows the comparison of the forces along the pile for incremental pile head displacements and the measured loads at 100mm pile head displacement. The method considerably underestimates the measured load in the pile by approximately 50%. Figure 5-83 shows the stresses measured along the pile after a pile head displacement of 100mm. Here it shows that the stress is also underestimated. Figure 5-84 shows the base response is underestimated, with a Q_c/Q_m value of 0.76. Figure 5-85 shows the overall load displacement response, and the UWA method underestimates the total capacity with a Q_c/Q_m of 0.58.

Case 41: This analysis varies the base resistance in the UWA method. The authors of the UWA method correlated the final filling ratio (FFR) to the $q_{b,pl}$; however, designers usually do not have access to this information until after pile has been installed. Therefore, the range of values of $q_{b,pl}$ of $0.1q_c$ to $0.3q_c$ is used. $0.6q_c$ is applied to the pile in these cases.

In addition, from the results of the RMS-error analysis and the results shown in Table 5-4, the UWA method has been found to overestimate the base capacity by about 50%. In this comparison, a reduction of q_b by 50% is included to assess the effects.

In general, similar trends were found for the sites. The results from Pigeon Creek only are shown.

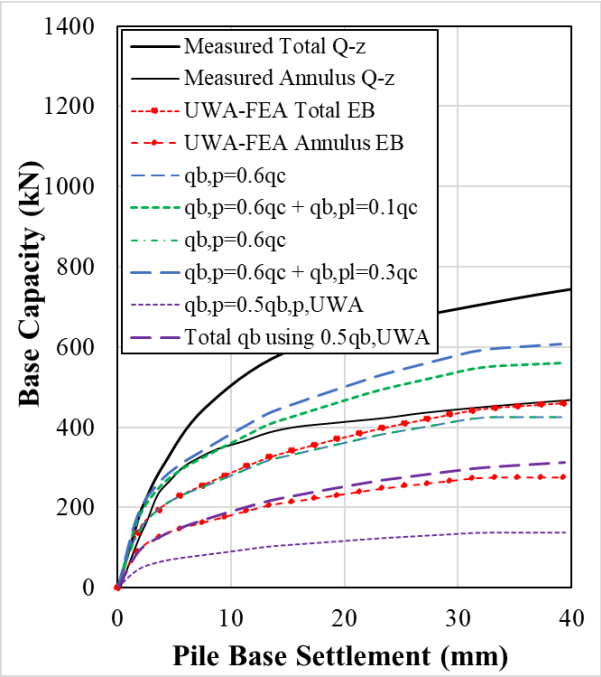

Figure 5-86 UWA-FEA estimation of pile base settlement vs measured load.

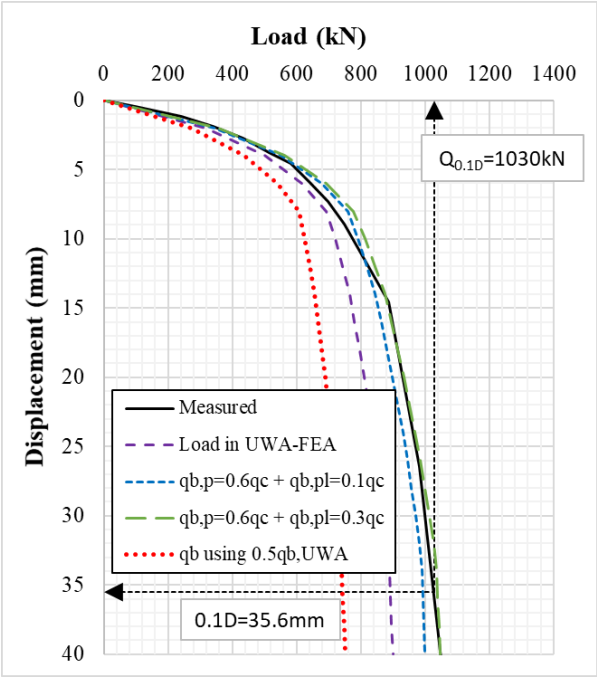

Figure 5-87 Load-displacement curve for UWA-FEA estimation against measured.

The comparison of the estimated base capacity to those measured is shown in Figure 5-86. In the analysis which adopts $0.6q_c$ at the base of the pile and $0.1q_c$ at the base of the plug, the total base capacity gives a Q_c/Q_m value of 0.78. When $0.6q_c$ is used at the base of the pile and $0.3q_c$ on the plug, the total capacity improves to Q_c/Q_m = 0.84. The reduction of q_b by 50% shows the lowest comparison with that measured, Q_c/Q_m = 0.43.

The load-displacement response (Figure 5-87) shows an improvement of Q_c/Q_m to 1.01 when the base resistance is distributed as $0.6q_c$ on the annulus and $0.3q_c$ on the plug. With $0.1q_c$ applied to the base of the plug the Q_c/Q_m is 0.96. The use of the 50% reduction of q_b gives a Q_c/Q_m value of 0.72.

Case 42: This UWA-FEA case investigated the effect on the mobilised internal shaft resistance, τ_{int}, to a change in the stiffness of the internal soil reaction curves. Although it was found that, in general, a stiffer interface enabled more of the plug to be mobilised, the variation in results was too small to be observed diagrammatically.

Case 43: This UWA-FEA case assesses the variation in pile response when the displacement-to-peak mobilised load, z, occurs at $0.0025D_o$, $0.005D_o$, and $0.02D_o$.

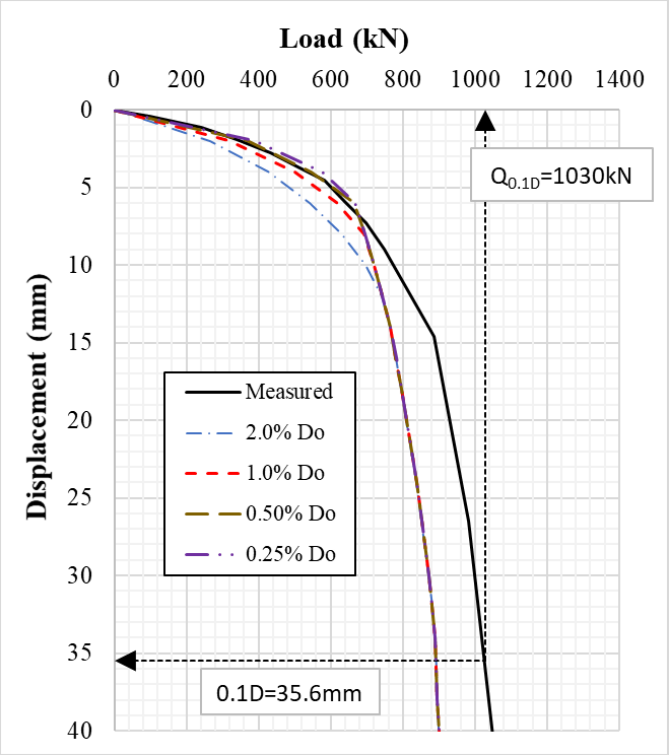

Figure 5-88 Comparison of the load-displacement responses for range of t-z curves with τ_{max} from the UWA-FEA. Pigeon Creek results.

The analyses all showed an effect on the initial stiffness but not the ultimate load, as shown in the results for the Pigeon Creek site, Figure 5-88.

Case 44: In this UWA-FEA the t-z curves adopted are those recommended by the DNV-OS-J101 (2016). As analysed in previous cases, these curves are applied as the external stress-strain relationship of the pile, adopting the limits on the ranges of the curve fitting factor, $0.5 < r_f < 0.98$, in the hyperbolic expression.

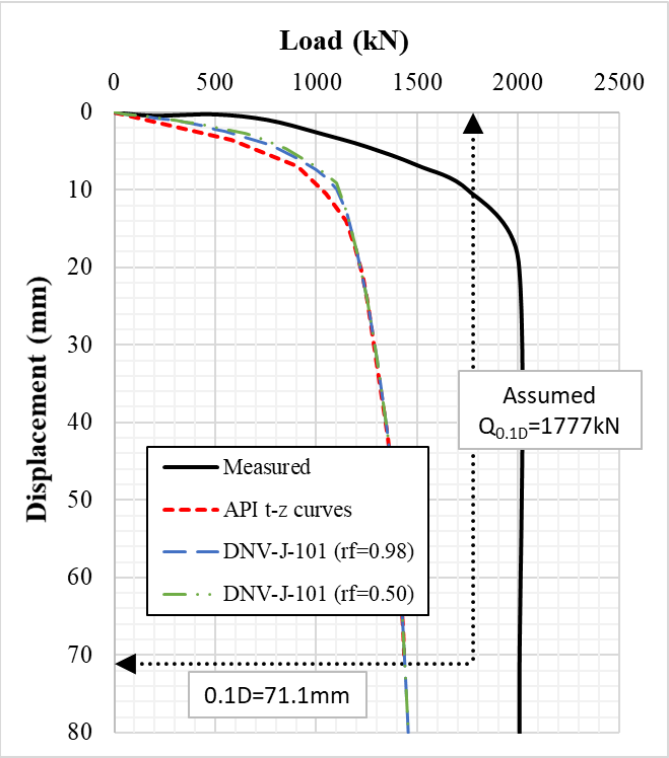

Figure 5-89 Load-displacement curve for UWA-FEA estimation against measured. Kwangyang Site results.

In general, the results were similar to those of the ICP-FEA whereby, there were no significant variations observed. The most observable variation due to the use of the API and DNV curves was found at the Kwangyang Plant site. Figure 5-89 shows the load-displacement responses for this site. Here a clear variation in initial stiffness is observed when the different curves are used. The results suggest that the DNV curves are marginally better at estimating the initial stiffness.

<u>Case 45</u>: This UWA-FEA investigates the use of a softer reaction at the base of the plug. Here the z/D_i is increased from 0.1 to 1.0. Figure 5-90 shows the comparison of the results from the Kwangyang Plant site as the clearest effect was observed.

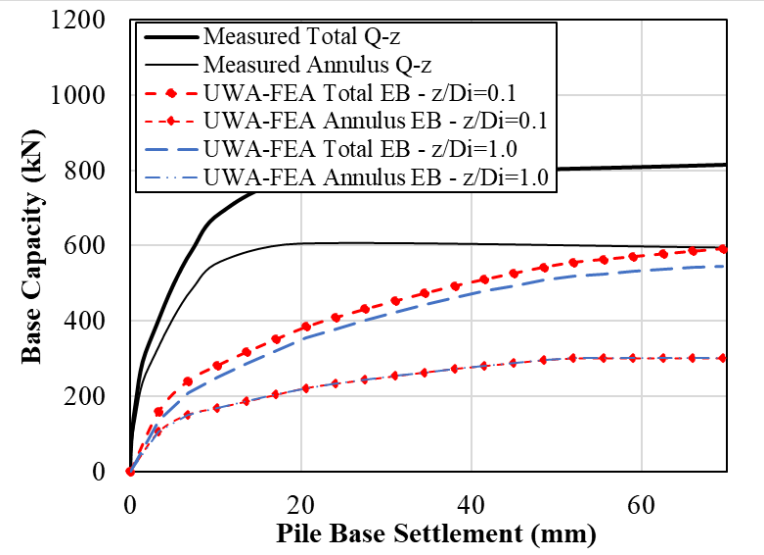

Figure 5-90 Comparison of the load-displacement responses for range of t-z curves with τ_{max} from the UWA-FEA. Kwangyang Plant results.

The trends observed here were similar to each of the sites. With a softer response at the base of the plug, the response at the base of the annulus is unchanged, but the stiffness of the plug resistance and the total capacity is reduced.

Case 46: This UWA-FEA examines the variation of the constrained modulus, M, using, as in earlier cases, K_{water}, G_{UWA} and E_{UWA}. These are compared to the results adopted for the default value of M, derived from the Lunne and Christophersen (1993). As the results are similar at each site, only the Pigeon Creek results are shown.

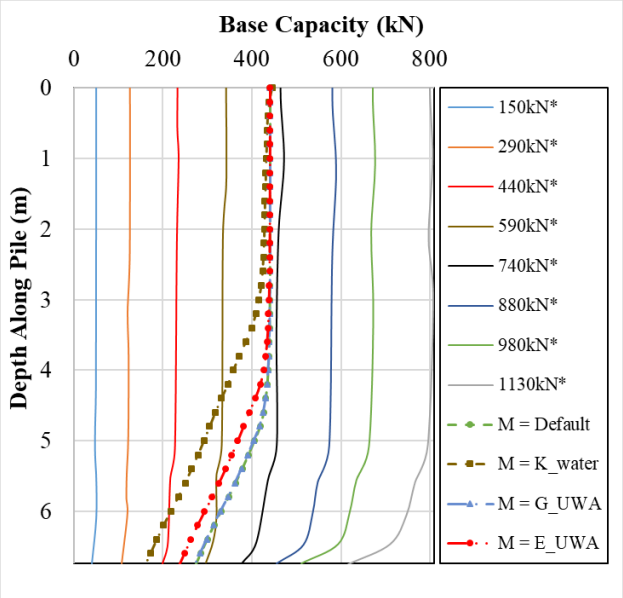

Figure 5-91 Mobilised internal shaft friction/base capacity. UWA-FEA estimation vs measured. Dotted lines are for F_t=880kN. Pigeon Creek results.

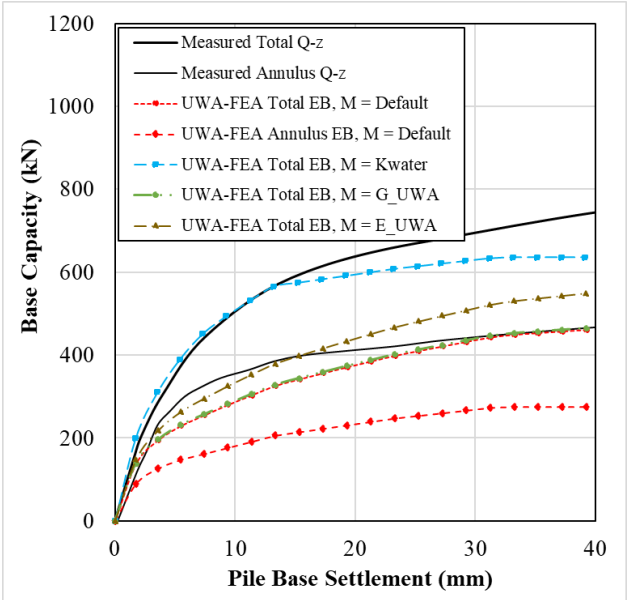

Figure 5-92 UWA-FEA estimation of pile base settlement vs measured load. Pigeon Creek results.

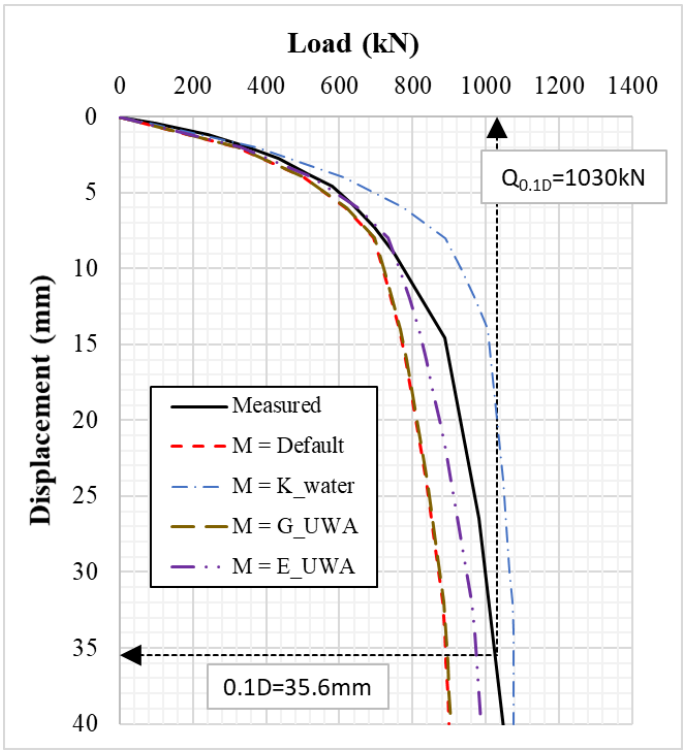

Figure 5-93 Load-displacement curve comparison of UWA-FEA estimates against measured. Pigeon Creek results.

Using the largest value of M, facilitates a much larger mobilised plug capacity and a marginal amount of increased base capacity (Figure 5-91), compared to when the default M values are used. In general, the total base capacity has not changed but to a greater effect, the distribution of the load. In addition, the use of larger values of M, in this case, causes less load to be supported by the annulus.

When $M = K_{water}$ this mobilises the largest base capacity, best matching the measured results with a Q_c/Q_m of 0.89 (Figure 5-92). The use of $M = E_{UWA}$ and G_{UWA} produces Q_c/Q_m of 0.76 and 0.64, respectively, for the total base capacity.

The load-displacement results for this case show trends that are similar to those in the other component behaviours, in that, the stiffer the plug the more load can be mobilised (Figure 5-93). When $M = K_{water}$, the initial stiffness is highest, as more of the base capacity is mobilised sooner.

Case 47: This UWA-FEA considered the effect on the overall load-displacement if the weight of pile and plug are included in the analysis. The results were similar to those for the API-FEA and ICP-FEA, in that there is little to no difference when these weights are included.

Case 48: This UWA-FEA considers the use of the factors that were found from the RMS-error calculation and Table 5-4. Here a factor of 2.0 is applied to σ'_{rc} on both the internal and external sides of the pile.

Pigeon Creek Site Results:

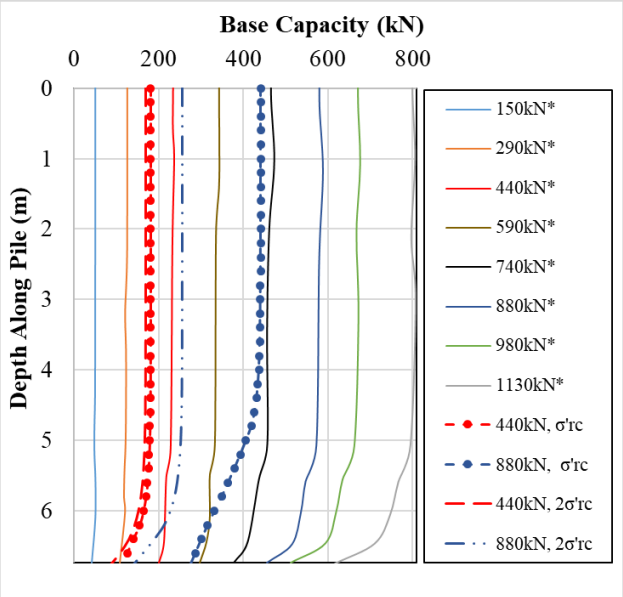

Figure 5-94 Internal shaft friction, UWA-FEA estimation vs measured.

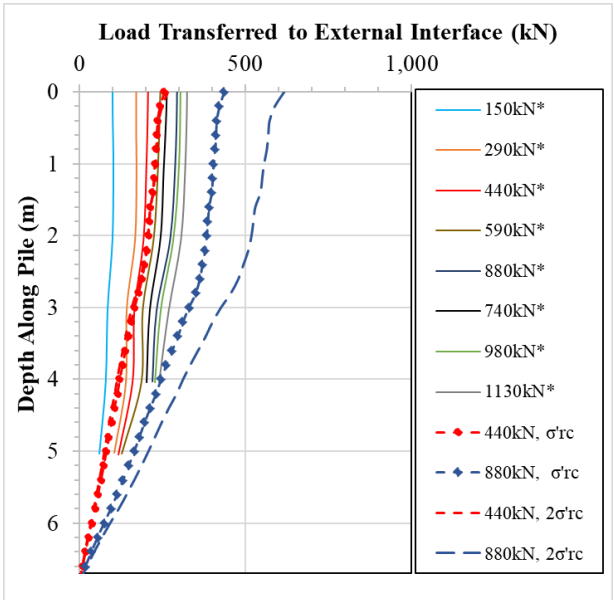

Figure 5-95 External shaft friction, UWA-FEA estimation vs measured.

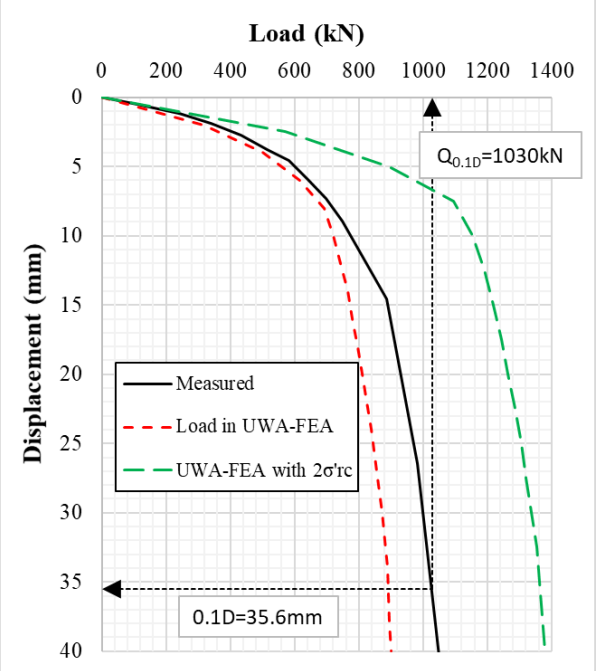

Figure 5-96 Load-displacement curve for UWA-FEA estimation against measured.

Figure 5-94 shows the comparison of the measured and estimated values of the internal shaft friction for pile head loads of 440kN and 880kN. The use of the factored (2×) σ'_{rc} generated less internal resistance than the unfactored case. This suggests that with a higher capacity more load is resisted by the external shaft (and therefore less to the base).

This is further demonstrated in Figure 5-95 where for a higher pile head load of 880kN, a larger load is supported by the external shaft for the condition where the factored σ'_{rc} is adopted. This occurs as the shaft capacity has doubled, allowing more load to be supported and therefore less capacity being required at the base of the pile. The smaller load of 440kN will therefore not see much variation when the factored σ'_{rc} is adopted, but when more capacity is required at 880kN, a clear variation is observed.

The load-displacement response shows an increase in Q_c/Q_m to 1.33 from a base case value of 0.87.

This corroborates the above discussion, that the initial stiffness has approximately doubled as a result of the increase in shaft friction in the factored σ'_{rc} case.

Kwangyang Site Results:

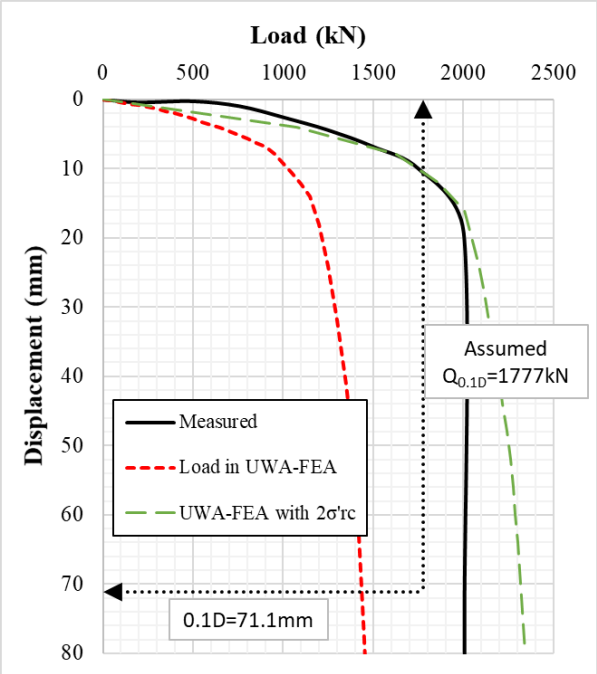

Figure 5-97 Load-displacement curve for UWA-FEA estimation against measured.

Figure 5-97 shows the comparison of the load-displacement for the Kwangyang Plant site. As discussed, the assumed capacity due to discrepancies in the case study have reduced the measured capacity of the pile. However, the results estimated when the factored σ'_{rc} is considered match the initial load response quite well. The Q_c/Q_m has increased from 0.81 to 1.33.

Euripides Site Results:

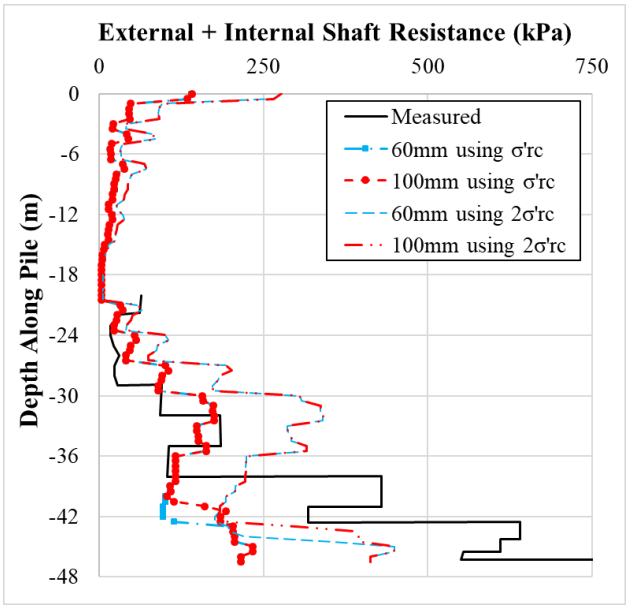

Figure 5-98 Total shaft friction, UWA-FEA estimation vs measured.

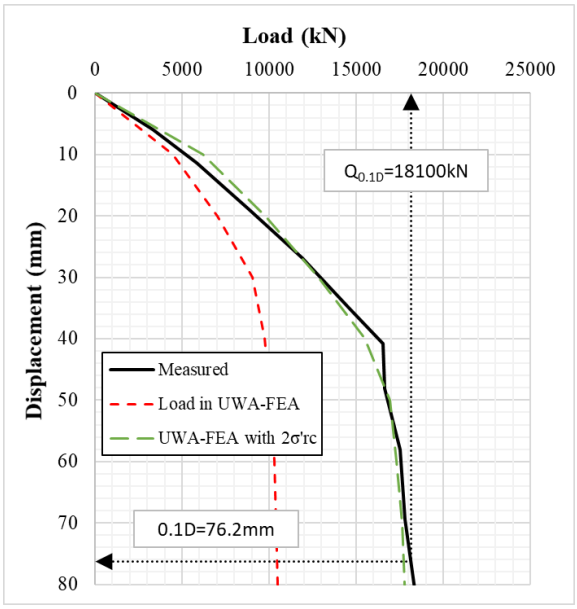

Figure 5-99 Load-displacement curve for UWA-FEA estimation against measured.

The use of $2\sigma'_{rc}$ has increased the estimated mobilised shaft friction along the pile length (Figure 5-98), improving the comparison to that measured. Figure 5-99 shows the load-displacement response comparison. By adopting a factored σ'_{rc}, the estimated values have significantly improved. The Q_c/Q_m for the total capacity has increased to 0.98 from 0.58.

5.3.2.4. Summary of Results

The results of the cases outlined above are summarised in Table 5-8. Unlike axially loaded piles in clay, which exhibit strain-softening after a peak capacity has been achieved, piles in sand generally continue to increase in capacity as the base is mobilised. This was observed at both the Pigeon Creek and the Euripides test sites and here the capacity is extracted after a pile head settlement of $0.1D_o$. At the Kwangyang Plant site, the ultimate values are suggested to be constant but modified as discussed, and this value used to perform the Q_c/Q_c comparison.

From Table 5-8, the variations to the API-FEA and UWA-FEA still both under-predict the capacities at each of the tested sites and the ICP-FEA is generally well averaged considering all test results.

Table 5-8 Summary of results

Case	Pigeon Creek		Kwangyang Plant - TP2		Euripides - Ic	
	Capacity at $0.1D_o$ (kN)	Q_c/Q_m	Capacity at $0.1D_o$ (kN)	Q_c/Q_m	Capacity at $0.1D_o$ (kN)	Q_c/Q_m
Measured Values	1030	-	1777	-	18100	-
API-FEA						
23	424	0.41	1343	0.76	9498	0.52
24	380	0.37	1288	0.72	9194	0.51
	410	0.40	1338	0.75	9432	0.52
	410	0.40	1343	0.76	9452	0.52
25	424	0.41	1343	0.76	9498	0.52
	424	0.41	1343	0.76	9498	0.52
	424	0.41	1343	0.76	9498	0.52
26	428	0.42	1343	0.76	9497	0.52
27	405	0.39	1285	0.72	9371	0.52
28	470	0.46	1583	0.89	11377	0.63
	444	0.43	1461	0.82	8876	0.49
	470	0.46	1580	0.89	9118	0.50
29	429	0.42	1343	0.76	9497	0.52
	429	0.42	1343	0.76	9497	0.52

Table 5-8 Summary of results (con'd).

Case	Pigeon Creek		Kwangyang Plant - TP2		Euripides - Ic	
	Capacity at $0.1D_o$ (kN)	Q_c/Q_m	Capacity at $0.1D_o$ (kN)	Q_c/Q_m	Capacity at $0.1D_o$ (kN)	Q_c/Q_m
Measured Values	1030	-	1777	-	18100	-
ICP-FEA						
30	1058	1.03	1513	0.85	19938	1.10
31	1338	1.30	1928	1.09	21861	1.21
	1391	1.35	2066	1.16	22321	1.23
32	1026	1.00	1509	0.85	19319	1.07
	1061	1.03	1512	0.85	19870	1.10
	1064	1.03	1513	0.85	19932	1.10
33	1065	1.03	1514	0.85	19938	1.10
	1065	1.03	1514	0.85	19938	1.10
	1065	1.03	1514	0.85	19938	1.10
34	1065	1.03	1513	0.85	19817	1.09
	1065	1.03	1513	0.85	19938	1.10
35	1058	1.03	1514	0.85	19969	1.10
36	965	0.94	1351	0.76	19214	1.06
37	1171	1.14	1608	0.91	20962	1.16
	1080	1.05	1565	0.88	20253	1.12
	1130	1.10	1600	0.90	20621	1.14
38	1065	1.03	1514	0.85	19938	1.10
	1065	1.03	1514	0.85	19938	1.10
39	1090	1.06	1577	0.89	22756	1.26
UWA-FEA						
40	892	0.87	1435	0.81	10464	0.58
41	993	0.96	1621	0.91	12237	0.68
	743	0.72	1258	0.71	9621	0.53
	1039	1.01	1696	0.95	12284	0.68
42	878	0.85	1404	0.79	10184	0.56
	900	0.87	1431	0.81	10439	0.58
	902	0.88	1435	0.81	10462	0.58
43	819	0.79	1435	0.81	10464	0.58
	818	0.79	1435	0.81	10464	0.58
	818	0.79	1435	0.81	10462	0.58
44	902	0.88	1436	0.81	10464	0.58
	902	0.88	1436	0.81	10464	0.58
45	874	0.85	1389	0.78	10398	0.57
46	1075	1.04	1867	1.05	13594	0.75
	895	0.87	1540	0.87	10651	0.59
	975	0.95	1671	0.94	11339	0.63
47	892	0.87	1435	0.81	10463	0.58
	892	0.87	1436	0.81	10463	0.58
48	1365	1.33	2320	1.31	17740	0.98

5.4. Recommendations from results

From the results of the analyses performed for the Pigeon Creek, Euripides and Kwangyang Plant test sites, recommendations can be suggested to improve the accuracy of the estimated response of OEPs in sands. These recommendations focus on the improved modelling of τ_{ext}, τ_{int} and q_b.

5.4.1. External Shaft

5.4.1.1. Ultimate Resistance, τ_{ext}

In sands the value of τ_{ext} is generally acceptable when using either the ICP-FEA or the UWA-FEA. This has not been found to be the case for the API-FEA as this method relies on the ultimate values derived from the API method that are significantly underestimated in sandy material. It is expected that in light of the results of the RMS-Error distribution observed in Figure 5-15, using the ICP method, no improvement would be gained by further work in sands. The UWA-FEA method is therefore chosen to be taken forward to assess whether improvements can be obtained.

See: Section 5.3.2.1, Case 1; Section 5.3.2.2, Case 30 & Case 39; and Section 5.3.2.3, Case 40 & Case 48.

5.4.1.2. Displacement to Mobilise τ_{ext}, z/D_o

It was found that the stiffer the t-z curves produced a better overall match to the measured response. This is achieved by a ratio of z/D_o of 0.0025. The initial stiffness of the load-displacement response is very sensitive to the stiffness of the t-z soil reaction curves as this mobilises initially. When using the ICP-FEA and the UWA-FEA, these methods have been found to improve the estimate of the initial stiffness at the Pigeon Creek site, but the comparisons at both the Kwangyang Plant site and the Euripides site are poorer when z/D_o = 0.0025 is used. The use of z/D_o = 0.01 is recommended to be taken forward.

See: Section 5.3.2.1, Case 25; Section 5.3.2.2, Case 33; and Section 5.3.2.3, Case 43..

5.4.1.3. t-z reaction curves – API vs DNV

In general, the initial stiffness of the load-displacement response is directly affected by varying the t-z relationships. When the ultimate values of all the t-z soil reaction curves are mobilised, the variation in the use of different soil reaction curves is insignificant as further capacity is now base dependent. In the different cases analysed using the ICP-FEA, the Pigeon Creek and Kwangyang Plant sites gave slightly better results when the DNV curves are used. At Euripides, the API curves were preferred as

in these cases the initial stiffness was better matched. In the UWA-FEA the use of the different curves did not give significant differences in the results. As any improvement in the estimation of stiffness is quite marginal, and the industry's experience with their use, the API t-z soil reaction curves will be used to progress this research.

See: Section 5.3.2.2, Case 34; and Section 5.3.2.3, Case 44.

5.4.1.4. ICP – *R** vs *R*

The use of the external radius, R, instead of the equivalent radius, R^*, in determining τ_f from the ICP-FEA method has been found to marginally increase the mobilised shaft resistance in the shorter piles. However, for the longer pile at Euripides, the effects were quite substantial, and this caused the overestimation of the measured capacity. It is therefore recommended to maintain the use of R^* in the calculation of τ_f.

See: Section 5.3.2.2, Case 39.

5.4.2. Internal Shaft

5.4.2.1. Internal Interface Resistance, τ_{int}

In the ICP and UWA design methods, τ_{ext} is determined by empirical correlations of field and laboratory test results. τ_{int} is not specifically defined in either method but indirectly accounted for in their definition of $q_{b,pl}$. Using the finite element variants of these methods however, it has been shown that τ_{ext} can be taken as the initial value of τ_{int}. The finite element process will then compute the mobilised value due to interactions with other components. If the full internal shaft capacity is mobilised, the load transferred to the base will be limited to the capacity at the base of the plug and the efficiency of the plug to convey the load to this base (constrained modulus dependent). Based on the configuration of the pile, the stresses will usually be confined to the active plug length, which is usually a few diameters from the base of the pile in sands, but much longer in clays.

See: Section 5.3.2.1, Case 1; Section 5.3.2.2, Case 30, Case 39; and Section 5.3.2.3, Case 40 & Case 48.

5.4.2.2. Constrained Modulus, *M*

In general, M has a direct influence on the total capacity of the pile and the stiffness of the response. Especially with the longer pile, as was the case with Euripides, the higher stiffness allows for a much

greater mobilisation of the base capacity. Although the preferred option is to derive M from soil testing, consolidation tests are not usually performed on sand to determine consolidation parameters (noting $M = 1/m_v$). The results from the study indicate that the Young's modulus, E, can be used as an estimate for M. The Author recommends care in using extremely high values of M as this can significantly increase the calculated value of $Q_{b,pl}$, as was found in the ICP-FEA and UWA-FEA. Using the ICP-FEA at the Euripides site, the use of $M = G_{ICP}$ or E_{ICP} gave acceptable results and at the Pigeon Creek site, using the UWA-FEA, the analysis performed using $M = E_{UWA}$ gave acceptable results.

Having observed the influence of the value of M on the overall results, the Author recommends that conservatively, M should be determined from the relationship by Lunne and Christophersen (1983).

See: Section 5.3.2.1, Case 28; Section 5.3.2.2, Case 37; and Section 5.3.2.3, Case 46.

5.4.2.3. Displacement to Mobilise τ_{int}, z_{peak}/D_i

At the Pigeon Creek and Kwangyang Plant sites, of the z_{peak}/D_i ratios considered, the stiffest ratio, of 0.0001, mobilised more of the base resistance of the soil plug. At the Euripides site, it was observed that this ratio allowed greater mobilisation of the internal shaft resistance, thereby enabling the creation of a rigid basal plug. In general, the use of a higher stiffness, such as 0.0001, is recommended when considering the z_{peak}/D_i component, as lower stiffnesses do not seem to replicate the measured behaviour.

See: Section 5.3.2.1, Case 24; Section 5.3.2.2, Case 32; and Section 5.3.2.3, Case 42.

5.4.3. Base Resistance

5.4.3.1. Resistance at pile base, $q_{b,p}$

The value of $q_{b,p}$ varies depending on the design method chosen.

Good estimates have been found when $q_{b,p}$ =0.7q_c was used in the ICP-FEA comparisons. This value was found to well predict the response at the Pigeon Creek and Kwangyang Plant sites, although marginally higher estimates were found at Euripides.

With the analyses using the UWA-FEA, the best matches were found when $q_{b,p} = 0.6q_c$ which was observed at the Pigeon Creek and Kwangyang Plant sites. A good match was also found at the Euripides site, however as only a single walled pile was used here, and due to the length of the pile, it is difficult to differentiate the distribution of load between the pile and plug.

As outlined in 5.4.1.1, as no further gain in capacity distribution is expected using the ICP method, the UWA-FEA method is analysed in more detail to explore whether improvements can be obtained. Therefore, using the UWA-FEA method, the end bearing resistance on the annulus, will be assumed to be $0.5q_{b,p}$.

See: Section 5.3.2.2, Case 31; and Section 5.3.2.3, Case 41.

5.4.3.2. Displacement to mobilise ultimate resistance of pile, $z_{b,p}/t$

A stiff annular base response will have a greater effect on the overall capacity if the D_o/t ratio is low. The value recommended of z/t, the displacement to mobilise the full annular resistance, is 0.1, as the use of this stiffness best replicated the observed behaviour at the three sites considered and using each of the finite element variants of the design methods in this study.

See: Section 5.3.2.1, Case 26; and Section 5.3.2.2, Case 35.

5.4.3.3. Stress-strain (constitutive) model of $q_{b,p}$

The Q-z relationship as per the API- RP 2GEO (2014), has been used in this exercise at the base of the annulus to represent the stress-strain relationship. The main variation has been the normalisation quantity, whereas API adopts the full base diameter, D_o, the wall thickness, t, was used to relate the stresses and strains in the mobilisation of annular resistance. It is therefore recommended to adopt the Q-z constitutive relationship from the API normalised by t instead of D_o, to fully mobilise $q_{b,p}$.

See: Section 5.3.2.1, Case 1, Case 26; Section 5.3.2.2, Case 30, Case 35; and Section 5.3.2.3, Case 40.

5.4.3.4. Resistance at plug base, $q_{b,pl}$

The value of $q_{b,pl}$ represents the ultimate resistance that can be transferred to the base of the plug. This quantity was found to vary between $0.1q_c$ to $0.3q_c$ as determined by Lehane *et al*. (2005); Salgado *et al*. (2002) and corroborated by this research exercise. The ICP method suggests that this value is $0.3q_c$ and when adopted into this work, in the ICP-FEA, this has been found to give results

that match the measured values at the Pigeon Creek and Kwangyang sites. This value however marginally overestimates the ultimate value and overall response at the Euripides site.

Using the UWA-FEA, when $q_{b,pl} = 0.3q_c$, the response at the Pigeon Creek site was underestimated, a good match was found at the Kwangyang site and an overestimated response was observed at the Euripides site. Using the default value of $q_{b,pl}$ from the UWA method at all three sites, this value was also underestimated.

Similar to the value adopted for $q_{b,p}$, with regards to the base of the plug, it is recommended that the end bearing resistance assume $0.5q_{b,pl}$, where $q_{b,pl}$ is the UWA's default approach. The intention is to obtain an improved overall distribution of capacity of OEPs in sands, to match or improve on the ICP method as in Table 5-3.

See: Section 5.3.2.2, Case 31; and Section 5.3.2.3, Case 41.

5.4.3.5. Displacement to mobilise ultimate resistance at base of plug, $z_{b,pl}/D_i$

Traditionally the displacement to mobilise the base of the plug has not been isolated from the base of the entire pile. In sands, an OEP with a low D_o/t ratio is susceptible of forming a rigid basal sand plug after a degree of relative displacement. In sands, OEPs with high D_o/t ratios will not form the internal arches necessary to confine the stresses near to the annulus, negating the formation of a rigid basal plug. In the analyses performed, the reduction in the stiffness at the base of the plug did not improve the comparison with the measured data but the opposite was observed at each of the three sites using each of the finite element design methods considered. The displacement to obtain the peak resistance of the soil plug, $q_{b,pl}$, is therefore recommended to be $0.1D_i$.

See: Section 5.3.2.1, Case 27; Section 5.3.2.2, Case 36; and Section 5.3.2.3, Case 45.

5.4.3.6. Stress-strain (constitutive) model of $q_{b,pl}$

Similar to that of the annulus, the Q-z relationship as per the API- RP 2GEO (2014), has been used in this exercise at the base of the plug to represent the stress-strain relationship. The main variation in this case is the normalisation quantity which adopts the internal pile diameter, D_i, to relate the stresses and strains. It is therefore recommended to adopt the Q-z constitutive relationship from the API normalised by D_i instead of D_o, to fully mobilise $q_{b,pl}$.

See: Section 5.3.2.1, Case 1 & Case 27; Section 5.3.2.2, Case 30 & Case 36; and Section 5.3.2.3, Case 40 & Case 45.

5.4.4. Miscellaneous

5.4.4.1. Pile and plug weights

In general, there is a negligible variation in the estimated load-displacement response when the pile and the plug weights are included in the analysis. Observable variations were in Case 29 using the API-FEA analyses, however this did not have a great effect on the overall load-displacement relationship. When using the ICP-FEA and UWA-FEA the effects were found to be quite small.

The weights of the pile and plug will continue to be included in the analyses even though their effects are minimal.

See: Section 5.3.2.1, Case 29; Section 5.3.2.2, Case 38; and Section 5.3.2.3, Case 47.

6. New FEA Method for OEPs

This chapter draws on the conclusions from Chapter 4 for clays and Chapter 5 for sands, to derive a new method of estimating the overall response of OEPs. From each of the cases presented, the variants that produced trends that better matched the measured responses are used to deduce the methodologies in clays and sands. In each of the following sections, the new finite element method is initially outlined and input parameters from each of the relevant case studies are applied to validate the method. As within the database, some of the test sites were comprised of sands and clays, applicable parameters are used at these sites to estimate the overall OEP response in a layered stratigraphy. This procedure is aimed at improving the estimate of the overall response with an improved base model implemented. An assessment of the performance of the new procedure is then done at the end of the clay and sand sections and compared to the results when only the direct capacity methods are used. This is not performed for the layered section as only a limited number of these sites are available. The new methods are then compared to an industry-based method using sands and clays, and some final considerations are provided on base capacity and the definition of plugging.

6.1. Base Capacity of OEPs in CLAYS

This section introduces the modified finite element method for OEPs in clay, aimed at improving the overall and base capacity response estimated.

In clays, there are a limited number of tests available to derive the base capacity. This is due to the believed low contribution of the base, to the overall capacity, and the cost of pile testing. In Chow (1997), 5 tests are quoted but this is then reduced to 3 tests in Jardine (2005), where reliable strain gauge data is available. From the detailed sensitivity study performed in Chapters 4 in clays, it was found that the mobilisation of the total end bearing in clays is dependent on several factors:

$$Q_b = f\left(L, L_{pl}, w_{b,p}, D_o, t, F_t, M, s_u, \delta_f, D_i\right) \tag{66}$$

Additional factors will depend on the input variables required in the API or ICP design method used. To best account for the combined effects of these factors under loading, a numerical approach is required.

6.1.1. Mobilisation of Annulus Capacity

The mobilisation of the full base capacity is generally considered to occur within a vertical displacement of $0.1D_o$. The resistance below the annulus has been found to have a much stiffer mobilisation than that of the plug (Paik *et al.*, 2003; Joseph *et al.*, 2017). The displacement required to fully mobilise the annulus has been investigated in Chapter 4 and found to better match the measured data at $0.1t$.

6.1.2. Mobilisation of Plug Capacity

The base capacity of the plug in an OEP in clay will be dominated by its undrained strength. With any increase in axial stress, due to an applied axial load, there cannot be an increase in the internal shaft friction without drainage, which will not readily occur. As loading continues, undrained behaviour suggests that the mean effective stress will remain constant, and as the plug capacity mobilises from the base, more of the plug length will become activated, presumably through the action of pore water pressure in the soil column. For a fully unplugged condition to occur, $L_a \geq L_{pl}$. Matsumoto *et al.* (1995) demonstrated the contribution of the soil plug by drilling out the plug within an OEP, testing the pile, and comparing the results to those of a matching pile with its plug intact. It was found that for different configurations of piles, this contribution varies. This suggests that if the full capacity of the plug can be achieved, the ultimate capacity of the pile will be larger than solely relying on the external shaft friction and end bearing on the annulus.

It can also be shown that the total stress, relative to depth, in a clay plug is:

$$\frac{d\sigma_v}{dz} = \gamma + \frac{4\alpha s_u}{D_i} \tag{67}$$

which does not lead to an exponential increase in base capacity when integrated over the length of the plug.

The full contribution of the base of the plug is assumed to occur after a relative displacement equal to approximately $0.1D_i$. For short piles, with low D/t ratios, the full ultimate shaft resistance is achieved quite rapidly, resulting in further loading being resisted by the base. The base resistance of the annulus is stiffer than that of the plug and would therefore become fully mobilised initially as

loading continued. Depending on the pile diameter however, after $0.1D_i$ of base displacement, the mobilised plug capacity would vary.

In terms of limits, as the internal shaft friction mobilises, the integral of the resistance over the length of the plug is limited to the bearing capacity of the soil at the plug's base. Therefore:

$$Q_{b,pl} = \int_0^{L_{pl}} \tau_{int} D_i \pi \, . \, dz \; \leq \; q_{b,pl} A_{pl} \tag{68}$$

which can be related to the API's method of assessing if plugging would occur. Depending on the pile configuration and plug length, if sufficient load is applied, the ultimate value of $\tau_{int} D_i \pi$ will be mobilised along the full extent of L_{pl}. If this occurs, the plug will behave in a fully unplugged manner. If only part of the plug becomes active, L_a, the plug behaves in a partially plugged manner.

In the double walled pile tests performed in clays, Doherty *et al.* (2010) found that during jacking installation, the load mobilised an active plug length of $3D_o$ which is longer than the typical $(1.0 \text{ to } 2.0)D_o$ observed in sands. This agrees with the results of this research project which has found that in clays, there is a smaller EB at the base of the plug, however more of the plug length is mobilised under axial load.

As discussed earlier in this work, the application of the load to the pile head causes compression of the steel pile and mobilises τ_{ext}, τ_{int} and $q_{b,p}$. For any discussion of the development of the base capacity, it is therefore also necessary to consider the efficiency of the load-transfer mechanisms. Due to the inherent difficulty in considering all these input parameters, a finite element method is recommended.

6.1.3. Modified API-FEA method for Clays

Based on the results of the finite element case study analysis, the recommendations are implemented in this section to improve the estimation of pile capacity. This is called the mod-API-FEA method which is derived using the recommendations listed in Section 4.4 with the intention of improving the estimation of overall pile head response and load distribution. However, as with all design methods, to ensure reliability, the method needs to be validated using more specific tests. Table 6-1 sets out the input parameters for the modified API-FEA design method.

Table 6-1 Input parameters for mod-API-FEA in clays.

Resistive Component	Resistance Input	Recommended Value
External Soil	τ_{ext}	API method (αs_u)
	$z_{p,e}/D_o$	0.01
	t-z reaction curves	API
Internal Soil	τ_{int}	τ_{ext}
	$z_{p,i}/D_i$	0.001
	M	(2000 - 4000) s_u
Annulus	$q_{b,p}$	$1.6q_c$
	$z_{b,p}/t$	0.1
	Q-z reaction curve	API
Plug Base	$q_{b,pl}$	$0.2q_c$
	$z_{b,pl}/D_i$	0.1
	Q-z reaction curve	API

Additional considerations and comments are stated below:

- **Softening $\delta_{ult}/\delta_{peak}$:**

  This ratio is to be determined from ring shear tests and applied as the reduction factor in the t-z soil reaction curves.

- **End Bearing Pile, $q_{b,p}$:**

  Earlier researchers found the end bearing of a pile in clay was approximately $9s_u$. However, the tests performed at some sites (such as Pentre) found that this was much higher, and it is thought reasonable to accept the current trend to relate the end bearing of the pile to the measured q_c values. The following is the recommended end bearing resistance from back analyses, consideration of the ICP method and the assumption that at the base of the annulus the soil will be drained.

  $$q_{b,p} = 1.6q_c \tag{69}$$

  Due to the limited data, this factor should later be fine-tuned to account for the ranges of over-consolidation ratios.

- **Constrained Modulus, M**

  M is more accurately deduced by $1/m_v$, which is the inverse of the coefficient of volumetric compressibility, a drained parameter. As the soil plug is undrained, $M \rightarrow \infty$. From the results

of the analysis performed in Chapter 4, the definition of M in Table 6-1 has proven adequate.

- **End Bearing Plug, $q_{b,pl}$:**

  The following expression is adopted as the resistance below the plug, selected as a lower bound derived from an interpretation of the results presented in previous chapters and on double-walled pile tests in clays (Doherty *et al.*, 2010):

$$\frac{q_{b,pl}}{q_c} = 0.20 \tag{70}$$

- **Pile and plug weights:**

  The weights of these components will be included, although they have a minor effect.

6.1.4. Validation

One of the main issues surrounding the mobilisation of the base capacity is the validation of the procedure. The measurements obtained from strain gauge data at the base of a pile is assumed to give the base resistance on the pile. This strain gauge however gives the measurements resulting from the interaction between the pile, the internal and external soil, and end bearing pressure on the annulus. In many of the test results where the base capacity of the plug is given, this capacity is derived from the compression of the base of the pile itself. In some tests the strain gauges at the base of the pile were damaged during installation (such as during the Pentre tests) therefore the strain gauge closest to the annulus was used. At times this location was several diameters above the pile base (such as with the Shanghai piles). Depending on this distance, the contribution of higher stresses from the compression of the internal plug may not have been accurately interpreted.

The true response of $q_{b,pl}$ can only be measured using an instrumented double walled pile system. This arrangement effectively isolates the internal and external shaft capacities. The annular load can be determined directly from the strain gauges at the base and the plug capacity is the integral of the internal shaft friction. This is an expensive procedure and tests are very limited, especially in clay soils. The Author recommends that more double walled pile tests are performed such as those at the Kinnegar test site.

The methodology determined from the analysis performed in Chapter 4 for the axial capacity of OEPs in clays, and outlined above, is applied here to each of the case studies using VIRTUPLUG.

The diagrams shown in the following sections are the comparisons of the estimated responses using the new methodology and the measured values. These show the estimated shear stress or pile load with depth, base response, load-displacement and overall load-transfer plots. In general, the solid lines represent the measured values and the dotted lines are those estimated, unless where specifically stated. Where no response data is available, the quoted value is shown on the diagram.

6.1.4.1. Kinnegar OE-3

At this site the double walled pile was used, however here the piles were installed and tested in a series of jacked intervals. Results were extracted from the instrumentation on the pile during jacking in 250mm push intervals. The pile however had a relatively small diameter of 168mm with a 2m test length. The results of this test have been included but due to the jacked-in nature of the pile and lack of a load-displacement response, the estimated capacity is not very reliable. Since there are no load-displacement responses available, capacities were estimated based on the strain gauge results at the end of each push increment. From these tests in clay, the end bearing resistance on the annulus ranged from (0.8 – 1.2)q_c, whereas at the base of the plug, the resistance was calculated to range between 0.2q_c and 0.8q_c. In addition, both τ_{ext} and τ_{int} achieved a common ultimate value as the pile embedment increased and τ_{ext} for the OEP, was smaller in the CEP of the same D_o.

The analysis results show that the total capacity was overestimated (Figure 6-1) with Q_c/Q_m=1.24. In the load-transfer diagram (Figure 6-2), the measured results show that there is compression at the base of the plug that propagates upwards. The compression occurs along the active plug length demonstrating that the end condition is not fully plugged. The proposed FE method is unable to accurately capture this trend as $q_{b,p}$ and $q_{b,pl}$ are very small. The method clearly overestimates the shaft friction, and this affects the total mobilised capacity along the pile. The method also estimates that there is a very small contribution from $Q_{b,pl}$, however this can be due to the assumptions adopted when extracting the measured data.

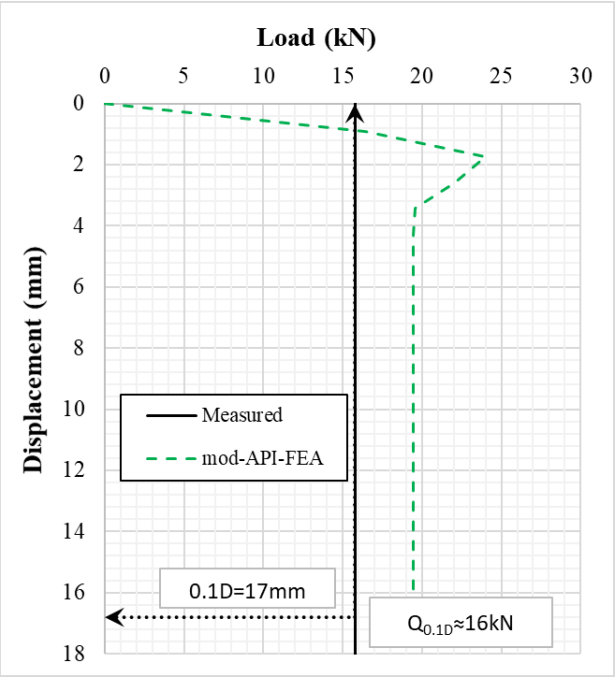

Figure 6-1 Load-displacement curve for mod-API-FEA estimation against measured.

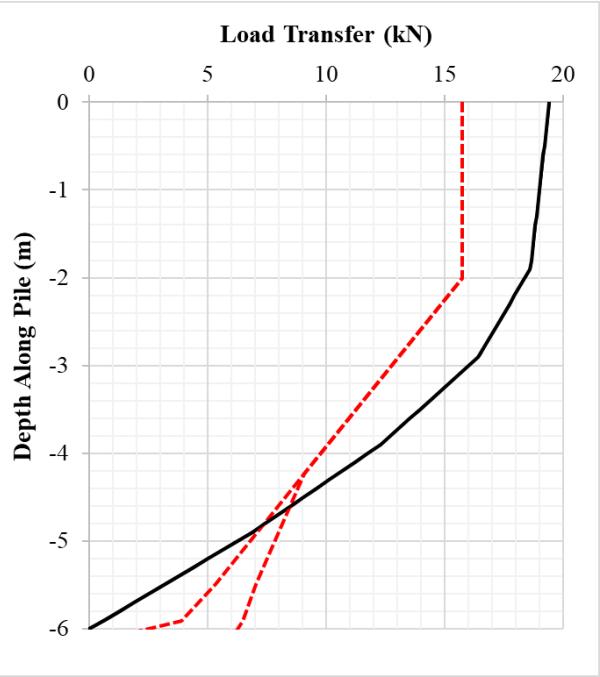

Figure 6-2 Load-transfer diagram for mod-API-FEA estimation at $w_t = 0.1D_o$. Dotted lines are measured values.

6.1.4.2. Pentre LDP

The analysis performed in Chapter 4 showed that the plates at the base of the internal channels did not seem to greatly affect the development of $q_{b,pl}$. In this analysis, using the mod-API-FEA, the plates are modelled to ensure robustness. This procedure however, does not seem to properly capture the base response (Figure 6-4) as Q_c/Q_m is 0.26. The load-displacement response, in Figure 6-5, however shows that the shaft resistance is very well matched, but a different peak capacity is obtained. As the base is underestimated and the shaft overestimated, the higher peak can be attributed to the sensitivity of the pile to the contribution of the shaft. This is credible here due to the length of the pile. Post-peak, q_b is correctly estimated to not contribute further capacity from the annulus nor plug base. The Q_c/Q_m here is 1.23.

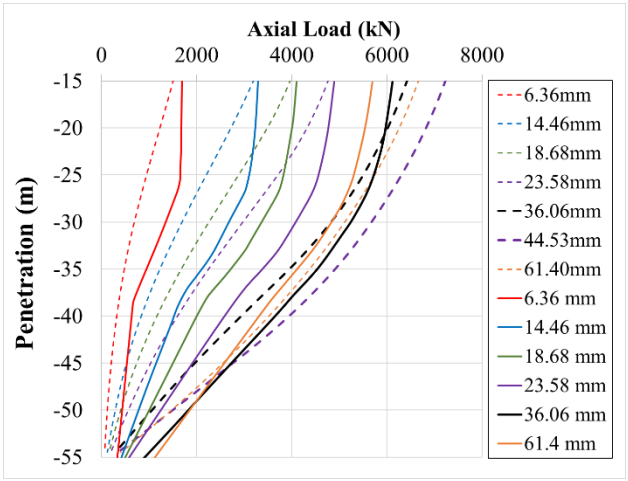

Figure 6-3 Axial load distribution in pile, mod-API-FEA estimation vs measured.

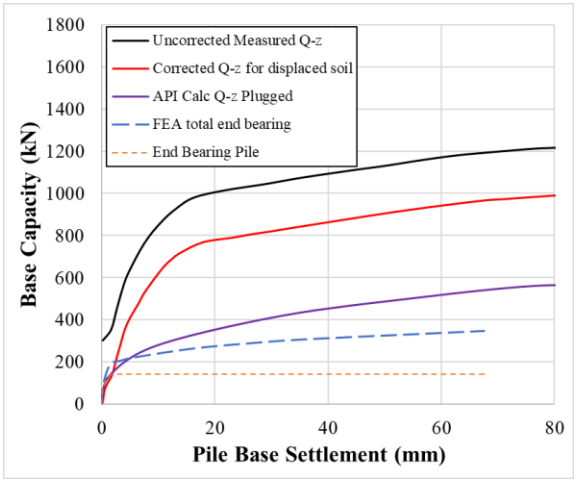

Figure 6-4 mod-API -FEA estimation of pile base settlement vs measured load.

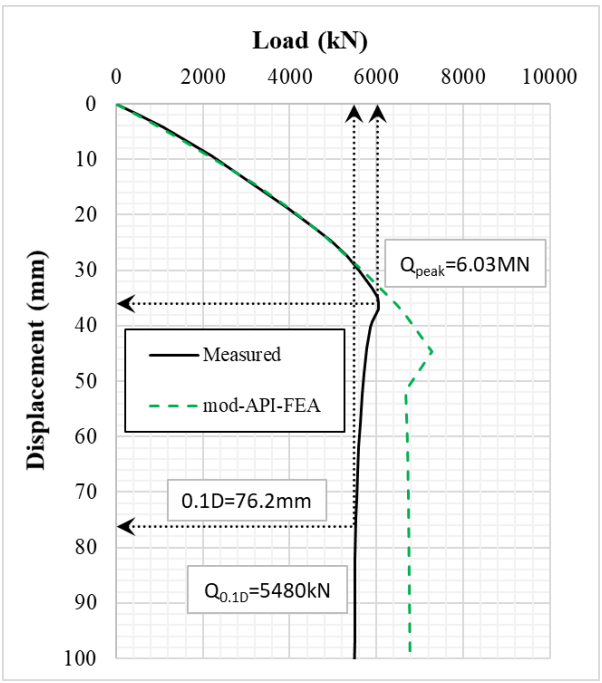

Figure 6-5 Load-displacement curve for mod-API -FEA estimation against measured.

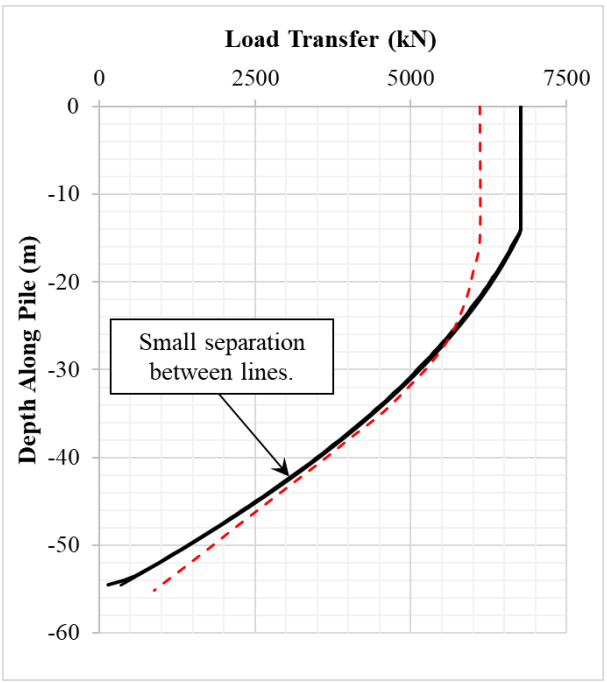

Figure 6-6 Estimated load-transfer diagram for mod-API -FEA estimation at w_t = 0.1D_o. Dotted lines are measured single-walled axial pile load.

The load-transfer plot also best combines these findings for this test. The Pentre piles were single-walled piles and therefore no accurate interpretation of $q_{b,pl}$ can be made. However, the comparison is, in general, quite good showing the capacity of shaft and end bearing at a pile head displacement of 0.1D_o. Here the end bearing on the pile and plug is estimated to be quite low and that the internal shaft is mobilised along most of the shaft implying an unplugged pile. This matches the suggestion that the capacity of the plug base is low and as the pile is loaded a clay plug will distribute the load along a larger active plug length as there is no exponential increase in radial plug stress near the base.

6.1.4.3. Tilbrook LDP

The mod-API-FEA method underestimates the shaft friction at this site. Due to the length of the pile, the overall capacity is sensitive to this underestimation. The development of the shaft resistance along the pile length is shown in Figure 6-7 and the axial load in the pile is shown in Figure 6-8.

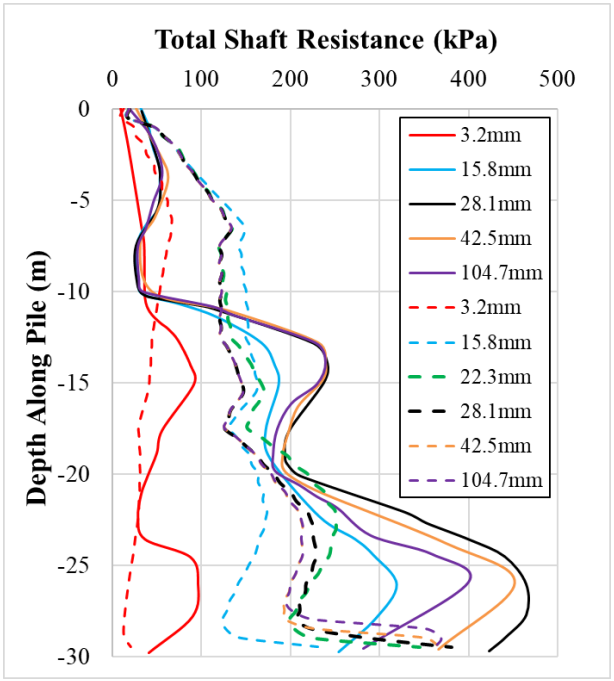

Figure 6-7 Total stress, mod-API-FEA estimation vs measured.

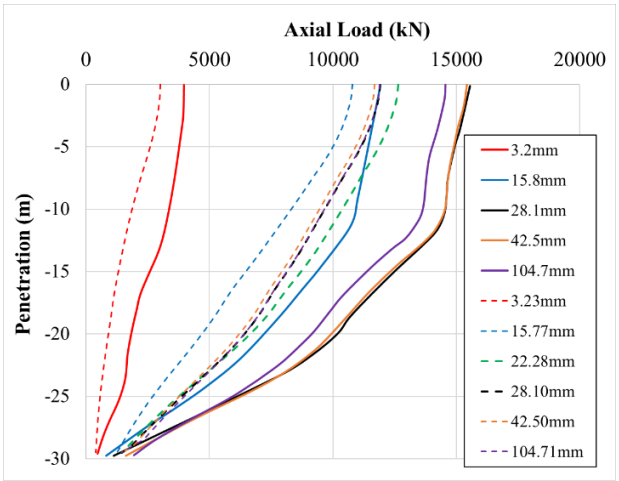

Figure 6-8 Axial load in pile, API-FEA estimation vs measured.

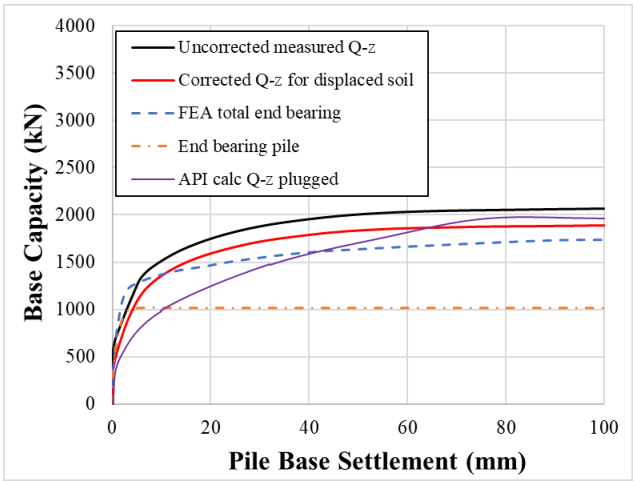

Figure 6-9 API-FEA estimation of pile base settlement vs measured load.

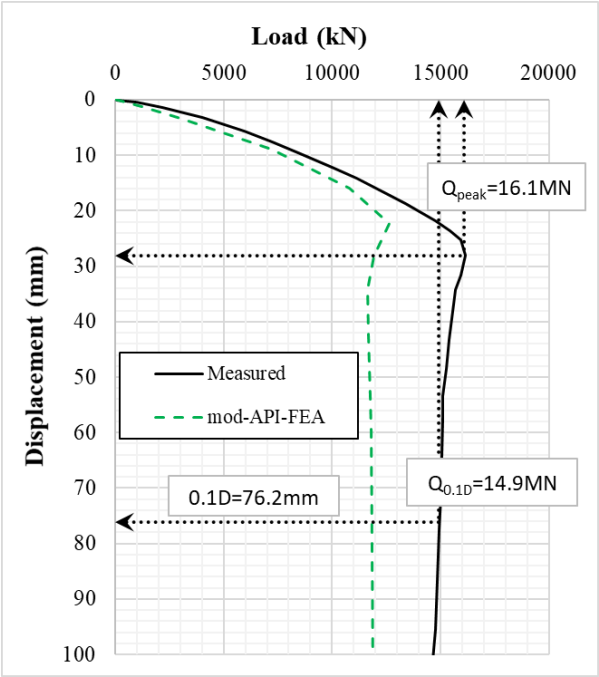

Figure 6-10 Load-displacement curve for mod-API-FEA estimation against measured.

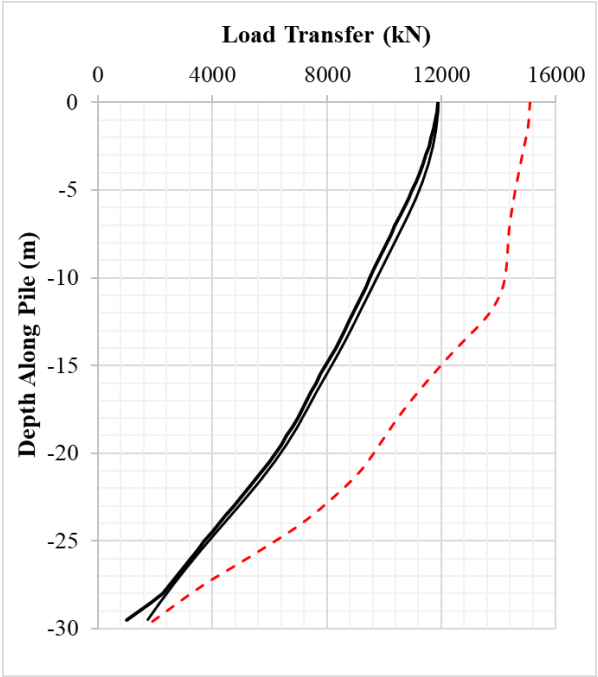

Figure 6-11 Load-transfer diagram for mod-API-FEA estimation at $w_t = 0.1D_o$. Dotted lines are measured single-walled axial pile load.

In terms of end bearing, the mod-API-FEA shows a good match at this site. Figure 6-9 shows the end bearing data and here, a good comparison of the mobilised, and estimated total base response is observed with Q_c/Q_m = 0.89. This is a better match than that observed at Pentre, the main difference between these sites being the over-consolidated nature of the clays, of which Tilbrook is the higher. Both end bearings were estimated by the equivalent factor on q_c, which suggests that possibly additional factors, unaccounted for, are contributing to this difference in capacity.

The load-displacement response (Figure 6-10) shows the effect of the underestimated shaft, with essentially a softer initial stiffness and lower achieved peak. Here the Q_c/Q_m ratio is 0.80. The load-transfer plot further expands this result and effectively demonstrates the effect of the underestimated shaft (Figure 6-11). The plot also shows that most of the capacity has been gained from the shaft, even though the shaft friction has been underestimated. The axial load in the pile is also shown in the diagram, and although from a single walled pile test, the method seems to have accurately computed the load-transfer at the base. Also, the method estimates that the full plug length is mobilised, due to the small separation of the internal and external load along the pile, suggesting a fully unplugged base condition.

6.1.4.4. Noetsu Bridge T1

In these tests, there was a peak load capacity observed but this was not as distinct as usually observed in OEPs tested in clay stratigraphies. This could have been due to the loading and unloading of the pile, preventing the pile from attaining its peak capacity. In addition, the pile was also relatively short, although L/D_o >10, and both τ_{ult} and q_b were underestimated by the mod-API-FEA method. Figure 6-12 shows that the developed axial load in the pile is not well predicted due to this underestimation. No base response was available for this site however, a base capacity of 500kN was suggested to occur at peak load. When the measured total base capacity is compared to the estimated response, the Q_c/Q_m ratio is 0.84 (Figure 6-13). The soil here is described as soft clay, which if taken as a normally consolidated material, would be similar to the Pentre pile, as the end bearing is underestimated. The underestimation of both components has a clear effect on the overall capacity. This is observed in Figure 6-14, where the loading cycles are also included in the response for comparison. The Q_c/Q_m ratio here is 0.63. The load-transfer diagram summarises these findings (Figure 6-15) but also shows the mobilisation of the full plug suggesting an unplugged pile. The axial load in the single pile is again overlaid in this diagram and the extent of the underestimation of the pile capacity is clearly observed.

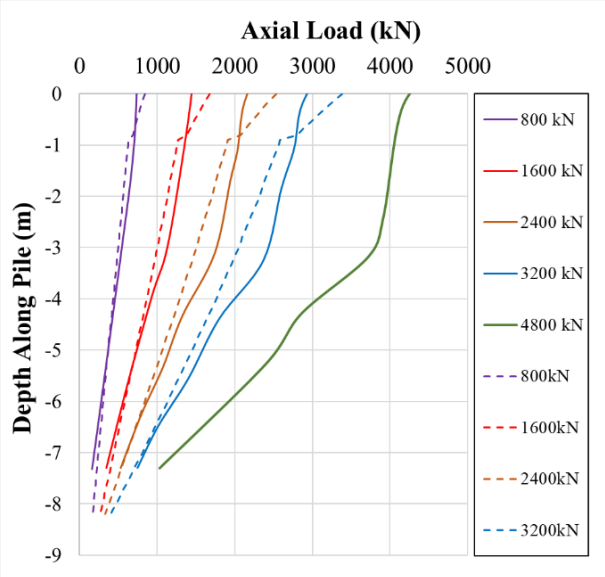

Figure 6-12 Axial load in pile, mod-API-FEA estimation vs measured.

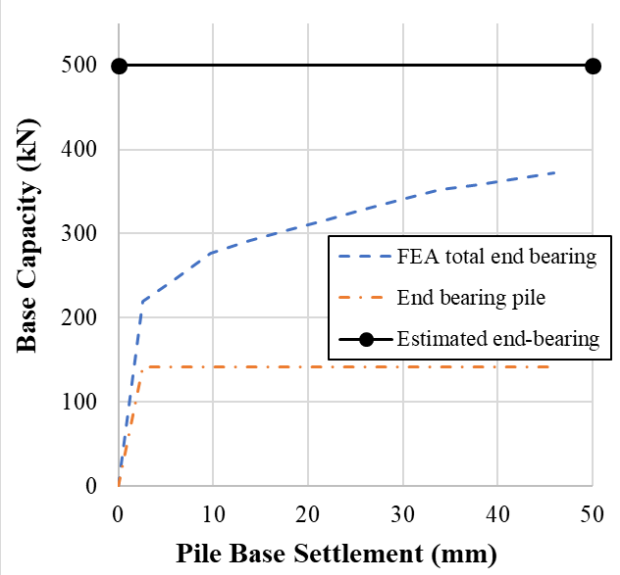

Figure 6-13 mod-API-FEA estimation of pile base settlement vs measured load.

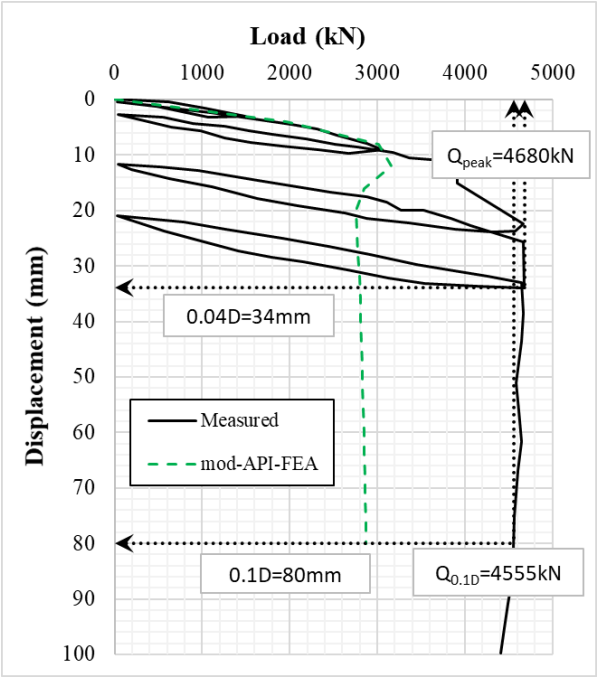

Figure 6-14 Load-displacement curve for mod-API-FEA estimation against measured.

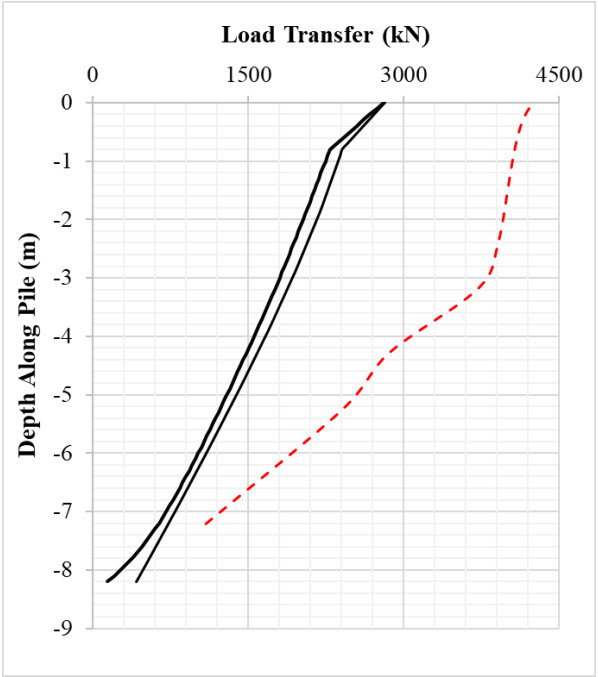

Figure 6-15 Load-transfer diagram for mod-API-FEA estimation at $w_t = 0.1D_o$. Dotted lines are measured single-walled axial pile load.

At this site, two piles were tested. Pile T1 was tested under conditions of loading and unloading to a pile head displacement of approximately 200mm. Pile T2 had quite similar dimensions, embedment depths and driving records, however the internal plug was removed to 0.5m below the base prior to testing. A separate assessment was performed on pile T2 and the results compared.

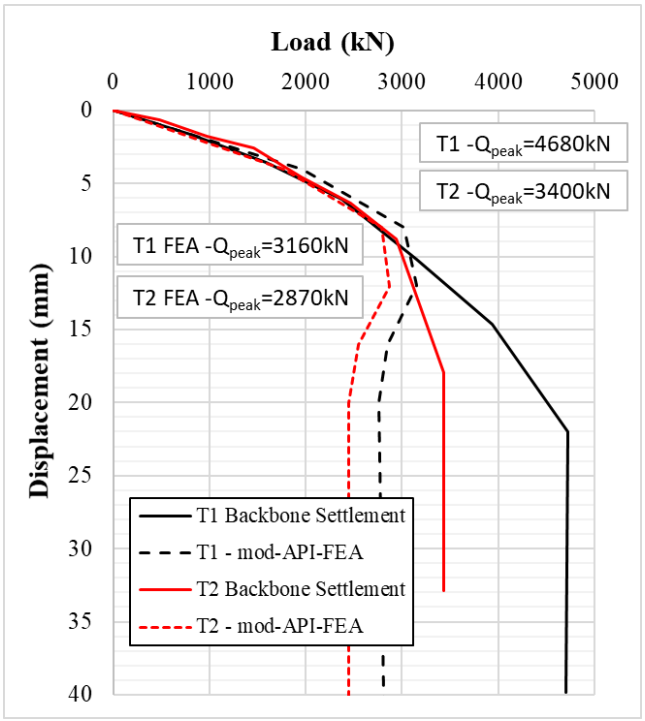

Figure 6-16 Load-displacement curve for the mod-API-FEA estimation against measured, comparing results from T1 and T2 backbone curves.

In the test results from pile T2, there was also no clear peak load observed. Figure 6-16 shows the backbone curve of the load-displacement response and the difference between the two responses (solid black and red lines) can be considered as the total end bearing contribution from the pile and plug. The difference between the peak capacities was measured as 1280kN. This capacity is not necessarily the end bearing however as the method of drilling out the plug was not specified. Depending on this method,

significant pile disturbance would occur which affects τ_{ext}. The diagram shows that the measured initial slopes are quite similar, indicating that the external shaft friction provided the initial resistance followed by gradual mobilisation of the base. From these results, the accuracy of the suggested 500kN as the measured base capacity is highly doubtful. This may only be the load measured in the pile, with the additional capacity supported by the plug. The mod-API-FEA method estimates the initial slopes quite well but the later response is not adequately captured. With no base resistance included in the analysis using the T2 pile parameters, the difference in total capacity estimated is equivalent to the base contribution, which is much lower than that measured. There is also quite a large difference in the offsets of total capacity of T1 and T2, between the estimated and measured.

6.1.4.5. Kansai Bridge T1

Although this is a layered site containing both sands and clays, with the base of the pile founded in sand, this site is predominantly clay and is therefore classified as a clay site. The layers of sand are treated as providing limited axial capacity.

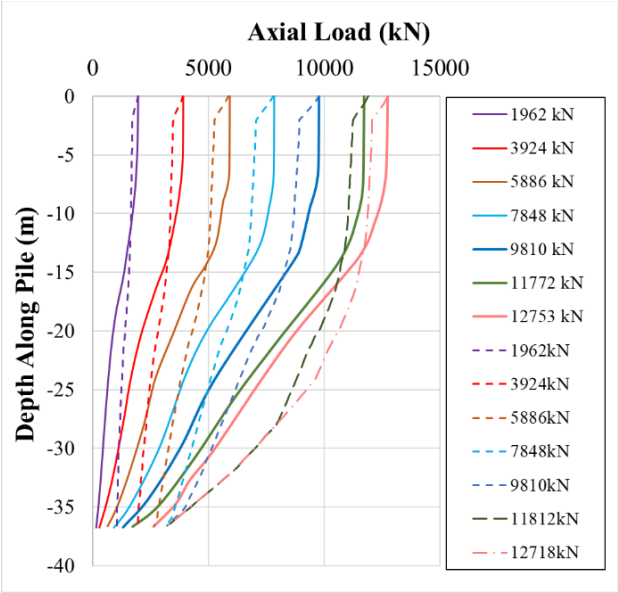

Figure 6-17 Axial load in pile, mod-API-FEA estimation vs measured.

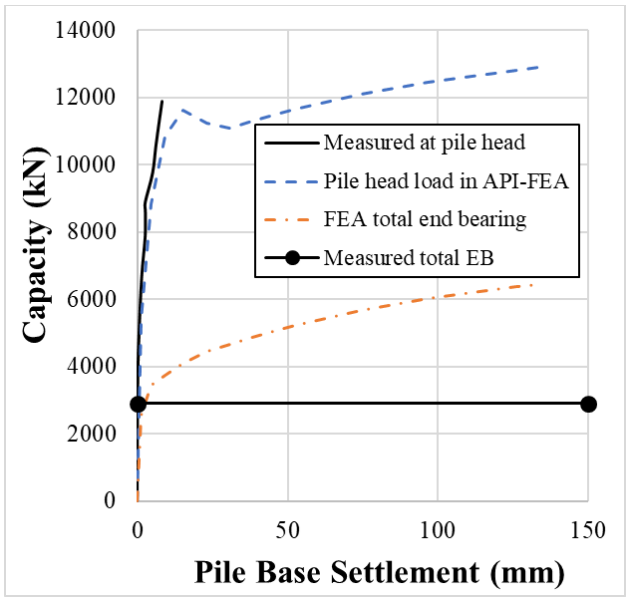

Figure 6-18 mod-API-FEA estimation of pile base settlement vs measured load.

The axial load estimated in the pile (Figure 6-17) is shown to compare well with the measured data using the mod-API-FEA. However, the estimated values show considerably less capacity than measured in the sand layers, suggesting that more capacity is actually provided by these layers than actually considered. The pile head load relative to the base displacement was provided for this site

and shown to be a good match (Figure 6-18). In addition, the overall base capacity was provided as 2900kN, which is indicated in the figure, although no response was provided.

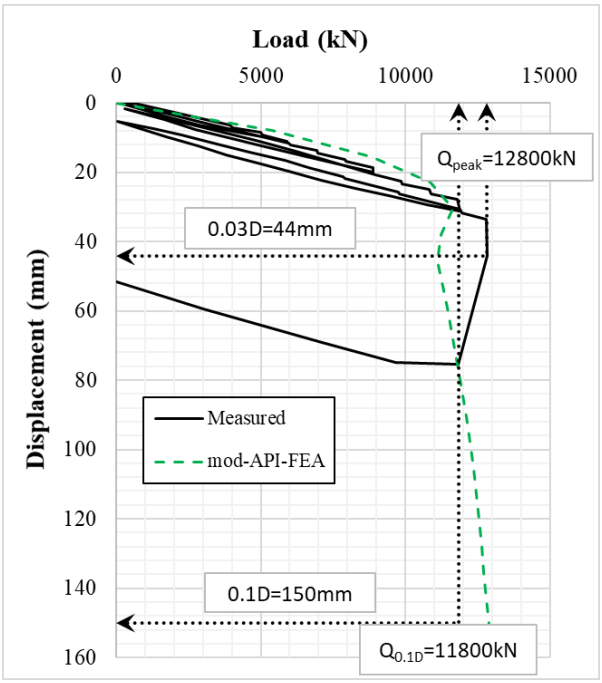

Figure 6-19 Load-displacement curve for mod-API-FEA estimation against measured.

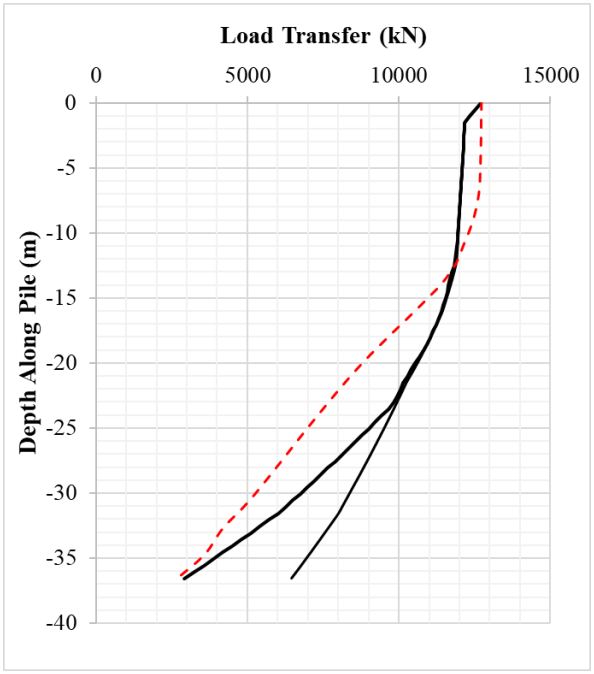

Figure 6-20 Load-transfer diagram for mod-API-FEA estimation at $w_t = 0.1D_o$.

Figure 6-19 shows the load-displacement response and the Q_c/Q_m ratio here is 1.09. Figure 6-20 shows the comparison of the estimated load transfer plot and measured axial load in the pile. The development of the load along the pile is not well captured here and can potentially be due to the provision of additional axial capacity from the sand layers, which were modelled to provide limited capacity contribution in this analysis.

6.1.4.6. Empire Tests

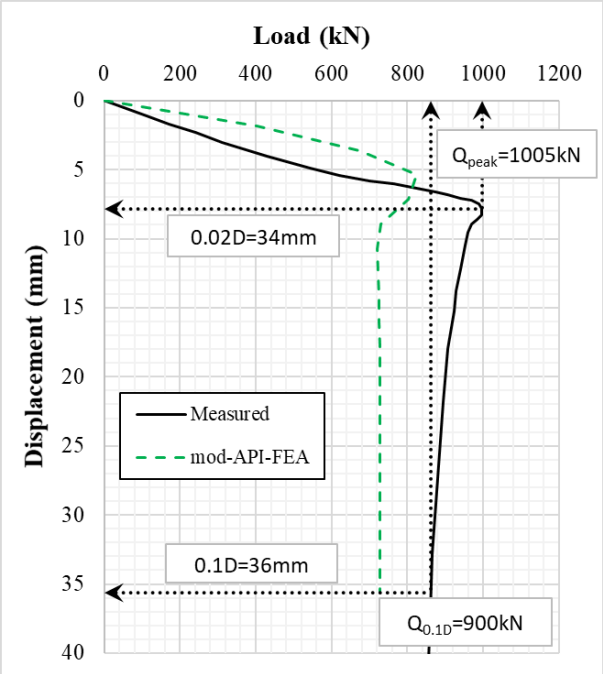

Figure 6-21 Load-displacement curve for mod-API-FEA estimation against measured for Empire 1.

At the Empire site there were four pile tests performed. The results of these tests were compared with the load-displacement estimates using the mod-API-FEA method. As all the comparisons gave quite similar results, only the analysis results from the pile test at Empire 1 is provided in Figure 6-21. The Q_c/Q_m ratios and responses for all the Empire sites are quite uniform ranging from 0.67 to 0.81.

6.1.4.7. Kontich Tests

The values of M adopted in these tests was $4000s_u$, which allowed the mobilisation of capacity to $w_t = 0.1D_o$. This value of M is considered appropriate to match the measured stiffness profile.

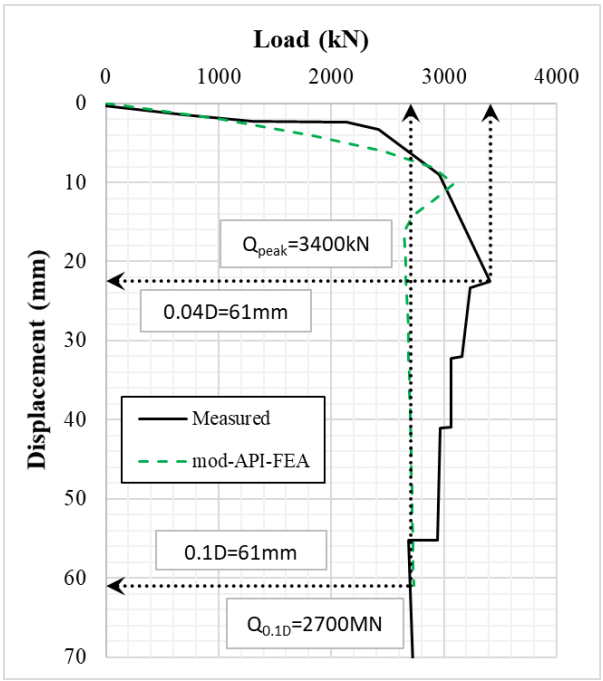

Figure 6-22 Load-displacement curve for mod-API-FEA estimation against measured for Kontich 1.

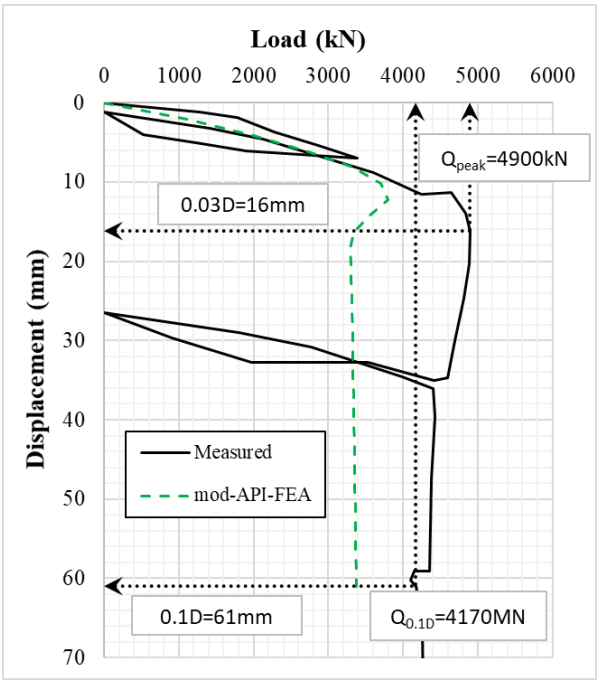

Figure 6-23 Load-displacement curve for mod-API-FEA estimation against measured for Kontich 2.

Figure 6-22 and Figure 6-23 show the comparison between the estimated and measured load-displacement response for Kontich tests 1 & 2, with Q_c/Q_m ratios of 1.01 and 0.81, respectively.

6.1.4.8. West Sole B Tests

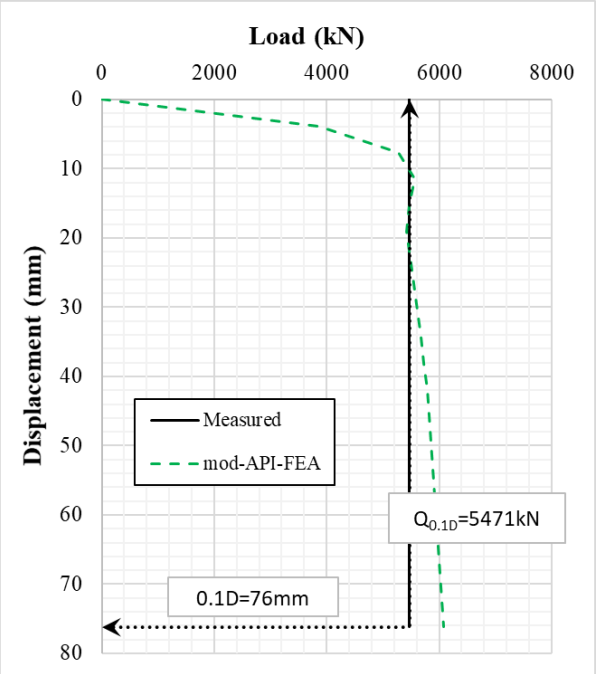

Figure 6-24 Load-displacement curve for mod-API-FEA estimation against measured for West Sole 2 – B9.

In the West Sole conductor pile tests, no load-displacement responses were found in the literature; however, the ultimate compressive capacities were provided and used in the comparisons. Due to the similarity of the results, only one representative pile test analysis, B9, is shown. Figure 6-24 shows the comparison of the load-displacement response for this test. The Q_c/Q_m ratios for the "B" series tests (1 to 5) ranged from 0.64 to 1.11.

6.1.4.9. West Sole A Tests

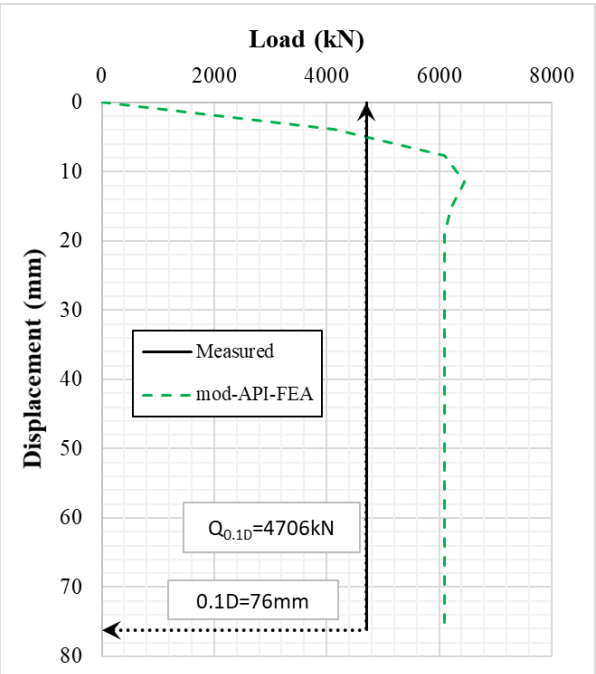

Figure 6-25 Load-displacement curve for mod-API-FEA estimation against measured for West Sole 7 – A9.

The West Sole "A" series tests are those performed on a conductor pile with a driving shoe. Again, at this location, only one representative site is selected due to the similarity of the analysis results. Figure 6-25 shows the load-displacement response for the West Sole pile, Test A9. The Q_c/Q_m ratios for all the "A" series tests (6 to 10) ranged from 0.75 to 1.29.

6.1.5. Summary Table – Clays

This section summarises the analysis results for the test cases previously discussed for OEPs in clays. Table 6-2 summarises the results of the analysis performed using the mod-API-FEA method and provides the measured data for each site for comparison. The Q_c/Q_m ratios from this table are also shown in Figure 6-26 to Figure 6-28, for the total, shaft and base capacities, where these are compared to those values estimated using the API method directly. It is observed here that, in general, there is a reduction of the total estimated capacity when the results from the mod-API-FEA method are compared to the API method directly. There are also slight variations observed in the comparisons of the Q_c/Q_m ratios for the shaft and base capacities.

A summary of statistical values is shown in Table 6-3. Here it shows that, in general, the static spreadsheet-based calculation of the API method estimates the overall capacity and distribution of capacity between the shaft and base well. The mean value of total capacity estimated by the mod-API-FEA is lower than that of the API method. However, this is directly related to the consideration of the reduced shaft resistance under loading. The mod-API-FEA includes the reduction to the residual shaft friction, determined by $\tan \delta_{ult} / \tan \delta_{peak}$, whereas the direct API method does not. The mod-API-FEA also includes the explicit modelling of the soil plug mobilisation in the analysis. The value of μ is therefore lower but more representative of the actual expected behaviour, if all database site tests are considered.

The values obtained by the mod-API-FEA also provides the non-linear load-displacement response to the user, which is not estimated by the API capacity calculation directly.

Table 6-2 Comparison of measured capacities and values derived from the modified API-FEA approach.

Site Number	Site	D (m)	D/t	L/D	Measured			mod-API-FEA					
					Total Capacity (kN)	Total Shaft Friction (kN)	Total End Bearing (kN)	Total Capacity (kN)	Total Shaft Friction (kN)	Total End Bearing (kN)	Q_c/Q_m Total Capacity	Q_c/Q_m Total Shaft Friction	Q_c/Q_m Total End Bearing
1	Kinnegar	0.168	18.7	36.3	16	10	6	19	19	0.00	1.24	2.00	0.00
2	Pentre - LDP	0.762	50.8	72.2	5480	4268	1212	6735	6420	315	1.23	1.50	0.26
3	Tilbrook - LDP	0.762	25.4	39.4	14900	12985	1915	11865	10163	1702	0.80	0.78	0.89
4	Noetsu Bridge	0.800	66.1	10.4	4555	4055	500	2872	2453	419	0.63	0.60	0.84
5	Kansai Bridge	1.500	68.2	24.7	11800	8900	2900	12882	6435	6446	1.09	0.72	2.22
6	Empire 1*	0.356	29.7	42.7	900	650	250	729	661	68	0.81	1.02	0.27
7	Empire 2	0.356	29.7	42.7	1731	941	790	1178	1067	111	0.68	1.13	0.14
8	Empire 3	0.356	29.7	34.3	1839	1089	750	1234	1084	149	0.67	1.00	0.20
9	Empire 4	0.356	29.7	34.3	2125	995	1130	1453	1269	184	0.68	1.28	0.16
10	Kontich 1	0.610	24.0	33.0	2700	1740	960	2730	2226	505	1.01	1.28	0.53
11	Kontich 2	0.610	24.0	38.5	4170	3430	740	3374	504	2870	0.81	0.15	3.88
12	West Sole 1	0.762	24.0	7.9	3051	1726	1325	2601	1094	1507	0.85	0.63	1.14
13	West Sole 2*	0.762	24.0	11.8	5471	2642	2829	6079	1876	4203	1.11	0.71	1.49
14	West Sole 3	0.762	24.0	15.7	6681	4457	2224	4287	2872	1415	0.64	0.64	0.64
15	West Sole 4	0.762	24.0	19.7	6788	4510	2278	5020	3917	1102	0.74	0.87	0.48
16	West Sole 5	0.762	24.0	23.6	8344	6023	2321	7025	4960	2066	0.84	0.82	0.89
17	West Sole 6	0.762	24.0	7.9	3051	2438	613	2569	1098	1470	0.84	0.45	2.40
18	West Sole 7*	0.762	24.0	11.8	4706	2873	1833	6094	1876	4218	1.29	0.65	2.30
19	West Sole 8	0.762	24.0	15.7	5533	4466	1067	4334	2872	1462	0.78	0.64	1.37
20	West Sole 9	0.762	24.0	19.7	6619	5240	1379	4955	3916	1039	0.75	0.75	0.75
21	West Sole 10	0.762	24.0	23.6	8344	6734	1610	6912	4959	1953	0.83	0.74	1.21

* pile test which most represents site.

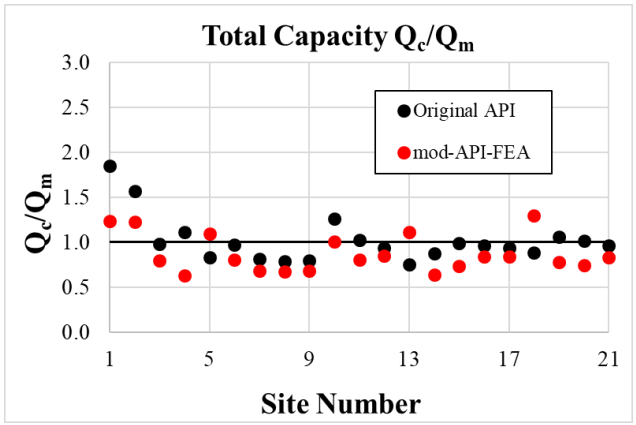

Figure 6-26 Comparison of the Q_c/Q_m of the total capacity using the original API and mod-API design method.

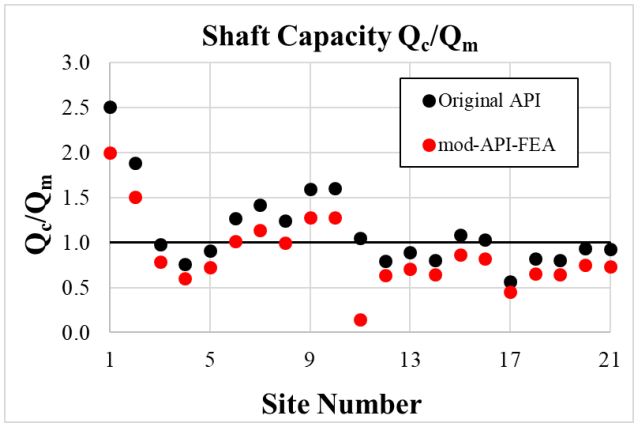

Figure 6-27 Comparison of the Q_c/Q_m of the shaft capacity using the original API and mod-API-FEA design method.

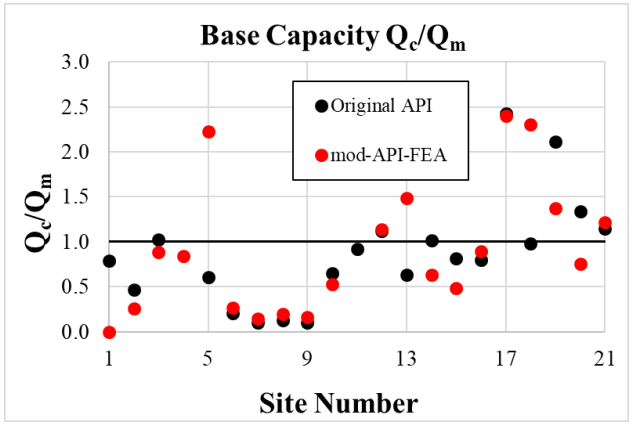

Figure 6-28 Comparison of the Q_c/Q_m of the base capacity using the original API and mod-API-FEA design method.

Table 6-3 Mean and standard deviation of Q_c/Q_m using the OEP validation database for clays using mod-API-FEA method.

Statistic	API			mod-API-FEA		
	Total Force Estimated	Shaft Friction	Total End Bearing	Total Force Estimated	Shaft Friction	Total End Bearing
μ	1.020	1.136	1.020	0.873	0.875	1.050
σ	0.261	0.453	0.910	0.201	0.389	0.944
COV	0.256	0.399	0.892	0.230	0.445	0.899

6.2. Base Capacity of OEPs in SANDS

This section introduces the modified finite element method for OEPs in sands, aimed at improving the overall and base capacity response estimated.

In sands, the base capacity is dominated by a combination of the resistance below the annulus and shearing induced dilation within the plug. In sands, there are also much more tests that focus on the end bearing capacity, and as previously shown there are four tests in the database in which large scale double-walled piles are used. From the detailed sensitivity study performed in Chapter 5, the influences on the base capacity need to consider a number of factors:

$$Q_b = f\left(L, L_{pl}, w_{b,p}, D_o, t, F_t, M, \delta_{cv}, \sigma'_{v0}, K_0, D_i\right) \quad (71)$$

Additional parameters are also required depending on the design method selected and the combination of these factors, to determine the base contribution to capacity, is best achieved using a numerical method.

6.2.1. Mobilisation of Annulus Capacity

Similar to the argument outlined for clays, the compaction of the soil at the base of the annulus of driven OEPs will be high. The stiffness of $q_{b,p}$ will therefore be greater than the stiffness of $q_{b,pl}$. The analysis performed in Chapter 5 suggests that in sands, $q_{b,p}$ will occur at an annular displacement of $0.1t$. This is also further corroborated by Paik *et al*. (2003) and Joseph *et al*. (2017).

6.2.2. Mobilisation of Plug Capacity

To facilitate the formation of a sand plug, there is a need of an overburdened pressure, the amount of which is dependent on the configuration of the pile and soil properties. This was also determined by Kishida & Isemoto (1977) who suggested that the inactive plug length ($L_{pl} - L_a$) in a sandy plug is less compacted but the presence of which is crucial to active plug formation. The length of soil plug needed to form a rigid basal plug varies depending on the properties of the pile-soil-plug arrangement which can range from $1.0D_o$ to $3.0D_o$. It can be shown that the effective stress, relative to depth, in the soil plug is:

$$\frac{d\sigma'_v}{dz} = \gamma' + \frac{4(\sigma'_v K \tan\delta)}{D_i} \quad (72)$$

which when integrated over the length of the plug leads to an exponential increase in σ'_v at the base. This phenomenon occurs in sand due to its frictional properties. The action of the sand grains increases the radial stress at the base of the plug, which is compounded by the overburden stress from the column of sand above this level. This is similar to the "reverse silo effect". In the "silo effect" the assumption is that in a silo, the stress between the grains and the sides of a silo becomes constant with depth. In the reverse silo effect the opposite occurs. As the grains are being pushed upwards the stress increases exponentially, essentially locking in the soil and forming a stiff plug. In general, the larger the plug length the greater the radial stress in the plug.

The behaviour of a soil plug comprised mainly of sand and subjected to an axial stress is different to that of a soil plug comprised mainly of clay. In an offshore environment, the pile is installed through water, the pore water pressure will not change dramatically during loading as the drainage path is relatively long. Therefore, for both sands and clays, undrained/partially drained behaviour should be considered to occur.

Similar to clays, the behaviour of OEPs in sands is quite complex and a finite element or other numerical method is recommended to simultaneously account for the various influences on their engineering behaviour.

6.2.3. Modified UWA-FEA method in Sands

The following sections outline the new modified methodology in sands, recommended to improve the estimation of the distribution of capacity to the external shaft and end bearing components in OEPs, in sands. This is based on the recommendations summarised in Section 5.4. Table 6-4 sets out the input parameters for the modified UWA-FEA design method.

Table 6-4 Input parameters for mod-UWA-FEA in sands.

Resistive Component	Resistance Input	Recommended Value
External Soil	τ_{ext}	$\tau_f = \left(\frac{f}{f_c}(2\sigma'_{rc} + \Delta\sigma'_{rd})\right)\tan\delta_{cv}$
	$z_{p,e}/D_o$	0.01
	t-z reaction curves	API
Internal Soil	τ_{int}	τ_{ext}
	$z_{p,i}/D_i$	0.001
	M	Lunne & Christophersen (1983)
Annulus	$q_{b,p}$	$0.50q_c(0.15 + 0.45{A_{rb}}^*)$
	$z_{b,p}/t$	0.1
	Q-z reaction curve	API
Plug Base	$q_{b,pl}$	$0.50q_c(0.15 + 0.45{A_{rb}}^*)$
	$z_{b,pl}/D_i$	0.1
	Q-z reaction curve	API

Additional considerations include:

- **External Shaft Resistance, τ_{ext}**

  The existing relationships to estimate τ_{ext} were outlined in Chapter 2.6. From the RMS-error assessment performed in Chapter 5 using the database results, the shaft friction was underestimated by a factor of 2.0. If this factor was applied to σ'_{rc}, effectively doubling the radial effective stress, in Equation (73), this converts the expression to:

$$\sigma'_{rc} = 0.06\, q_c\, (\sigma'_{v0}/P_a)^{0.13}\, (h/R)^{-0.38} \tag{73}$$

  This new ultimate shaft resistance should now improve the comparison with the measured shaft resistances.

- **Constrained Modulus, M**

  M is determined from the relationship by Lunne and Christophersen (1983), unless measured directly in sample testing.

- **End Bearing, q_b**

  The relationships that are currently used to compute the end bearing resistance are as follows:

$$\frac{q_b}{q_c} = 0.15 + 0.45{A_{rb}}^* \tag{74}$$

$${A_{rb}}^* = 1 - FFR\left(\frac{{D_i}^2}{{D_o}^2}\right) \tag{75}$$

$$FFR \approx \min\left[1, \left(\frac{D_i}{1.5}\right)^{0.2}\right] \quad (76)$$

From the RMS-error assessment performed in Chapter 5, the contribution of the base to the estimated capacities in the database, showed an overestimation by a factor of 2.0. If 0.50 was applied to Equation (74), this gives:

$$\frac{q_b}{q_c} = 0.50(0.15 + 0.45{A_{rb}}^*) \quad (77)$$

Using this adjustment, the slope as outlined in the Lehane *et al*. (2005) can be adapted as per the expression in Equation (77) and the new line can be drawn as shown in Figure 6-29.

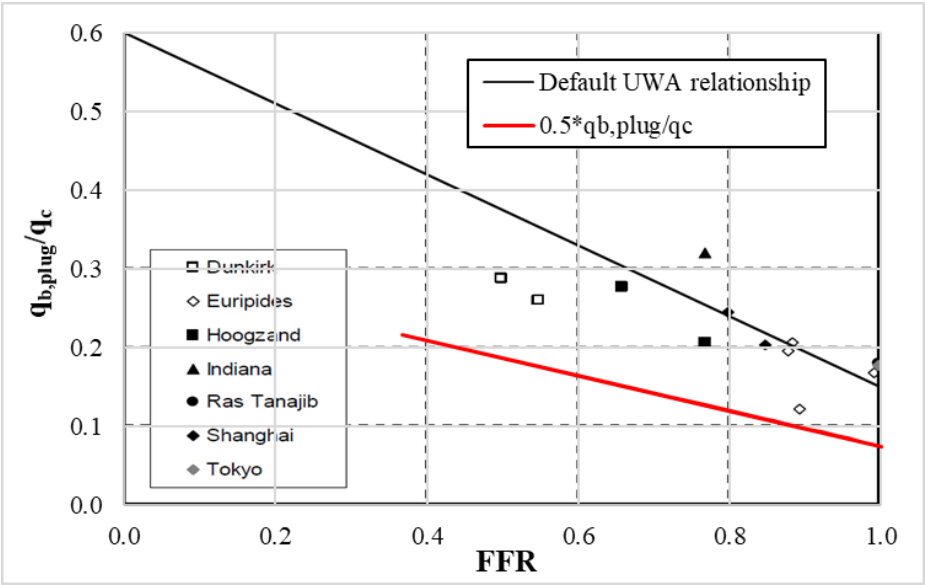

Figure 6-29 Ratio of q_{plug} to the averaged q_c value versus FFR, plus a factored version (Adapted from Lehane *et al*., 2005).

q_b is applied as the same resistance over the base of $q_{b,p}$ and $q_{b,pl}$.

- **Pile and plug weights**

  The weights of these components will be included, although they have been shown to have no real influence on the results.

6.2.4. Validation

Each of the test sites identified in Chapter 5 is now analysed using the principles outlined above and the estimated response using the new UWA-FEA method is shown. Where available, the response is compared with measured data at each site. These were performed using both the displacement or force-controlled methods where applicable in VIRTUPLUG.

Where the required data is available, solid lines represent the measured values and the dotted lines are those estimated, unless specified otherwise. A summary of the variation of the Q_c/Q_m values for total capacity is presented at the end of the validation assessments in Table 6-5.

6.2.4.1. Pigeon creek

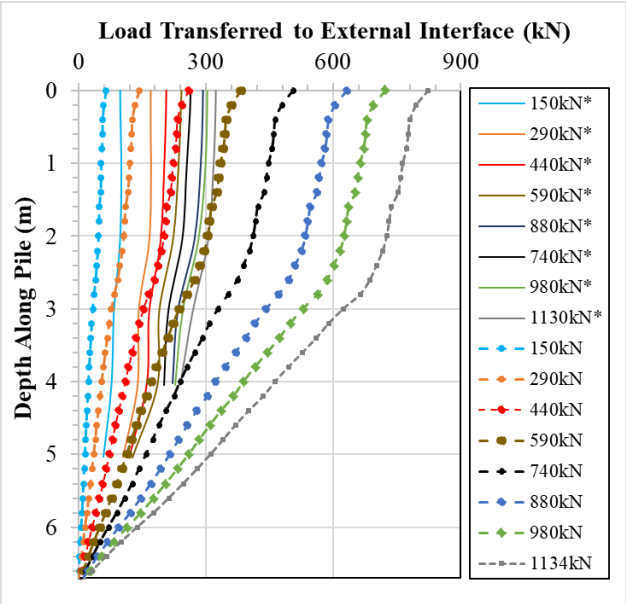

Figure 6-30 Axial load distribution in pile, UWA-FEA estimation vs measured.

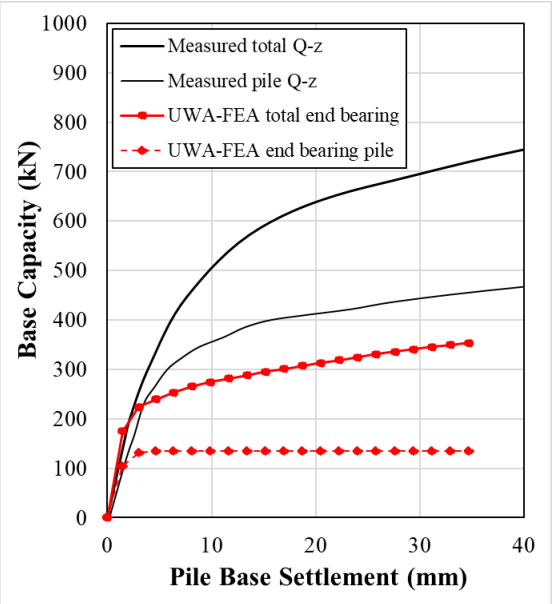

Figure 6-31 UWA-FEA estimation of pile base settlement vs measured load.

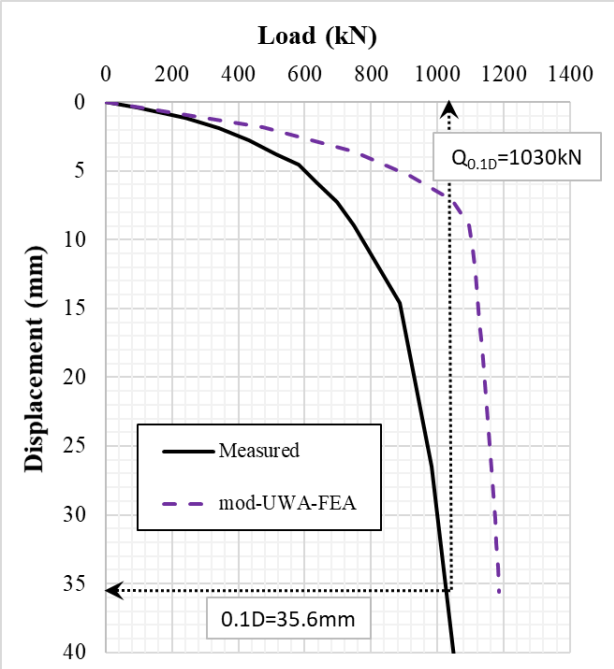

Figure 6-32 Load-displacement curve for UWA-FEA estimation against measured.

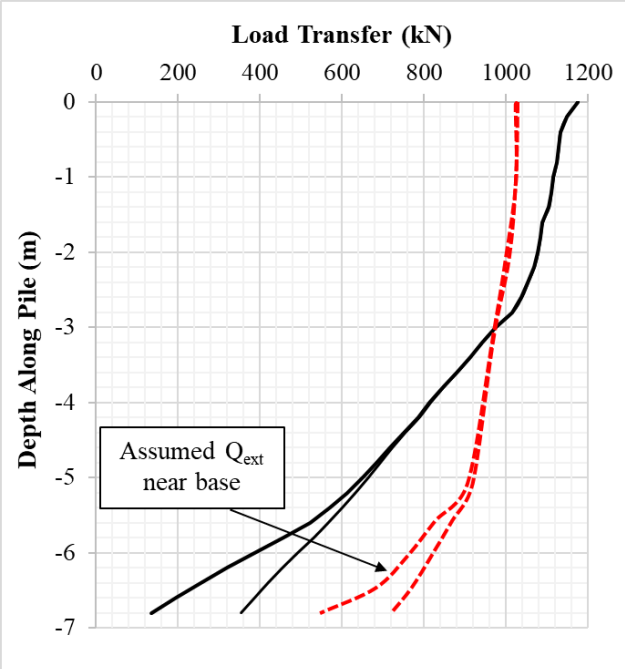

Figure 6-33 Load-transfer diagram for UWA-FEA estimation at $w_t = 0.1D_o$. Dotted lines represent measured values.

From the results, the mod-UWA-FEA method is shown to overestimate the axial load transferred to the external pile, Q_{ext}, shown in Figure 6-30. Figure 6-31 shows that using the mod-UWA-FEA

methodology, the overall base capacity is underestimated with a Q_c/Q_m ratio of 0.49. It appears that at this site, the mod-UWA-FEA is not effective in predicting the measured base nor shaft response. The higher shaft friction also causes an increase in the stiffness of the pile which directly affects the initial slope of the load-displacement response (Figure 6-32). From Table 6-5 however, this is a marginal improvement with Q_c/Q_m of 1.15. A full load-transfer diagram can be produced for this site (Figure 6-33) and shows that although the estimated capacity is within 25%, the load distribution is not ideal. Also, due to missing data along the base of the external pile, these results are not very reliable. The base capacities of the pile and plug are well captured in this figure and reflect the results of the base response, although not well estimated by the mod-UWA-FEA method. The estimated active plug length, L_a however, is almost the same as that measured.

6.2.4.2. Kwangyang Plant TP-1

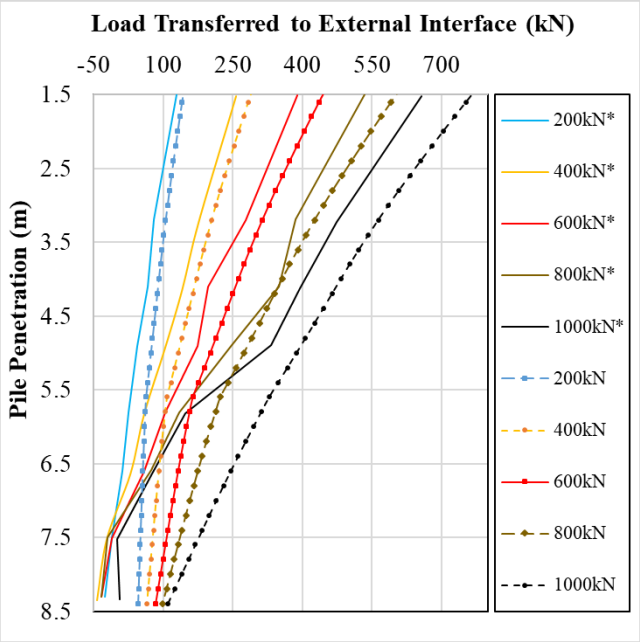

Figure 6-34 Axial load distribution in pile, mod-UWA-FEA estimation vs measured.

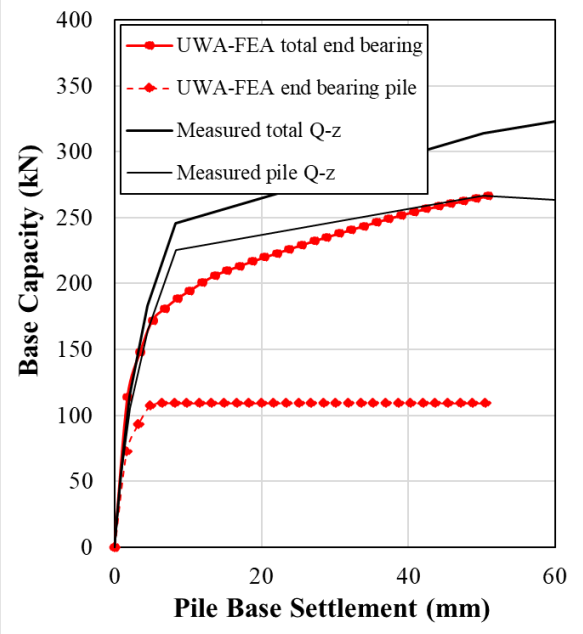

Figure 6-35 mod-UWA-FEA estimation of pile base settlement vs measured load.

At this site, the mod-UWA-FEA shows an improved match of the mobilisation of Q_{ext} at different increments of loading (Figure 6-34). Here, there is some disparity between the measured and estimated results at the base, due to the welding together of the internal and external double walled pile system causing a degree of tensile load-transfer. Figure 6-35 shows that the base capacity of the plug is highly overestimated however the total end bearing is still underestimated. This suggests that the end bearing approximation using the mod-UWA-FEA may not be the most ideal in this case. Due

to the differences in the load-transfer to the external shaft friction, the initial response of the load-displacement relationship is very stiff, leading to a much higher capacity estimated and Q_c/Q_m increasing from 1.10 to 1.16 (Figure 6-36). Figure 6-37 shows that in general there is a good match between the results, however due to the welded configuration of the double walled pile, the load transfer at the base is not easily deciphered.

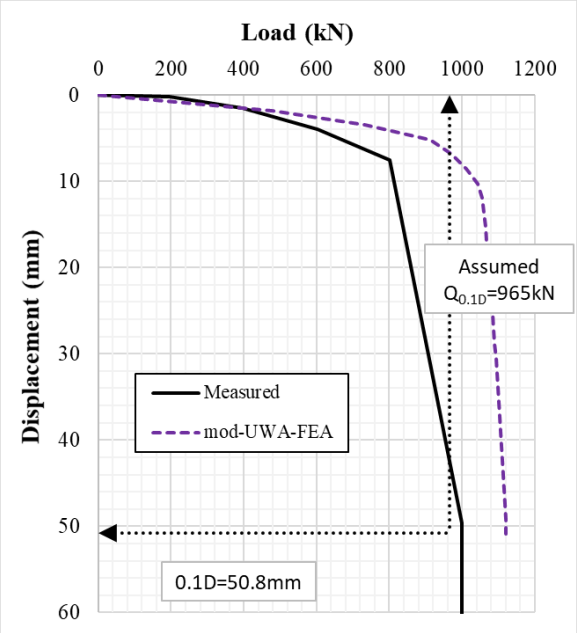

Figure 6-36 Load-displacement curve for mod-UWA-FEA estimation against measured.

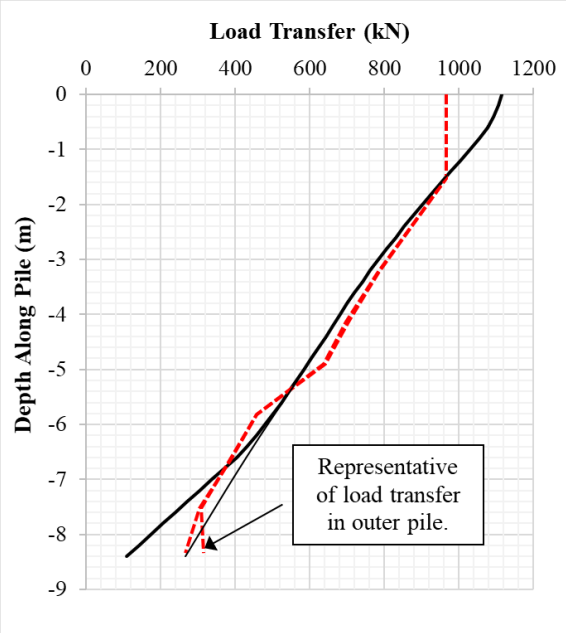

Figure 6-37 Load-transfer diagram for mod-UWA-FEA estimation at w_t = 0.1D_o. Dotted lines represent measured values.

6.2.4.3. Kwangyang Plant TP-2

Here, the results of the method are quite similar to those of the previous test. The base response is shown for comparison in Figure 6-38. The pile head load-response diagram (Figure 6-39) demonstrates that the mod-UWA-FEA does quite well in estimating the measured response, however the assumed reduction, due to the inconsistencies in the reported results, is lower than that estimated. The Q_c/Q_m is 1.18 for the total pile capacity.

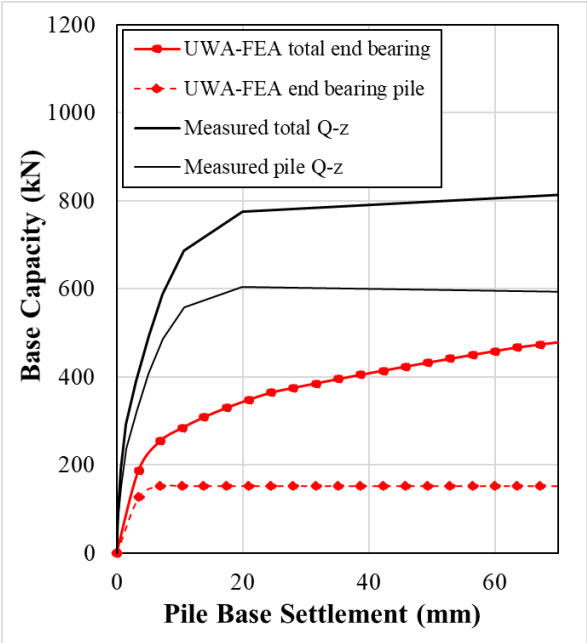

Figure 6-38 mod-UWA-FEA estimation of pile base settlement vs measured load.

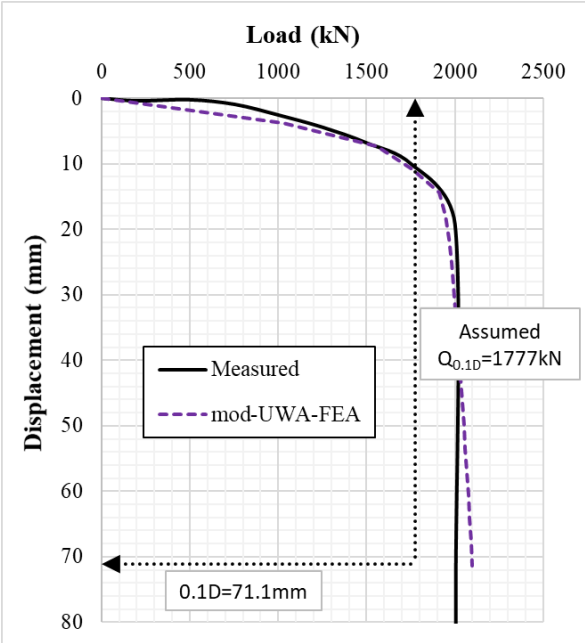

Figure 6-39 Load-displacement curve for mod-UWA-FEA estimation against measured.

6.2.4.4. Kwangyang Plant TP-3

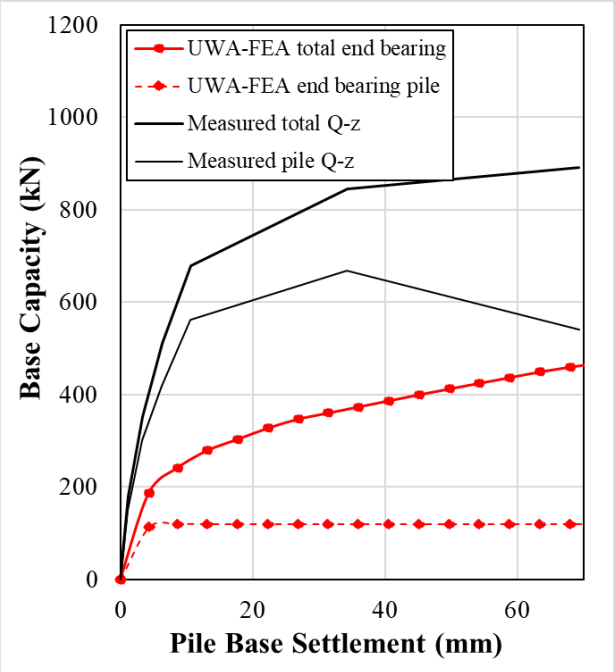

Figure 6-40 mod-UWA-FEA estimation of pile base settlement vs measured load.

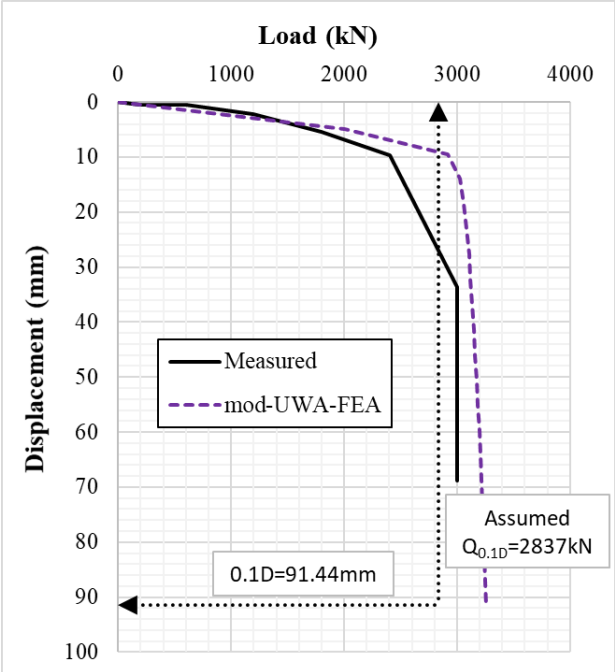

Figure 6-41 Load-displacement curve for mod-UWA-FEA estimation against measured.

Figure 6-40 and Figure 6-41 are shown here to demonstrate the similar predictability of the method between tests at this site.

6.2.4.5. Mobile Bay Test Piles

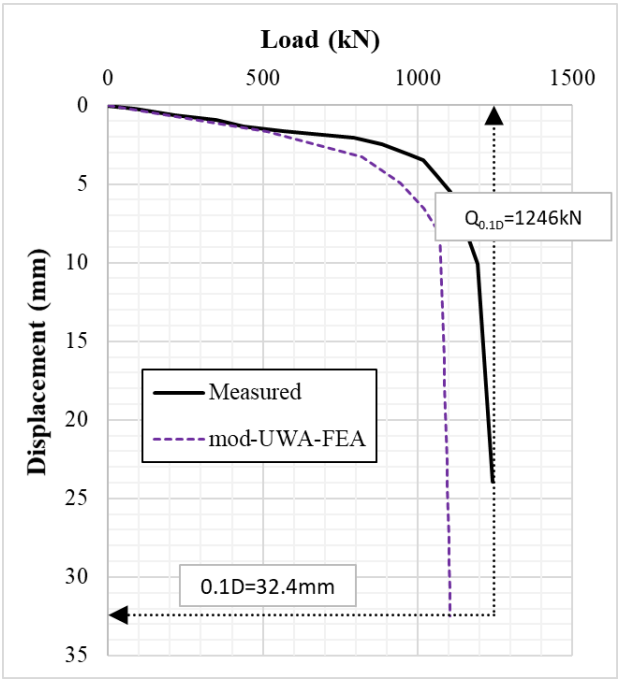

Figure 6-42 Load-displacement curve for mod-UWA-FEA estimation against measured for Mobile Bay AL-1.

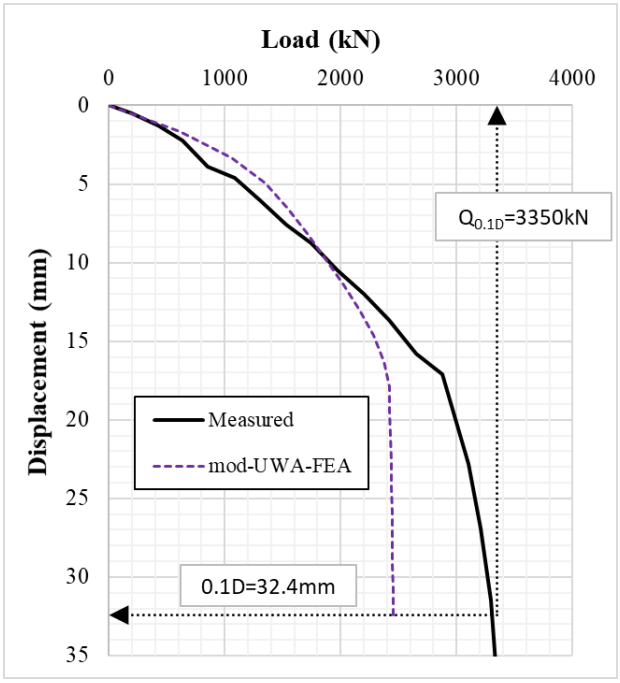

Figure 6-43 Load-displacement curve for mod-UWA-FEA estimation against measured Mobile Bay AL-2.

There was very limited data available for these sites. Using the mod-UWA-FEA, with the available data, there was an improvement observed in the overall estimate of load-displacement as shown in Figure 6-42, with Q_c/Q_m of 0.89, and Figure 6-43, with Q_c/Q_m values of 0.73.

6.2.4.6. Hoogzand 1-C

In Beringen *et al*. (1979), results were quoted after a pile head settlement of $0.15D_o$, however pile capacity is obtained after a pile head settlement of $0.1D_o$. Data is therefore extracted after this displacement.

The mobilisation of axial load in the pile is displayed in Figure 6-44. Here it is shown that the new method is generally able to match the measured distribution along the pile. The measured axial load, gradually mobilises the shaft friction, as the slope of the lines reduce, up to a load of about 1000kN. Afterwards, these lines become parallel and further capacity is obtained from the end bearing only. Figure 6-45 shows the comparison of the estimated and measured values. The initial slope of the curve, that tapers after about 600kN, shows that the end bearing on the pile is higher but not well captured by the method. Here the underestimation is by approximately 50%.

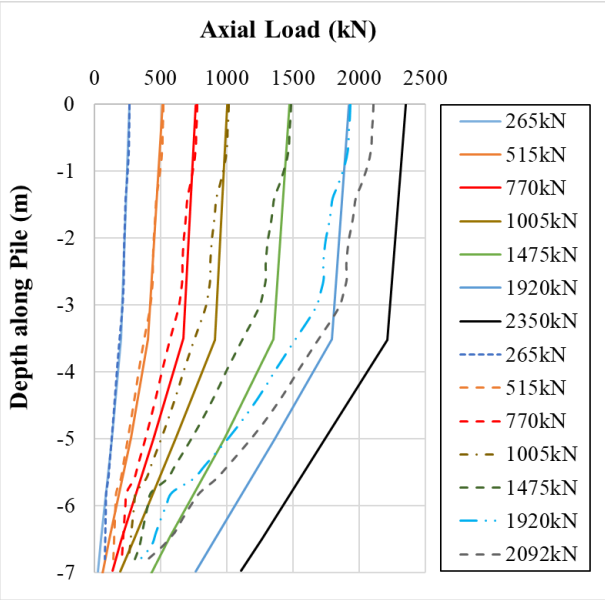

Figure 6-44 Axial load distribution in pile, mod-UWA-FEA estimation vs measured.

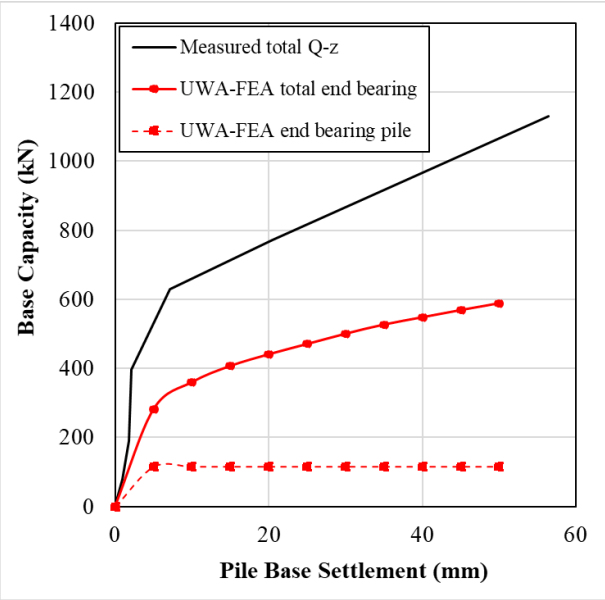

Figure 6-45 mod-UWA-FEA estimation of pile base settlement vs measured load.

The load-displacement diagram, Figure 6-46, shows that the Q_c/Q_m value is 1.01, which is an improvement given that the pile head response is estimated here, and 0.99 was previously obtained when the UWA method was used directly. The initial slope of the curve also matches well, suggesting that the predicted initial stiffness from the shaft is well modelled. The shallower slope, due to base mobilisation is also well matched. Beringen *et al.* (1979) indicated that the top of the plug was stationary relative to the pile head during loading. This was assumed to be due to a plugged response; however, partial plugging was most likely to have been the cause, with compression at the base of the sand plug causing dilation and confinement as loading is applied.

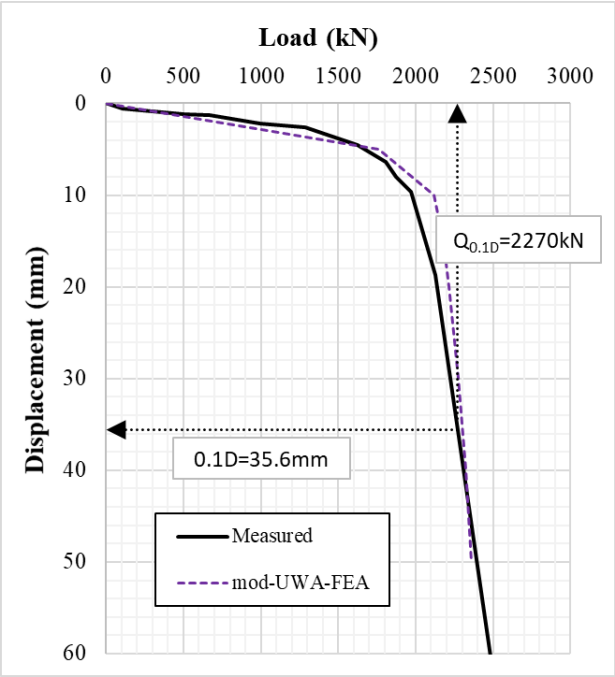

Figure 6-46 Load-displacement curve for mod-UWA-FEA estimation against measured.

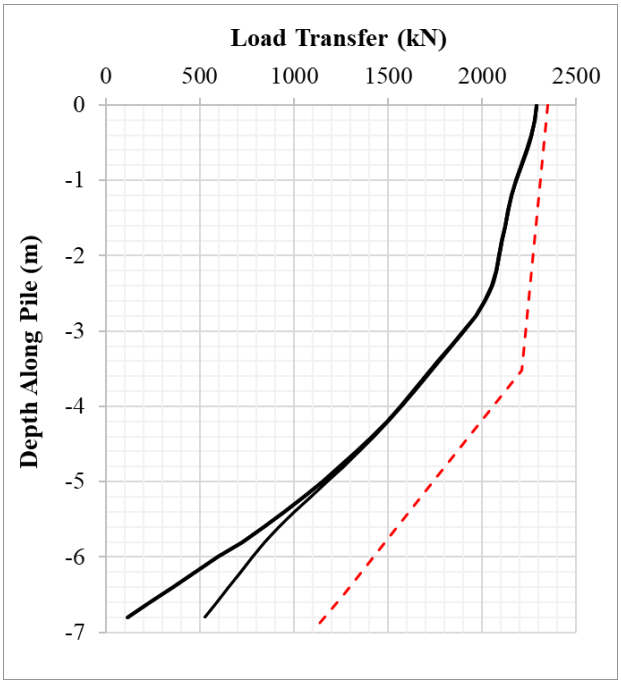

Figure 6-47 Load-transfer diagram for mod-UWA-FEA estimation at $w_t = 0.1D_o$. Dotted lines represent measured single-walled axial pile load.

From Figure 6-47, which shows the estimated load-transfer in the pile, the compression of the soil plug occurred along its active length, L_a, which is estimated here to be about $5D_o$, which is less than L_{pl}. This also suggests partial plugging was the prominent failure mode of the base. From this comparison it is observed that the method, which estimates a gradual distribution of load along the shaft and the end bearing on the pile, can be improved. This may lead to estimated values of L_a that are closer to that observed in OEPs in sandy soils (about 2-3D_o).

6.2.4.7. Hoogzand 3-C

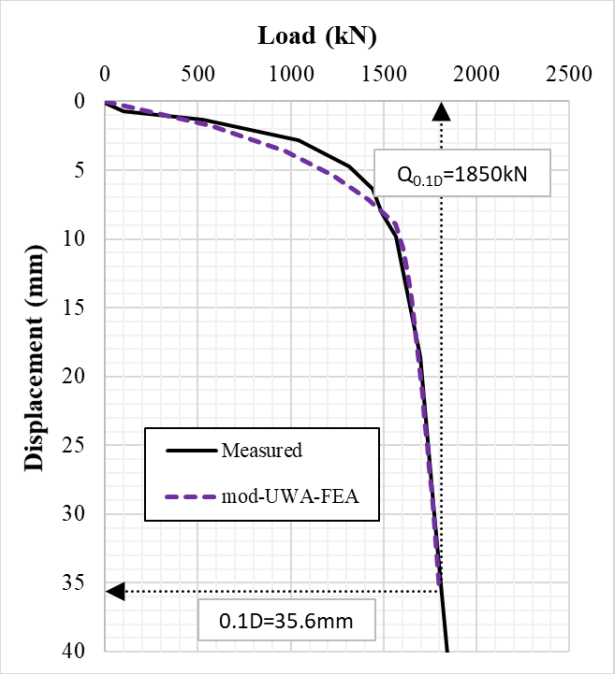

Figure 6-48 Load-displacement curve for mod-UWA-FEA estimation against measured.

Figure 6-48 shows a good match when the estimated and measured load-displacement responses are compared. The Q_c/Q_m value of the method has improved from 1.19 to 0.97.

6.2.4.8. Dunkirk C1-C

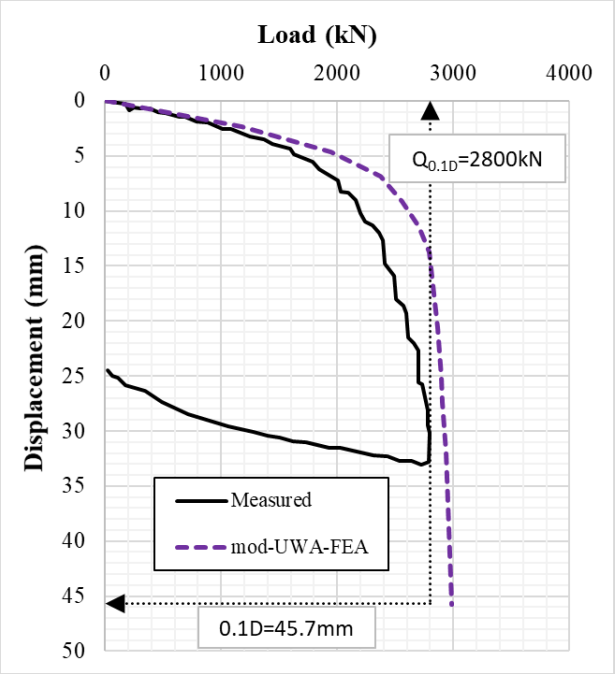

Figure 6-49 Load-displacement curve for mod-UWA-FEA estimation against measured.

Figure 6-49 gives the comparison of the load-displacement response. A good approximation is observed with a Q_c/Q_m ratio of 1.07, however the predicted initial slope is slightly stiffer than the measured response.

6.2.4.9. Euripides 1a

The Euripides analysis cases (1a, 1b, 1c & II) gave similar results, therefore only those from test 1a are presented.

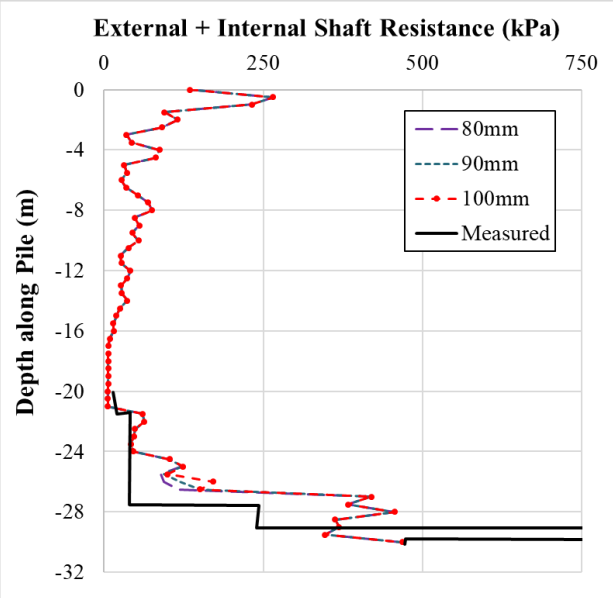

Figure 6-50 Total shaft friction, mod-UWA-FEA estimation vs measured at $w_t \approx 80$mm.

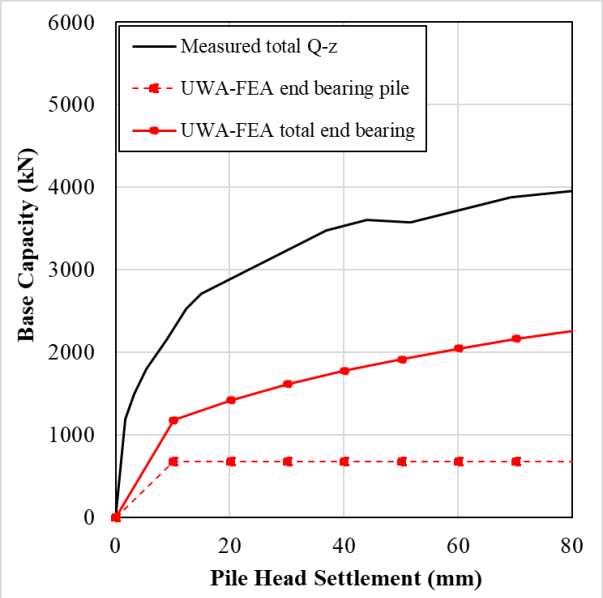

Figure 6-51 mod-UWA-FEA estimation of pile base settlement under a $w_t = 0.1D_o$ vs measured load.

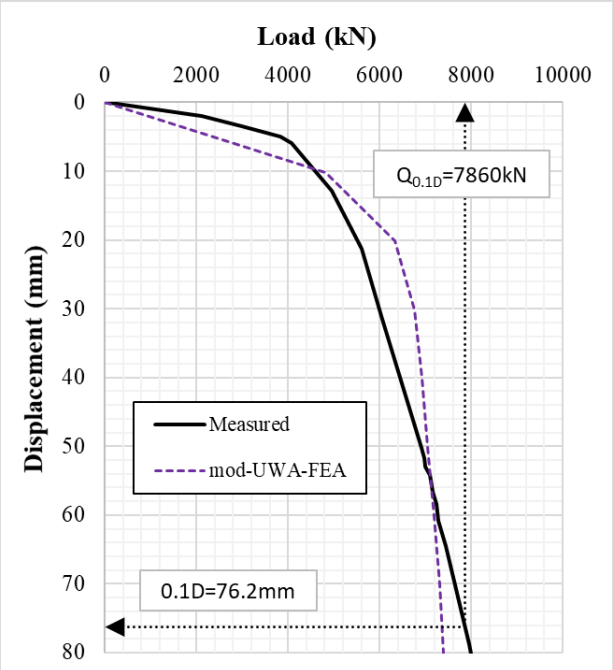

Figure 6-52 Load-displacement curve for mod-UWA-FEA estimation against measured.

Figure 6-50 shows that the mod-UWA-FEA can well estimate the total shaft resistance along the base of the pile length, as there is a very good match between the values. The base response is similar to the previous cases and shows that the method underestimates, in general, both $Q_{b,p}$ and $Q_{b,pl}$ (Figure 6-51). In terms of the load-displacement however, there is a very good match of the initial stiffness, when the axial support is governed by the shaft friction, and in the flatter part of the response, when the base capacity is mobilised (Figure 6-52). This agreement in response occurs even though the base capacity is underestimated. The Q_c/Q_m for the load-displacement is 0.94.

6.2.4.10. Tokyo Bay TP

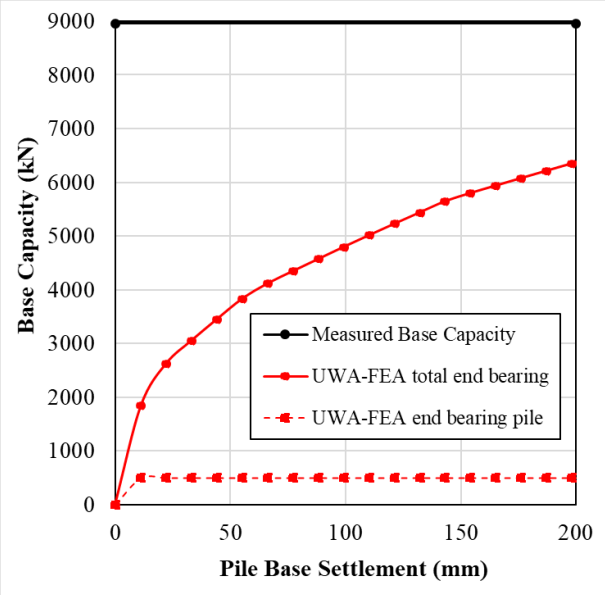

Figure 6-53 mod-UWA-FEA estimation of pile base settlement vs measured load.

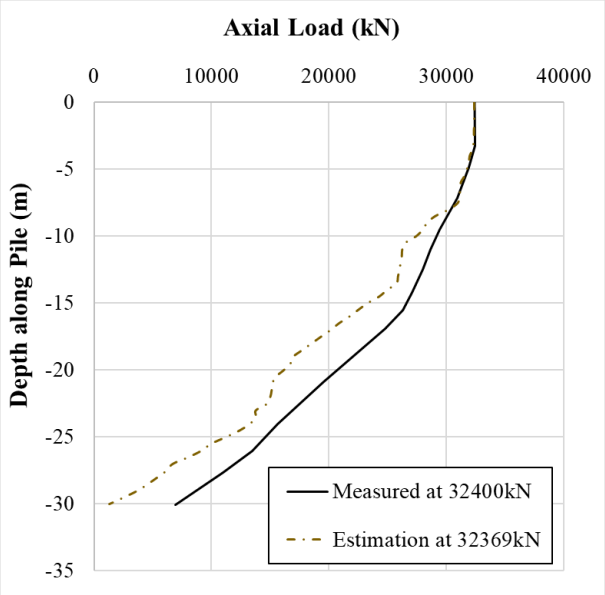

Figure 6-54 Axial load distribution in pile, mod-UWA-FEA estimation vs measured.

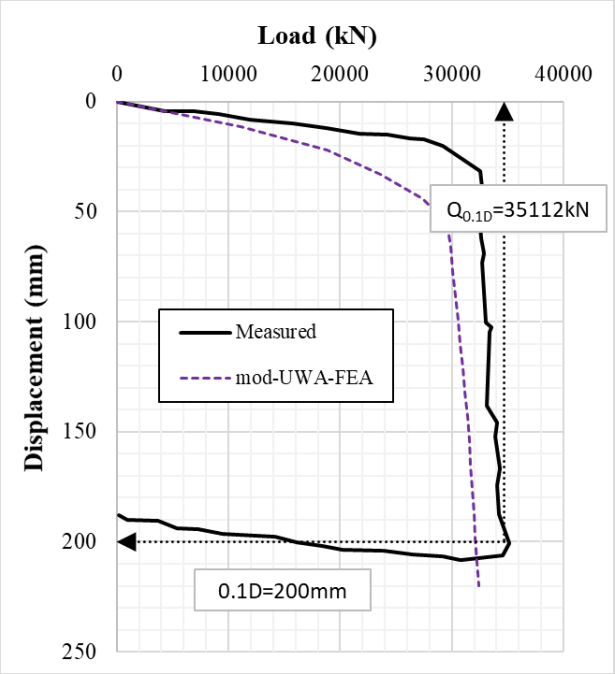

Figure 6-55 Load-displacement curve for mod-UWA-FEA estimation against measured.

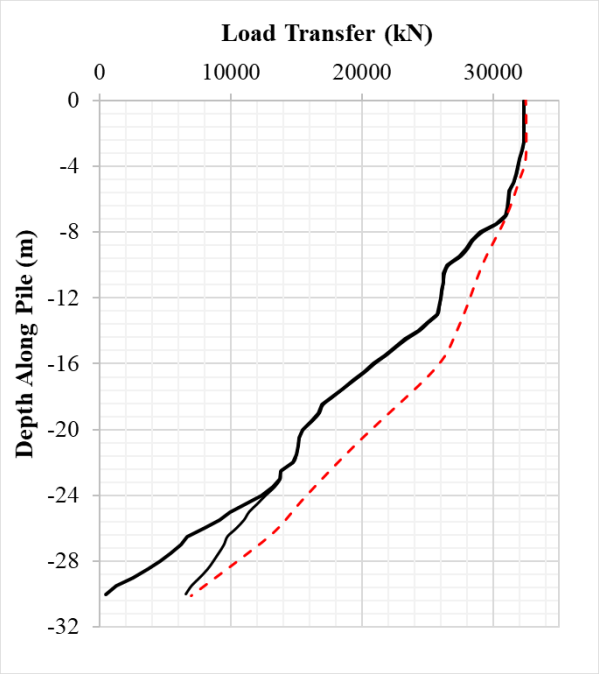

Figure 6-56 Theoretical load-transfer diagram for mod-UWA-FEA estimation at $F_t \approx$ 32,400kN.

The case study in Shioi *et al.* (1992) provided results for the base and shaft at w_t=0.02D_o. The base would most likely not have achieved its ultimate capacity at this point and no Q-z reaction curve is available. Figure 6-53 therefore shows the estimated base response from the mod-UWA-FEA method and the measured base capacity derived from the sum of the base load at w_t=0.02D_o and the increase in total capacity to w_t=0.1D_o. The axial load along the pile was also available, here at a pile head

load of 32,400kN, this distribution is compared with that estimated in Figure 6-54. The shaft capacity seems to be adequate at this load, but these results also depict the low contribution of the pile base estimated here.

The load-displacement diagram observes a good match of stiffness along the full pile head response (Figure 6-55) and the method has also improved Q_c/Q_m from 0.79 to 0.91. The large proportion of base capacity mobilised over a large displacement is also well replicated.

The load-transfer diagram is shown in Figure 6-56 at a pile head load, F_t of 32,400kN. At this load, the measured pile head displacement was $0.02D_o$, and the estimated was $0.1D_o$. The estimated total base capacity at this load, using VIRTUPLUG, was approximately 6372kN, however the measured base capacity is not yet fully developed here to the 8958kN.

6.2.4.11. Drammen 16-P1-11

The load-displacement response is provided for the pile test 16-P1-11.

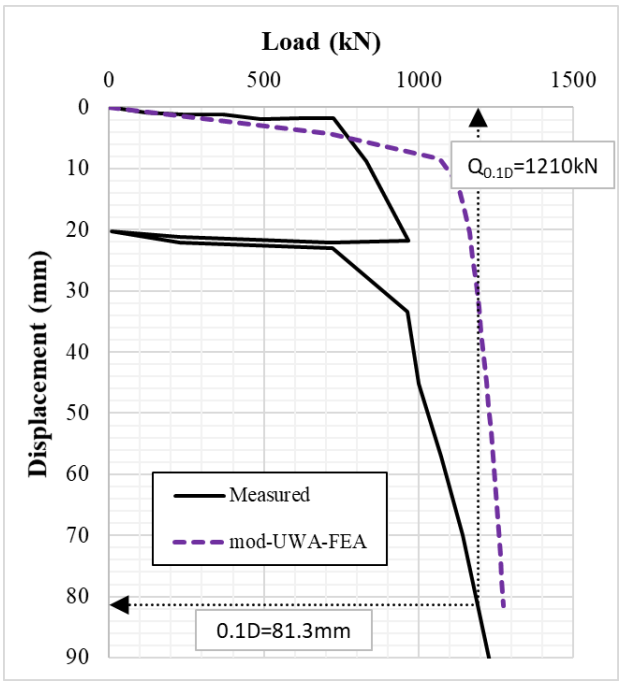

Figure 6-57 Load-displacement curve for mod-UWA-FEA estimation against measured.

This pile was subjected to cyclic loading, and as can be seen in the load-displacement response in Figure 6-57, the response follows the Masing's behaviour, as upon unloading and re-loading, the response reconnects to the original load-displacement path. Under compressive loading the match is quite good with a Q_c/Q_m, at $0.1D_o$, of 1.05, however the original UWA method estimated 0.98.

6.2.4.12. Drammen 16-P1-15

No load-displacement results are available here, therefore a linear relationship is assumed. This data is obtained from Tvedt & Fredriksen (2003) and Yang *et al*. (2015). The results for the 25-P1-25 tests were quite similar and therefore not included.

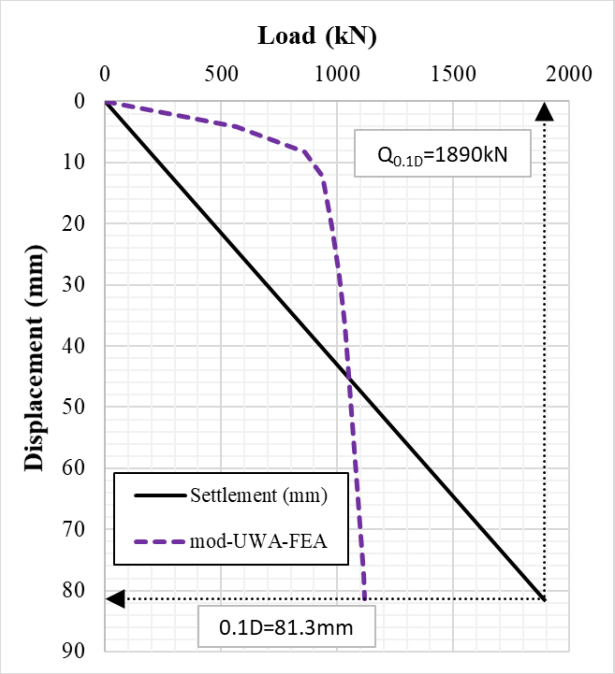

Figure 6-58 Load-displacement curve for mod-UWA-FEA estimation against measured.

Figure 6-58 shows the comparison of the estimated load-response for this site and the assumption of a linear relationship from the origin to the capacity at w_t=0.1D_o. The Q_c/Q_m value has decreased from 0.73 to 0.59.

6.2.4.13. Hound Point – P0-C

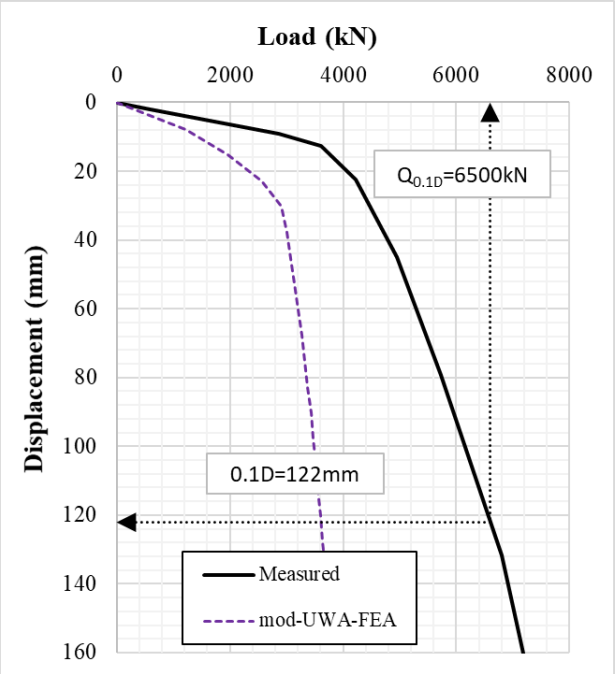

Figure 6-59 Load-displacement curve for mod-UWA-FEA estimation against measured.

The comparison of load-displacement response is shown in Figure 6-59. Here the Q_c/Q_m has reduced from 0.96 to 0.56. The underestimation of this capacity is mainly due to the large proportion of clay present in the upper part of the pile, which cannot be modelled using the UWA method. Also a greater contribution from the base capacity was computed using the UWA method, however, using the mod-UWA-FEA the distribution was better balanced although achieving a lower total capacity.

6.2.4.14. Shanghai ST-1

This site is comprised of a 28m initial clay layer, followed by sandy silt. Within the geotechnical engineering database however, this case study by Pump *et al.* (1998), is considered a sand site. Any parameterisation of this soil, used as input to the UWA method, will therefore have inherent assumptions adopted for the thick clay layer. In addition, the methodology of the UWA method predicts much lower capacities in the sand layers, due to the low values of area ratio (A_{rs}) and friction fatigue (h/D) here, as opposed to using the ICP method, which estimates a much higher capacity. The differences are evident here due to the high variation in the estimated shaft capacities, especially where the clay layers are assumed to provide no additional capacity. There are also differing values of q_c published for the site from Pump *et al.* (1998) and Yang *et al.* (2015).

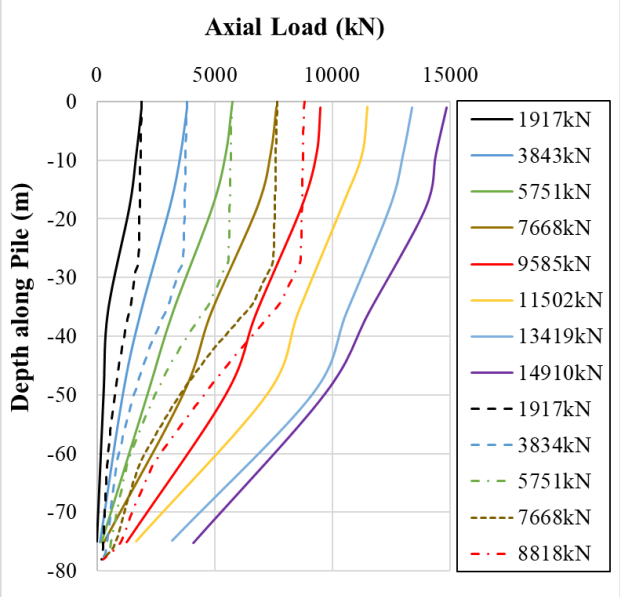

Figure 6-60 Axial load distribution in pile, mod-UWA-FEA estimation vs measured.

Figure 6-60 shows the comparison of the axial load in the pile. The slope of the estimated values (dotted lines) are vertical in the clay layers and generally uniform in the sand layers. From the measured results (solid lines), it is evident that the pile acquires a large proportion of capacity in the clay layers. This is observed from the uniform slope of these measured values, which suggests that the mod-UWA-FEA methodology cannot solely be used here. The base of the pile bears in sand; however, the capacity of the annulus is greatly underestimated by the method. As the ICP method considers both sands and clays, a better correlation may be possible using a modified ICP-FEA method in layered stratigraphies. This is considered in Section 6.3.

Figure 6-61 shows the load-displacement response. The piles at the Shanghai site were subjected to many cycles, and those up to w_t=0.1D_o are shown in the diagram. The applicability of the Masing's rule for piles under combined loading and unloading is again observed here. The Q_c/Q_m was found to be 0.61, an improvement from the previous 0.53 using the UWA method directly.

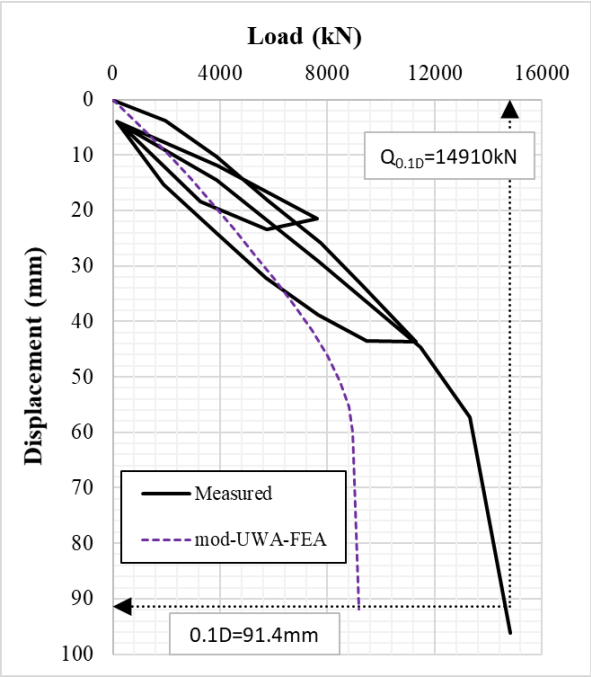

Figure 6-61 Load-displacement curve for mod-UWA-FEA estimation against measured.

Due to the underestimation of the overall capacity at the site using the mod-UWA-FEA, the accuracy of the load-transfer diagram is low and not included. Also, the results from Shanghai ST-2 tests were derived from the same site data as those from ST-1, with an increased pile length of 0.1m. The comparison of the analysis results is similar to those shown in this section and therefore not included.

6.2.4.15. Ras Tanjib C

The loading and unloading performed at this site did not achieve a pile head displacement of $0.1D_o$.

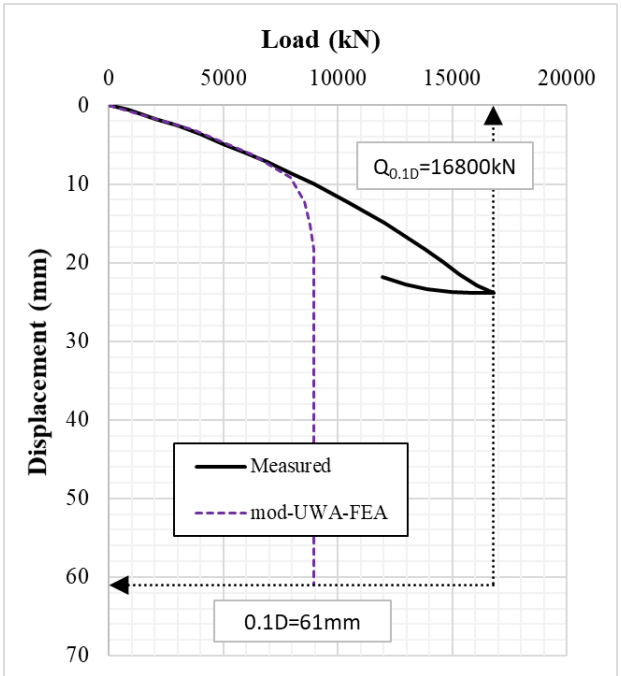

Figure 6-62 Load-displacement curve for mod-UWA-FEA estimation against measured.

Figure 6-62 shows the available load-displacement results and compares these to what was estimated by the mod-UWA-FEA method. The Q_c/Q_m here has remained constant at 0.53. From the load-displacement diagram, the shaft friction has clearly been underestimated here. The measured q_c values were used, so this could be attributed to higher δ_{cv} values than the default input adopted.

6.2.5. Summary Table – Sands

Table 6-5 summarises the results of the analysis performed using the mod-UWA-FEA method. These values were referred to in the previous discussion but better displayed diagrammatically in Figure 6-63 to Figure 6-65. As can be observed from these figures, after all these changes, there has been little shift in the Q_c/Q_m values for total capacity, the shaft capacity seems to have been improved but now seems generally overestimated, and the base capacity seems to have also improved but now underestimated.

Table 6-6 shows the statistical summaries of the Q_c/Q_m values for the total, shaft and base capacities. Here it shows that:

- considering all the changes that have been employed in the use of the mod-UWA-FEA, there is not much variation in total capacity found using this method and the UWA method directly.
- considering the shaft friction, the applied factor of 2.0 on σ'_{rc} has caused the Q_c/Q_m value to increase from 0.823 to 1.228. This suggests that a factor of (say) 1.5 on σ'_{rc} may be more appropriate and is therefore recommended to achieve be a better estimate of the shaft capacity using the mod-UWA-FEA method.
- considering the end bearing, the factor of 0.5 applied to q_b has caused the Q_c/Q_m value to reduce from 1.682 to 0.556, suggesting that this was too low. A factor of 0.75 applied to q_b is therefore recommended when using the mod-UWA-FEA method .
- there are no great improvements observed in the standard variations of the summarised results between the mod-UWA-FEA and the UWA methods.

It is noted that the results of the mod-UWA-FEA are determined based on the estimated responses obtained after a pile head displacement of $0.1D_o$, rather than a direct, static method. This means that a non-linear load-displacement response is produced, providing further, more detailed information to the user, rather than a linear response.

Table 6-5 Comparison of measured capacities and values derived from the modified UWA-FEA approach.

Site Number	Site	D (m)	D/t	L/D	Measured			mod-UWA-FEA					
					Total Capacity (kN)	Total Shaft Friction (kN)	Total End Bearing (kN)	Total Capacity (kN)	Total Shaft Friction (kN)	Total End Bearing (kN)	Q_c/Q_m Total Capacity	Q_c/Q_m Total Shaft Friction	Q_c/Q_m Total End Bearing
1	Pigeon creek	0.356	11	20	1029	310	719	1186	833	354	1.15	2.68	0.49
2	Kwangyang Plant TP1	0.508	10	17	965	651	314	1122	855	267	1.16	1.31	0.85
3	Kwangyang Plant TP2	0.712	14	16	1777	943	834	2097	1618	480	1.18	1.72	0.58
4	Kwangyang Plant TP3	0.914	18	17	2837	1947	890	3261	2759	501	1.15	1.42	0.56
5	Mobile Bay AL1	0.324	13	47	1246	-	-	1105	990	115	0.89	-	-
6	Mobile Bay AL2	0.324	13	132	3350	-	-	2454	2209	245	0.73	-	-
7	Hoogzand 1-C	0.356	22	20	2270	1310	960	2303	1774	529	1.01	1.35	0.55
8	Hoogzand 3-C	0.356	18	15	1850	-	-	1798	1144	655	0.97	-	-
9	Dunkirk C1-C	0.457	34	22	2800	-	-	2988	2429	560	1.07	-	-
10	Euripides 1a	0.763	21	40	7860	3860	4000	7364	5138	2227	0.94	1.33	0.56
11	Euripides 1b	0.763	21	51	12600	9400	3200	12942	10671	2271	1.03	1.14	0.71
12	Euripides 1c	0.763	21	62	18100	14150	3950	16875	14640	2236	0.93	1.03	0.57
13	Euripides II	0.763	21	61	17980	13410	4570	16797	14529	2267	0.93	1.08	0.50
14	Tokyo Bay TP	2.000	59	15	35112	25938	8958	32120	25748	6372	0.91	0.99	0.71
15	Drammen 11	0.813	65	14	1210	-	-	1273	989	285	1.05	-	-
16	Drammen 15	0.813	65	18	1890	-	-	1119	766	352	0.59	-	-
17	Drammen 25	0.813	65	31	2700	-	-	1856	1523	333	0.69	-	-
18	Hound Point P0-C	1.220	50	21	6500	4000	2500	3610	2038	1572	0.56	0.51	0.63
19	Shanghai ST-1	0.914	46	86	14910	10720	4190	9167	8368	798	0.61	0.78	0.19
20	Shanghai ST-2	0.914	46	87	16000	13600	2400	9177	8379	798	0.57	0.62	0.33
21	Ras Tanjib C	0.610	21	30	16800	-	-	8950	7881	1069	0.53	-	-

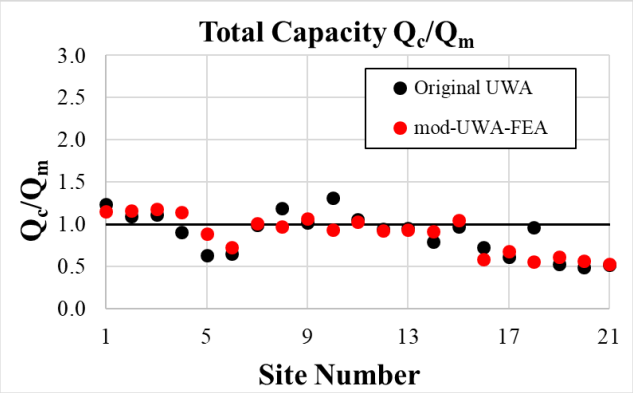

Figure 6-63 Comparison of the Q_c/Q_m of the total capacity using the original UWA and mod-UWA-FEA design method.

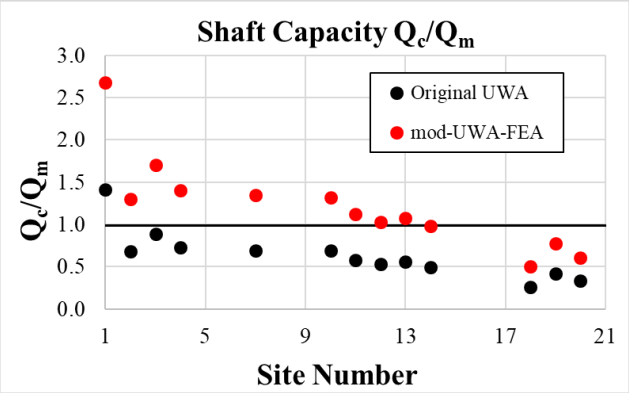

Figure 6-64 Comparison of the Q_c/Q_m of the shaft capacity using the original UWA and mod-UWA-FEA design method.

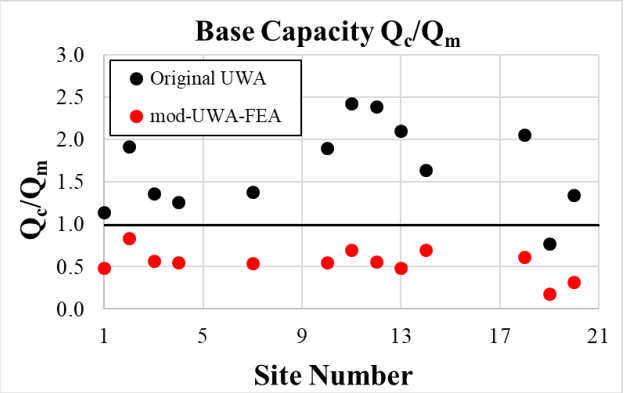

Figure 6-65 Comparison of the Q_c/Q_m of the base capacity using the original UWA and mod-UWA-FEA design method.

Table 6-6 Mean and standard deviation of Q_c/Q_m for the OEP validation database for sands using mod-UWA-FEA method.

Statistic	UWA			mod-UWA-FEA		
	Total Force Estimated	Shaft Friction	Total End Bearing	Total Force Estimated	Shaft Friction	Total End Bearing
μ	0.894	0.823	1.682	0.889	1.228	0.556
σ	0.246	0.415	0.508	0.215	0.529	0.159
COV	0.275	0.504	0.302	0.242	0.431	0.287

6.3. Capacity of OEPs in Layered Soils

In the field, it is quite uncommon to find stratigraphies that are uniformly clays or sands. In some of the cast studies that were presented, such as the predominantly clay site at Kansai Bridge, or predominantly sand sites at Shanghai, these did have some layers of either sands or clays respectively. The methodologies outlined in Sections 6.1 and 6.2 were developed to determine the behaviour of OEPs in either all-clays or all-sands, respectively. In the pile design methods analysed, each has some shortcoming in one or another soil type or in layered soils. As found in the evaluation of each method's performance in Sections 4.2 and 5.2, the API method may be good in clays, but not very accurate in sands. Similarly, it was observed that the ICP may be good in sands but inaccurate in some clay stratigraphies. In addition, the API was found to be better than the ICP in clays due to the minimal quantity of soil parameters required to produce acceptable designs. The UWA method was found to be quite good in sands but cannot be used for pile design in layered stratigraphies.

Given these shortfalls, when designing in layered soils some compromise must be allowed and therefore, a modified ICP-FEA method is recommended.

6.3.1. Modified ICP-FEA method in Layered Soils

The following sections outline the new recommended methodology to improve the estimation of capacity distribution to the external shaft and end bearing components in OEPs, in layered soils.

6.3.1.1. Clays

Table 6-7 Input parameters for mod-ICP-FEA in clay layers.

Resistive Component	Resistance Input	Recommended Value
External Soil	τ_{ext}	$\tau_f = \sigma'_{rc} \tan \delta_f$ (σ'_{rc} from ICP)
	$z_{p,e}/D_o$	0.01
	t-z reaction curves	API
Internal Soil	τ_{int}	τ_{ext}
	$z_{p,i}/D_i$	0.001
	M	(2000 - 4000) s_u
Annulus	$q_{b,p}$	$1.6q_c$
	$z_{b,p}/t$	0.1
	Q-z reaction curve	API
Plug Base	$q_{b,pl}$	$0.2q_c$
	$z_{b,pl}/D_i$	0.1
	Q-z reaction curve	API

Additional considerations include:

- **Softening $\delta_{ult}/\delta_{peak}$:**

  This is to be determined from ring shear tests and applied as the reduction factor in the t-z curves.

- **External Shaft Resistance, τ_{ext}**

  In clays, the loading factor (K_f/K_c) taken as 80% in this work and introduced into the ICP method by Lehane (1992) considered the softening of clays under loading. Within the FEA method, this reduction is catered for by the t-z soil reaction curves, preferably derived from ring-shear testing. To avoid the double-counting error, this factor is to be removed.

- **End Bearing Pile, $q_{b,p}$**

  In a similar way to the expression derived for the base resistance of OEPs in clay, the following is recommended, assuming that the soil below the annulus of the pile will always become drained:

$$\frac{q_{b,p}}{q_c} = 1.6 \tag{78}$$

- **End Bearing Plug, $q_{b,pl}$**

  The following expression is adopted as the base resistance below the plug, selected as a lower bound derived from the resistance at the base of double walled pile tests (Doherty et al. 2010):

$$\frac{q_{b,pl}}{q_c} = 0.20 \tag{79}$$

6.3.1.2. Sands

Table 6-8 Input parameters for mod-ICP-FEA in sand layers.

Resistive Component	Resistance Input	Recommended Value
External Soil	τ_{ext}	ICP method ($\sigma'_{rf} \tan \delta_{cv}$)
	$z_{p,e}/D_o$	0.01
	t-z reaction curves	API
Internal Soil	τ_{int}	τ_{ext}
	$z_{p,i}/D_i$	0.001
	M	Lunne & Christophersen (1983)
Annulus	$q_{b,p}$	$1.0q_c$
	$z_{b,p}/t$	0.1
	Q-z reaction curve	API
Plug Base	$q_{b,pl}$	$0.2q_c$
	$z_{b,pl}/D_i$	0.1
	Q-z reaction curve	API

Additional considerations include:

- **External Shaft Resistance, τ_{ext}**

  In sands, the existing relationships as per the ICP-2005 method is to be maintained.

- **End Bearing Pile, $q_{b,p}$**

  Chow (1997) noted that the ratio of base resistance below the annulus to the q_c value, $q_{b,p}/q_c$ ranged from 0.91 to 4.3, depending on diameter and density. It is noted however that the density will be related to by the measured q_c values. The following lower bound is therefore accepted as appropriate:

$$\frac{q_{b,p}}{q_c} = 1.0 \tag{80}$$

- **End Bearing Plug, $q_{b,pl}$**

  The following expression is adopted as the base resistance below the plug, selected as a lower bound derived from the resistance at the base of bored piles in sands (Lehane et al. 2002):

$$\frac{q_{b,pl}}{q_c} = 0.20 \tag{81}$$

- **Pile and plug weights**

  The weights of these components will be included for both sands and clays even though their effect is small.

6.3.2. Validation

In the validation of this method, tests previously analysed, with OEPs in layered stratigraphies and included in the geotechnical engineering database are used. Over time this database can be contributed to and modified, thereby enhancing the accuracy of the predictions.

6.3.2.1. Kansai Bridge T1

Properties of the sand at this site were derived from the main paper (Matsumoto *et al.*, 1992) and where unavailable, default values were adopted.

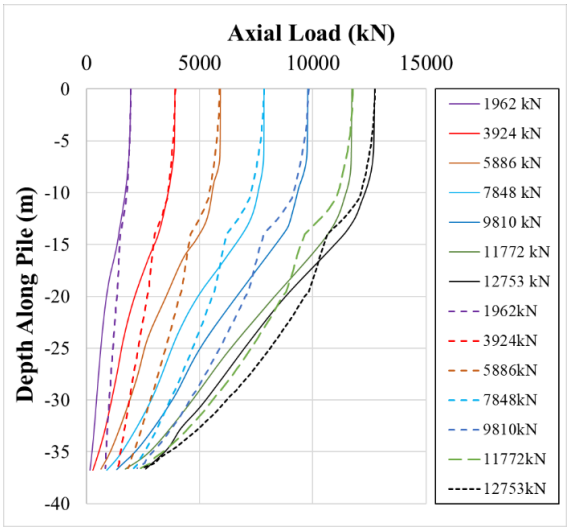

Figure 6-66 Axial load distribution in pile, mod-ICP-FEA estimation vs measured.

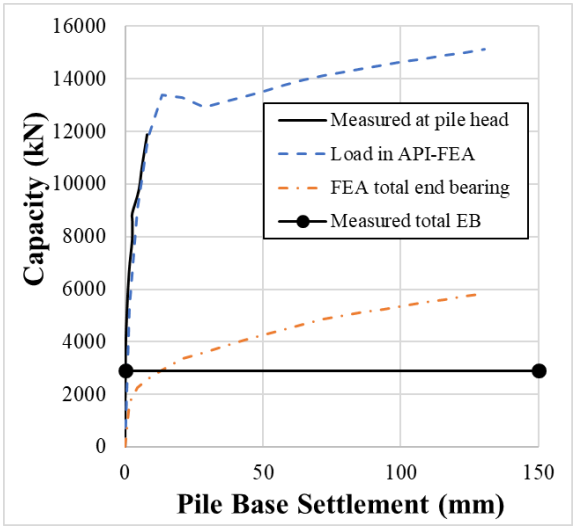

Figure 6-67 mod-ICP-FEA estimation of pile base settlement vs measured load.

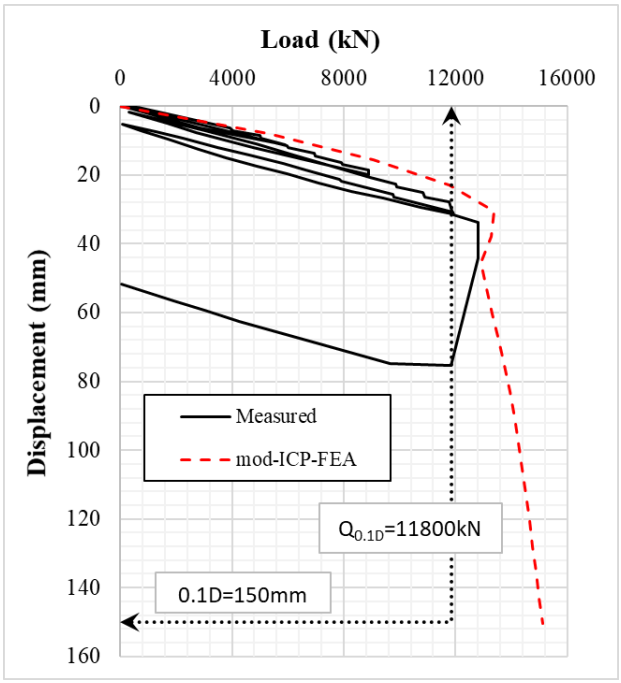

Figure 6-68 Load-displacement curve for mod-ICP-FEA estimation against measured.

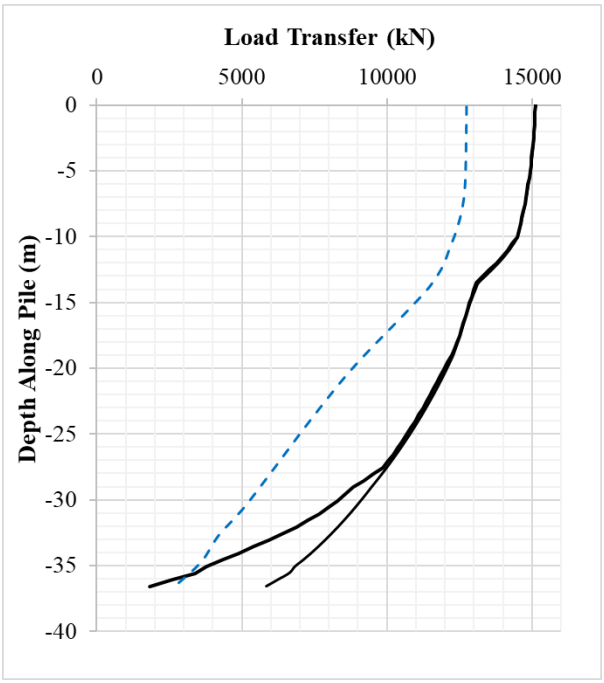

Figure 6-69 Load-transfer diagram for mod-ICP-FEA estimation at $w_t = 0.1D_o$. Dotted lines represent measured single-walled axial pile load.

The axial load along the pile is shown in Figure 6-66. This diagram can be compared to that showed earlier in Figure 6-17 where this site was considered as clay only. Using the mod-ICP-FEA, the slopes of the mobilised axial loads are quite similar to those measured, suggesting that the method is an improvement on the original modification. In terms of the base response, although the previous case did show a good match, there is also an improvement observed in Figure 6-67, compared to the previous results of Figure 6-18. The overall load-displacement response however shows that the capacity is overestimated. Figure 6-68 portrays a result, similar to a backbone curve encompassing the measured response. The Q_c/Q_m for this analysis is 1.27. The load-transfer diagram for this

analysis is shown in Figure 6-69 at w_t=0.1D_o. As the mod-ICP-FEA method over-predicts the capacity, this is also represented in this diagram, although the annulus capacity is well captured. In addition, this method estimates a much shorter active plug length, by about 5m than previously estimated. This suggests that with the contribution of the clay layers, under the same pile head displacement, less plug capacity is needed (or mobilised) to support the load.

6.3.2.2. Hound point P0-C

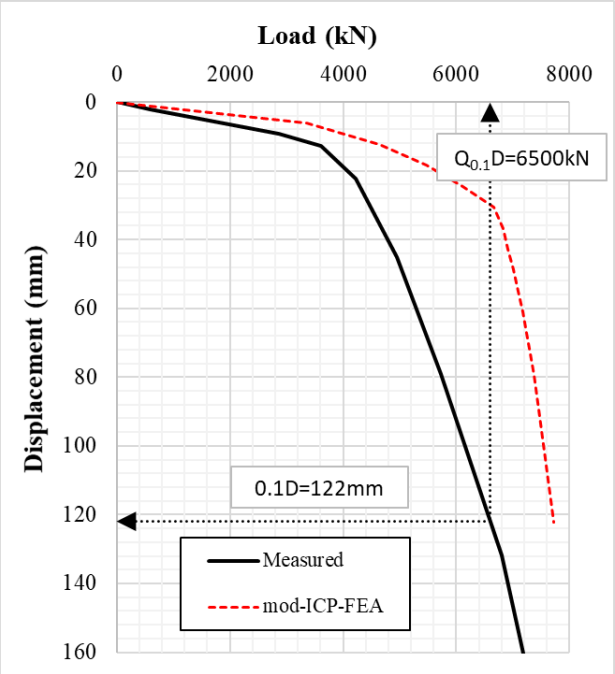

Figure 6-70 Load-displacement curve for Layered -FEA estimation against measured.

As outlined in Section 6.2.4.13, a large proportion of clay is present at this site and the UWA method is specific to sands. Using the mod-ICP-FEA, Figure 6-70 shows the comparison between the estimated and measured load-displacement response. In this analysis, the use of the mod-ICP-FEA method shows a high initial stiffness which leads to an over-estimation of the capacity (Q_c/Q_m = 1.19). This high initial stiffness is caused by the higher stiffness of the shaft, from the inclusion of the clay layers in the model. Observing the measured results, these suggest that the contribution of the shaft to the total capacity, should be less, based on the length of the initial part of the curve with a high stiffness. The base capacity however, which is generally the capacity gained over the shallower gradient in the load-displacement response, should be larger. The estimated shaft friction is therefore suggested to be overestimated and the base capacity underestimated by the mod-ICP-FEA method.

6.3.2.3. Shanghai ST-1

The properties of the clay at this site were extracted from Pump *et al.* (1998) and Gao *et al.* (1986).

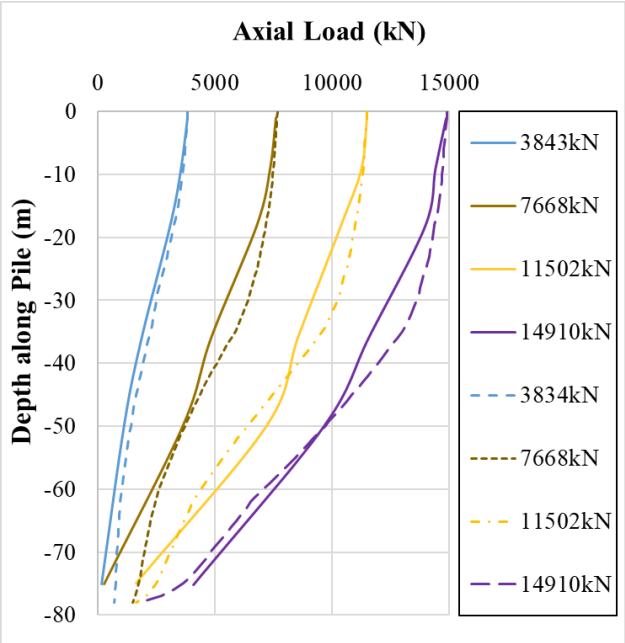

Figure 6-71 Axial load distribution in pile, Layered-FEA estimation vs measured.

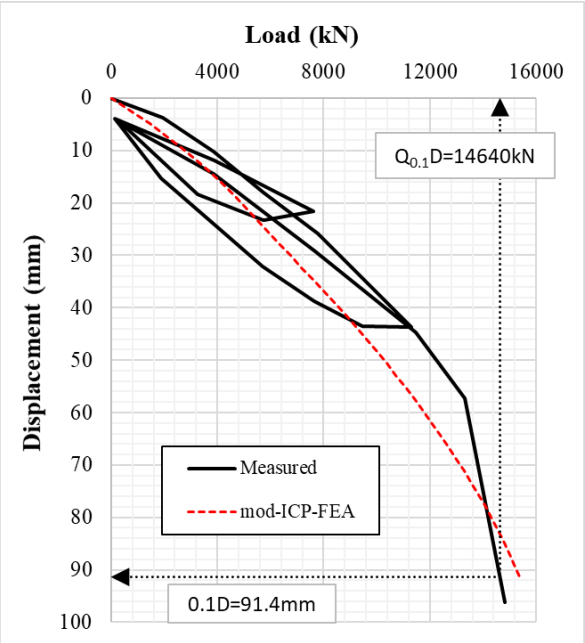

Figure 6-72 Load-displacement curve for Layered -FEA estimation against measured.

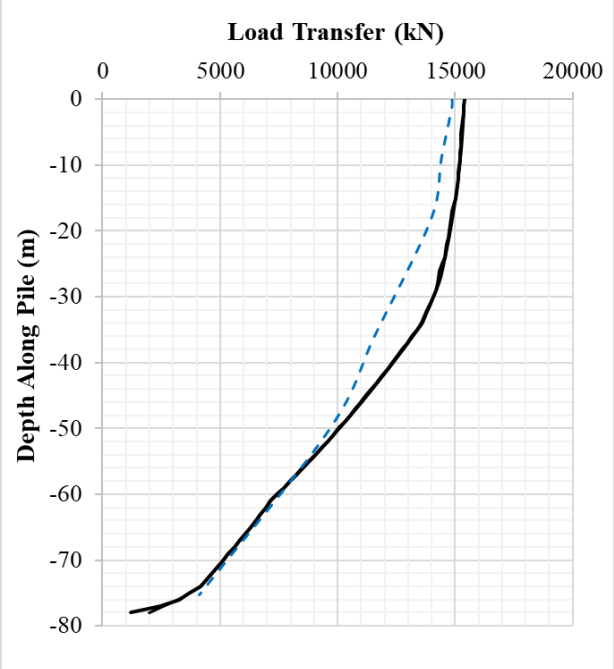

Figure 6-73 Load-transfer diagram for mod-ICP-FEA estimation at w_t = 0.1D_o. Dotted lines are measured single-walled axial pile load.

Using the mod-ICP-FEA, Figure 6-71 shows the axial load in the pile. Comparing these results to those in Figure 6-60, finds that the new method can mobilise much more capacity than the previous method. Here the additional contribution of the clay layers allowed a better match to the overall load-response, suggesting that these layers ought not to be omitted. Figure 6-72, shows the highly improved results, where the Q_c/Q_m is now 1.05 compared to a previous 0.61. In the sand analysis, Section 6.2.4.14, no load-transfer plot was shown due to the high variation in total mobilised capacity. As the results in this analysis have improved, the load-transfer diagram at w_t=0.1D_o is included (Figure 6-73) and corroborates the above observations. Also, the estimated contribution of the plug is quite low with a small L_a. Similar observations were also found with the results at Shanghai ST-2.

In general, the use of the mod-ICP-FEA has been able to better capture the measured responses of open-ended piles in layered stratigraphies.

6.4. Comparison with the Commercial Code OPILE

Using the method developed above, these results are now compared against those from an industry method of computing pile head response. OPILE is a pile design program that determines the effects on piles subjected to lateral, axial and torsional loads, displacements and rotations. OPILE was developed by Cathie and Associates Ltd and accepts input of stratigraphy and pile properties. OPILE adopts pile design methods including the API, ICP and UWA to inform the design of piles, it however does not directly model the plug. This program is well established, and the results from OPILE will be compared to those of the modified methods at the Euripides and Pentre sites using VIRTUPLUG.

6.4.1.1. Pentre LDP

The pile tests at Pentre is used to compare the results estimated by the mod-API-FEA method with those determined when the parameters are derived directly from the API and ICP methods and input into OPILE.

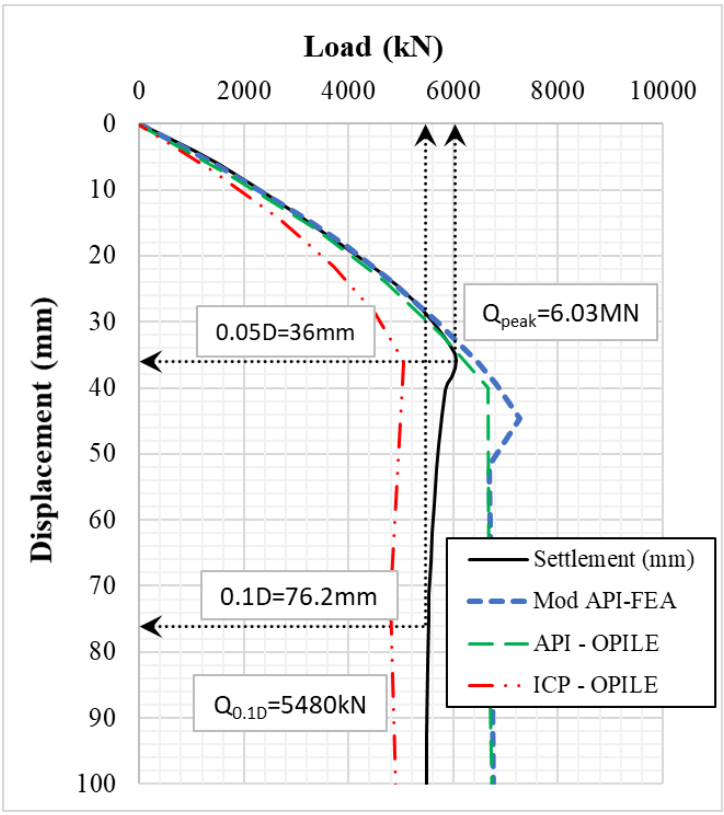

Figure 6-74 Load-displacement curve comparing those measured with the results from OPILE-API/ICP and the mod-API-FEA method suggested in this study.

The load-displacement diagram is shown in Figure 6-74. The values of Q_c/Q_m are given in Table 6-9.

Table 6-9 Comparison of Q_c/Q_m for the Pentre - LDP test using the OPILE and the mod-API-FEA results against the measured data.

Component	Q_c/Q_m			
	OPILE-API	OPILE-ICP	API direct	mod-API-FEA
Total	1.22	0.88	1.57	1.23
Shaft	1.47	0.98	1.88	1.50
Base	0.35	0.53	0.46	0.26

In this example, the mod-API-FEA over-predicts the capacity and the distribution can be improved. However, this is the case for all the methods used here.

6.4.1.2. Euripides 1c

The pile tests at Euripides (Test 1c) will now be used to compare the results estimated by the mod-UWA-FEA, as set out in Section 6.2.3, with those determined when the methodology, derived directly from the API, ICP and UWA methods, are input into OPILE.

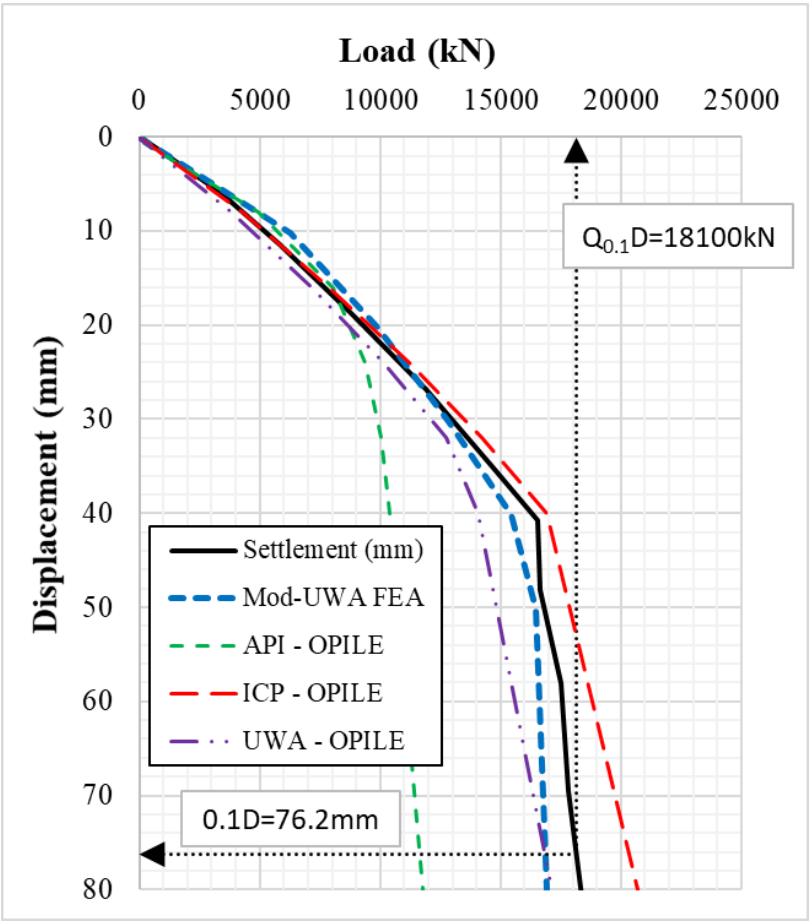

Figure 6-75 Load-displacement curve comparing those measured with the results from OPILE using the API, ICP and UWA methods, and the mod-UWA-FEA method suggested in this study.

The load-displacement diagram is shown in Figure 6-75. Here the response estimated by the mod-UWA-FEA has the best match to the measured data. The distribution of Q_c/Q_m is expanded on in Table 6-10.

Table 6-10 Comparison of Q_c/Q_m for the Euripides 1c test using the OPILE and the mod-UWA-FEA results against the measured data.

Component	Q_c/Q_m				
	OPILE-API	**OPILE-ICP**	**OPILE-UWA**	**UWA direct**	**mod UWA-FEA**
Total	0.64	1.12	0.93	0.95	0.93
Shaft	0.54	1.15	0.78	0.54	1.03
Base	1.01	1.04	1.45	2.40	0.57

In this example, although the distribution in the ICP method gives better results, the mod UWA-FEA has improved the distribution of the loads computed directly by the UWA.

6.5. Considerations on Capacity, Load-Transfer and Plugging

6.5.1. Pile and End Bearing Capacity

The capacity of an OEP is defined as the total capacity that can be supported after a pile head displacement of $0.1D_o$. However, this cannot be determined accurately when simplified expressions for the shaft friction and the base capacities are used. In OEPs, the shaft capacity is initially mobilised followed by the base. However, the full ultimate capacity of the shaft may not be mobilised at w_t=$0.1D_o$ and at this displacement, only a fraction of the ultimate base capacity may be mobilised. Some researchers have suggested methods for the total contribution of the base, but this entirely depends on the configuration of the pile, the installation method, the load applied and characteristics of the soil. In long piles, less of the base capacity may be mobilised but in weak stratigraphies, this will not be the case. In shorter piles, more of the base may be mobilised, however, to determine the percentage contribution, simplified methods do not accurately estimate this distribution. This research work has shown that numerical or FE methods are better at estimating the distribution given the number of factors that influence the result.

In terms of the displacement required to achieve full base capacity, depending on the stiffnesses of the interacting components, the full base capacity will never be reached in some OEPs, due to the large displacements necessary to mobilise base capacity. In these cases, it may be inaccurate to sum

both total shaft and end bearing capacities to obtain the total capacity, as the base capacity may or may not be mobilised within (the serviceability requirements) a pile head settlement of $0.1D_o$.

6.5.2. Load-Transfer in OEPs

From the initial testing that was performed on OEPs by Kishida (1967) (or even earlier by Széchy, 1959 & 1961), we have learnt that under loading, the behaviour of the resistive components in OEPs is different to those in CEPs. As the load is transferred through the different components, their interaction is the cause of this disparity.

As the OEP is loaded, the stiffness of the external shaft is usually highest, and mobilises initially as the pile deforms and load is transferred to the surrounding soil. This is then followed by the mobilisation of the end bearing on the annulus which transfers the load into the soil below. Internally, the shaft resistance is mobilised, but this load can only be transferred to the base of the plug, the effective transfer of which depends on the stiffness (M) of the combined layers of the plug and the stiffness of the soil at the base of the plug. The ultimate capacity of the plug is limited to the bearing capacity of the soil below its base. The relative displacement required to facilitate this process depends on the stiffnesses of these components.

The behaviour of the plug was found to be quite different in sands and clays. In sands, a larger value of base resistance was found in the analyses due to the interaction of the components exponentially increasing the rigidity of the soil at the base of the plug. In clays, the base resistance was found to be relatively lower, with the overall contribution of the plug usually small. The active plug length in clays was also much higher, which is most probably due to the loading of the pore water within the clay as the axial stress increased, suggesting unplugged behaviour.

6.5.3. Definition of Pile Plugging

From the analyses performed and the results discussed, the original definitions of a plugged and unplugged pile need to be refined.

The plugged condition is currently defined as the presence of a rigid plug of soil at the base of OEPs which effectively creates a CEP. In spite of this, Jardine *et al.* (2005) found that this led to a (50%) smaller capacity than at the base of CEPs. The base capacity, after $w_{b,p}$=$0.1D_o$, in a CEP will not

equal that of an OEP due to the softer load-transfer process. The transferral process that limits the mobilised capacity in an OEP is not observed in a CEP after an equivalent base displacement. During the installation of a CEP, the soil at the base of the pile becomes compressed and compacted, thereby increasing its bearing capacity. However, at the base of OEPs, although more compaction would be expected at the base of the annulus, a much less compacted state would be observed at the base the plug. This has been observed in CPT testing in the soil plug, after load tests performed at the Noetsu Bridge (Matsumoto et al, 1995).

A plugged OEP therefore does not strictly occur. The base settlement required to mobilise the full plug capacity will vary depending on the installation method, soil type, pile configuration and rate of loading. OEPs will therefore always act in a partially-plugged or fully unplugged (coring) mode under axial load. The mode depends on the active plug length mobilised. Researchers that consider a pile plugged are essentially assuming that the active plug length is very short; however, the capacity will not be the same compared to that of an equivalent CEP.

7. Conclusions and Recommendations

This work has investigated three established design methods for OEPs to determine if the use of a more accurate model of the plug is used, a better distribution of the applied load can be obtained. An initial investigation was made to each design method in clays (Section 4.2) and sands (Section 5.2) to determine if a factor could be applied to the shaft and base components to improve the overall distribution. The results of this analysis were then used in a finite element method which was specifically designed for this research and models the pile-plug-soil interaction (Chapter 3). The method was tested using a series of cases, using input from the design methods, to determine the key influences on open-ended pile behaviour and deduce recommendations for improvement of the method. The recommendations were used to determine a modified finite element variant of the design methods, and suggestions made on the most applicable stratigraphies where these methods should be applied. The research has found that although a thorough scientific process was followed, the results in Table 6-3 for clays and Table 6-6 for sands, suggest that the recommended method gives some nominal improvement to the distribution, although the improvement is not very evident from the values. The main improvement however, is the effective modelling the soil plug and capturing this behaviour better than what is currently performed in the industry. The main issue found with this task is its validation, as within the geotechnical engineering database for OEPs, there is a high variation in the reliability of measured shaft and base loads.

7.1. Conclusions

1. In long and slender piles, the shaft friction usually develops initially under axial static load, causing a very steep initial gradient of the load-displacement curve. In these piles, the pile compression causes more of the shaft friction to mobilise and a proportion of the end bearing may develop before the full shaft reaches its ultimate capacity. The initial slope of OEPs in sands with high L/D ratios is usually due to the shaft mobilisation and the shallower slope is due to the end bearing development (test case results in Chapter 4 and 5).

2. The only way to accurately determine the capacity of the plug is via the strains measured along the inner pile of a double wall arrangement. The Author suggests that in future research or experimentation using double walled piles, the inner and outer shaft capacity, and the end bearing on the annulus should be measured independently.
3. The load-transfer diagram, outlined in Chapter 2.9, gives a good representation of the load distributed to the resistive components of the pile. This diagram clearly depicts the load transferred to the annulus, plug base and external shaft. In addition, it can also give information on the active plug length which can inform the interpretation of a partially plugged or fully unplugged pile.
4. A one-dimensional finite element method which models the pile-soil-plug interaction and adopts the guidance outlined in this study is recommended for the analysis of OEPs. Design parameters to be input into the modified methods are to be obtained from the API, ICP and UWA methodologies with the recommendations outlined within this document.
5. The finite element variants of the design methods have been explored and the following conclusions have been reached:
    - The mod-API-FEA seems best suited for use in all-clay stratigraphies as demonstrated in Section 6.1.4. Table 6-3 shows the improvement in the estimated distribution, noting that the FEA method considers softening along the pile shaft, so these values would be lower.
    - The ICP method was shown to estimate the capacity distribution well in all-sand stratigraphies but was not as good as the API method in estimating the capacity distribution in all-clay stratigraphies (Table 4-3). This suggests that the mod-ICP-FEA method is the better design method for use in all-sand stratigraphies, noting that the estimated resistances for shaft and end bearing from the ICP methodology are the most critical component of the method. From the assessment performed using the sites with layered stratigraphies, Section 6.3.1, the mod-ICP-FEA is also the preferred method at these sites.
    - The mod-UWA-FEA method was investigated further in Section 6.2, following the results obtained in Section 5.2. The results shown in Table 6-6 were not as expected, demonstrating

that the originally estimated factor on σ'_{rc} was too high, and the factor on q_b was too low. As a result, intermediate factors of 1.5 and 0.75, applied to σ'_{rc} and q_b, respectively, in the mod-UWA-FEA method, are expected to improve the capacity distribution and are therefore recommended.

6. The research has also been able to outline a method for improving the Q-z relationship at the base of open-ended piles in Section 2.10, adopting the recommendations of Chapter 6. This method of computing the Q-z relationship could potentially be used to improve the model of the base capacity of OEPs. The recommended procedure for the updated Q-z curve is to:
   - adopt the suggestions presented in Section 6.1, 6.2 and 6.3 to obtain design and FE parameters to model the shaft and end bearing response;
   - compute the separate base response of the annulus and plug via the derived FE approach;
   - superimpose these responses to obtain the new Q-z soil reaction curve;
   - use these curves in conjunction with the API's t-z soil reaction curves to better estimate the axial resistance of an open-ended pile in a structural model.
7. Historically, the concept of a plugged pile was defined to facilitate an easier design process. From this study it has been found that all OEPs behave in either a partially-plugged or fully-unplugged mode. Relative displacement at the base of an OEP causes the mobilisation of the internal shaft friction which mobilises the soil plug. The base of the plug column then reacts against the soil below the plug and the total load transferred is limited by the bearing capacity of this component. For an efficient load-transfer, the stiffness of the individual components needs to be quite high. In clays, undrained strength parameters define the stiffness of the plug leading to a much longer active plug length mobilised (Chapter 4). In sands, an exponential increase in the mean effective stress is usually observed, due to dilation especially near the base, which causes the active plug length to be relatively short, usually about 1-2 times the external diameter of the pile (Chapter 5).
8. In Section 6.4, the mod-API-FEA and mod-UWA-FEA methods have been compared against OPILE, an established numerical and industry pile design software which does not directly model

the plug, and these new FE methods have proven to give quite good results.

7.2. Recommendations

Based on the results of this work, the following suggestions are recommended:

1. Further work is to be done on the constrained modulus value with depth. For sands this has been estimated using the measured q_c values at the site and the relationships outlined by Lunne and Christophersen (1983). In clays this has been taken as a factor of up to $4000s_u$.
2. One of the main assumptions used in this work is the wishing-in-place of the OEP. By making this assumption, the residual stresses are assumed to be zero in both soil and pile which can cause the end bearing to be underestimated and friction to be overestimated (Kraft 1990). The Author suggests that more work can be done on driveability, which has the potential to directly inform the initial residual stress in the pile and soil after driving. This will therefore improve the estimate of static pile capacity.
3. The end bearing on the annulus of an open-ended pile should be related to the averaged q_c value at its intended depth. In this study, simple factors were applied based on available data to replicate the trends observed. However, in fine-tuning these factors, additional parameters such as OCR, derived using friction and pore-pressure ratios from CPT measurements, should be considered, and then validated against the measured strains at the Pentre and Tilbrook sites. Once updated, this should improve the estimate of resistance below the annulus and plug, and further increase the capability of the numerical method.

8. References

1. American Petroleum Institute Recommended Practice 2GEO, Geotechnical and Foundation Design Considerations, API RP 2GEO, Apr 2011. Addendum issued Oct 2014.
2. Atkins confidential report, (2013).
3. Benson, A. Taylor, P., Guinard, M., 2013. Atkins Technical Note TN001 – Study 2a & 2b: Axial Pile Capacity Method and Pile Plugging. For DONG Energy.
4. Brucy, F., Meunier, J. and Nauroy, J.F., 1991. Behaviour of pile plug in sandy soils during and after driving. In *Proc. Offshore Technol. Conf., Houston*, OTC-6514.
5. Chow, F. *Investigations into displacement pile behaviour for offshore foundations*. PhD. Diss. Imperial College London (University of London), 1997.
6. Clarke, J., 1993. Large Scale Pile Tests in Clay. Thomas Telford, London.
7. Clausen, C.J.F., Aas, P.M., & Karlsrud, K. (2005). Bearing capacity of driven piles in sand, the NGI approach. In M. J. Cassidy, & S. Gourvenec (Eds.), Proc. of the *Int. Sym. on Frontiers in Offshore Geotechnics* (Perth, Australia ed., Vol. n/a, pp. 574-580). The Netherlands: CRC Press/Balkema.
8. Cox, W.R., Solomon, I.J. and Cameron, K., 1993. Instrumentation and calibration of two 762 mm diameter pipe piles for axial load tests in clays. In *Large-scale pile tests in clay* (pp. 217-236). Thomas Telford Publishing.
9. Coyle, H.M. and Reese, L.C., 1966. Load transfer for axially loaded piles in clay. *J. of the Soil Mech. and Fdns Div., 92(2),* pp.1-26.
10. Coyle, H.M. and Sulaiman, I.H., 1967. Skin friction for steel piles in sand. *J. of the Soil Mech. and Fdns Div., 92(6),* pp. 261-278.
11. Darragh, R., and R. Bell. Load tests on long bearing piles. *Performance of deep foundations.* ASTM International, 1969.
12. De Nicola, A. and Randolph, M.F., 1997. The plugging behaviour of driven and jacked piles in sand. *Geotechnique, 47(4),* pp.841-856.
13. Duncan, J.M. and Chang, C.Y., 1970. Nonlinear analysis of stress and strain in soils. *J. of the Soil Mech. and Fdns Div., 96(5),* pp. 1629-1653.
14. Gao, D.Z., Wei, D.D. and Hu, Z.X., 1986. Geotechnical properties of Shanghai soils and engineering applications. In *Mar. Geo. and Nearshore/Offshore Structures*. ASTM International.
15. Gibbs, C.E., McAuley, J., Mirza, U.A. and Cox, W.R., 1993. Reduction of field data and interpretation of results for axial load tests of two 762 mm diameter pipe piles in clays. In *Large-scale pile tests in clay* (pp. 285-345). Thomas Telford Publishing.
16. Heerema, E.P. and De Jong, A., 1980. An advanced wave equation computer program which simulates dynamic pile plugging through a coupled mass-spring system. In *Numerical methods in offshore piling* (pp. 37-42). Thomas Telford Publishing.
17. Hight, D.W., Lawrence, D.M., Farquhar, G.B., Mulligan, G.W., Gue, S.S. and Potts, D.M., 1996, January. Evidence for scale effects in the end bearing capacity of open-ended piles in sand. In *Proc. Offshore Technol. Conf., Houston*, OTC-7975.
18. Holeyman, A.E. ed., 2001. *Screw piles-installation and design in stiff clay*. CRC Press.
19. Houlsby, G.T., 2018, notes for Offshore Foundation Design module, Renewable Energy Marine Systems (REMS) 2018.

20. Houlsby, G.T. and Puzrin, A.M., 2006. Principles of hyperplasticity: an approach to plasticity theory based on thermodynamic principles. Springer Science & Business Media.

21. Iskander, M., 2011. Behaviour of Pipe Piles in Sand: Plugging & Pore-Water Pressure Generation During Installation and Loading. Springer Science & Business Media.

22. Jardine, R., Chow, F., Overy, R., and Standing, J., 2005. *ICP design methods for driven piles in sands and clays* (p. 112). London: Thomas Telford, 2005.

23. Jardine, R.J., Fourie, A., Maswoswe, J. and Burland, J.B., 1985. Field and laboratory measurements of soil stiffness. In Proc., *11th Int. Conf. on Soil Mech. and Fdn. Eng.* (Vol. 2, pp. 511-514). Rotterdam, The Netherlands: Balkema.

24. Jeong, S., Ko, J., Won, J. and Lee, K., 2015. Bearing capacity analysis of open-ended piles considering the degree of soil plugging. *Soils and Foundations*, 55(5), pp.1001-1014.

25. Jia, J., 2018. Axial Force–Displacement of Piles: t-z and Q-z Curve. In: Soil Dynamics and Foundation Modelling. Springer, Cham.

26. Joseph, T.M., Burd, H.J., Houlsby, G.T., and Taylor, P., 2018. One-dimensional finite element analysis of soil plug behaviour within open-ended piles. In Cardoso et al. (Eds.) *Proc. Of the 9th European Conference on Numerical Methods in Geotechnical Engineering (NUMGE 2018)*, Porto, Portugal. Vol. 2, pp. 1493-1500, Taylor and Francis Group, London.

27. Joseph, T.M., Houlsby, G.T., Burd, H.J. and Taylor, P., 2017, January. Finite Element Analysis of Soil Plug Behaviour within Open-Ended Piles. In *Offshore Site Investigation Geotechnics 8th Int. Conf. Proc.* (Vol. 628, No. 635, pp. 628-635). Society for Underwater Technology.

28. Kishida, H., 1967, September. The ultimate bearing capacity of pipe piles in sand. In *Proc. of the 3rd Asian Reg. Conf. on Soil Mech. and Fdn Eng., Haifa, Israel* (pp. 25-28).

29. Kishida, H., and Isemoto, N., 1977. Behaviour of sand plugs in open ended steel pipe piles. *Proc. 9th Int. Conf. on Soil Mech. and Fdn. Eng.*, Tokyo (Vol. 1, No. 1, pp. 601-604).

30. Kishida, H., Uesugi, M. and Susumu, M., 1985. Behaviour of dry sands in steel pipe piles. *Proc. 8th Southeast Asian Geotechnical Conf*., Kuala Lumpur.

31. Klevsjø, C., 2014. *Numerical Modelling of Cyclic Loading on Clay* (Master's thesis, Institutt for bygg, anlegg og transport).

32. Kolk, H. J., Baaijens, A. E., & Senders, M. (2005). Design criteria for pipe piles in silica sands. In M. J. Cassidy, & S. Gourvenec (Eds.), Proc. of the *Int. Sym. on Frontiers in Offshore Geotechnics* (Perth, Australia ed., Vol. n/a, pp. 711-716). The Netherlands: CRC Press/Balkema.

33. Kondner, R.L., 1963. Hyperbolic stress-strain response: cohesive soils. *J. of the Soil Mech. and Fdns Div., 89*(1), pp.115-144.

34. Kraft Jr, L.M., 1990. Computing axial pile capacity in sands for offshore conditions. *Marine Georesources & Geotechnology*, *9*(1), 61-92.

35. Kraft Jr, L.M., Cox, W.R. and Verner, E.A., 1981. Pile load tests: Cyclic loads and varying load rates. *J. Geotech. Geoenviron. Eng*., 107, pp. 1-19 (ASCE 16000).

36. Kraft Jr, L.M., Ray, R.P. and Kagawa, T., 1981. Theoretical t-z curves. *J. Geotech. Geoenviron. Eng., 107,* pp. 1543-61, (ASCE 16653).

37. Kulhawy, F.H. and Jackson, C.S., 1989, June. Some observations on undrained side resistance of drilled shafts. In *Fdn Eng.: Current principles and practices* (pp. 1011-1025). ASCE.

38. Kusakabe, O., Matsumoto, T., Sanadabata, I., Kosuge, S. and Nishimura, S., 1989, August. Report on questionnaire: Predictions of bearing capacity and drivability of piles. In *Proceedings of the 12th Int. Conf. on Soil Mech and Fdn. Eng., Rio de Janeiro, Brazil* (Vol. 5, pp. 2957-2963).

39. Lambson, M.D., Clare, D.G., Senner, D.W.F. and Semple, R.M., 1993. Investigation and interpretation of Pentre and Tilbrook Grange soil conditions. In *Large-scale pile tests in clay* (pp. 134-196). Thomas Telford Publishing.

40. Lehane, B.M. and Gavin, K.G., 2001. Base resistance of jacked pipe piles in sand. *J. Geotech. Geoenviron. Eng., 127*(6), pp.473-480.

41. Lehane, B.M., Jardine, R.J. and McCabe, B.A., 2003. Pile group tension cyclic loading: Field test programme. *Imperial College Consultants (ICON).*

42. Lehane, B.M. and Randolph, M.F., 2002. Evaluation of a minimum base resistance for driven pipe piles in siliceous sand. *J. Geotech. Geoenviron. Eng., 128*(3), pp.198-205.

43. Lehane, B.M., Schneider, J.A. and Xu, X., 2005. The UWA-05 method for prediction of axial capacity of driven piles in sand. In M. J. Cassidy, & S. Gourvenec (Eds.), Proc. of the *Int. Sym. on Frontiers in Offshore Geotechnics* (Perth, Australia ed., Vol. n/a, pp. 683-689). The Netherlands: CRC Press/Balkema.

44. Leong, E.C. and Randolph, M.F., 1991. Finite element analyses of soil plug response. *Int. J. for Numerical and Analytical Methods in Geomechanics, 15*(2), pp.121-141.

45. Liyanapathirana, D.S., Deeks, A.J., & Randolph, M.F., 1998. Numerical analysis of soil plug behaviour inside open-ended piles during driving. *Int. J. for Numerical and Analytical Methods in Geomechanics*, 22(4), 303-322.

46. Liyanapathirana, D.S., Deeks, A.J., & Randolph, M.F., 2001. Behaviour of Thin-Walled Open-Ended Piles During Driving. *In Computational Mechanics–New Frontiers for the New Millennium* (pp. 393-398).

47. Lüking, J. & Kempfert, H.G., 2013. Plugging effect of Open-Ended Displacement Piles. *Proc. of the 18th Int. Con. on Soil Mechanics and Geotech. Eng.*, Paris (pp. 2363-2366).

48. Lunne, T. and Christoffersen, H.P., 1983, January. Interpretation of cone penetrometer data for offshore sands. In *Proc. Offshore Technol. Conf., Houston*, OTC-4464.

49. Matsumoto, T., Sekiguchi, H., Shibata, T. and Fuse, Y., 1992. Performance of steel pipe piles driven in Pleistocene clays. In *Proc., 4th Int. Conf. Appl. Stress-Wave Theory to Piles* (pp. 293-298).

50. Mendoza, R.C., 2004. *Determination of Lateral Stresses in Boom Clay using a Lateral Stress Odometer* (Master's thesis, International Institute for Geo-Information Science and Earth Observation, Enschede, The Netherlands).

51. Murff, J.D. Raines, R.D. & Randolph, M.F., 1990. Soil plug behaviour of piles in sand. In *Proc. Offshore Technology Conference., Houston*, OTC-6421, pp 25-42.

52. O'Neill, M.W. and Raines, R.D., 1991. Load transfer for pipe piles in highly pressured dense sand. *Journal of Geotechnical Engineering, 117*(8), pp.1208-1226.

53. OPILE, Single pile axial and lateral analysis, 2018, Cathie and Associates.

54. Paik, K.H. and Lee, S.R., 1993. Behaviour of soil plugs in open-ended model piles driven into sands. *Marine Georesources & Geotechnology, 11*(4), pp.353-373.

55. Paik, K., Salgado, R., Lee, J. Kim, B. 2003. Behaviour of open-and closed-ended piles driven into sands. *J. Geotech. Geoenviron. Eng.* 129.4, pp. 296-306.

56. Pando, M.A., Ealy, C.D., Filz, G.M., Lesko, J.J. and Hoppe, E.J., 2006. A laboratory and field study of composite piles for bridge substructures (No. FHWA-HRT-04-043). United States. Federal Highway Administration. Office of Infrastructure Research and Development.

57. Pump, W., Korista, S. and Scott, J., 1998. Installation and load testing of deep piles in Shanghai alluvium. *In Proc. of the 7th Int. Con. on Deep Fdns., Vienna, Austria. Paper* (Vol. 13, pp. 1-3).

58. Ramsey, N., Sharma, S. and Lee, F., 2017, January. Multi-Laboratory Assessments of Cyclic Soil Behaviour. In *Offshore Site Investigation Geotechnics 8th Int. Conf. Proc.* (Vol. 1232, No. 1237, pp. 1232-1237), Society for Underwater Technology.

59. Randolph, M.F., Leong, E.C. and Houlsby, G.T., 1991. One-dimensional analysis of soil plugs in pipe piles. *Geotechnique*, 41(4), pp.587-598.

60. Randolph, M.F. and Wroth, C.P., 1978. Analysis of deformation of vertically loaded piles. *J. Geotech. Geoenviron. Eng.*, 104 (ASCE 14262).

61. Randolph, M.F. and Wroth, C.P., 1982. *Recent developments in understanding the axial capacity of piles in clay*. University of Oxford Department of Engineering Science.

62. Salgado, R., Lee, J., Kim, K., and Paik, K., 2002. *Load Tests on Pipe Piles for Development of CPT-Based Design Method*. Joint Transportation Research Program, Project No. C-36-45R, Report No: FHWA/IN/JTRP-2002/4.

63. Schneider, J.A., Xu, X. and Lehane, B.M., 2008. Database assessment of CPT-based design methods for axial capacity of driven piles in siliceous sands." *J. Geotech. Geoenviron. Eng.* 134.9 pp. 1227-1244.

64. Schneider, J.A., Xu, X., and Lehane, B.M., 2010. End bearing formulation for CPT based driven pile design methods in siliceous sands. In *2nd Int. Sym. on Cone Penetration Testing*.

65. Széchy, C.H., 1959. Tests with tubular piles. *Acta Technica* of the Hungarian Academy of Science, *Vol 24*, pp.181-219.

66. Széchy, C.H., 1961, July. The effect of vibration and driving upon the voids in granular soil surrounding a pile. In *Proc. 5th Int. Con. on Soil Mech. and Fdn. Eng., Paris* (Vol. 2, pp. 161-164).

67. Vijivergiya, V.N., 1977. Load-movement characteristics of piles. In *4th Symp. of Waterway, Port, Coastal and Ocean Div., ASCE* (Vol. 2, pp. 269-284).

68. Williams, R.E., Chow, F.C. and Jardine, R.J., 1997, May. Unexpected behaviour of large diameter tubular steel piles. In *Proc. Int. Conf. on Foundation Failures* (pp. 363-378). IES, NTU, NUS and Inst. Structural Engineers Singapore.

69. Woodward, R.J., Lundgren, R. and Boitano, J.D., 1961, July. Pile loading tests in stiff clays. In *Proc. 6th Int. Con. on Soil Mech. and Fdn. Eng, Paris* (pp. 177-184).

70. Xu, X., Schneider, J.A. and Lehane, B.M., 2008. Cone penetration test (CPT) methods for end-bearing assessment of open-and closed-ended driven piles in siliceous sand. *Can. Geo. J.*, *45*(8), pp.1130-1141.

71. Yang, Z., Jardine, R., Guo, W. and Chow, F., 2015. *A Comprehensive Database of Tests on Axially Loaded Piles Driven in Sand*. Academic Press.

Supplementary Material

Appendix A – Paper 1:
Finite Element Analysis of Soil Plug Behaviour within Open-Ended Piles

Joseph, T.M., Houlsby, G.T., Burd, H.J. and Taylor, P., 2017. Finite Element Analysis of Soil Plug Behaviour within Open-Ended Piles. In *Offshore Site Investigation Geotechnics 8th International Conference Proceeding* (Vol. 628, No. 635, pp. 628-635). Society for Underwater Technology.

FINITE ELEMENT ANALYSIS OF SOIL PLUG BEHAVIOUR WITHIN OPEN-ENDED PILES

TM Joseph, GT Houlsby and HJ Burd
Department of Engineering Science, University of Oxford, UK
P Taylor
Atkins Ltd, Warrington, UK

Abstract
Current design standards for offshore open-ended piles vary in their consideration of the soil plug's contribution to the pile's axial capacity and, indirectly, to its stiffness. API RP2 GEO (2011) and UWA-05 (Lehane et al., 2005) consider the contribution of the plug, but ICP-05 (Jardine et al., 2005) combines the plug capacity with the end bearing from the pile annulus. The current study critically examines the behaviour of the plug using a specifically-designed 1D finite element method, developed to model each component of the plug-pile-soil interaction. The load-transfer into the surrounding soil and base is modelled using non-linear axial soil reaction curves. Using this methodology, a theoretical assessment of the contribution of the soil plug to the pile axial performance can be made. The findings of this theoretical assessment are compared to the current treatment of soil plug response in the design standards.

1. Introduction

1.1 Outline of paper

The American Petroleum Institute's (API) method for axial pile capacity of driven open-ended piles (OEPs) is widely used in the offshore oil and gas industry. However, as the industry continues to develop, more reliable pile design methods, such as the Imperial College Pile (ICP) and the University of Western Australia's (UWA) methods have been developed. Each of these methods has improved the reliability of axial pile capacity prediction. However, additional research may assist in further optimising the pile length further. The current paper examines how plug capacity is analysed in each design method and examines the conditions controlling plugging post-installation under static loading in cohesionless soils.

The plug capacity is analysed with a 1D finite element analysis (FEA) design tool, specifically written for the investigation of plug behaviour, which computes the mobilisation of resistance in the pile, plug and surrounding soil. The FEA tool uses the external shaft friction and end bearing capacity from the API, ICP and UWA design methods. Soil reaction curves are applied to individual components allowing a gradual mobilisation of soil resistance. Total base capacities derived from the tool are compared with those calculated directly using the design methods to gain insight into the incremental mobilisation of each component of capacity. Piles with low ratios of length/diameter (L/D), such as offshore wind monopiles, are less prone to plugging than longer piles. This initial study examines jacket type piles with L/D ratios greater than 10.

One of the main difficulties encountered in calibrating the finite element model is the lack of published data on open-ended pile tests which effectively isolate the base and shaft capacity, and even less that isolate the internal shaft friction. As a result, a carefully selected database was used to validate the model and perform the comparisons.

1.2 Outline of pile plugging

When OEPs are driven or loaded, plug-pile interaction can occur in different modes. In a plugged mode the core of soil moves entirely with the pile and failure of the soil beneath the plugged pile occurs. In an unplugged mode, the core of soil remains approximately static, while the pile shears past the plug. The other mode is partially plugged where the soil column within the pile is essentially compressed from the base upwards without total shear failure.

Whilst most piles drive unplugged, principally because of dynamic effects causing failure at the soil-pile interface, their subsequent behaviour during

(quasi) static loading is less certain. This behaviour is governed by a number of factors including soil arching, high values of internal friction and strong dilatancy (Jardine et al., 2005). However, as pile length-to-diameter ratio increases the pile is less susceptible to plugging.

1.3 Pile plugging research

Soil plug behaviour has been investigated by various researchers, including Kishida (1967); Paikowsky (1989); Matsumoto and Takei (1991); Randolph et al. (1991); Salgado et al. (2002); Lehane and Randolph (2002); Jeong and Ko (2015). Some of these researchers suggest that piles fail in a plugged manner while others argue otherwise.

Under increasing load, the pile may retain its unplugged state or move to a partially or fully plugged condition. A fully unplugged pile will only develop when the cumulative internal shaft resistance is less than the base stress on the plug.

Early researchers such as Kishida and Isemoto (1977) found that the internal shaft resistance, τ_i, increases non-linearly towards the tip of the pile. Different researchers have proposed various explanations for this phenomenon. Paikowsky (1989) linked soil plugging to the internal arching behaviour of grains in a silo, similar to the shape of the soil layers in extruded tube samples. He suggested that the silo effect creates downward concave arches in the soil plug that increase the soil stresses and therefore τ_i near the base. He suggested that as the pile diameter increases, this arching is less effective and leads to plug failure (unplugging).

Randolph et al. (1991), suggested that when a load is applied to the base of the plug, the increasing axial stress causes an increased lateral stress thereby increasing τ_i (Figure 1). They suggested that this will increase exponentially with increasing ratio of plug length to internal pile diameter, L_{pl}/D_i. In their paper, a 1D plug analysis method for drained, undrained and partially drained soil is set out. For a drained cohesionless soil, the end bearing capacity is normally a result of pile plugging due to arching action within the plug. For undrained conditions, where insufficient time is available for drainage, the excess pore water pressure supports the load but without an increase in τ_i.

Experiments by Lehane and Gavin (2001) on model piles in sand, using a testing chamber, agree with the method outlined by Randolph et al. (1991). However, they also suggested that the sand near to the pile tip dilates, increasing the internal radial stress and the internal shaft friction thereby generating a plugged response.

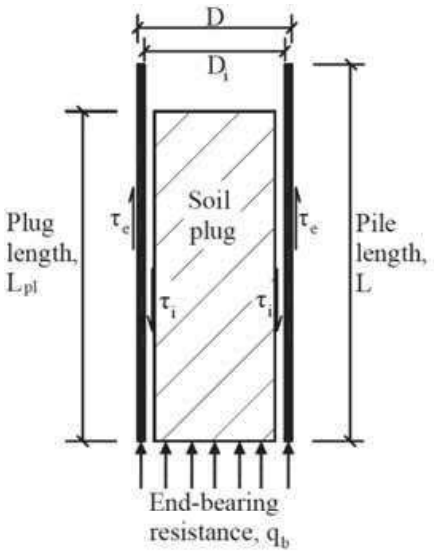

Figure 1: Pile, plug and base resistance interactions. The external and internal shaft friction are represented by τ_e and τ_i, respectively.

Chow (1997) and Jardine et al. (2005), concluded that plugging in sand is a function of pile diameter, relative density and the dilation properties of the soil along the internal pile walls. This research suggests that the greatest susceptibility to plugging occurs in small diameter piles installed in dense sand.

2. Industry methods of base capacity estimation

Each of the main design methods make varying assumptions and use derived relationships from different databases. The methods, therefore, typically do not produce equal pile lengths for a given set of design requirements.

2.1 The API method

The API considers the summation of the shaft resistance over the internal shaft area of the pile, $\int \tau_i P_i . dz$, where P_i is the internal pile perimeter integrated over the full pile length incrementally through thicknesses of height dz, compared to the end bearing (EB) capacity of the plug, $q_b A_{plug}$. The lesser of these is added to the end bearing on the pile annulus, $q_b A_{ann}$, to derive the end bearing capacity, Q_b.

$$Q_b \text{ (unplugged)} = q_b A_{ann} + \int \tau_i P_i . dz \quad (1)$$

$$Q_b \text{ (plugged)} = q_b \left(A_{ann} + A_{\text{plug}}\right) \quad (2)$$

where q_b = end bearing resistance, A_{ann} = area of the annulus, and A_{plug} = base area of the plug. The end bearing resistance on the base for sands is related to the effective overburden pressure by $q_b = N_q \sigma'_{vo}$ (where $8 \leq \text{N}_\text{q} \leq 50$) and a function of relative density.

There is no proof that the API base capacity is reliable, but rather simply, a track record of API designed piles not failing. Whilst the API has the advantage of simplicity, drawbacks include:

- This method is unreliable in silts and loose sands and underestimates capacity in dense sands (Lehane et al., 2005).
- The radial effective stress, σ'_r, is proven to change significantly non-linearly with depth (Jardine et al., 2005) but is assumed to increase proportionally with vertical effective stress.
- The stress regimes on either side of the pile wall are assumed equal even though these are likely to be different.

2.2 The ICP method

This design method assumes that the total pile capacity is fully mobilised after a pile head displacement of $0.1D$ (where D is the external diameter). The external shaft friction is considered explicitly but any contribution to base capacity from the internal shaft friction is lumped together within the annular end bearing (EB) capacity. Therefore it is difficult to isolate the mobilisation of the internal and external shaft friction capacities under gradually increasing load.

From a small dataset, two criteria were derived to predict plugged behaviour in cohesionless material. These are:

$$D_i(m) < 0.02[D_R(\%) - 30] \quad (3)$$

$$D_i/D_{CPT} < 0.083 q_c/P_a \quad (4)$$

where D_R = relative density, D_{CPT} = diameter of the CPT cone, q_c = cone tip resistance and P_a = atmospheric pressure. The corollary of these equations is that any pile with $D_i > 1.4\text{m}$ is considered to be unplugged.

Pile tests used to derive the ICP method demonstrate the base capacity, Q_b, is about 50% of that from equivalent sized closed-ended piles. This is due to the softer response of the base of the soil plug under axial load. This capacity reduction is therefore applied to derive the expression for base resistance, q_b, in OEPs that meet the plugging criteria.

$$Q_b \text{ (plugged)} = q_b(A_{ann} + A_{\text{plug}}) \quad (5)$$

$$q_b = q_c[0.5 - 0.25\, log(D/D_{CPT})] \quad (6)$$

To determine the unplugged resistance, this method indirectly allows for a contribution from internal shaft friction, τ_i, by the expression

$$q_b \text{ (unplugged)} = q_c \quad (7)$$

This method indicates that q_b on the annulus, is typically $0.7q_c$, due to the different geometry of the pile tip relative to a CPT cone. The remaining $0.3q_c$ is taken as the contribution from τ_i up 30 to 40 wall thicknesses (t) above the toe.

The ICP method has been based on the results of geotechnical testing in the laboratory and in the field. Although relatively detailed, it is noted that:

- There are no base response procedures.
- None of the interpretations from published research performed on the plug, such as Matsumoto and Takei (1991); Randolph et al. (1991); Salgado et al. (2002), are directly included in the ICP methodology.
- The method does not consider the length or the effects of a change in length of the plug to the behaviour of the OEP under static loading.

2.3 The UWA method

This method originated from research by the University of Western Australia on the comparison of the Fugro-04 method (Fugro, 2004), the ICP method and the NGI-04 method (Clausen et al., 2005) on behalf of the API Committee.

In the UWA method the soil plug is considered more directly by the use of the final filling ratio (FFR) value. This is the final value of the incremental filling ratio (IFR), the change in plug length to change of penetration during driving ($IFR = \Delta L_{pl}/\Delta L_p$) upon reaching the target pile penetration depth. When the $IFR = 0$, the pile is fully plugged, when $0 < IFR < 1.0$, the pile is partially plugged and when $IFR = 1.0$, the pile is unplugged. As the FFR cannot be known before installation, an empirical relationship is provided for it. The method indicates that if $L_{PL} > 5D_i$, then the pile will behave in a plugged manner under static loading irrespective of pile diameter. The method of computing Q_b for an open-ended pile using the UWA method is as follows:

$$Q_b \text{ (plugged)} = q_b\left(A_{ann} + A_{plug}\right) \quad (8)$$

$$q_b = q_c[0.15 - 0.45{A_{rb}}^*] \quad (9)$$

$${A_{rb}}^* = 1 - FFR\left({D_i}^2/D^2\right) \quad (10)$$

$$FFR \approx min[1, (D_i/1.5)^{0.2}] \quad (11)$$

Limitations of the UWA method include:

- It is adopted for use with sands only. Approximations have been outlined for thin clay layers, but this method is not applicable in typical layered stratigraphies or if the pile tip bears in a clay layer.
- No consideration of a change in the length of the plug is adopted in this method.

In addition, in all of these three methods, the pile is assumed rigid although the empiricism used to deduce each method, relies on the compression of the test pile to derive relationships.

3. Plug specific experimentation

If the behaviour of the soil plug is to be critically assessed, appropriate forms of pile testing are needed to isolate the internal and external soil behaviour. A double walled pile system can effectively separate the internal, external and end bearing resistances. The layout in Figure 2 is an example of this arrangement by Salgado et al. (2002). Similar work has been done by Paik and Lee (1993); Lehane and Gavin (2001); Doherty et al. (2010); Ko and Jeong (2015).

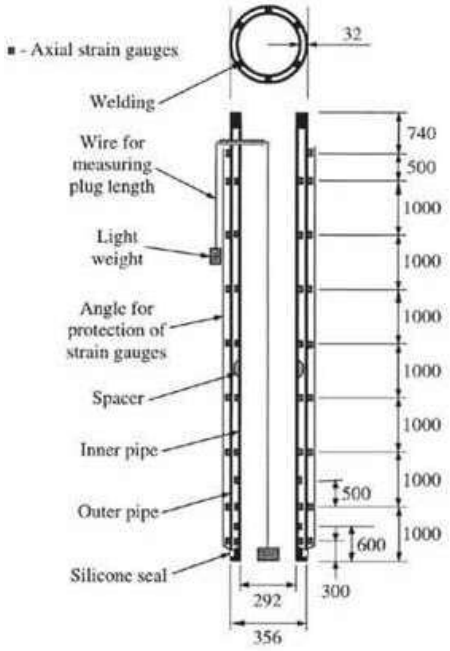

Figure 2: Schematic of open-ended test pile (Salgado et al., 2002)

The pile testing performed by Salgado et al. (2002) used an 8.24m long, instrumented, double walled pile. The internal pile extended below the external pile to form the end bearing on the annulus. Their interpretation of the base capacity mobilisation is shown in Figure 3. This diagram shows the vertical load in the soil plug after the final increment of load is applied. It can be seen that the total base capacity is distributed between the pile annulus and the plug. The majority of the plug load is seen to be transferred between the plug and the pile shaft by friction near the base of the plug.

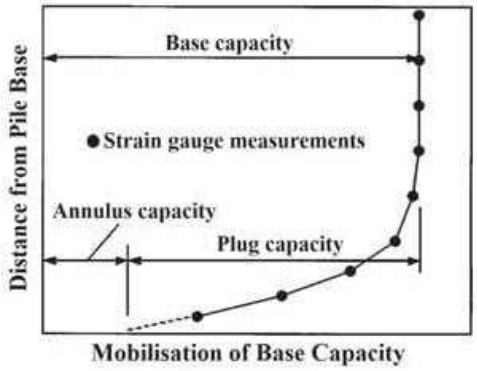

Figure 3: Mobilisation of base capacity (adapted from Salgado et al., 2002; Paik et al., 2003)

Further testing to the same scale was performed by Jeong and Ko (2015). Their findings were quite similar to the plug behaviour observed by Salgado et al. (2002) using this methodology. This behaviour specifically showed the following process as an open-ended pile is statically loaded:

- The load is initially taken by the upper part of the external pile which experiences elastic compression.
- The annulus resistance starts to mobilise with the mobilisation of the external shaft resistance over the entire length of the pile i.e. when the pile toe moves relative to the adjacent soil
- The internal shaft friction starts to mobilise at the same time as the annulus, with attenuating upward stresses.

None of the main pile design methods capture these processes directly and therefore do not enable the mobilisation and distribution of the internal and external shaft and annulus resistances to be identified seperately. This process can, however, be captured using a mathematical model which can be solved by using a finite element method. A modelling approach for this purpose is described below.

4. Analysis

A 1D finite element model is used to solve the equilibrium equations that balance the load in the pile, plug, soil, interfaces and on the base. The arrangement of the FEA is shown in Figure 4. Here the soil, pile and plug are discretised as 2-noded elements with the interfaces adopting 4-noded elements.

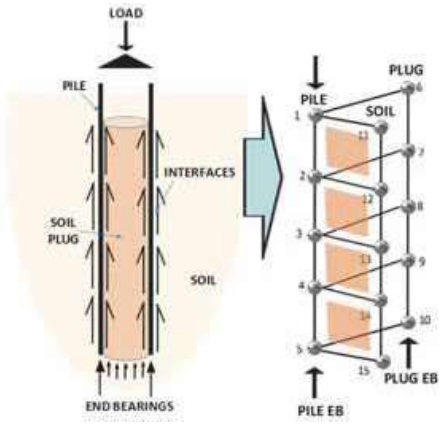

Figure 4: Simple discretised 1D model of pile-plug-soil, interfaces and bearing components

To validate the output of the FEA, the database assembled by Chow (1997); Jardine et al. (2005); Lehane et al. (2005); and Yang et al. (2015), was used, selecting only driven open-ended pipe piles, under static compression. The data from these tests were found to vary considerably. These range from only total capacity being provided to others where a detailed breakdown being available. Seven tests that matched these required criteria and which had at least a clear separation of shaft and base capacities were used in the analysis. In addition, the three double wall pile tests performed by Ko and Jeong (2015), were included in the analysis requiring q_c values to be correlated from standard penetration test (SPT) results using Kulhawy & Mayne (1990).

Table 1: Pile load tests considered for the analysis.

Test Number	Site	Reference Authors
1	Pigeon creek	Salgado et al. (2002)
2 – 4	Kwangyang Plant	Ko, J. & Jeong, S. (2015)
5	Hoogzand	Beringen (1979)
6 – 9	Euripedes	Kolk et al. (2005b)
10	Tokyo Bay	Shioi et al. (1992)

The measured site data and test pile lengths were used to calculate API, ICP and UWA capacities. The ultimate shaft and end bearing stresses from each method were used as input parameters to the finite element analysis with the non-linear axial load transfer methodology adopted from API RP2 GEO (2011). More specifically the parameters included:

- The external and internal shaft friction values, τ_e and τ_i respectively, with full mobilisation occurring at a shear displacement of $0.01D$ in each element. For this assessment, τ_e and τ_i were assumed equal, with full mobilisation occuring progressively during the FEA.
- The end bearing of a plugged pile, q_b, is applied separately to the annulus area and the plug area. The peak capacity occurrs at 1% of the wall thickness ($0.01t$) and 10% of the plug diameter ($0.1D_i$), respectively.
- Constant values of Young's modulus were deduced from interpreted values of shear modulus, from q_c, and applied as the axial stiffness of the plug per element.

The finite element method was then used to compute the strains and evaluate the displacements, stresses and forces in each of the components under increasing levels of axial load.

5. Results

There are a limited number of tests performed where the end bearing on the pile annulus and soil plug is specifically obtained. However, more test results are available for the total base capacity, Q_b. Figure 5 and Figure 6 show the values of the ratio of calculated to measured values (Q_c/Q_m) of total base capacity Q_b against the L/D and D/t ratio. The Q_c values are those computed directly from the respective design method (API, ICP or UWA) and those calculated using the new FEA (API-FEA, ICP-FEA or UWA-FEA) at a pile-head displacement of $0.1D$. As shown in the figures, using the Q_c values from FEA, the Q_c/Q_m ratios are close to unity indicating the FEA tool predicts base mobilisation more reliably than the design standards.

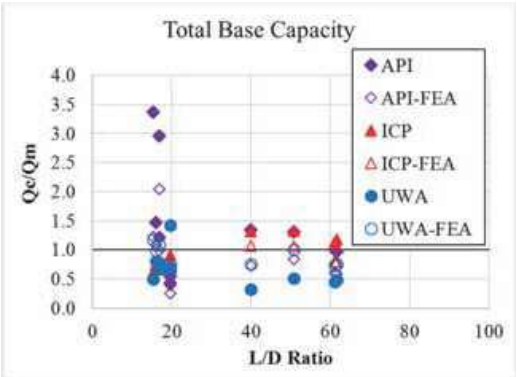

Figure 5: Distribution of Q_c/Q_m for the total base capacity against the pile slenderness ratio

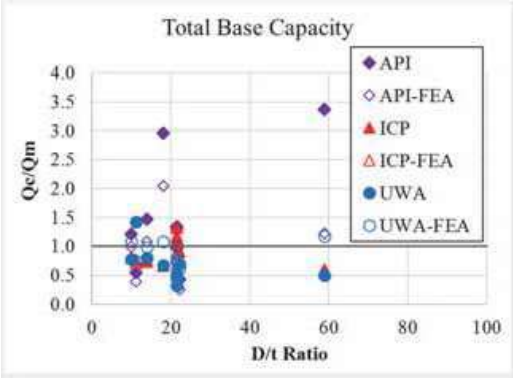

Figure 6: Distribution of Q_c/Q_m for the total base capacity against the pile diameter to thickness ratio

In Table 2 to Table 4, the ratios of Q_c/Q_m directly derived from the design methods are compared to those derived from the FEA for those sites where double walled piles have been used. The values are presented for each component so that their respective contribution can be clearly seen. The ratios of Q_c/Q_m for the end bearing on the pile and the total shaft friction, are constant, for both the direct calculations and the FEA as these components are the first components to be fully mobilised. The base capacity of the plug, and therefore the total base capacity, is directly affected by the use of the FEA.

Table 2: Ratio of Q_c/Q_m for the API and API-FEA analysis.

Test Location	Q_c/Q_m Ratio	Total Pile Capacity	Total Shaft Friction	Total End Bearing	End Bearing Pile	End Bearing Plug
Pigeon Creek	Direct	0.56	0.61	0.54	0.28	0.98
	FEA	0.46	0.61	0.39	0.28	0.57
K. Plant TP1	Direct	0.81	0.52	1.21	0.54	4.06
	FEA	0.72	0.52	0.99	0.54	2.94
K. Plant TP2	Direct	1.01	0.64	1.48	0.53	4.11
	FEA	0.84	0.64	1.08	0.53	2.62
K. Plant TP3	Direct	1.38	0.71	2.96	1.02	5.94
	FEA	1.10	0.71	2.04	1.02	3.62

Table 3: Ratio of Q_c/Q_m for the ICP and ICP-FEA analysis.

Test Location	Q_c/Q_m Ratio	Total Pile Capacity	Total Shaft Friction	Total End Bearing	End Bearing Pile	End Bearing Plug
Pigeon Creek	Direct	1.14	2.02	0.76	0.40	1.39
	FEA	1.10	2.02	0.71	0.40	1.24
K. Plant TP1	Direct	0.86	0.89	0.81	0.36	2.72
	FEA	0.85	0.89	0.80	0.36	2.69
K. Plant TP2	Direct	0.86	0.95	0.74	0.27	2.07
	FEA	0.85	0.95	0.73	0.27	2.02
K. Plant TP3	Direct	0.79	0.84	0.67	0.23	1.34
	FEA	0.79	0.84	0.67	0.23	1.34

Table 4: Ratio of Q_c/Q_m for the UWA and UWA-FEA analysis.

Test Location	Q_c/Q_m Ratio	Total Pile Capacity	Total Shaft Friction	Total End Bearing	End Bearing Pile	End Bearing Plug
Pigeon Creek	Direct	1.24	1.42	1.16	0.60	2.11
	FEA	0.95	1.42	0.74	0.60	0.98
K. Plant TP1	Direct	1.06	0.78	1.44	0.64	4.84
	FEA	0.91	0.78	1.09	0.64	3.00
K. Plant TP2	Direct	1.05	0.80	1.37	0.49	3.82
	FEA	0.89	0.80	0.99	0.49	2.37
K. Plant TP3	Direct	0.86	0.68	1.28	0.44	2.57
	FEA	0.80	0.68	1.08	0.44	2.07

For the tests at Kwangyang Plant, Ko and Jeong (2015), both the UWA direct and UWA-FEA methods display a better match to the measured total capacity, whereas both the ICP direct and ICP-FEA methods display a better match to the end bearing on the plug. The tests performed at Pigeon Creek, Salgado et al. (2002), provided soil plug and annulus stress-displacement and force-displacement results. The UWA-FEA was the closest match to the stress and force distributions, and is presented in Figure 7 and Figure 8 below. These diagrams show the mobilisation of stresses and forces in the annulus and plug which were directly measured or estimated by the FEA. The 'BASE' term is the stress averaged over the entire base area, or the summation of the total force provided by the pile annulus and plug. The results in Figure 8 can be matched to those in the UWA-FEA method in Table 4 for the pile annulus, plug and total base results. The plug stress mobilisation from the UWA-FEA method agrees well with the measurements. However, the FEA analysis over-estimates the initial stiffness of the annulus response and under-estimates the ultimate annular end bearing. Refinements can be made to reduce these differences.

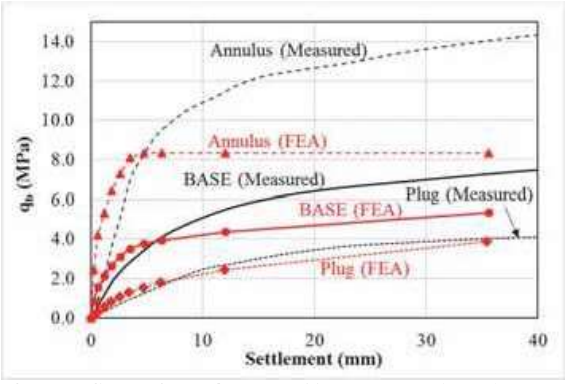

Figure 7: Comparison of measured base stress and UWA (FEA) estimates vs pile head settlement. Data from the Pigeon Creek test site (Salgado et al., 2002).

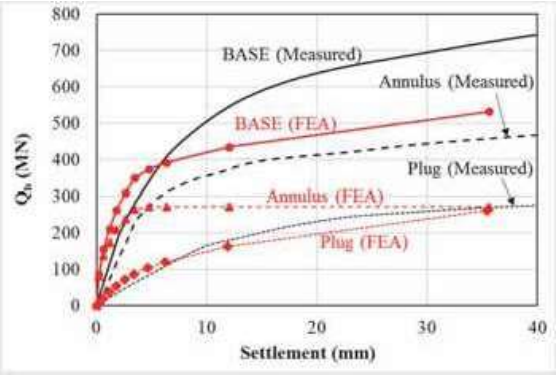

Figure 8: Comparison of measured base capacity and UWA (FEA) estimates vs pile head settlement. Data from the Pigeon Creek test site (Salgado et al., 2002).

Table 5 presents a comparison of the data from the four test sites where double walled piles are used. This includes the Area Ratio (A_{ann}/A_{plug}) and the ratio of the measured end bearing forces on the annulus and plug $(Q_{b,ann}/Q_{b,plug})$. These two values are observed to be quite different.

Table 5: Comparison of D/t, L/D, Area and EB Force Ratios.

Test Location	D/t Ratio	L/D Ratio	Area Ratio (A_{ann}/A_{plug})	Measured EB Force Ratio ($Q_{b,ann}/Q_{b,plug}$)
Pigeon Creek	11	20	0.49	1.70
Kwangyang Plant TP1	10	17	0.56	4.25
Kwangyang Plant TP2	14	16	0.36	2.79
Kwangyang Plant TP3	18	17	0.27	1.54

6. Discussion

The methodology used to estimate the end bearing capacity in the API, ICP and UWA design methods is different. Each has been based on the results of various investigations on base capacity. From the tests on double walled piles, the isolation of the internal, external and base capacities was possible and with this a better understanding of the stresses near to the pile tip. As indicated by Salgado et al. (2002), due to the exponential increase in the value of τ_i, the values of end bearing on the annulus can be misinterpreted due to the high compression of piles at this level.

As a simplification, the process of applying the computed base stress over the entire base area has its merit due to the complexity involved in estimating the contribution of the soil plug under an applied load. To consider the pile response accurately however, a model that integrates τ_i over the active plug length, as load is applied, is required. This can be done using finite elements or a similar medium. Here, the individual components can be sequentially mobilised under incremental load. It has been demonstrated, in Figure 5 and Figure 6, that the established pile design methods, especially the ICP and UWA produce data scattered about unity for the ratio of Q_c/Q_m on base capacity. The mean values are 0.95 and 1.65 respectively. A close inspection however of Table 2 to Table 4, in general, shows that the end bearing values on the pile annulus have Q_c/Q_m values that are less than 0.5 and end bearing values on the soil plug that are much greater than 1.5. This suggests that the design methods for OEPs underestimate the contribution of the pile's annulus and overestimate the contribution of the soil plug. These effects may compensate for each other to produce an improved estimate of the base capacity; however, the overall distribution of base capacity is inadequately proportioned between annulus and plug. Table 5 shows a clearer representation of the extent of this unequal distribution. If the distributions of stress were similar over the entire base, then the area ratio and the measured EB force ratios would be similar, and as can be seen, they are not.

The FEA can model the compression of the pile and plug separately under an applied static load. As shown by the results of many researchers, the response of an OEP is analogous to that of a pile-within-a-pile. None of the design methods directly consider this, and as can be seen from Figure 5 and Figure 6 combining the ICP and UWA methods with the FEA tool, in general, does improve the estimation of total base capacity. Using this finite element method to compute the pile capacity has shown that the response of the components of pile resistance can be obtained but further work needs to be done on its implementation so that it best captures the base response of OEPs.

7. Conclusions

It has been shown that the CPT based design methods may be good at predicting the overall base capacity of an OEP but the reliability of these base capacity predictions is limited. Also, the distribution and rate of mobilisation of these capacities may not be accurately captured. The double walled pile test data shows that the stress at the base of the plug is much less than is attributed to it by the design methods and the opposite occurs for the end bearing on the pile. The authors present a means of capturing this behaviour more accurately using a finite element

procedure which effectively isolates the individual components. Some comparisons with the measured data from these tests are also presented. Further work is still required to accurately refine this finite element procedure to ensure that its full capabilities are demonstrated and that it improves our ability to estimate OEP response.

8. Acknowledgments

The authors acknowledge the contribution of the ESPRC and Atkins Ground Engineering (c/o Dr. David French) for the funding of this research work and Claire Delgal, Acquisition Librarian at the ICE, London for the supply of database material.

9. References

American Petroleum Institute Recommended Practice 2GEO, Geotechnical and Foundation Design Considerations, API RP 2GEO, Apr 2011.

Chow, F Investigations into displacement pile behaviour for offshore foundations (1997). PhD Thesis. Imperial College, London (University of London).

Clausen CJF, Aas PM and Karlsrud K. (2005). Bearing capacity of driven piles in sand, the NGI approach. In: Gourvenec S and Cassidy M (eds.) *Proc. Int. Symp. Frontiers in Offshore Geotechnics, ISFOG 2005*. London: Taylor Francis, 677-682.

De Nicola A and Randolph MF. (1997). The plugging behaviour of driven and jacked piles in sand. *Geo-technique* 47(4): 841-856.

Doherty P, Gavin K and Gallagher D. (2010). Field investigation of base resistance of pipe piles in clay. *J. Geotech. Eng.* 163: 13-22.

Fugro Engineers BV. (Fugro) (2004). Axial pile capacity design method for offshore driven piles in sand, P-1003, Issue 3, to API, August 2004.

Jardine R, Chow F, Overy, R and Standing, J. (2005). ICP design methods for driven piles in sands and clays. London: Thomas Telford.

Jeong S, Ko J, Won J and Lee K. (2015). Bearing capacity analysis of open-ended piles considering the degree of soil plugging. *Soils and Foundations* 55(5): 1001-1014.

Ko J and Jeong S. (2015). Plugging effect of open-ended piles in sandy soil. *Can. Geotech J.* 52: 535-547

Kishida H and Isemoto N. (1977). Behaviour of sand plugs in open ended steel pipe piles. Proc. 9th Int. Conf. on Soil Mech. and Foundation Engineering, Tokyo, 601-604.

Lehane BM and Gavin KG. (2001). Base resistance of jacked pipe piles in sand. *J. Geotech. Geoenviron. Eng.* 128(3): 198-205.

Lehane BM and Randolph MF (2002). Evaluation of a Minimum Base Resistance for Driven Pipe Piles in Siliceous Sands. *J. Geotech. Geoenviron. Eng*. 127(6): 473-480.

Lehane BM, Schneider JA and Xu X. (2005). The UWA-05 method for prediction of axial capacity of driven piles in sand. In: Gourvenec S and Cassidy M (eds.) *Proc. Int. Symp. Frontiers in Offshore Geotechnics, ISFOG 2005*. London: Taylor Francis, 683-689.

Matsumoto T and Takei M. (1991). Effects of soil plug on behaviour of driven pipe piles. *Soils and Foundations* 31(2): 14-34.

Paik K and Lee S. (1993). Behaviour of soil plugs in open ended model piles driven into sands. *J. Marine Geotech* 11: 353-373.

Paik K, Salgado R, Lee J and Kim B. (2003). Behaviour of open-and closed-ended piles driven into sands. *J. Geotech. Geoenviron. Eng.* 129(4): 296-306.

Paikowsky SG. (1989). A static evaluation of soil plug behaviour with application to the pile plugging problem. PhD. Dissertation. Massachusetts Institute of Technology, USA.

Randolph MF, Leong EC and Houlsby GT. (1991). One-dimensional analysis of soil plugs in pipe piles. *Geotechnique* 41(4): 587-598.

Salgado R, Lee J, Kim K and Paik K. (2002). Load tests on pipe piles for development of CPT based design method. Final Report FHWA/IN/JTRP-2002/4 for the Indiana Department of Transportation and the US Department of Transportation Federal Highway Administration.

Schneider JA, Xu X and Lehane BM. (2008). Database assessment of CPT-based design methods for axial capacity of driven piles in siliceous sands. *J. Geotech. Geoenviron. Eng.* 134(9): 1227-1244.

Schneider JA, Xu X and Lehane BM. (2010). End bearing formulation for CPT based driven pile design methods in siliceous sands. Proc. 2nd Int. Sym. on Cone Penetration Testing, paper 18.

Xu X, Schneider JA and Lehane BM. (2008). Cone penetration test methods for end-bearing assessment of open-and closed-ended driven piles in siliceous sand. *Canadian Geotechnical J.* 45(8): 1130-1141.

Yang Z, Jardine R, Guo W and Chow F. (2015). A Comprehensive Database of Tests on Axially Loaded Piles Driven in Sand. Zhejiang Academic Press.

Appendix B – Paper 2:
One-dimensional finite element analysis of soil plug behaviour within open-ended piles

Joseph, T.M., Burd, H.J., Houlsby, G.T., and Taylor, P., 2018. One-dimensional finite element analysis of soil plug behaviour within open-ended piles. In *Eur. Conf. on Numerical Methods in Geotechnical Engineering IX*, Porto, Portugal.

Numerical Methods in Geotechnical Engineering IX – Cardoso et al. (Eds)
© 2018 Taylor & Francis Group, London, ISBN 978-1-138-33203-4

One-dimensional finite element analysis of the soil plug in open-ended piles under axial load

T.M. Joseph, H.J. Burd & G.T. Houlsby
Department of Engineering Science, University of Oxford, UK

P. Taylor
Atkins Ltd., Warrington, UK

ABSTRACT: In the offshore industry, open-ended steel piles are primarily designed using one of three pile design methods: the API (2011), the ICP (2005) and the UWA (2005). The soil plug, inside the pile, is considered differently in each of the methods, producing different pile lengths due to the varying assumptions adopted. A one-dimensional finite element method has been used to analyse the behaviour of the resistive components of the soil-pile-plug system. This adopts the principle of virtual work to solve the coupled differential equations enabling the contribution of each component to be isolated. Using this method, a more realistic axial pile response can be modelled which directly influences the behaviour of the soil plug. Predictions from the method have been compared to the results of double walled pile tests which show the mobilisation of the external shaft friction from the top downwards, and the internal friction from the base upwards.

1 INTRODUCTION

Many different methods are used to design offshore open-ended piles (OEP). Few of these consider the contribution of the soil plug directly and none of these methods model its behaviour accurately. Investigation of the behaviour of the soil plug has shown that the plug is mobilised from the base upwards. The compression of instrumented piles has been used to establish empirical pile design methods. However, in design, a rigid pile is often assumed, thereby simplifying the process. Improved modelling which captures the different responses of the soil, pile and plug, and the interaction between them, can only be achieved using a numerical approach, where a mathematical procedure is used to solve the equations of equilibrium that governs the soil-pile-plug response. A one-dimensional finite element (FE) procedure of this sort is presented in this paper.

The FE procedure has been used in combination with three pile design methods: the API (2011) method, the ICP (2005) method, and the UWA (2005) method, to produce a FE variant of each. A case study is presented which examines the predicted response from each FE variant and compares these to published pile test data.

2 FINITE ELEMENT ANALYSIS

2.1 *Open ended pile model*

Consider an OEP as shown in Figure 1 with an axially applied load F_t. In this system, the elastic pile is assumed to be in equilibrium as the load applied at the pile head is balanced by the summation of the external and internal shear stresses, $\tau_o(z)$ and $\tau_i(z)$, respectively, plus the end-bearing resistance $q_{p,b}$ on the base of the pile annulus. The action of τ_i is supported by the end-bearing resistance across the base of the plug, $q_{pl,b}$. Each of these components has separate stiffnesses which are mobilised at different rates to support the pile. These stiffnesses and the relative displacement across the interfaces dictate the mobilisation of the interface shear stresses, and the end bearing resistance. In this model, zero thickness interface layers are assumed.

2.2 *Strong and weak forms of the equations of equilibrium*

For the resistive components for the OEP, the axial stress, σ_p, that acts on the cross-sectional pile area, A_p, satisfies the following strong (differential equation) form (compression positive):

$$\frac{d\sigma_p}{dz}A_p + \tau_e P_e + \tau_i P_i = 0 \quad (1)$$

where τ_e, τ_i = shear stress in the external and internal interfaces, respectively; and P_e, P_i = external and internal perimeter of the pile, respectively. The plug satisfies the separate equilibrium equation (compression positive):

$$\frac{d\sigma_{pl}}{dz}A_{pl} - \tau_i P_i = 0 \quad (2)$$

where, σ_{pl} = the axial stress in the plug and A_{pl} = the cross-sectional area of the plug.

Equations (1) and (2) are converted to the weak (virtual work) form by multiplying by an arbitrary set of virtual displacements, δw, and integrating over the pile length (L) and plug length (L—L_{pl}) as appropriate. The application of the boundary conditions at the limits of the pile and plug is then used to obtain an expression which balances the virtual work associated with the applied load and the sum of the internal virtual work terms, giving:

$$\begin{aligned}\delta w_t\left(F_t\right) = \delta w_{p,b}F_{p,b} - \int_0^L \sigma_p A_p\left(\frac{d\left(\delta w_p\right)}{dz}\right)dz \\ + \delta w_{pl,b}F_{pl,b} - \int_{L-L_{pl}}^L \sigma_{pl}A_{pl}\left(\frac{d\left(\delta w_{pl}\right)}{dz}\right)dz \\ + \int_0^L \delta w_s \tau_s P_e dz + \int_{L-L_{pl}}^L \left(\delta w_p - \delta w_{pl}\right)P_i\tau_i dz \\ + \int_0^L \left(\delta w_p - \delta w_s\right)P_e\tau_e dz\end{aligned} \quad (3)$$

where δw_t = pile head virtual displacement; $\delta w_{p,b}$ = pile base virtual displacement; δw_p = virtual displacement along the pile shaft; $\delta w_{pl,b}$ = plug base virtual displacement; δw_{pl} = virtual displacement along the soil plug; δw_s = external soil virtual displacement; and τ_s = shear stress in the soil. Equation (3) may be expressed as:

$$0 = \delta W_E + \delta W_I \quad (4)$$

where δW_E and δW_I are expressions for the external and internal virtual work, respectively.

The external virtual work is associated with the applied load at the top of the pile:

$$\delta W_E = -\left(\delta w_t F_t\right) \quad (5)$$

The internal virtual work is associated with the internal stresses in the pile, the plug and the interfaces. This is given by:

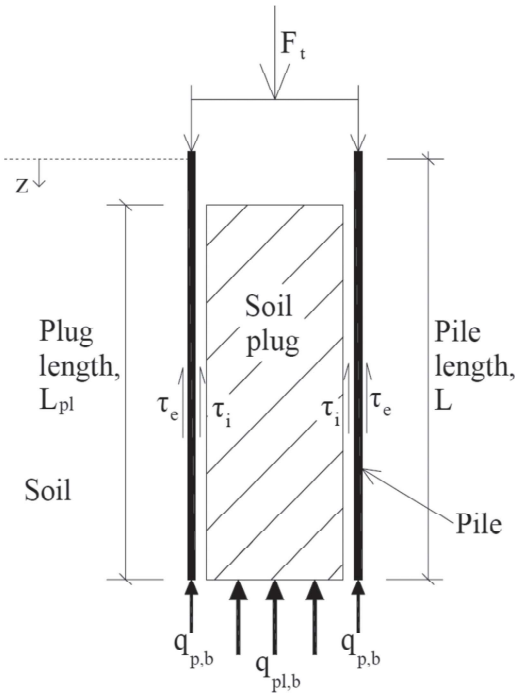

Figure 1. Pile, plug and base resistance interactions.

$$\begin{aligned}\delta W_t = \delta w_{p,b}F_{p,b} - \int_0^L \sigma_p A_p\left(\frac{d\left(\delta w_p\right)}{dz}\right)dz \\ + \delta w_{pl,b}F_{pl,b} - \int_{L-L_{pl}}^L \sigma_{pl}A_{pl}\left(\frac{d\left(\delta w_{pl}\right)}{dz}\right)dz \\ + \int_0^L \delta w_s \tau_s P_e dz + \int_{L-L_{pl}}^L \left(\delta w_p - \delta w_{pl}\right)P_i\tau_i dz \\ + \int_0^L \left(\delta w_p - \delta w_s\right)P_e\tau_e dz\end{aligned} \quad (6)$$

3 FINITE ELEMENT PROCEDURE

The virtual work equations specified above are used to determine a set of discretized 1D finite element equations using the standard Galerkin approach. The OEP is discretised as a series of finite elements along its entire length. The pile, plug and soil are modelled as sets of 2-noded line elements. The pile-soil and pile-plug interfaces are modelled as 4-noded, zero-thickness, interface elements; these interface elements are used to connect the pile elements to the (internal) plug elements and the (external) soil elements. The end-bearing of the pile and plug are modelled as lumped elements. Figure 2 indicates diagrammatically the general form of the finite element model.

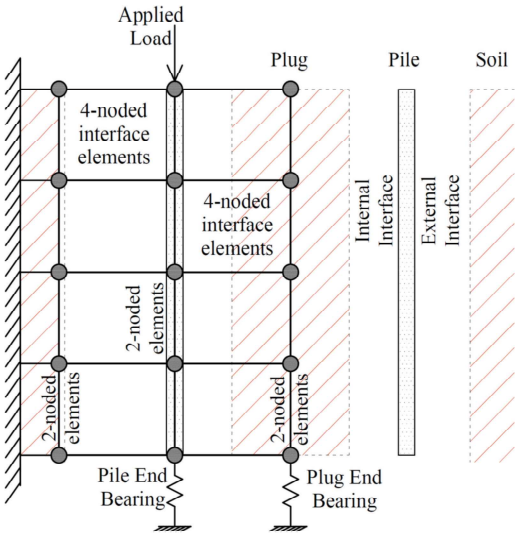

Figure 2. Simple discretised model of pile-plug-soil, interfaces and end bearing components.

The axial displacements within each element are related to the nodal displacements via Lagrangian shape functions The displacements and strains determined using this approach are:

$$w = \mathbf{N}\boldsymbol{w}_e \quad \text{and} \quad \frac{dw}{dz} = \mathbf{B}\boldsymbol{w}_e \tag{7}$$

where $\boldsymbol{N}$ is the shape function matrix; $\boldsymbol{w}_e$ is the vector of element nodal displacements; and $\boldsymbol{B}$ is a matrix formed from the derivative of the element shape function, $\boldsymbol{N}$.

3.1 *Pile base*

The pile base is a lumped element and therefore adopts the value of an equivalent point load:

$$\boldsymbol{f}_{p,b} = F_{p,b} \tag{8}$$

3.2 *Pile*

The virtual work term for the pile is:

$$\int_0^L \sigma_p A_p \left(\frac{d\left(\delta w_p\right)}{dz} \right) dz \tag{9}$$

Adopting the Lagrangian shape functions and their derivatives, and on the basis of the Galerkin approach, the virtual work associated with the pile is approximated by:

$$\sum_{pile\ elements} \delta \boldsymbol{w}_e^T \int_0^L \boldsymbol{B}^T \sigma_p A_p .dz \tag{10}$$

The internal force within each pile element is determined from:

$$\boldsymbol{f}_{element,p} = \int_{elements} \boldsymbol{B}^T \sigma_p A_p .dz \tag{11}$$

3.3 *Plug base*

The plug base is also a lumped element and adopts a point load value as:

$$\boldsymbol{f}_{pl,b} = F_{pl,b} \tag{12}$$

3.4 *Plug*

The virtual work expression for the plug is:

$$\int_{L-L_{pl}}^{L} \sigma_{pl} A_{pl} \left(\frac{d\left(\delta w_{pl}\right)}{dz} \right) dz \tag{13}$$

Converting to the Galerkin form gives:

$$\sum_{plug\ elements} \delta \boldsymbol{w}_e^T \int_{L-L_{pl}}^{L} \boldsymbol{B}^T \sigma_{pl} A_{pl} .dz \tag{14}$$

The internal force within each of the plug elements is then determined from:

$$\boldsymbol{f}_{element,pl} = \int_{elements} \boldsymbol{B}^T \sigma_{pl} A_{pl} .dz \tag{15}$$

3.5 *Soil*

The virtual work expression is:

$$\int_0^L \delta w_s \tau_s P_e dz \tag{16}$$

This gives the Galerkin form as:

$$\sum_{soil\ elements} \delta \boldsymbol{w}_e^T \int_0^L \boldsymbol{N}^T \tau_s P_e .dz$$

The internal force within each of the soil elements is determined from:

$$\boldsymbol{f}_{element,s} = \int_{elements} \boldsymbol{N}^T \tau_s P_e .dz \tag{17}$$

3.6 *Internal interface*

Adopting the Langrangian shape functions, the virtual work (Galerkin form) of the 4-noded internal interface elements is:

$$\sum_{int-int\ elements} \delta \boldsymbol{w}_e^T \int_{L-L_{pl}}^{L} \boldsymbol{N}^T \tau_i P_i .dz \tag{18}$$

The internal force within each 4-noded internal interface element is:

$$\boldsymbol{f}_{element,int-int} = \int_{elements} \boldsymbol{N}^T \tau_i P_i .dz \tag{19}$$

3.7 *External interface*

Similarly, adopting the Langrangian shape functions, the virtual work (Galerkin form) of the 4-noded external interface elements is:

$$\sum_{ext-int\ elements} \delta \boldsymbol{w}_e^T \int_{0}^{L} \boldsymbol{N}^T \tau_i P_i .dz \tag{20}$$

The internal force within each 4-noded external interface element is:

$$\boldsymbol{f}_{element,\ ext-int} = \int_{elements} \boldsymbol{N}^T \tau_i P_i .dz \tag{21}$$

3.8 *Assembly*

The global internal force vector ($\boldsymbol{F}_{INT}$) is obtained by assembling the individual forces of the nodes for each element and the base node for the pile and the plug. A similar assembly process is performed for the virtual displacement vector ($\delta \boldsymbol{w}$). This process is performed by using an assembly function [°] which populates the internal forces vector, displacements vector and the stiffness matrix employing an appropriate degree of freedom mapping:

$$\begin{aligned} \boldsymbol{F}_{INT} = {} & \mathbb{A}\left[\boldsymbol{f}_{p,b} \right] - \mathbb{A}\left[\boldsymbol{f}_{element,p} \right] \\ & + \mathbb{A}\left[\boldsymbol{f}_{pl,b} \right] - \mathbb{A}\left[\boldsymbol{f}_{element,pl} \right] \\ & + \mathbb{A}\left[\boldsymbol{f}_{element,s} \right] + \mathbb{A}\left[\boldsymbol{f}_{element,int-int} \right] \\ & + \mathbb{A}\left[\boldsymbol{f}_{element,ext-int} \right] \end{aligned} \tag{22}$$

$$\begin{aligned} \delta \boldsymbol{w} = {} & \mathbb{A}\left[\delta W_{p,b} \right] - \mathbb{A}\left[\boldsymbol{\delta w}_p \right] + \mathbb{A}\left[\delta W_{pl,b} \right] - \mathbb{A}\left[\boldsymbol{\delta w}_{pl} \right] \\ & + \mathbb{A}\left[\boldsymbol{\delta w}_s \right] + \mathbb{A}\left[\boldsymbol{\delta w}_{i,i} \right] + \mathbb{A}\left[\boldsymbol{\delta w}_{e,i} \right] \end{aligned} \tag{23}$$

The internal work is now written as:

$$\delta W_I = \delta \boldsymbol{w}^T \boldsymbol{F}_{INT} \tag{24}$$

The external virtual work is assembled in the same manner, giving:

$$\delta W_E = -\delta \boldsymbol{w}^T \mathbf{F}_{EXT} \tag{25}$$

From Equation (4):

$$0 = \delta \boldsymbol{w}^T \left(\mathbf{F}_{INT} - \mathbf{F}_{EXT} \right) \tag{26}$$

As the virtual displacements are arbitrary on the basis of the first lemma of variational calculus:

$$\boldsymbol{G} = 0 = \left(\mathbf{F}_{INT} - \mathbf{F}_{EXT} \right) \tag{27}$$

The vector equation, $\boldsymbol{G} = 0$, is solved using the modified Newton-Raphson method.

4 CASE STUDY

The selected case study consists of a double wall pile test that was performed in Pigeon Creek, Indiana, USA. The soil comprised predominantly gravelly sand to a depth of 13 m. CPT data available for the site is presented in Figure 3. The test pile was 8.24 m long with dimensions as shown in Figure 4. This was driven to the required depth and loaded incrementally to failure. The separation of the pile walls and the installation of strain gauges over their lengths allowed the differential response of both pile walls to be measured. The results of these tests are published in Salgado et al. (2002) and Paik et al. (2003). Using this published

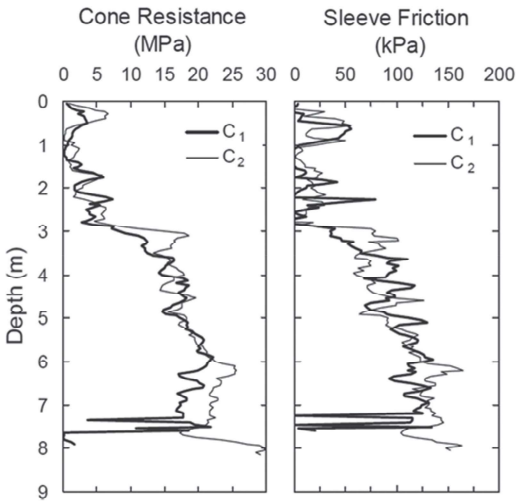

Figure 3. q_c and f_s. measurements (Salgado et al., 2002).

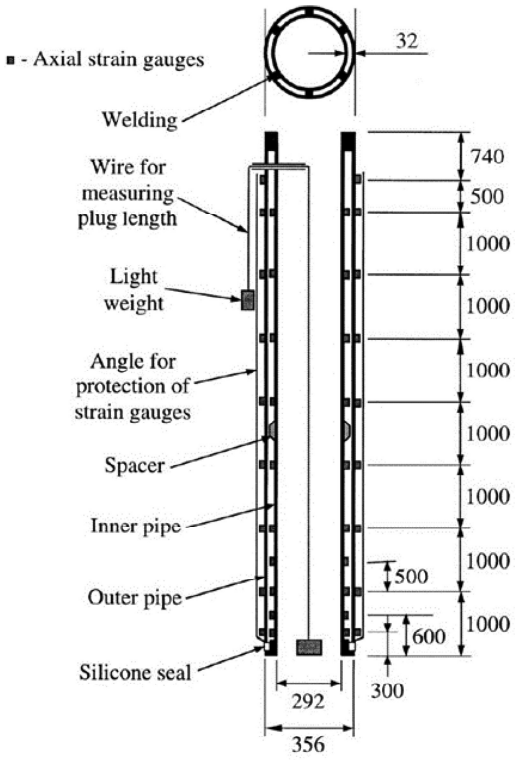

Figure 4. Double-walled open-ended test pile (Salgado et al., 2002).

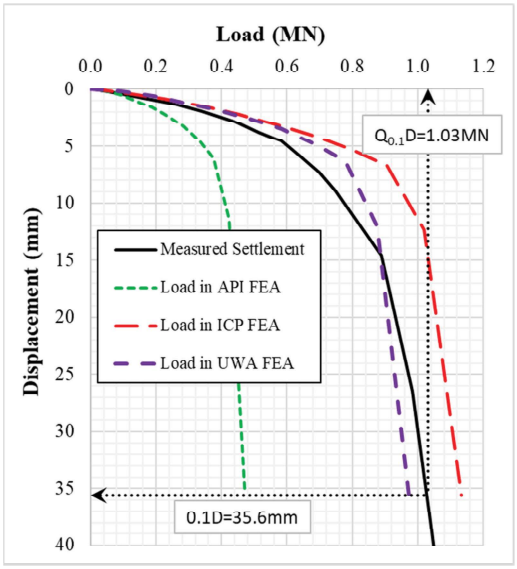

Figure 5. Load displacement responses using FE variants of the API, ICP and UWA design methods.

data, a comparison is made of these results and those estimated by the FE procedure adopting the input parameters of the design methods to obtain their FE variants.

The ultimate external shaft friction, τ_{ult}, and the ultimate end bearing resistance, q_{ult}, are input to the FE procedure from the design methods. By using the design methods directly, without the FE procedure, each predicts a plugged pile, therefore q_{ult} is applied over the area of both the annulus and the pile plug.

In addition, the Q-z and t-z soil reaction curves, taken directly from the API, are specified as constitutive models in the finite element analysis and employed for the ICP and UWA methods. The t-z soil reaction curves are applied to both the external and internal sides of the pile with τ_{ult} applied as the limiting resistance on both sides.

The computed pile head load-displacement responses are presented in Figure 5. Here it is shown that the estimated capacity from the API-FEA significantly underpredicts the capacity at a pile head displacement of $0.1D$, where D is the external pile diameter, with the ratio of calculated to measured capacity, $Q_c/Q_m = 0.45$. The ICP-FEA and UWA-FEA methods both estimate the capacity to within 10% of the measured value.

Using the FE model, the mobilised base capacity, which includes the internal shaft and annular end bearing capacity on the pile, can be extracted under the action of loads applied at the pile head. This has been done for each of the three design methods and presented in Figure 6 to Figure 8. The dotted lines represent the FE estimated values and the solid lines are those measured. These figures demonstrate the ability of the FE model to mobilise the soil plug from the base upwards; a characteristic not currently possible with the existing design methods.

From Figure 6 the API-FEA does not mobilise the full measured internal loads, as the overall capacity is lowest, therefore a smaller load is attributed to each component. The ICP-FEA (Figure 7) and the UWA-FEA (Figure 8) both demonstrate an improved but under-estimation of the development of the base capacity although this is not fully developed to match the measured loads.

The external shaft friction developed along the pile can be extracted from the FE model and compared to the load measured along the external pile in the pile tests. These comparisons are presented in Figure 9 to Figure 11. During the installation, some of the strain gauges below 4 m and 5 m were damaged resulting in missing data.

For a pile head load of 1130 kN, the resulting shaft friction measured along the pile ranged from

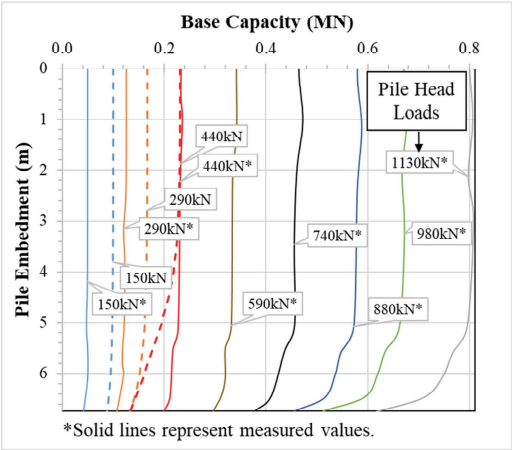

Figure 6. Comparison of measured base capacity to estimates using the API-FEA procedure with axial pile head loads.

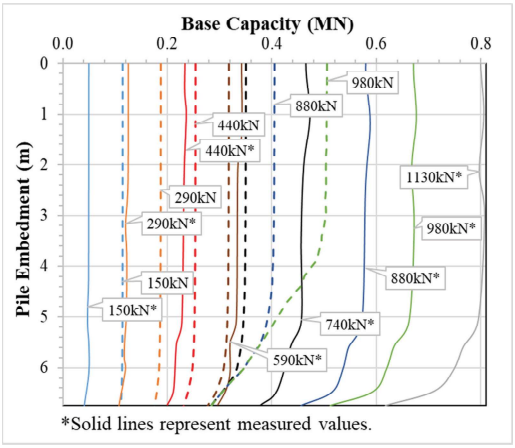

Figure 8. Comparison of measured base capacity to estimates using the UWA-FEA procedure with axial pile head loads.

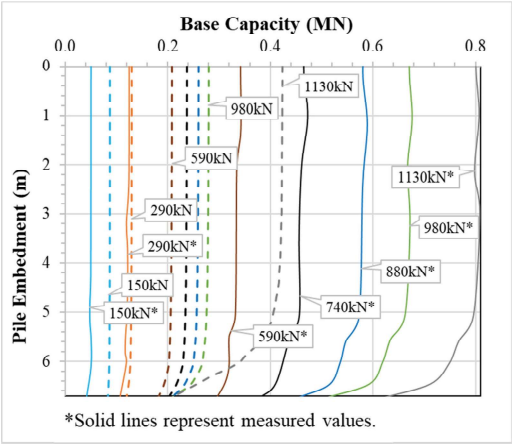

Figure 7. Comparison of measured base capacity to estimates using the ICP-FEA procedure with axial pile head loads.

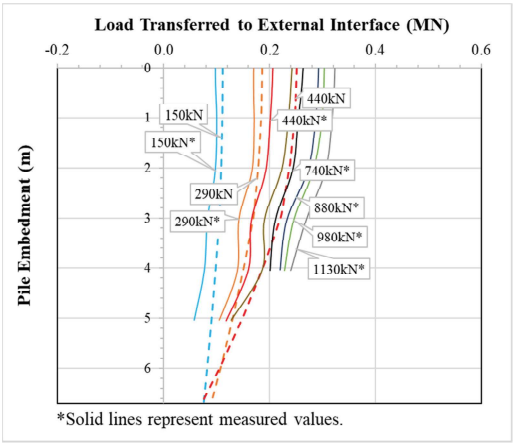

Figure 9. Comparison of measured load distribution along external pile to estimates of external shaft capacity using the API-FEA procedure with axial pile head loads.

approximately 320 kN to 240 kN in the pile segments. The API-FEA procedure (Figure 9) shows that the full load measured in the pile was not mobilised as the maximum FEA value estimated was 440 kN. The ICP-FEA procedure (Figure 10) estimates a maximum of 500 kN in the top segment of the pile. The UWA-FEA (Figure 11) estimates a similar load of approximately 500 kN in the top segment, however this is achieved under a smaller pile head load. This comparison demonstrates that, with the assumptions adopted, whilst ICP and UWA provide good estimates of total pile capacity (Figure 5), none of the design methods predict the relative contributions from the base and shaft identified by the FEA.

Figure 12 to Figure 14 compares the mobilisation of the end bearing capacity. The API-FEA comparison shows that the base capacity of both the annulus and the plug is underpredicted; the total base capacity is approximately 40% of that measured. The ICP-FEA improves the accuracy of model with an estimation of total end bearing of about 70% of that measured. The total base capacity from the UWA-FEA method is the best approximation with 75% of the measured capacity estimated. In these plots however, the distribu-

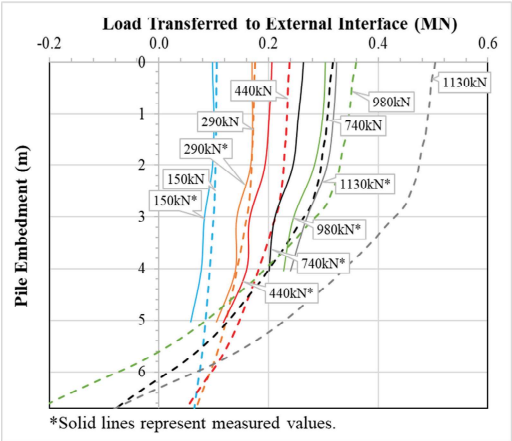

Figure 10. Comparison of measured load distribution along external pile to estimates of external shaft capacity using the ICP-FEA procedure with axial pile head loads.

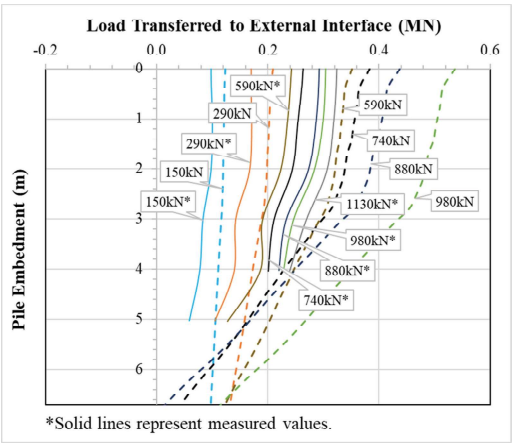

Figure 11. Comparison of measured load distribution along external pile to estimates of external shaft capacity using the UWA-FEA procedure with axial pile head loads.

tion of base capacity between the annulus and soil plug, from the FE analysis, is somewhat different to that measured.

5 DISCUSSION

The equation of equilibrium used to represent a loaded open-ended pile has been solved using a finite element procedure. This method has been unique in that the soil-pile-plug model has been incorporated. The use of the Galerkin method with Lagrangian shape functions is used to represent the various components of the model. Three existing pile design methods were used in the FE model to estimate the capacities and response of these components.

The design methods have derived their capacities based on detailed studies of existing pile test data. These relate the ultimate compressive capacity of

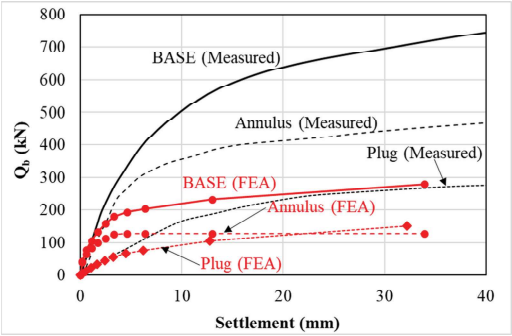

Figure 12. Comparison of measured base capacity and API-FEA estimates vs pile head settlement.

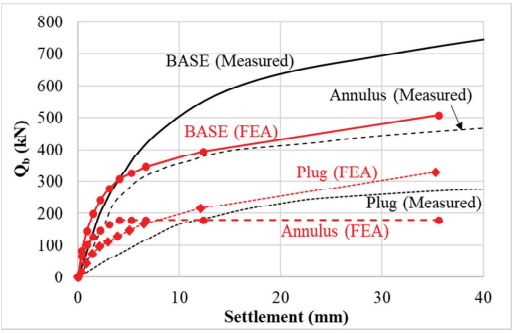

Figure 13. Comparison of measured base capacity and ICP-FEA estimates vs pile head settlement.

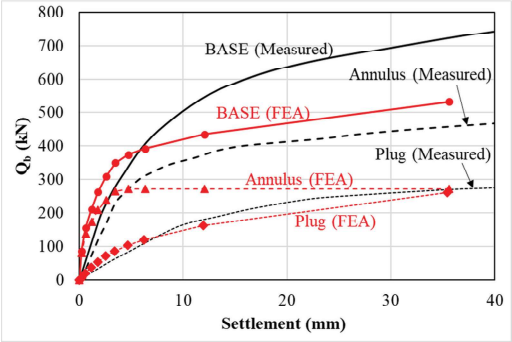

Figure 14. Comparison of measured base capacity and UWA-FEA estimates vs pile head settlement.

the pile to detailed soil test results and derived behaviours of the interface and end bearing. These were deduced for general use by the industry with a rigid pile assumption. The true behaviour of the pile under loading however, is to compress and modelling this response in design is usually an unsophisticated process combining simple soil reaction curves and an elastic pile in a Winkler-type analysis. The finite element model presented here, however, enables a forensic examination of the responses of the individual pile components.

Using the geotechnical engineering database, such as Yang et al. (2015), the ICP and the UWA pile design methods have been shown to provide improved estimates of pile capacity. This tendency was also found in the case study presented in Figure 5 where these methods estimate the measured pile capacity within 10% accuracy.

The end bearing behaviour is difficult to predict. Each of the pile design methods presented adopts a different approach to estimate this behaviour since each considers the response of the pile tip, plug base and internal shaft friction differently. In each method, if the pile is considered 'plugged', the base resistance is applied over the full base area. In the case study, the measured resistance at the base of the pile was approximately 14 MPa which is similar to the measured q_c values. As shown in Figure 6 to Figure 8, with small loads applied, the pile tip provides the only contribution to end bearing. As more load is applied, this quantity rapidly increases demonstrating the high stiffness of this component.

The mobilisation of the plug's capacity was clearly observed in the case study due to the double walled pile configuration. As shown in Figure 6 to Figure 8, as the load increases, the plug capacity is gradually mobilised. This behaviour was replicated in the FE model. Essentially, the plug conveys load from the pile to the soil beneath the base of the plug. The interaction between the pile and the internal plug will therefore influence the end bearing capacity. If the efficiency of load transfer is considered perfect, all the load that is resisted by the internal plug-pile interface is supported by the end bearing of the plug. Also, as demonstrated by Randolph et al. (1991) and other researchers, for drained sandy soils, the compression from the base of a confined soil plug will cause lateral expansion thereby increasing the internal interface stress from the pile tip, attenuating upwards the pile shaft.

The stiffness and capacity of the plug's base is difficult to determine due to the parameters involved in the mobilisation. Again considering sandy soils, these parameters include: the interface friction angle, δ_{cv}, between the pile and plug, accounting for the interface roughness between the two materials; the effective stress in the soil, σ'_{v0}, which depends on the density and length of the plug; a factor that considers the dilatant behaviour of sand when subjected to shearing, K_0; and the confinement stress of the plug, which is dependent on the internal diameter of the pile, D_i. This confinement stress increases with a reducing D_i, and influences the end bearing resistance. Therefore, in sands:

$$q_{pl,b} = f\left(\delta_{cv}, \sigma'_{v0}, K_0, \frac{1}{D_i}\right) \tag{28}$$

Due to the number of factors included in mobilisation, the plug stiffness is much lower than that of the pile tip. Current estimates of plug capacity, such as Lehane et al. (2015) suggest 0.2 to 0.3 of the measured q_c.

The mobilised resistance of the external shaft friction is shown in Figure 9 to Figure 11. The UWA demonstrates the best match of the measured to estimated data followed by the ICP and then the API method. However, both the ICP and UWA methods appear to significantly over-estimate the external shaft capacity.

In general, the pile design methods have been shown to underestimate the end bearing capacity. Figure 14, which highlights the base response of the UWA method, shows that the use of the ultimate values coupled with the API's Q-z soil reaction curves has the best comparison to the values measured. Further work is to be done to improve on this trend.

It is therefore observed from the use of the FE model that the design methods do not readily predict the base and shaft capacity contributions in open-ended piles.

6 CONCLUSIONS

The numerical procedure presented herein has been able to demonstrate that by using finite elements, a critical analysis can be performed on the behaviour of the individual components of an open-ended pile. A case study is presented which compares published results from physical testing using a double walled pile, to those estimated by a simple one-dimensional FE procedure, adopting the ultimate design parameters from three pile design methods, coupled with the API's axial soil reaction curves. The procedure has shown that with the ICP and UWA parameters adopted, the overall capacity is well estimated, however the mobilised distribution of load across each of the resistive components is not well matched. In addition, the true response and capacity of the soil plug is not well captured by the design methods considered. Further work is therefore necessary to ensure that the mobilised stiffness of the individual

components required to support axial loads are accurately considered in design. One approach to achieving this is by further improvement of the soil-pile-plug model using a FE procedure.

ACKNOWLEDGEMENTS

This work was supported by grant EP/L016303/1 for Cranfield University and the University of Oxford, Centre for Doctoral Training in Renewable Energy Marine Structures—REMS (http://www.rems-cdt.ac.uk/) from the UK Engineering and Physical Sciences Research Council (EPSRC). The authors also acknowledge the contribution of Atkins (c/o Andrew Benson and Dr David French) for the support of this research work.

REFERENCES

American Petroleum Institute Recommended Practice 2GEO, Geotechnical and Foundation Design Considerations, API RP 2GEO, Apr 2011.

Burd, H. 2015. Finite Element Analysis of Axially Loaded Pile. Internal document.

Khennane, A. 2013. Introduction to finite element analysis using MATLAB and Abaqus". Boca Raton: CRC Press.

Jardine, R., Chow, F., Overy, R. & Standing, J. 2005. *ICP design methods for driven piles in sands and clays*. London: Thomas Telford.

Lehane, B.M. & Gavin, K.G. 2001. Base resistance of jacked pipe piles in sand. *J. Geotech. Geoenviron. Eng.* 128(3): 198–205.

Lehane, B.M. & Randolph, M.F. 2002. Evaluation of a Minimum Base Resistance for Driven Pipe Piles in Siliceous Sands. *J. Geotech. Geoenviron. Eng*. 127(6): 473–480.

Lehane, B.M., Schneider, J.A. & Xu, X. 2005. The UWA-05 method for prediction of axial capacity of driven piles in sand. In: Gourvenec S and Cassidy M (eds.) 2005. *Proc. Int. Symp. Frontiers in Offshore Geotechnics, ISFOG 2005.* London: Taylor Francis, 683–689.

Lehane, B.M., Schneider, J.A. & Xu, X. 2005. CPT based design of driven piles in sand for offshore structures. Report Number: 05345. University of Western Australia: Geomechanics Group Publication.

Joseph, T.M., Houlsby, G.T., Burd, H. & Taylor, P. 2017. Finite Element Analysis of Soil Plug Behaviour Within Open-Ended Piles. SUT OSIG, London, Sept 2017.

Paik, K., Salgado, R., Lee, J. & Kim, B. 2003. Behaviour of open-and closed-ended piles driven into sands. *J. Geotech. Geoenviron. Eng.* 129(4): 296–306.

Randolph, M.F., Leong, E.C. & Houlsby, G.T. 1991. One-dimensional analysis of soil plugs in pipe piles. *Geotechnique* 41(4): 587–598.

Salgado, R., Lee, J., Kim, K. & Paik, K. 2002. Load tests on pipe piles for development of CPT based design method. Final Report FHWA/IN/JTRP-2002/4 for the Indiana Department of Transportation and the US Department of Transportation Federal Highway Administration.

Smith, I.M. & Griffiths, D.V. 2004. *Programming the finite element method*. Chichester: John Wiley & Sons.

Wood, D.M. 2004. Geotechnical modelling. Applied Geotechnics Vol. 1. Abingdon: Spon Press.

Yang, Z., Jardine, R., Guo, W. & Chow, F. 2015. *A Comprehensive Database of Tests on Axially Loaded Piles Driven in Sand.* London: Academic Press.

Appendix C – Manual:
VIRTUPLUG Program Manual with Source Code